

**EXPERIMENTAL INVESTIGATIONS OF A COMMON
RAIL DIRECT INJECTION DIESEL ENGINE USING
BIODIESEL BLENDS IN REACTIVITY CONTROLLED
COMPRESSION IGNITION MODE**

TEOH YEW HENG

**FACULTY OF ENGINEERING
UNIVERSITY OF MALAYA
KUALA LUMPUR**

2016

**EXPERIMENTAL INVESTIGATIONS OF A COMMON
RAIL DIRECT INJECTION DIESEL ENGINE USING
BIODIESEL BLENDS IN REACTIVITY CONTROLLED
COMPRESSION IGNITION MODE**

TEOH YEW HENG

**THESIS SUBMITTED IN FULFILMENT OF THE
REQUIREMENTS FOR THE DEGREE OF DOCTOR
OF PHILOSOPHY**

**FACULTY OF ENGINEERING
UNIVERSITY OF MALAYA
KUALA LUMPUR**

2016

UNIVERSITY OF MALAYA
ORIGINAL LITERARY WORK DECLARATION

Name of Candidate: **TEOH YEW HENG**

Matric No: **KHA110004**

Name of Degree: **DOCTOR OF PHILOSOPHY**

Title of Thesis: **EXPERIMENTAL INVESTIGATIONS OF A COMMON RAIL
DIRECT INJECTION DIESEL ENGINE USING BIODIESEL
BLENDS IN REACTIVITY CONTROLLED COMPRESSION
IGNITION MODE**

Field of Study: **ENERGY (ALTERNATIVE FUEL)**

I do solemnly and sincerely declare that:

- (1) I am the sole author/writer of this Work;
- (2) This Work is original;
- (3) Any use of any work in which copyright exists was done by way of fair dealing and for permitted purposes and any excerpt or extract from, or reference to or reproduction of any copyright work has been disclosed expressly and sufficiently and the title of the Work and its authorship have been acknowledged in this Work;
- (4) I do not have any actual knowledge nor do I ought reasonably to know that the making of this work constitutes an infringement of any copyright work;
- (5) I hereby assign all and every rights in the copyright to this Work to the University of Malaya ("UM"), who henceforth shall be owner of the copyright in this Work and that any reproduction or use in any form or by any means whatsoever is prohibited without the written consent of UM having been first had and obtained;
- (6) I am fully aware that if in the course of making this Work I have infringed any copyright whether intentionally or otherwise, I may be subject to legal action or any other action as may be determined by UM.

Candidate's Signature

Date:

Subscribed and solemnly declared before,

Witness's Signature

Date:

Name:

Designation:

ABSTRACT

In recent years, rapid growth in population, development, and industrialization have led to a high demand for energy worldwide. Biofuels from bio-based products can be considered an alternative to fossil fuels used in the transport sector. However, the use of biodiesel in conventional diesel combustion engines has usually caused lower thermal efficiency and higher in specific fuel consumption. Using alternative fuels and switching to promising combustion technologies such as low temperature combustion (LTC) are reliable approaches to address this issue. This research aims to use biofuels as an alternative energy source for engines operating in reactivity controlled compression ignition (RCCI) dual-fuel combustion mode. In the first stage, a test cell system was developed, which consisted of a single cylinder diesel engine, dynamometer and combustion analyzer system. This was followed by the extensive conversion and integration of the high pressure common-rail injection to the test engine for providing high degree of flexibility in the control of injection parameters. In the second stage, an experimental investigation to study the effects of palm and Jatropha biodiesel fuels on the engine performance, emissions, and combustion characteristics of the converted engine was performed under different load operations. The test fuels included a conventional diesel fuel and eight different blends of palm and Jatropha biodiesel fuels. During the third stage, parametric studies dealing with injection timing and exhaust gas recirculation (EGR) variation by using neat palm biodiesel were performed and compared with baseline diesel. In the final stage, the effects of diesel/ biodiesel strategies on dual-fuel combustion were investigated. This dual-fuel combustion mode proposes port fuel injection of gasoline and direct injection of diesel/ biodiesel fuel with rapid in-cylinder fuel blending. Engine performance, emissions, and cylinder pressure trace were sampled and analyzed under different experiment schemes. The results indicated that the in-house

developed ECU is capable of real-time control and monitoring of the injection parameters. The second stage experimental results revealed that the biodiesel blended fuels had a significant influence on the brake specific fuel consumption (BSFC) at all the engine load conditions examined. In general, the use of neat and blends of biodiesel resulted in a reduction in brake specific nitrogen oxide (BSNO_x), brake specific carbon monoxide (BSCO), smoke emissions, shorter ignition delay (ID), and shorter combustion duration regardless of the load conditions. Besides, the third stage experimental results indicated that both the injection timing and EGR variation had a prominent effect on the engine performance, emissions and combustion characteristics with baseline diesel and neat biodiesel operation. Based on the highest brake thermal efficiency (BTE) and the reasonable NO_x level, thus the optimum injection timing is found to be 11°BTDC for both the baseline diesel and biodiesel operation. Introduction of EGR has effectively reduced the NO_x emissions, but has increased the smoke emissions. In the last stage experiment, the results showed that the engine operating under RCCI dual-fuel combustion mode could achieve high efficiency with near zero NO_x and smoke emissions.

ABSTRAK

Kebelakangan ini, pertumbuhan populasi yang pesat, pembangunan dan perindustrian telah mengakibatkan keadaan permintaan yang tinggi terhadap tenaga di seluruh dunia. Biofuel daripada produk berasaskan bio bakal dianggap sebagai pengganti alternatif untuk bahan api fosil yang digunakan dalam sektor pengangkutan. Walau bagaimanapun, penggunaan biodiesel dalam enjin diesel pembakaran konvensional biasanya menyebabkan kecekapan haba yang rendah dan spesifik penggunaan bahan api yang tinggi. Penggunaan sumber bahan api alternatif dan pengenalan teknologi pembakaran yang menjanjikan seperti *low temperature combustion (LTC)* boleh dianggap sebagai pendekatan yang boleh dipercayai untuk menangani isu ini. Kajian ini bertujuan untuk menggunakan biofuel sebagai sumber tenaga alternatif untuk operasi enjin dengan mod pembakaran dwi-bahan api *reactivity controlled compression ignition (RCCI)*. Pada peringkat pertama, sistem pengujian telah dibangunkan, dimana ia terdiri daripada enjin diesel berombok satu, *dynamometer* dan sistem penganalisis pembakaran. Ini diikuti dengan konversi dan integrasi system suntikan *common-rail* bertekanan tinggi terhadap enjin ujian bagi menyediakan fleksibiliti yang tinggi dalam kawalan masa suntikan, kuantiti suntikan dan membolehkan suntikan beracara pelbagai. Pada peringkat kedua, siasatan ujikaji terhadap kesan bahan api biodiesel *Jatropha* dan sawit terhadap prestasi enjin, pengeluaran ekzos, dan ciri-ciri pembakaran di bawah operasi beban yang berbeza telah dilakukan. Bahan api ujian termasuk diesel konvensional dan lapan campuran bahan api biodiesel. Pada peringkat ketiga, kajian parametrik terhadap perubahan pemasaan suntikan dan edaran semula gas ekzos (EGR) dengan menggunakan biodiesel sawit telah dijalankan dan dibandingkan dengan diesel konvensional. Pada peringkat akhir, kesan strategi diesel/ biodiesel terhadap pembakaran dwi-bahan api telah dijalankan. Mod pembakaran tersebut melibatkan suntikan *port* bahan api petrol serta suntikan terus bahan

api diesel/ biodiesel dengan pencampuran bahan api *rapid* dalam silinder. Prestasi enjin, pengeluaran ekzos, dan tekanan silinder telah disampel dan dianalisis untuk setiap skim eksperimen. Keputusan eksperimen peringkat pertama menunjukkan bahawa sistem ECU yang dibangunkan mampu mengawal dan memantau parameter suntikan bahan api. Keputusan eksperimen peringkat kedua mendedahkan bahawa pencampuran bahan api biodiesel mempunyai pengaruh yang besar ke atas brek penggunaan bahan api tertentu (BSFC) untuk semua keadaan beban enjin diperiksa. Secara umumnya, penggunaan biodiesel dan campurannya menyebabkan pengurangan brek oksida nitrogen tertentu (BSNO_x), brek karbon monoksida tertentu (BSCO), pelepasan asap, pengurangan lengah pencucuhan (ID), dan tempoh pembakaran lebih cepat untuk setiap keadaan beban. Selain itu, keputusan eksperimen peringkat ketiga menunjukkan bahawa kedua-dua masa suntikan dan EGR variasi mempunyai kesan penting ke atas prestasi enjin, pelepasan ekzos dan ciri-ciri pembakaran bagi enjin beroperasi dengan diesel dan biodiesel. Berdasarkan kecekapan brek tertinggi haba (BTE) dan tahap pelepasan NO_x yang munasabah, maka masa suntikan optimum didapati berlaku pada 11° BTDC untuk enjin operasi dengan kedua-dua diesel dan biodiesel. Pendedahan EGR telah mengurangkan pelepasan NO_x dengan efektif, tetapi telah meningkatkan pelepasan asap. Untuk pengujian tahap terakhir, keputusan eksperimen menunjukkan bahawa enjin yang beroperasi di bawah mod pembakaran dwi-bahan api RCCI mempunyai keupayaan untuk mencapai kecekapan yang tinggi dengan pelepasan NO_x dan asap yang hampir sifar.

ACKNOWLEDGEMENTS

I would like to special thanks to my supervisors Professor Dr. Masjuki Hj. Hassan and Associate Professor Dr. Md. Abul Kalam for their helpful guidance, encouragement and assistance. Without their help, progress could never have been made on this thesis. I also express my sincere gratitude to the Ministry of Higher Education (MOHE) of Malaysia and University of Malaya for financial support through UMRG (grant number RG145-12AET), HIR grant (UM.C/HIR/MOHE/ENG/07), and Postgraduate Research Grant (PPP) (grant number PG035-2012B). I am grateful to the University of Science Malaysia and Ministry of Education Malaysia (SLAB/SLAI Programme) for the scholarship which enabled me to undertake a PhD program at the University of Malaya. I also would like to convey appreciation to all faculty members and staff of the Department of Mechanical Engineering, University of Malaya for giving opportunity to prepare and conduct this research. I also would like to thank to all members in “Centre for Energy Sciences” research group for their valuable ideas and discussion. I am thankful for their aspiring guidance, invaluable constructive criticism and friendly advice. I am sincerely grateful to them for sharing their truthful and illuminating views on a number of issues related to the thesis. Additional thanks to Mr. Sulaiman Ariffin for his technical help and assistance.

A special thanks to my family and my beloved wife, How Heoy Geok. Words cannot express how grateful I am to them for all of the sacrifices that they have made on my behalf.

TABLE OF CONTENTS

Abstract	iii
Abstrak	v
Acknowledgements	vii
Table of Contents	viii
List of Figures	xii
List of Tables.....	xx
NOMENCLATURES	xxii
ABBREVIATIONS	xxiii
CHAPTER 1: INTRODUCTION	1
1.1 Overview.....	1
1.2 Research background.....	6
1.3 Problem statement	13
1.4 Research objectives	15
1.5 Research novelty and contribution	16
1.6 Scope of study.....	17
1.7 Organization of dissertation.....	18
CHAPTER 2: LITERATURE REVIEW	20
2.1 Introduction.....	20
2.2 Overview.....	20
2.3 Internal combustion engine.....	23
2.4 Diesel engine emissions regulation	24
2.5 Strategies to improve CI engine pollutant emissions	26
2.6 Biodiesel combustion in a CI engine	28

2.7	LTC strategies: the diesel engine salvation	30
2.7.1	Homogeneous charge preparation strategies	32
2.7.1.1	External mixture preparation.....	33
2.7.1.2	In-cylinder mixture preparation	36
2.8	LTC control strategies	42
2.8.1	Exhaust gas recirculation (EGR).....	42
2.8.2	Fuel modification	43
2.9	Diesel engine fuel delivery system.....	45
2.10	Diesel fuel injection system conversion	48
CHAPTER 3: RESEARCH METHODOLOGY		51
3.1	Introduction.....	51
3.2	Biodiesel selection	54
3.3	Test fuels.....	55
3.4	Engine operating conditions	61
3.5	Test engine.....	64
3.6	Common-rail fuel injection system conversion.....	65
3.6.1	Fuel rail and supply pump.....	67
3.6.2	Engine controller unit (ECU)	70
3.6.3	Fuel injector.....	80
3.7	Engine test bed setup	91
3.8	Combustion analyzer system setup.....	96
3.9	Exhaust gas recirculation (EGR) setup.....	100
3.10	Calculation methods	111
3.10.1	Engine performance	111
3.10.2	Combustion analysis.....	111
3.11	Statistical and equipment uncertainty analysis	112

CHAPTER 4: RESULTS AND DISCUSSION.....	114
4.1 Introduction.....	114
4.2 Engine-out responses of the converted common-rail fuel injection system.....	115
4.2.1 Effect of injection timing variation	115
4.2.2 Effect of injection pressure variation	119
4.2.3 Effect of injection strategies.....	126
4.2.4 Summary	130
4.3 Effect of biodiesel blends on common-rail diesel engine.....	131
4.3.1 Performance analysis.....	131
4.3.2 Emissions analysis.....	135
4.3.3 Combustion analysis.....	143
4.3.4 Vibration analysis.....	151
4.3.5 Summary	154
4.4 Effect of Injection timing.....	155
4.4.1 Performance analysis.....	155
4.4.2 Emissions analysis.....	158
4.4.3 Combustion analysis.....	162
4.4.4 Summary	167
4.5 Effect of EGR	168
4.5.1 Performance analysis.....	168
4.5.2 Emissions analysis.....	171
4.5.3 Combustion analysis.....	174
4.5.4 Strategy for simultaneous BSNO _x -smoke reduction	178
4.5.5 Summary	180
4.6 Effect of dual-fuel combustion	181
4.6.1 SOI timing sweep at constant EGR.....	181

4.6.1.1	Performance analysis.....	182
4.6.1.2	Emissions analysis.....	185
4.6.1.3	Combustion analysis	189
4.6.2	Dual-fuel with EGR sweep.....	195
4.6.3	Summary	197
CHAPTER 5: CONCLUSIONS AND RECOMMENDATION		199
5.1	Conclusions	199
5.2	Recommendation	202
REFERENCES.....		203
APPENDIX A		226
APPENDIX B		228

LIST OF FIGURES

Figure 1.1: Forecast of global population growth, GDP and energy demand (Colton, 2014).	3
Figure 1.2: ASEAN primary energy consumption (2011 - 2040).....	3
Figure 1.3: ASEAN energy demand by sector.....	4
Figure 1.4: Past and projected global CO ₂ emissions by source (Nejat et al., 2015).....	5
Figure 1.5: Energy related CO ₂ emission of ASEAN (International Energy Agency (IEA), 2013).	6
Figure 1.6: Plot of NO _x and soot formation regions on Φ -T plane with various combustion strategies (Folkson, 2014).	12
Figure 2.1: Worldwide exhaust emission testing procedures and standards (Delphi, 2015).	25
Figure 2.2: Comparison of SI, CI and HCCI engine (Clean combustion research centre, 2015).	31
Figure 2.3: Mixture preparation strategies.	33
Figure 2.4: Early implementations of external mixture formation.	34
Figure 2.5: Pulsed injection strategy for early in-cylinder injection (Baumgarten, 2006).	37
Figure 2.6: Early in-cylinder diesel direct injection strategies.	37
Figure 2.7: Nissan MK-concept: effects of EGR, retarded injection timing (IT) and increased swirl on exhaust emissions and thermal efficiency (Kimura et al., 2001).	39
Figure 2.8: Schematic of the MK combustion concept (Kimura et al., 2002).	40
Figure 2.9: Schematic diagrams of the (a) conventional diesel engine. (b) NADI TM for an early injection.....	41
Figure 2.10: Methods for controlling LTC phasing (Stanglmaier & Roberts, 1999).	42
Figure 2.11: Heat-release traces for iso-octane and PRF80 (Sjöberg & Dec, 2007).	44
Figure 2.12: Development of injection pressure of diesel engine (Mahr, 2004).	47
Figure 2.13: Comparison of injection pressures (Denso Corporation, 2007).	47

Figure 2.14: Key factors for diesel fuel injection system development (Mahr, 2004). ..	48
Figure 3.1: Schematic representation of the research methodology.	51
Figure 3.2: Transesterification of triglycerides with alcohol.	55
Figure 3.3: Single cylinder diesel engine.	64
Figure 3.4: Schematic diagram of the experimental setup.	66
Figure 3.5: Fuel delivery setup with pump driven by electric motor.	68
Figure 3.6: Schematic of the fuel system.	68
Figure 3.7: External and cross sectional views of the suction control valve (Denso Corporation, 2007).	70
Figure 3.8: Intake fuel quantity variation via duty cycle control (Denso Corporation, 2007).	70
Figure 3.9: Arduino Mega 2560 microcontroller as ECU.	73
Figure 3.10: Sensors arrangement.	74
Figure 3.11: Outline diagram of the ECU interface with sensors and actuator.	74
Figure 3.12: PID closed loop engine speed control scheme.	75
Figure 3.13: Timing diagram of the pickup coil and encoder signals aligned with the SOICU, PWCU, port and direct fuel injection output signals.	76
Figure 3.14: Programming flow chart for SOICU.	77
Figure 3.15: Programming flow chart for PWCU.	78
Figure 3.16: Fuel injection interface program tab.	79
Figure 3.17: Fuel injection pulse train.	79
Figure 3.18: Diesel solenoid injector (Delphi France SAS, 2007).	81
Figure 3.19: Denso port fuel injector.	81
Figure 3.20: Common-rail injector mounted on the engine cylinder head.	82
Figure 3.21: Images showing the Delphi injector (a) nozzle hole diameter, and (b) nozzle holes arrangement.	82

Figure 3.22: Schematic of the port fuel injection system.....	83
Figure 3.23: Port fuel injector injection quantity versus pulse-width at constant pressure of 400 kPa (Calibration fluid: Gasoline).....	86
Figure 3.24: Direct injector injection quantity versus pulse-width under different rail pressure (Calibration fluid: Diesel).....	86
Figure 3.25: Common-rail fuel injector driver control logic pulse signal and current across solenoid coil with PWM.	90
Figure 3.26: Flyback diode across the coil of common-rail injector.	90
Figure 3.27: Common-rail fuel injector current profile management interface program tab.....	91
Figure 3.28: SuperFlow™ 4” turbine type airflow meter. Note that the fan blades are clearly visible in the photo on the right.....	93
Figure 3.29: Type-K thermocouple mounted in the exhaust stream.....	94
Figure 3.30: Operation principle of Kobold positive displacement gear wheel flow meter.	94
Figure 3.31: LabVIEW software user interface screen shot.	95
Figure 3.32: High-speed data acquisition system setup and integration with combustion analyzer system.	99
Figure 3.33: Exhaust gas recirculation.....	100
Figure 3.34: EGR system setup.....	101
Figure 3.35: Schematic of the EGR system.	102
Figure 3.36: Exhaust and intake air sampling trains with sensors connected to the Arduino Mega 2560 microcontroller.....	104
Figure 3.37: Schematic diagram of the mixing point of intake fresh air and exhaust gas.	106
Figure 3.38: Visualization of the intake charge content with and without use of EGR.	106
Figure 3.39: Horiba MEXA-700λ air-to-fuel ratio analyzer and the UEGO sensor.....	107
Figure 3.40: MEXA-700λ O ₂ reading interface program tab.	107

Figure 3.41: EGR valve position sensor chart.	109
Figure 3.42: Outline diagram of the microcontroller interface with EGR valve.	109
Figure 3.43: EGR interface program tab.....	109
Figure 3.44: EGR valve characteristic curve.	111
Figure 4.1: Effect of SOI timing on engine torque under various engine speed and load conditions under a constant injection pressure of 600 bar, without EGR and diesel fuel with compression ignition (maximum torque as indicated with circle).	116
Figure 4.2: Combustion pressure and HRR curves at various SOI timings under 1500 rpm, 50% load and under a constant injection pressure of 600 bar and without EGR.....	117
Figure 4.3: Effect of SOI timing on the first and second HRR peaks and ignition delay at 1500 rpm, 50% load and under a constant injection pressure of 600 bar and without EGR.	118
Figure 4.4: NO _x and smoke emission with various SOI timing at 1500 rpm, 50% load and under a constant injection pressure of 600 bar and without EGR.....	119
Figure 4.5: Closed-loop response of the rail pressure with 100 bar (for 300-1000 bar) and 200 bar (for 1000-1800 bar) step change at various engine speed of (a) 1000 rpm, (b) 1500 rpm, and (c) 2000 rpm, 50% load. All tests were conducted without EGR.....	120
Figure 4.6: Engine BTE for varying rail pressure and engine speed (SOI _{1000 rpm} = 4° BTDC, SOI _{1500 rpm} = 12° BTDC, and SOI _{2000 rpm} = 16° BTDC). All tests were conducted without EGR and at 50% load.....	121
Figure 4.7: NO _x emission for varying rail pressure and engine speed (SOI _{1000 rpm} = 4° BTDC, SOI _{1500 rpm} = 12° BTDC, and SOI _{2000 rpm} = 16° BTDC). All tests were conducted without EGR and at 50% load.....	123
Figure 4.8: Smoke emission for varying rail pressure and engine speed (SOI _{1000 rpm} = 4° BTDC, SOI _{1500 rpm} = 12° BTDC, and SOI _{2000 rpm} = 16° BTDC). All tests were conducted without EGR and at 50% load.....	124
Figure 4.9: Effect of injection pressure on HRR peak, ignition delay and combustion duration at 1500 rpm, 50% load setting (SOI _{1500 rpm} = 12° BTDC). All tests were conducted without EGR.	124
Figure 4.10: Combustion pressure and HRR curves at various fuel injection pressure under (a) 1000 rpm, (b) 1500 rpm, and (c) 2000 rpm, 50% load (SOI _{1000 rpm} = 4° BTDC, SOI _{1500 rpm} = 12° BTDC, and SOI _{2000 rpm} = 16° BTDC). All tests were conducted without EGR.....	125

Figure 4.11: Effect of fuel injection strategies on (a) BTE, (b) smoke, (c) NO _x emissions, and (d) peak pressure rise rate at various fuel injection pressures, under 1500 rpm, 50% load, SOI _{Pilot} = 30° BTDC, SOI _{Main} = 12° BTDC, and SOI _{Post} = -5° BTDC. All tests were conducted without EGR.	128
Figure 4.12: Combustion pressure and HRR curves at various fuel injection strategies under (a) 400 bar, (b) 800 bar, and (c) 1200 bar, at engine speed of 1500 rpm, 50% load, SOI _{Pilot} = 30° BTDC, SOI _{Main} = 12° BTDC, and SOI _{Post} = -5° BTDC. All tests were conducted without EGR.	129
Figure 4.13: BSFC with Jatropha biodiesel blends compared with diesel fuel at various BMEP. All tests were conducted without EGR.	132
Figure 4.14: BSFC with palm biodiesel blends compared with diesel fuel at various BMEP. All tests were conducted without EGR.	132
Figure 4.15: Brake thermal efficiency (BTE) with Jatropha biodiesel blends compared with diesel fuel at various BMEP. All tests were conducted without EGR.	134
Figure 4.16: Brake thermal efficiency (BTE) with palm biodiesel blends compared with diesel fuel at various BMEP. All tests were conducted without EGR.	134
Figure 4.17: BSCO with Jatropha biodiesel blends compared with diesel fuel at various BMEP. All tests were conducted without EGR.	136
Figure 4.18: BSCO with palm biodiesel blends compared with diesel fuel at various BMEP. All tests were conducted without EGR.	137
Figure 4.19: Relative air-fuel ratio with Jatropha biodiesel blends compared with diesel fuel at various BMEP. All tests were conducted without EGR.	137
Figure 4.20: Relative air-fuel ratio with palm biodiesel blends compared with diesel fuel at various BMEP. All tests were conducted without EGR.	138
Figure 4.21: Variations in BSNO _x emissions with different engine loads and fuel types for Jatropha biodiesel fuels. All tests were conducted without EGR.	139
Figure 4.22: Variations in BSNO _x emissions with different engine loads and fuel types for palm biodiesel fuels. All tests were conducted without EGR.	140
Figure 4.23: EGT with Jatropha biodiesel blends compared with diesel fuel at various BMEP. All tests were conducted without EGR.	141
Figure 4.24: EGT with palm biodiesel blends compared with diesel fuel at various BMEP. All tests were conducted without EGR.	141

Figure 4.25: Smoke level with Jatropha biodiesel blends compared with diesel fuel at various BMEP. All tests were conducted without EGR.	142
Figure 4.26: Smoke level with palm biodiesel blends compared with diesel fuel at various BMEP. All tests were conducted without EGR.	143
Figure 4.27: In-cylinder pressure and HRR versus crank angle for Jatropha biodiesel blends at a BMEP of (a) 0.1 MPa and (b) 0.6 MPa. All tests were conducted without EGR.	146
Figure 4.28: In-cylinder pressure and HRR versus crank angle for palm biodiesel blends at a BMEP of (a) 0.1 MPa and (b) 0.6 MPa. All tests were conducted without EGR. .	147
Figure 4.29: Variations in mass fraction burned for diesel and Jatropha biodiesel blends at a BMEP of 0.1 MPa and without EGR.	150
Figure 4.30: Variations in mass fraction burned for diesel and palm biodiesel blends at a BMEP of 0.1 MPa and without EGR.	150
Figure 4.31: Variations in RMS of acceleration for diesel and Jatropha biodiesel blends at different engine loads and without EGR.	152
Figure 4.32: Variations in RMS of acceleration for diesel and palm biodiesel blends at different engine loads and without EGR.	152
Figure 4.33: Variations in peak pressure rise rate for diesel and Jatropha biodiesel blends at different engine loads and without EGR.	153
Figure 4.34: Variations in peak pressure rise rate for diesel and palm biodiesel blends at different engine loads and without EGR.	153
Figure 4.35: BSFC with PME compared with diesel fuel at various SOI timings and without EGR.	156
Figure 4.36: Brake thermal efficiency at different SOI timing conditions and without EGR.	157
Figure 4.37: BSNO _x emissions at different SOI timing conditions and without EGR. .	159
Figure 4.38: In-cylinder mean gas temperature curves for (a) baseline diesel, (b) PME at various SOI timings and without EGR.	159
Figure 4.39: Smoke emissions at different SOI timing conditions and without EGR. .	160
Figure 4.40: Exhaust gas temperature variation at different SOI timing conditions and without EGR.	162

Figure 4.41: Combustion pressure, heat release rate and injector current profiles for diesel and PME fuel at SOI of 11°BTDC and without EGR.....	164
Figure 4.42: Total burning angle as a function of SOI timing for diesel and PME fuel and without EGR.	164
Figure 4.43: Combustion pressure curves for (a) baseline diesel and (b) PME at various SOI timings and without EGR.	166
Figure 4.44: BSFC with PME compared with diesel fuel at various EGR rates.	169
Figure 4.45: Exhaust gas O ₂ concentration with PME compared with diesel fuel at various EGR rates.	169
Figure 4.46: BTE with PME compared with diesel fuel at various EGR rates.....	170
Figure 4.47: BSNO _x and smoke emission with various EGR rates.	173
Figure 4.48: Intake and exhaust air CO ₂ concentration with PME compared with diesel fuel at various EGR rates.	173
Figure 4.49: In-cylinder pressure, HRR and injector current signal versus crank angle for engine operated with PME (top) and baseline diesel (bottom) at various EGR rates...	176
Figure 4.50: Ignition delay at various EGR rates for engine operation with baseline diesel and PME fuels.	177
Figure 4.51: Maximum combustion pressure at various EGR rates for engine operation with baseline diesel and PME fuels.	178
Figure 4.52: BSNO _x –smoke opacity plot for the tested fuels.	180
Figure 4.53: BSFC at various SOI timing for dual fuel operation diesel/gasoline and PME/gasoline fuels, with 30%EGR.....	183
Figure 4.54: BTE at various SOI timing for dual fuel operation of diesel/gasoline and PME/gasoline fuels, with 30%EGR.....	185
Figure 4.55: BSNO _x emissions at various SOI timing for dual fuel operation of diesel/gasoline and PME/gasoline fuels, with 30%EGR.	186
Figure 4.56: CA50 at various SOI timing for dual fuel operation of diesel/gasoline and PME/gasoline fuels, with 30%EGR.....	187
Figure 4.57: BSHC emissions versus SOI timing sweeps with 30% EGR for dual fuel operation of diesel/gasoline and PME/gasoline fuels.	188

Figure 4.58: BSCO emissions versus SOI timing sweeps with 30%EGR for dual fuel operation of diesel/gasoline and PME/gasoline fuels.	188
Figure 4.59: Effect of SOI timing on combustion pressure and heat release rate for dual fuel operation of diesel/gasoline and PME/gasoline with 30% EGR.	192
Figure 4.60: Effect of SOI timing variation on the coefficient of variation of indicated mean effective pressure for dual fuel operation of diesel/gasoline and PME/gasoline with 30% EGR.	192
Figure 4.61: Comparison of 100 cycles of cylinder pressure under various SOI timings for diesel/gasoline dual fuel operation with 30% EGR.....	193
Figure 4.62: Comparison of 100 cycles of cylinder pressure under various SOI timings for PME/gasoline dual fuel operation with 30% EGR.....	194
Figure 4.63: Influence of EGR variation on performance, emissions and combustion characteristics for engine operation with dual fuel combustion of diesel/gasoline and PME/gasoline.	196

LIST OF TABLES

Table 1.1: Development of United States, European Union and Japan emission average limit values for PM and NO _x from heavy-duty vehicles (TransportPolicy.net, 2014). ..	10
Table 2.1: EU emission standards for heavy-duty diesel engines: steady-state testing (DieselNet, 2012).	26
Table 2.2: Comparison of SI, CI and HCCI combustion engines.	32
Table 2.3: Overview of LTC acronyms from literature.	33
Table 2.4: Overview of external mixture preparation strategy implemented in gasoline-fuelled LTC engines.	35
Table 2.5: Comparison of the common-rail fuel injection system with the conventional mechanical pump-line-nozzle system.	50
Table 3.1: Engine test details.	52
Table 3.2: Fuel properties of petroleum diesel, gasoline, PME, JME and biodiesel blends.	58
Table 3.3: GC/FID operating conditions.	59
Table 3.4: Fatty acid composition of neat PME and JME fuel.	60
Table 3.5: Characteristics of single-cylinder engine.	64
Table 3.6: Specifications of the retrofitted test engine.	65
Table 3.7: Supply pump specifications.	69
Table 3.8: High-pressure common-rail specifications.	69
Table 3.9: Technical specifications of the Arduino Mega 2560 microcontroller.	73
Table 3.10: Injection current profile key parameters for common-rail injector.	91
Table 3.11: SuperFlow TM airflow meter calibration data.	93
Table 3.12: Measuring components, ranges and resolution of the AVL DICOM 4000 gas analyzer and DiSmoke 4000 smoke analyzer.	96
Table 3.13: Technical specifications of K-33 ICB 30% CO ₂ sensor.	102
Table 3.14: List of measurement accuracy and percentage uncertainties.	113

Table 4.1: Crank angle position corresponding to certain percent mass fraction burned for all Jatropha biodiesel blends under various BMEPs.....	148
Table 4.2: Crank angle position corresponding to certain percent mass fraction burned for palm biodiesel blends under various BMEPs.....	149
Table 4.3: Experimental conditions.	182

University of Malaya

NOMENCLATURES

μs	Microsecond	s
BMEP	Brake Mean Effective Pressure	MPa
BSCO	Brake Specific Carbon Monoxide	g/kWhr
BSFC	Brake Specific Fuel Consumption	g/kWhr
BSHC	Brake Specific Hydrocarbon	g/kWhr
BSNO _x	Brake Specific Nitrogen Oxide	g/kWhr
BTE	Brake Thermal Efficiency	%
CA	Crank Angle	-
CA10	Mass Fraction Burned of 10%	°CA
CA50	Mass Fraction Burned of 50%	°CA
CA90	Mass Fraction Burned of 90%	°CA
EGR	Exhaust Gas Recirculation	%
EGT	Exhaust Gas Temperature	°C
HRR	Heat Release Rate	J/°CA
Hz	Hertz	s ⁻¹
ID	Ignition Delay	°CA
IMEP	Indicated Mean Effective Pressure	MPa
ISFC	Indicated Specific Fuel Consumption	g/kWhr
IT	Injection Timing	°CA
MPRR	Maximum Pressure Rise Rate	bar/°CA
Mtoe	Million Tons of Oil Equivalent	tonne
PW	Pulse Width	μs
λ	Relative Air-Fuel Ratio	-
Φ	Equivalence Ratio	-

ABBREVIATIONS

AOAC	Association of Analytical Communities
AOME	Algal Oil Methyl Ester
ARC	Active Radical Combustion
ASTM	American Society for Testing and Materials
ATAC	Active Thermo-Atmosphere Combustion
ATDC	After Top Dead Center
BAU	Business As Usual
BP	British Petroleum
BTDC	Before Top Dead Center
CAD	Computer Aided Design
CAI	Controlled Auto-Ignition
CCD	Charge Coupled Device
CFD	Computational Fluid Dynamics
CI	Compression Ignition
CN	Cetane Number
CO ₂	Carbon Dioxide
COV	Coefficient of Variance
CR	Compression Ratio
D	Baseline Diesel
DAQ	Data Acquisition
DI	Direct Injection
DOC	Diesel Oxidation Catalyst
DPF	Diesel Particulate Filter
ECU	Engine Controller Unit
EEV	Enhanced Environmentally friendly Vehicles
EGR	Exhaust Gas Recirculation
EGT	Exhaust Gas Temperature
EIA	Energy Information Administration
ELR	European Load Response
EN	European Standards
ESC	European Stationary Cycle
EU	European Union
FAME	Fatty Acid Methyl Ester
FID	Flame Ionization Detector
GC	Gas Chromatography
GDP	Gross Domestic Product
GHG	Greenhouse Gas
Gt	Giga tones
GUI	Graphical User Interface
HC	Hydrocarbon
HCCI	Homogenous Charge Compression Ignition
HCDC	Homogenous Charge Diesel Combustion
HCLI	Homogenous Charge Late Injection

HEUI	Hydraulic Electric Unit Injection
HiMICS	Homogeneous charge intelligent multiple injection combustion system
HiMICS	Multiple Injection Combustion System
HRR	Heat Release Rate
HTHR	High Temperature Heat Release
I/O	Input and Output
ICP	Integrated Circuit Piezoelectric
ID	Ignition Delay
IEA	International Energy Agency
ISR	Interrupt Service Routine
IT	Injection Timing
JB10	10% Jatropha biodiesel + 90% petroleum diesel by volume
JB100	100% Jatropha biodiesel by volume
JB30	30% Jatropha biodiesel + 70% petroleum diesel by volume
JB50	50% Jatropha biodiesel + 50% petroleum diesel by volume
JME	Jatropha Methyl Ester
KOH	Potassium Hydroxide
LPG	Liquefied Petroleum Gas
LTC	Low Temperature Combustion
LTHR	Low Temperature Heat Release
LTR	Low Temperature Reactions
MK	Modulated Kinetics
MON	Motor Octane Number
MULDIC	Multiple Stage Diesel Combustion
NADI™	Narrow Angle Direct Injection
NO	Nitric Oxide
NO _x	Nitrogen Oxide
nPAH	Nitric Polycyclic Aromatic Hydrocarbons
NVO	Negative Valve Overlap
O ₂	Oxygen
OBD	On-Board Diagnostic
OI	Octane Index
Pa	Pascal
PAH	Polycyclic Aromatic Hydrocarbon
PB10	10% Palm biodiesel + 90% petroleum diesel by volume
PB100	100% Palm biodiesel by volume
PB30	30% Palm biodiesel + 70% petroleum diesel by volume
PB50	50% Palm biodiesel + 50% petroleum diesel by volume
PCCI	Premixed Charge Compression Ignition
PCI	Premixed Compression Ignited Combustion
PFI	Port Fuel Injection
PI	Port Injection
PID	Proportional-Integral-Derivative
PLC	Programmable Logic Controllers

PM	Particulate Matter
PME	Palm Methyl Ester
PPCI	Partially Premixed Charge Compression Ignition
PREDIC	Premixed Diesel Combustion
PRF	Primary Reference Fuels (Iso-Octane/ n-Heptane Mixture)
PW	Pulse Width
PWCU	Pulse-Width-Modulation Control Unit
PWM	Pulse-Width-Modulation
RCCI	Reactivity Controlled Compression Ignition
R _g	Gasoline Ratio
RMS	Root Mean Square
RON	Research Octane Number
rpm	Revolution per Minute
SCCI	Stratified Charge Compression Ignition
SCR	Selective Catalytic Reduction
SI	Spark Ignition
SO ₂	Sulfur Dioxide
SOC	Start of Combustion
SOI	Start of Injection
SOICU	Start of Injection Control Unit
SVO	Straight Vegetable Oil
SwRI	Southwest Research Institute
TDC	Top Dead Center
TS	Toyota-Soken Combustion
TTL	Transistor-Transistor Logic
UEGO	Universal Exhaust Gas Oxygen
uHC	Unburned Hydrocarbon
UNIBUS	Uniform Bulky Combustion System
VCR	Variation of Compression Ratio
VOC	Volatile Organic Compounds
VVT	Variable Valve Timing
WHSC	World Harmonized Stationary Cycle
WOT	Wide Open Throttle

CHAPTER 1: INTRODUCTION

1.1 Overview

Energy plays a vital role in our daily life. In recent years, rapid growth in population, development, and industrialization have led to a high demand for energy worldwide. As shown in Figure 1.1, by 2040 the estimated world population will reach 9 billion, from approximately 7 billion in 2010. This additional 2 billion people will need energy. Over the same period, the projected 30% growth in global population will also translate into a rise in gross domestic product (GDP) of around 140% in 2040, compared with that of 2010. According to this trend, the forecasted global energy demand will increase by around 35% in 2040 compared to the demand in 2010, with an average growth rate of 1.1% (Colton, 2014). From the ASEAN side, the total primary energy consumption of ASEAN, in 2011, was equivalent to Japan, which is around 444 Mtoe (Japan TIOEE, 2013). It is forecasted that, in 2040, ASEAN energy consumption will increase to 1186 Mtoe, rising at an annual rate of 3.1%. Furthermore, Indonesia will exceed Japan's energy consumption in 2035 and it is predicted that they will become fifth largest energy consumer of the world. However, as Malaysia and Thailand population growth will decelerate from 2025, their primary energy consumption rate will be slower than other ASEAN countries. The statistical representation of past and projected ASEAN primary energy consumption for the period 2011 – 2040 is shown in Figure 1.2 (Mofijur et al., 2015).

Generally, global energy demand is predominantly from the following sources: crude oil, natural gas and coal. Among this, the automotive internal combustion engine is a major user of oil and gas. The global economy depends heavily on crude oil, particularly in the transportation sector. This scenario is due to the fact that crude oil has a characteristic of

high energy density and better handling facility. In fact, fossil diesel is widely used in heavy-duty vehicles due to their extensive availability, the provision of subsidies by governments and the reliability of diesel engines. According to the International Energy Agency (IEA), the global energy demand will rise by 37% from 2014 to 2040 (International Energy Agency (IEA), 2014), and it is forecasted that fossil fuels will contribute 80% of this demand (McEwen, 2015). Besides, it is predicted that the world energy consumption in the transportation sector will increase by an average of 1.1% per year (U.S. Energy Information Administration (EIA), 2013), whereas energy demand for transportation sector in ASEAN will be rising at a rate of 2.7% annually (International Energy Agency (IEA), 2013). The rapid increase in transportation sector can be seen in Indonesia, Malaysia, Thailand and the Philippines. Energy demand by industrial sector was the highest in 2011 and in 2035, rising from 120 Mtoe to 225 Mtoe, as indicated in Figure 1.3.

It must be emphasized that it is certain that eventually the fossil fuels will be exhausted. These resources are finite and are predicted to be exhausted in less than another 100 years. However, few models forecasted that it will be depleted in less than 45 years (British Petroleum (BP), 2010; Sharma & Singh, 2009). In addition, current reserves of liquid fuel have the capacity to meet only half of the usual energy demand until 2023 (Owen et al., 2010). This massive drift of fossil fuel consumption has severely affected environmental quality, including global warming, eutrophication, deforestation, photochemical smog, ozone depletion and acidification (Bare et al., 2012).

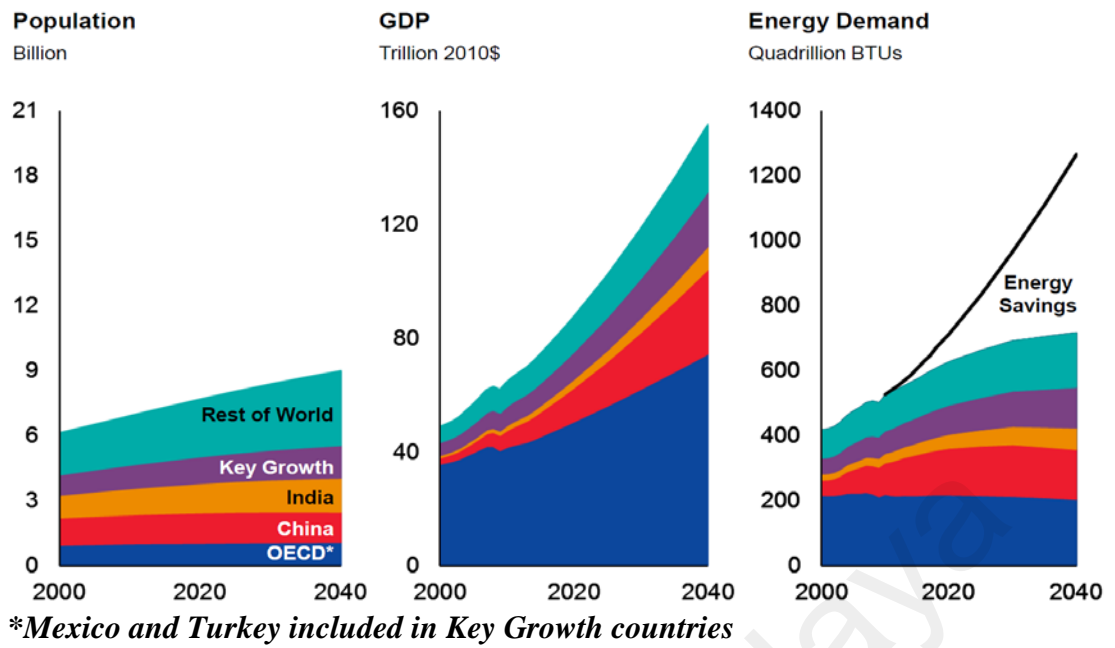


Figure 1.1: Forecast of global population growth, GDP and energy demand (Colton, 2014).

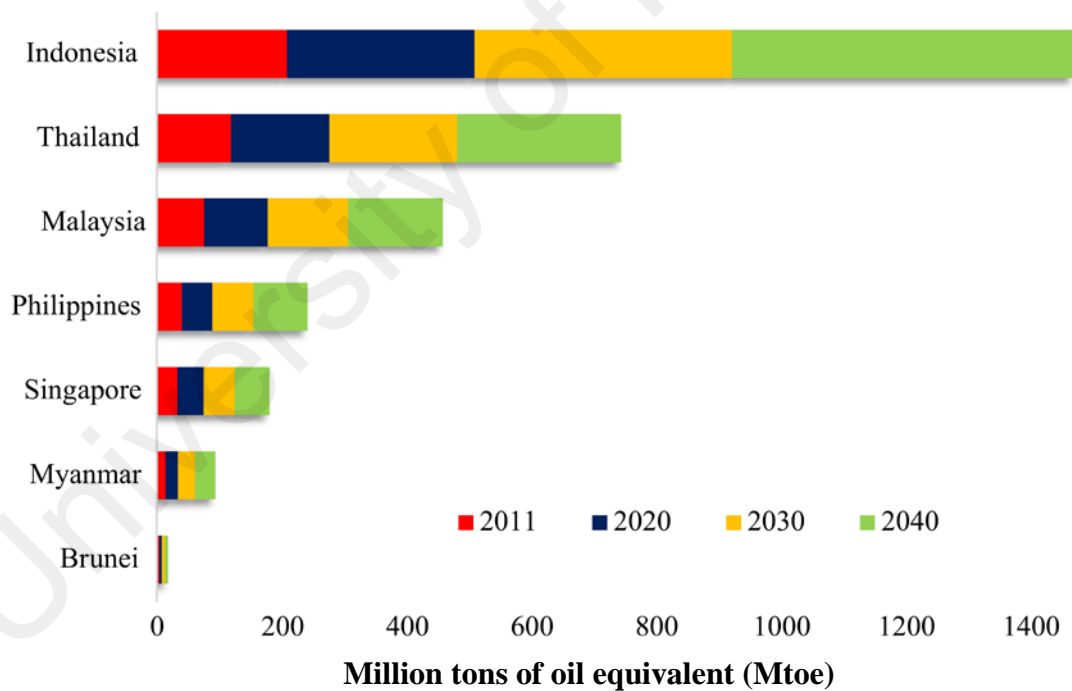


Figure 1.2: ASEAN primary energy consumption (2011 - 2040).

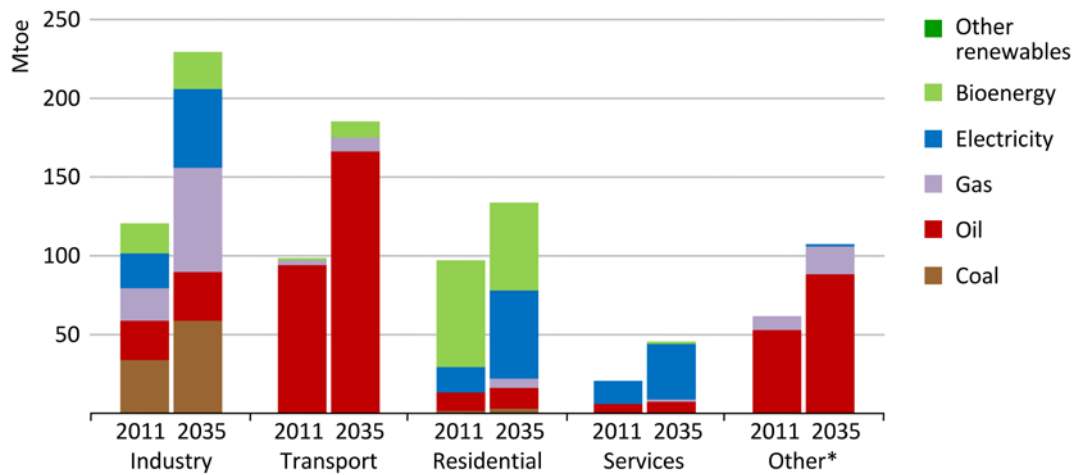


Figure 1.3: ASEAN energy demand by sector.

Carbon dioxide (CO₂), nitrogen oxide (NO), unburned hydrocarbon (HC) and volatile organic compounds (VOC) are the primary air pollutants emitted through the combustion of fossil fuels. In particular, CO₂ gas is the primary greenhouse gas (GHG) contributor and the production trend through human activities has increased dramatically every year. Figure 1.4 shows the global CO₂ emissions by source (Nejat et al., 2015). As can be seen, transport emissions are projected to quadruple between 2015 and 2030, reflecting a strong increase in demand for cars and growth in aviation. Besides, the energy related CO₂ emission of ASEAN would increase to 2.3 Gt (Giga tones) in 2035 from 1.2 Gt in 2011, which is 6.1% of global emission, as shown in Figure 1.5 (International Energy Agency (IEA), 2013). If the effects of CO₂ on the climate are disregarded, the rise in global temperatures of 2 °C could cause the extinction of up to a million species and loss of hundreds of millions of human lives (Ahmad et al., 2011). In this regard, with participation of over 120 heads of government, the 2009 Copenhagen Climate Change Summit was the largest meeting of world leaders in history to track national commitments to curb global warming. At the Summit, world leaders from key countries underscored how clean and renewable energies sustainably produced from biological sources can help decrease GHG emissions, enhance food security, spur economic growth and reduce poverty in the world (NRDC, 2015). Climate action is also taken seriously in most of the

European Union (EU) countries. The EU has independently introduced two key directives to resolve the environmental effects associated with transport (Gilpin et al., 2014). As a mitigation measure for reducing GHG emissions, the first directive is to promote the utilization of biofuels and other renewable fuels for transport (Directive 2009/28/EC, 2009). The second regulates specific pollutants from compression-ignition engines used in vehicles (Directive 2005/55/EC, 2005) as a medium-term mitigation measure for air pollutants. Consequently, it is clear that the world is confronted with the twin crises of fossil fuel depletion and environmental degradation that are hotly debated issues nowadays. Mitigating both of these issues requires changes in the fuel mix with cleaner renewable alternative fuels and savings on the utilization of fossil fuels (Bollen & Brink, 2014). It is believed that substitution of even a small fraction of total consumption by alternative fuels will contribute a significant positive impact on the economy and the environment of any country (Anand et al., 2011).

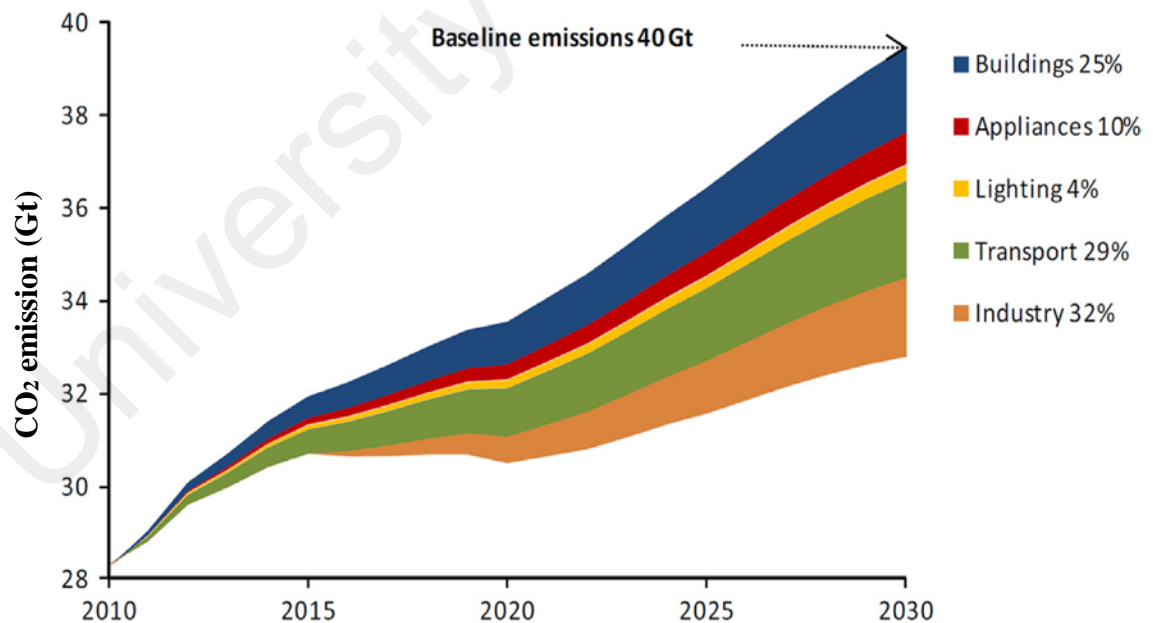


Figure 1.4: Past and projected global CO₂ emissions by source (Nejat et al., 2015).

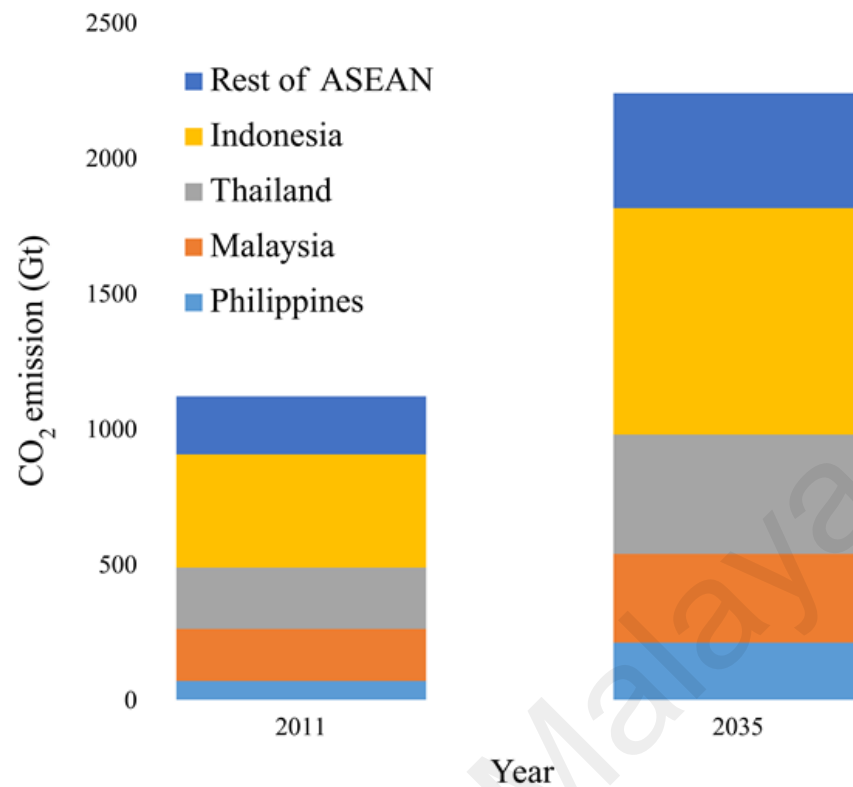


Figure 1.5: Energy related CO₂ emission of ASEAN (International Energy Agency (IEA), 2013).

1.2 Research background

In the present scenario of worldwide energy crisis coupled with its detrimental impact on the environment, the world is being compelled to focus on developing clean alternative fuel that is economically competitive, technically feasible, easily available, and environmentally acceptable (Liaquat et al., 2010; Mofijur et al., 2013; Tesfa et al., 2012). Biofuels from bio-based products are alternatives to fossil fuels used in the transport sector. They are renewable, can improve the energy security of a country by reducing dependency on volatile foreign markets, and producing them can ease unemployment. As an alternative to diesel fuel, biodiesel is one of the most promising and ideal choices due to its environmentally adaptable behaviour and similar physicochemical properties to that of fossil diesel fuel. Furthermore, its content is minimally toxic, highly biodegradable, has a higher cetane number, and an absence of aromatic compounds and sulfur, thus making it a more desirable alternative to diesel (Anand et al., 2011). Biodiesel can be derived from straight vegetable oils, edible and non-edible plants, recycled waste cooking

oils, and animal fat (Agarwal, 2007; Mofijur et al., 2012). Biodiesel in its neat or blended form can be used in diesel engines without modification of the engine or fueling process, thus greatly simplifying the system's integration and adoption. The idea of operating plant oils as fuels for diesel engines is not novel. This concept had been demonstrated as far back as 1900 by Rudolf Diesel using groundnut oil as a fuel running in his newly developed compression ignition (CI) engine (Murugesan et al., 2009). Soon afterwards, however, the utilization of clean vegetable oils became unattractive due to the rapidly developing petroleum industry and the cheap supply of fossil fuel at that time. Today, following more than a century-long detour in the petroleum age, vegetable oils are again being used as fuel in the transport sector. With rising environmental awareness, advancing technologies, great support from farmers, and soaring oil prices, biofuels have become a popular alternative energy source for internal combustion engines and could be an important fuel like petroleum (Babu & Devaradjane, 2003).

Biodiesel, typically known as fatty acid methyl ester (FAME), can be produced from vegetable oils or animal fats by using the transesterification process and have been widely evaluated in diesel CI engines over many years. If straight vegetable oil (SVO) is used as a fuel without being converted to biodiesel, it may lead to the build-up of carbon deposits inside the combustion chamber, injector coking, oil ring sticking and gelling of the engine lubricant oil in the diesel engine (Atabani et al., 2013). This is mainly due to the relatively higher viscosity and lower volatility of SVO than standard diesel fuel, thus negatively impacting the engine operation life span. In the biodiesel industry, one of the most popular ways to reduce SVO viscosity is through the use of the transesterification process (Demirbas, 2008). In this process, a larger quantity of alcohol is added into vegetable oil to shift the chemical reaction toward the production of methyl esters in the presence of a catalyst. Globally, there are more than 350 oil-bearing crops identified as prospective feedstocks for the production of biodiesel (Mofijur et al., 2014). Depending upon

environmental and climatic conditions, the biodiesel feedstock varies from country to country, for example rapeseed and sunflower in Europe, soybean in North America, palm in Southeast Asia, and Coconut in tropic and sub-tropical regions. (Murugesan et al., 2009). On the other hand, other non-edible oils such as *Jatropha curcas*, *Moringa oleifera*, *Calophyllum inophyllum*, *Pongamia pinnata*, *Sterculia foetida*, *Croton megalocarpus*, and *Madhuca indica (Mahua)* etc. are also increasingly popular all over the world (Atabani et al., 2013). Different feedstocks of biodiesel will have different fatty acid composition content. These variations can affect fuel properties such as cetane number, viscosity, density, heating value and low temperature properties. (Puhan et al., 2010). All these physicochemical properties of biodiesel fuel have a strong relation with engine performance, exhaust emissions and combustion characteristics. In general, the use of biodiesel and its blends result in a slight loss in power, torque reduction and higher BSFC. Besides that, most of the emissions reduced with biodiesel and its blends, but with a slight increase in the NO_x (An et al., 2012; Keskin et al., 2008; Kim & Choi, 2010; Mohammadi et al., 2012; Song & Zhang, 2008; Tesfa et al., 2012). However, some studies also found relatively lower NO_x emissions from using biodiesel and its blends (Armas et al., 2010; Baiju et al., 2009; Cheung et al., 2009; Sharma et al., 2009).

Internal combustion engines were introduced over a century ago, and since then they have played a significant role in transportation. They have shaped the world in which we live and their future development will be driven by emissions legislation and other social and economic factors. Essentially, there are two predominant types of internal combustion engines: the Spark Ignition (SI) and Compression Ignition (CI) engine. However, both have disadvantages such as low thermal efficiency in the SI engine and high production of NO_x and particulate matter in the CI engine (Maurya & Agarwal, 2014). Due to the adverse effects of these emissions on human health and the environment, they are now subjected to legislative limits (Agarwal, Gupta, et al., 2011). Approximately one-third

share of total vehicles sold in the USA and Europe are diesel-powered (Jayed et al., 2011). However, the emission standards for these vehicles have been progressively tightened over time (ref. Table 1.1) and this limits its use (TransportPolicy.net, 2014). Generally, there are three strategies that can be implemented to diesel engines to attain lower emission limits, namely alternative fuels (Masum et al., 2013; Sajjad et al., 2014), new combustion mechanism (Valentino et al., 2012) and exhaust emissions after-treatment (Lilik & Boehman, 2011). However, there is a trade-off relationship between emissions reduction and performance improvement. As an example, EGR is an effective way to reduce NO_x emissions, but over use could result in higher soot levels and fuel economy penalties (Asad et al., 2015). In addition, after-treatment systems such as DPF (Diesel Particulate Filters) (Bensaid & Russo, 2011), DOC (Diesel Oxidation Catalyst) (Glewen et al., 2011), and SCR (Selective Catalytic Reduction) (Vallinayagam et al., 2013) have been proven their effectiveness in controlling Particulate Matter (PM) and NO_x emissions, but this increases the cost and complexity of the engine (Parks Ii et al., 2010). Therefore, there is a need to develop alternative combustion strategies that are able to minimize the after-treatment system requirement and thus reduce related costs. It is generally believed that the future engine will be featured with alternative compound combustion involving an integration of both the gasoline engine and diesel engine, taking into consideration both low emissions and high efficiency (Reitz & Duraisamy, 2015).

Table 1.1: Development of United States, European Union and Japan emission average limit values for PM and NO_x from heavy-duty vehicles (TransportPolicy.net, 2014).

Region	Regulation and year	Average Standard Values (g/kWh)	
		NO _x	PM
United States	2002-2004	2.7	0.13
	2007	1.6	0.013
	2010	0.27	0.013
European Union	Euro III (2000)	5	0.1
	Euro IV (2005)	3.5	0.02
	Euro V (2008)	2	0.02
	Euro VI (2013)	0.2-1.0	0.01-0.02
Japan	2003-2004	3.38	0.18
	2005	2	0.27
	2009-2010	0.7	0.01

Recently, another type of promising combustion strategy has evolved called low temperature combustion (LTC), in addition to SI and CI. LTC is an in-cylinder approach of advanced combustion strategies for the simultaneous reduction of PM and NO_x emissions (Dec, 2009; Northrop et al., 2011). It can be adopted in any size of transportation engine, ranging from small (Lemberger & Floweday, 2009; Wu et al., 2010), light-duty (Okude et al., 2004; Shimazaki et al., 2003) and heavy-duty engines (Musculus et al., 2008; Singh et al., 2007; Srinivasan et al., 2007) to large ship engines (Agarwal, 2011). Various LTC concepts including homogenous charge compression ignition (HCCI) (Bendu & Murugan, 2014; Gan et al., 2011; Han et al., 2015; Juttu et al., 2007; Su et al., 2003; Urushihara et al., 2003), uniform bulky combustion system (UNIBUS) (Hasegawa & Yanagihara, 2003), modulated kinetics (MK) (Kimura et al., 1999), premixed charge compression ignition (PCCI) (Aoyama et al., 1996; Jia et al., 2015; Torregrosa et al., 2013), homogeneous charge diesel combustion (HCDC) (Himabindu & Mahalakshmi, 2007; Himabindu et al., 2008; Odaka et al., 1999), homogeneous charge late injection (HCLI) (Cook et al., 2008), and reactivity controlled compression ignition (RCCI) (Benajes et al., 2015; Li et al., 2015) are being intensively investigated as potential future alternatives for more efficient internal combustion

engines. Although various acronyms have been assigned to this new combustion process, they still refer to the common fundamental characteristics of a premixed fuel-air mixture and auto-ignited combustion, with the goal of lowering combustion temperatures to advantageously alter the chemistry of NO_x and/or soot formation. Figure 1.6 indicates the plot of local equivalence ratio (Φ) versus flame temperature (T) with various combustion strategies. It can be observed that NO_x forms in the region of low equivalence ratio and at high temperature (i.e. > 2200 K), whilst soot formation, takes place in the rich mixture zone above 1800 K. Conventional diesel combustion is unavoidable from the formation zones of NO_x and soot, but LTC techniques like PCCI, HCCI and RCCI avoid these zones and reduce NO_x and soot simultaneously.

HCCI combustion is one of the earliest and simplest diesel combustion methods for achieving low NO_x and soot emissions in a CI engine. However, this combustion process reveals some technical challenges that need to be addressed prior to the widespread implementation of this strategy. HCCI combustion is driven mainly by chemical kinetics of in-cylinder fuel-air mixtures. Thus, the lack of direct ignition control on the auto-ignition timing, very rapid heat release, and high pressure rise rate restricts the operational load range of the HCCI engine (Cerit & Soyhan, 2013). Therefore, coupling between the fuel injection event and the combustion event is desirable in order to have flexible control over the combustion process on a cycle-to-cycle basis (Dempsey et al., 2013). This has prompted the study of PCCI combustion, which combines the characteristics of conventional diesel combustion and HCCI. In the PCCI combustion strategy, two injections in one complete engine cycle is typically used to operate the engine. A fraction of fuel is injected at a very early stage to create a lean mixture, while the other injection is timed close to TDC to act as a combustion trigger. The early injected fuel greatly enhances fuel-air mixing prior to combustion starting, thus soot formation can be suppressed in the first place. In PCCI combustion, high fuel injection pressure is typically

used to improve the mixing process, and a high EGR ratio is used for reduction of NO_x (Weall & Collings, 2007). The use of EGR permits longer ignition delay for the main fuel injection, allowing extra time for the injected fuel to mix more thoroughly with the air. With the combination of these strategies, the combustion can be separated from the injection event while a correlation between them still presents (Zhang, Xu, et al., 2011).

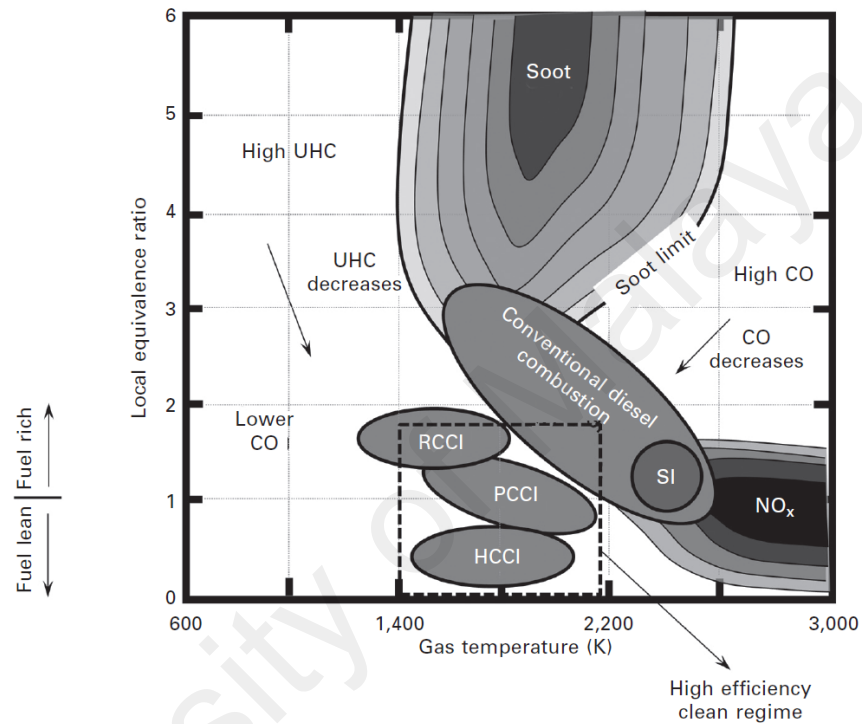


Figure 1.6: Plot of NO_x and soot formation regions on Φ -T plane with various combustion strategies (Folkson, 2014).

However, there remains formidable challenges to currently available LTC technologies due to their high HC, CO emissions, and narrow operating regimes that may be related to complications in ignition control. Occasionally, the problems are serious enough to cause higher BSFC (Bhave et al., 2005; Ekoto et al., 2009). Generally, the low load limit is constrained by ignition stability and high cycle-to-cycle combustion instability, whereas high load operation is limited by excessively high maximum combustion pressure, rapid pressure rise and knocking combustion (Das et al., 2014). Therefore, a new emerging dual fuel engine combustion strategy, called RCCI by Kokjohn et al. (Kokjohn et al., 2009) is worth investigating. RCCI is a dual fuel engine combustion technology that was

developed at the University of Wisconsin-Madison Engine Research Center laboratories. RCCI is a dual fuel engine combustion technology and offers better control of combustion and resolves the load range limitation issue of HCCI and PCCI strategies (Reitz & Duraisamy, 2015). As the name implies, the RCCI combustion approach employs in-cylinder fuel blending with at least two fuels of different reactivity injected at specific times in the engine cycle to control the in-cylinder charge reactivity and thus optimize combustion timing, duration, and magnitude. Usually, RCCI uses port injection of relatively low reactive fuel (i.e. gasoline) along with the direct injection of high reactive fuel (i.e. diesel) to control in-cylinder charge conditions. Mixing fuels of varied reactivity in the cylinder offers another powerful dimension of combustion control parameters. Reitz's investigations have demonstrated that an engine operating with the RCCI strategy can gain back about 20% in fuel efficiency compared to conventional diesel combustion while still meeting PM and NO_x emissions without after-treatment (Reitz, 2010).

1.3 Problem statement

Usually, the common-rail injection system can be found in multi-cylinder diesel engines used in passenger cars and trucks. However, they are too large and complicated, and it is almost impossible to have full access to the stock ECU to reconfigure the injection parameters. Besides, it is rare indeed that a commercially available single-cylinder diesel engine is equipped with an electronically controlled fuel injection system largely due to the high cost of implementation. Additionally, the common-rail injection system offered many advantages including of improvement in thermal efficiency, fuel economy, and cleaner exhaust emissions compared to a conventional mechanical system. Thus, its introduction in a single-cylinder diesel engine should be an interesting idea. Further, the advanced fuel injection system also offers the possibility to perform multiple injection to simultaneously reduce smoke and NO_x emission. Therefore, this study focuses on the investigation of injection parameters with baseline diesel on a modified single-cylinder

engine test rig equipped with a high-pressure common-rail injection system. This would involve with the development of a fully controlled common-rail fuel injection single-cylinder diesel engine for research studies. The developed system must be able to provide flexible control of injection parameters such as injection timing, injection pressure, and number of injections in a cycle of operation, which enables a more advanced combustion study.

The use of biodiesel in conventional diesel combustion engines has usually caused higher NO_x and specific fuel consumption (Al-Dawody & Bhatti, 2013; Palash et al., 2013; Rahman et al., 2013). Using alternative fuels and switching to promising combustion technologies such as LTC can be reliable approaches to addressing this issue (Kakaee et al., 2015). In fact, LTC is a promising concept for NO_x emission reduction not only for petroleum diesel, but also for biodiesels (Veltman et al., 2009). However, the main challenge for most LTC strategies is higher HC and CO emissions that result from low combustion temperature and higher EGR rate. Using an oxygenated fuels such as biodiesel can be a good alternative to this problem, and yet these fuels are derived from renewable sources. In addition, a number of LTC engine research is currently being carried out worldwide, but not in Malaysia. This study would establish a good starting point for LTC engine research in Malaysia, specifically dealing with the newest and promising approach of the RCCI combustion system. Also, biofuels have received renewed interest due to its less polluting and renewable nature as opposed to petroleum fuels. Therefore, this research study focuses on the utilization of biofuels as alternative energy sources for engines operating in RCCI dual-fuel combustion mode.

1.4 Research objectives

Many previous studies (Chauhan et al., 2012; Ong et al., 2014; Raheman & Ghadge, 2007; Vedharaj et al., 2013) into biodiesel fuel have examined the engine-out responses of a conventional mechanical pump-line-nozzle fuel injection system. With this fuel injection system, the lower compressibility and the viscosity of the biodiesel will usually lead to an advanced start of injection, resulting in higher NO_x emissions (Lapuerta et al., 2008). These effects could be eliminated by using common-rail fuel injection technology, in which fuel pressurization is independent of injection timing (Leahey et al., 2007). Thus far, most of the research about biodiesel, including the study of its effect on engine performance, emissions and combustion characteristics, has been performed under relatively low EGR levels (i.e. <30%) (Lattimore et al., 2016) and with an engine equipped with a conventional pump-line-nozzle injection system (Pradeep & Sharma, 2007; Saravanan, 2015; Tsolakis et al., 2007). The engine-out responses under higher EGR (>30%) conditions have not yet been sufficiently investigated. In the case of palm biodiesel fuel, it contains about 11.7% oxygen content in the fuel composition and has a higher cetane number than petro-diesel (Chong et al., 2015), which gives great opportunities to optimize the engine performance and emissions under higher EGR levels. Consequently, the aim of this study is to investigate the impact of neat palm oil methyl ester (PME) combustion in a diesel engine equipped with a common-rail injection system with higher EGR rate. In addition, to the best of author's knowledge, there is limited study on engine operating on biofuels in RCCI combustion mode. In a RCCI dual-fuel combustion engine system, biodiesel fuel has a higher cetane number and higher oxygen content and can be used as the ignition source. Apparently, combining the two, LTC and biofuels, could potentially address both the emissions and efficiency challenges observed with petroleum–diesel based low temperature combustion (Tompkins & Jacobs, 2012).

Therefore, this research study focuses on the utilisation of biofuels as an alternative energy source for engines operating in RCCI dual-fuel combustion mode.

The objectives of the present study can be summarized as follows:

- To develop a common-rail direct injection engine based on the conventional pump-line-nozzle injection system diesel engine.
- To investigate the engine performance, emissions, combustion and vibration characteristics using palm biodiesel and its blends, Jatropha biodiesel and its blends, and baseline diesel fuel.
- To study the effect of injection parameters and EGR variation on engine performance, emissions and combustion characteristics using neat palm biodiesel and diesel fuel.
- To study the engine performance, emissions and combustion characteristics using diesel and biodiesel as direct injection fuels for achieving RCCI combustion mode.

1.5 Research novelty and contribution

The original contribution of the present study includes the development of various keys experimental setup, engine performance, emissions and combustion characteristics of biodiesels fuel in common-rail injection engine and RCCI combustion engine. Furthermore, this study also offer better understanding of the performance of biodiesel fuel in an engine equipped with various promising NO_x reduction strategies such as injection timing retardation, EGR and low temperature combustion. This will contribute to introducing of biodiesel in RCCI advanced combustion engine. The summary for contributions of the present research is as follow:

1. Developed a fully controlled fuel injection system that could operate with multiple injectors to accommodate RCCI combustion mode.

2. Explored the impact of higher EGR rate (i.e. >30%) on diesel and biodiesel engine performance, emissions and combustion characteristics.
3. Proposed of diesel engine operating in RCCI combustion mode and fueled with oxygenated fuel of biodiesel.
4. Established a good starting point for low temperature combustion (LTC) engine research in Malaysia, especially dealing with the newest and promising approach of RCCI combustion system.

From the outcome of this study, a number of research papers have been published in the high impact internal journal and conference proceedings. The publication list are presented in Appendix A.

1.6 Scope of study

The scope of this research work is as follows:

- i. Engine test cell design, fabrication and setup. This includes the engine dynamometer and load bank, sensors and instrumentation, data acquisition system and data post processing.
- ii. Convert a pump-line-nozzle direct injection diesel engine into a common-rail high-pressure injection direct injection diesel engine. The conversion includes designing and fabricating the flexible fuel supply system and selection of common-rail fuel injector. Independent control of the injection parameters was achieved using a custom-built engine controller unit (ECU).
- iii. Produce biodiesel from *Jatropha curcas* oil and palm oil. Physicochemical properties of the produced biodiesel have been measured and compared with ASTM D6751 standard. Moreover, the fatty acid composition of methyl ester has also been determined.

- iv. Analyze the effect of injection parameter and EGR variation on the engine performance, emissions and combustion characteristics.
- v. Engine testing for common-rail direct injection diesel engine using various palm biodiesel blends, Jatropha biodiesel blends and baseline diesel fuels. The engine-out responses were analyzed in terms of engine power, exhaust emissions and combustion characteristics.
- vi. Convert a CI diesel engine into a dual-fuel RCCI combustion engine. The conversion includes designing and fabricating an additional port injection fuel supply system, EGR system integration and selection of port fuel injector. Additional ECU for port fuel injection system has also been designed and developed.
- vii. Dual-fuel RCCI engine testing with gasoline as premix fuel and diesel/biodiesel as direct injection fuel. The effects of fuel type, fuel injection timing, and EGR rate on engine power, exhaust emissions and combustion characteristics have been investigated.

1.7 Organization of dissertation

The dissertation comprises of five chapters. The organization of each chapter is set out as follows:

Chapter 1 presents the overview of the research topic. It begins by discussing the overview of the present and future global energy scenario. This is followed by background research that indicates the significance of biodiesel and the technological progress in internal combustion engine toward meeting increasingly stringent emission standards. Problem statement, research objectives and scope of study are also included in this chapter.

Chapter 2 consists of the literature review of the previous studies regarding the related areas of the research. For instance, combustion of petroleum diesel and biofuels in

conventional CI engine, impact of biofuel on engine-out responses, introduction of various LTC strategies and their impact on NO_x and PM emissions, etc.

Chapter 3 describes the methodology of this study. In this section, a brief illustration of the equipment used for fuel sample preparation and fuel property characterization has been elaborated. Experimental apparatus setup includes engine modification, fuel delivery system construction, test bed configuration, ECU development and instrumentation have been described in detail. The test procedure and the analyzers for acquiring combustion data have also been presented.

Chapter 4 is dedicated to showing all the results of this study and the results have been discussed with reference to previous studies.

Chapter 5 provides the conclusion and further recommendations for work that can be continued by future research work.

CHAPTER 2: LITERATURE REVIEW

2.1 Introduction

This literature review is separated into nine sections and begins with an overview of current energy scenario, engine technologies advancement and diesel engine exhaust emissions regulation. This is followed by a review of the strategies to improve diesel engine pollutant emissions as well as the biodiesel combustion in conventional CI engines. Furthermore, the review is followed with the introduction of various LTC strategies, how it differs from conventional combustion, and an overview of practical applications. The chapter then moves on to review the LTC control strategies. Finally, diesel engine fuel injection systems and conversion are reviewed and the potential they offer in engine development is covered.

2.2 Overview

The increasing trend of energy consumption can be related to two primary factors, mainly: (1) a change in lifestyle; and (2) the significant growth of population. Two of the main contributors are the transportation and the basic industry sectors. This increase in energy demand has been met using fossil resources (crude oil, natural gas and coal, principally), which have caused serious environmental impacts including global warming, acidification, deforestation, ozone depletion, eutrophication and photochemical smog, among others (Körbitz, 1999). The last few years experienced the Deepwater Horizon oil spill in the Gulf of Mexico, the Fukushima-Daiichi nuclear accident in Japan, and the Arab Spring, which led to oil supply disruptions from Middle East (International Energy Agency (IEA), 2012). These trends and incidents, when considered together, emphasizes the need to rethink our global energy system.

Owen et al. (Owen et al., 2010) reported that current proven reserves of liquid fuels have the capacity to serve just over half of Business As Usual (BAU) demand until 2023. Therefore alternative fuels or biofuels are becoming increasingly important due to environmental and energy concerns (Agarwal, 2007). The U.S. Energy Information Administration (EIA) provides a projection of the world's consumption of marketed energy from all fuel sources through to 2035, which supports the increasing trend of renewable energy consumption (US Energy Information Administration, 2011). This also reports renewable energy as the world's fastest growing form of energy with the renewable share of total energy use increasing from 10% in 2008 to 14% in 2035 in EIA reference case. In addition, the International Energy Agency (IEA) states that biofuels could provide 27% of total transport fuel and contribute, in particular, to the replacement of diesel, kerosene and jet fuel by 2050 (International Energy Agency (IEA), 2011). The projected use of biofuels could avoid around 2.1 Giga tones (Gt) of CO₂ emissions per annum when produced sustainably. The Kyoto Protocol was a significant step for the reduction of CO₂ and five other greenhouse gases as it set a legally-binding target on quantitative emission reductions for industrialized nations. It also indirectly introduced the concept of "carbon neutral fuel". There are many emission standards, focusing on regulating pollutants released by automobiles and other powered vehicles, which generally specify certain limiting value of the emissions of NO_x, PM or soot, CO, or volatile hydrocarbons. Recently, automotive manufacturers have invested a lot of cost and effort in order to meet stringent regulations on exhaust emissions. This resulted in a new generation of diesel engines that are more environmentally friendly and are in no way inferior to gasoline engines in terms of performance. In comparison with gasoline engines, diesel engines have better output torque, reliability and durability. Further, they burn 30% less fuel and emit 25% less CO₂ on average (Sellerbeck et al., 2007).

The unprecedented fuel consumption and environmental degradation highlight the necessity of developing renewable and clean alternative fuels. Among the various alternative fuels, biofuels including biodiesel and alcohol has become the focus of research because of its reproducibility and non-toxicity. Biodiesel is always regarded as a promising diesel substitute for its similar properties with diesel and even better performance in engines including lower PM and HC emissions (Veltman et al., 2009). The attractive characteristics of biodiesel include its higher cetane number, non-toxic emissions, bio-degradability, absence of sulphur and aromatic compounds along with having characteristics of renewability and beneficial effects on the environment (Atabani et al., 2012; Atadashi et al., 2012). For many years, an enormous number of researchers around the world have tested biodiesel/blends in CI engines. In general, some performance deficiency in terms of engine power loss, torque reduction, and brake specific fuel consumption (BSFC) have been reported and it is mainly due to the lower energy content of biodiesel compared to petroleum diesel. In terms of emissions, reductions in CO, HC, SO₂, polycyclic aromatic hydrocarbon (PAH), nitric polycyclic aromatic hydrocarbons (nPAH) and PM have been reported. However, the major drawback of biodiesel/blends is higher NO_x emissions in comparison with diesel fuel (Aydin & İlkılıç, 2010; Dhar et al., 2012; Xue et al., 2011).

LTC in diesel engines is gaining interest after its initial development dating back to 1979 (Onishi et al., 1979). It is now widely demonstrated across a breadth of applications, including light-duty (e.g. passenger cars) (Akagawa et al., 1999; Jacobs et al., 2005; Lechner et al., 2005; Takeda et al., 1996) and heavy-duty (e.g. large trucks) (Alriksson & Denbratt, 2006; Hardy & Reitz, 2006; Musculus, 2006; Simescu et al., 2003). Despite the success demonstrated with LTC, some concerns still remain regarding its ability to maintain the high efficiency accustomed in conventional diesel combustion. Such concerns include decreased fuel conversion efficiency and increased HC and CO

concentrations. Additionally, biodiesel is also gaining interest as an augmenting fuel to petroleum diesel. Similar to LTC, the effect of biodiesel on efficiency and emissions is well-reported (Agarwal, 2007; Monyem & Gerpen, 2001). Both poor combustion phasing and increased concentrations of unburned HC and CO concentrations are blamed for lower fuel conversion efficiency with petroleum-diesel-based LTC (Knight et al., 2010). Furthermore, the use of different fuels with LTC offers promise for overcoming these challenges (Junjun et al., 2009; Kim et al., 2008; Lilik & Boehman, 2011).

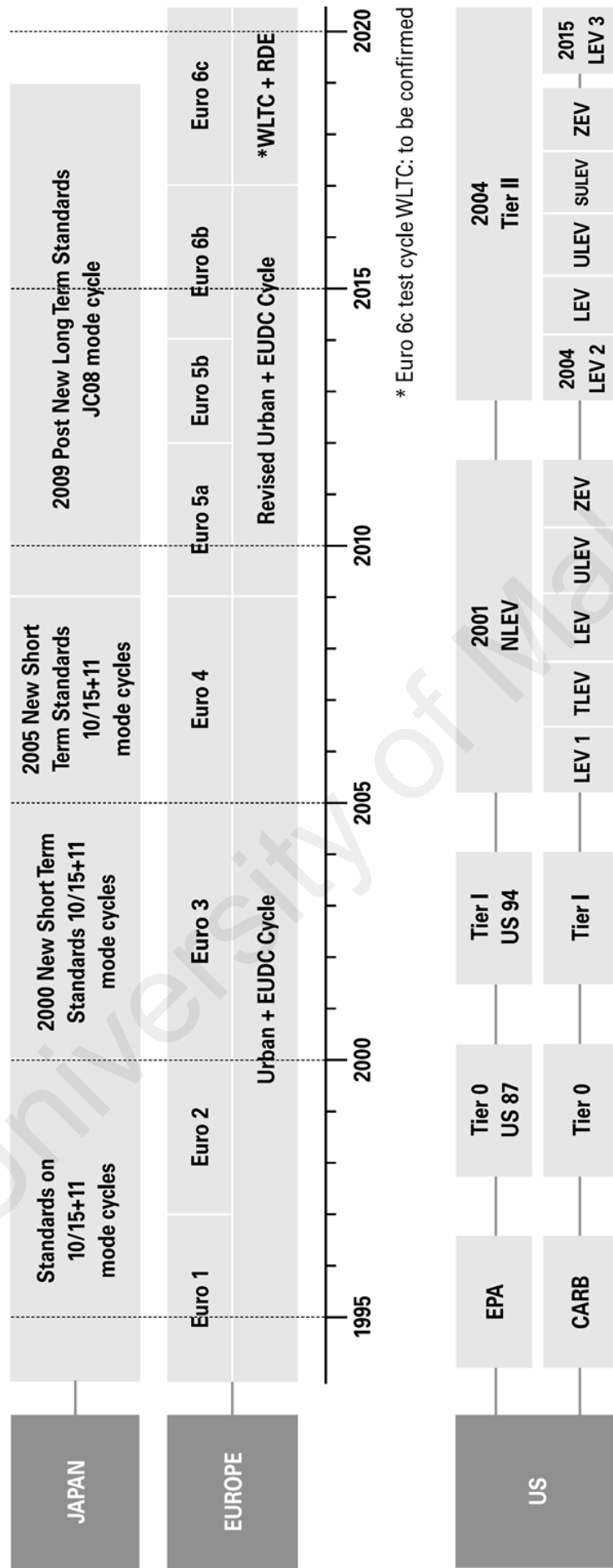
2.3 Internal combustion engine

The internal combustion engine works upon very simple principles. However, there are a lot of aspects that require sophisticated controls and implementation in order to achieve the highest engine efficiency. The internal combustion engine is an energy conversion device, which extracts mechanical power from the heat energy of fuel oxidation. Generally, the working principle of an internal combustion engine is relatively simple. First, air is drawn into the engine combustion chamber and used as the working fluid of the system. Then the air inlet of the combustion chamber is closed to form an enclosed volume inside the engine. Fuel is combusted inside that enclosed combustion chamber for heat addition to the air. With the added heat energy, the pressure of the air in the combustion chamber is elevated, thus exerting force directly on the moving piston of the engine to produce mechanical work. Finally, the burned products are expelled from the combustion chamber to leave room for the induction of fresh air and ready for the next cycle. In reality, these processes of course are more complicated and implemented in many different ways, but they hold true for every internal combustion engine. Fundamentally, internal combustion engines can be categorized based on the method of fuel ignition, namely the SI and CI engine. The SI gasoline engine was developed by Otto in 1876, while the CI diesel engine was invented by Diesel in 1892. The engine can be

further categorized based on the operating cycle, which are commonly the two-stroke or four-stroke cycle engine.

2.4 Diesel engine emissions regulation

Diesel engine's emissions have improved significantly over the last 40 years because of advancements in engine technology, emission controls, and fuel preparation (Ouenou-Gamo et al., 1998). Diesel engines emit a wide range of gaseous and particulate phased organic and inorganic compounds with higher amounts of aromatics and sulfur. The particles have hundreds of chemicals adsorbed onto their surfaces; comprising many recognized or suspected mutagens and carcinogens. The gaseous phase also contains many toxic chemicals and irritants. These have serious adverse effects on human health and environmental impact (Ackerman et al., 2000; Eldering & Cass, 1996; USEPA, 2002). The composition of diesel exhaust varies considerably depending on engine type, operating conditions, fuel, lubricating oil, and whether an emission control system is present. Generally, exhaust contains a higher amount of PM, NO_x, CO, unburned hydrocarbon (HC) and smoke. Worldwide testing procedures and exhaust emission standards are shown in Figure 2.1. The European Union's criteria emissions regulations for heavy-duty diesel engines are commonly known as Euro I to Euro VI. The first standard (Euro I) was introduced in 1992 (DieselNet, 2012). The most recent legislation, Euro VI, is basically comparable in stringency to the US 2010 standard and became effective in 2013. It also introduces emissions limits in terms of particle number, new testing requirements including off-cycle and in-use testing, and more strict on-board diagnostic (OBD) requirements. Russia introduced regulations based on Euro IV beginning in 2010 and based on Euro V targeting for 2014. Malaysia has begun adopting European emissions regulations for light-duty vehicles since 1997 and is targeting to implement Euro IV by early 2016 (UNEP, 2013).



European Union countries: Austria, Belgium, Bulgaria, Cyprus, the Czech Republic, Denmark, Estonia, Finland, France, Germany, Greece, Hungary, Ireland, Italy, Latvia, Lithuania, Luxembourg, Malta, Netherlands, Poland, Portugal, Romania, Slovakia, Slovenia, Spain, Sweden, United Kingdom.

Figure 2.1: Worldwide exhaust emission testing procedures and standards (Delphi, 2015).

Table 2.1: EU emission standards for heavy-duty diesel engines: steady-state testing (DieselNet, 2012).

Stage	Date	Test	CO	HC	NO _x	PM
			g/kWh			
Euro I	1992, ≤ 85 kW	ECE R-49	4.5	1.1	8	0.612
	1992, > 85 kW		4.5	1.1	8	0.36
Euro II	1996.1		4	1.1	7	0.25
	1998.1		4	1.1	7	0.15
Euro III	1999.10 EEV only	ESC & ELR	1.5	0.25	2	0.02
	2000.1		2.1	0.66	5	0.10 ^a
Euro IV	2005.1		1.5	0.46	3.5	0.02
Euro V	2008.1		1.5	0.46	2	0.02
Euro VI	2013.01	WHSC	1.5	0.13	0.4	0.01

^a - PM = 0.13 g/kWh for engines < 0.75 dm³ swept volume per cylinder and a rated power speed > 3000 rpm

2.5 Strategies to improve CI engine pollutant emissions

In CI engines, the majority of studies on the comparisons between diesel and biodiesel have been based on the standard setting of an engine using fossil diesel fuel. Also, it is generally agreed upon that the formulation of fuel composition can enhance the biodiesel combustion performance and tailpipe emissions. However, the experimental results indicated that it was not easy to keep NO_x emissions neutral while reducing other pollutants simply through fuel reformulation (Keskin et al., 2007; Qi et al., 2011; Qi, Chen, et al., 2009; Qi et al., 2010). Therefore, modification of the engine operating parameters such as injection strategies and exhaust gas recirculation (EGR) may be possible to optimize the engine emissions due to the difference in combustion characteristics and chemical composition between diesel and biodiesel. In a diesel engine, improvements in the fuel injection parameters can be employed to reduce engine emissions and improve fuel economy. Injection parameters such as injection pressure, injection duration, injection timing, and fueling are the key injection parameters which can significantly affect the performance and emissions of an engine. For instance, the combustion efficiency and ignition delay will change as the injection timing is varied

because of the effect of mixture formation (Sayin et al., 2009). Numerous studies revealed that injection timing retardation reduces NO_x emissions (Park et al., 2011; Sayin et al., 2008; Zhu et al., 2013). With late injection timing, the peak cylinder pressure decreases and results in lower peak combustion temperatures and consequently, NO_x emissions diminish. Conversely, advancing the injection timing decreases HC and CO emissions. In another study (Hariram & Mohan Kumar, 2012), the effect of injection timing on the performance, combustion and emission parameters was investigated in a single cylinder, mechanical pump-line-nozzle injection system using algal oil methyl ester (AOME) blended fuels (i.e. 5, 10 & 20% blend). The test result revealed that the advancement in injection timing of 5° crank angle from the rated static injection timing of 345° crank angle caused a reduction in brake specific fuel consumption, HC, CO and smoke, and increase the combustion pressure, heat release rate, brake mean effective pressure (BMEP) and NO_x emissions. In another related study, Ganapathy et al. (Ganapathy et al., 2011) demonstrated an improvement in engine performance and emissions when the fuel injection pressure and injection timing were optimized for Jatropha biodiesel operation. The experiment was conducted in a single-cylinder diesel engine that was equipped with a mechanical pump-line-nozzle injection system. The fuel injection timing was varied with a 5° crank angle on either side of the rated static injection timing (345° crank angle).

Another effective approach to reduce NO_x emissions from a petrol–diesel engine is by means of the EGR technique which is a pretreatment approach. However, using EGR alone has some drawbacks in that it could reduce energy efficiency, operational stability and a trade-off in terms of soot emissions (Shahir et al., 2015). In this regard, others have investigated the effects of combining biodiesel and EGR. The general outcome from these studies was that combining EGR and biodiesel was an effective strategy to reduce NO_x and/or PM (Qi et al., 2011). Pradeep and Sharma (Pradeep & Sharma, 2007) adjusted the EGR levels (5–25%) and engine load on a single-cylinder engine and found that biodiesel

emitted more smoke at lower loads and less smoke at higher loads when compared to diesel fuel. Tsolakis et al. (Tsolakis et al., 2007) found that the use of biodiesel fuel could reduce the smoke and NO_x from a single-cylinder engine with EGR (i.e. 10% and 20%) under certain engine conditions when compared to diesel. FOME (fish oil methyl ester) and its blends have been tested in a diesel engine by Bhaskar et al. (Bhaskar et al., 2013). They show that a blend fuel with 20% vol of FOME produces nearly the same brake thermal efficiency with lower unburned hydrocarbon, carbon monoxide and soot emissions, but higher NO_x emissions compared to diesel fuel. They found that NO_x emissions can be reduced with the use of EGR. EGR flow-rates of 10%, 20% and 30% were examined in their study. The authors suggested that 20% EGR flow rate be optimum for 20% FOME blend considering the emissions of NO_x and soot.

2.6 Biodiesel combustion in a CI engine

Aside from differences in engine structure, the way of controlling engine load, engine operating speed or the type of fuel being used, the most substantial factor that differentiates SI and CI engines is the combustion process. While the energy is stored in the fuel as chemical energy, the engine is extracting energy from the heat energy that is released from the fuel. This clearly shows the importance of the combustion process for a heat engine. The heat addition process in CI engines is achieved through the auto-ignition of fuel that is injected into the hot compressed air inside the combustion chamber. The fuel must be mixed well with the air and provided suitable condition to form combustible fuel-air mixture, before it can be oxidized and attained effective heat release process. Four major factors are involved in that process, namely; (1) In-cylinder air condition; (2) Fuel injection; (3) Combustion chamber design; and (4) In-cylinder air motion. Diesel engine combustion is a complex phenomenon. Various processes affect the efficient combustion such as atomization and evaporation of the fuel, mixing of the fuel with surrounding gases, self-ignition, oxidation, turbulence induced by air and fuel

jet, the possible interaction of the fuel jet with the cylinder walls, heat transfer between the fuel and the surrounding gases, and between combustion gases and the cylinder walls (Tauzia et al., 2006). The homogeneous air–fuel mixing in time is largely influenced by the combustion chamber geometry and the fuel injection characteristics (Semin et al., 2008). The higher fuel injection pressure will lead to a faster combustion rates, thus resulting in higher combustion chamber gas temperature. This is because of the increasing vaporization rate of spray fuel and reduction of its penetration into the combustion chamber (Purushothaman & Nagarajan, 2009). The experimental indicator diagram determines the shape and magnitude of the cylinder pressure diagram. It can also serve the purpose of determining the heat release (Rakopoulos et al., 2006).

The properties of both the pure and blended biodiesel have great influence on engine performance and emissions, since it has different physical and chemical properties from those of diesel fuel. Further research is required to find out more about the properties of biodiesel and their effects on combustion and the fuel injection system, if this fuel is used in diesel engines without any modification (Qi, Geng, et al., 2009). Though several advantages can be obtained with the application of biodiesel, few of its inherent properties are to be ameliorated in order to overcome the limitations (Mofijur et al., 2012). Biodiesel has higher viscosity than petroleum diesel (Shahabuddin et al., 2012). Studies have indicated that increasing blend ratios and thus viscosity, can lead to reduced atomization quality of the injected fuel. The consequences are increasing in the average droplet diameter of the sprayed fuel and the breakup time (Alptekin & Canakci, 2009; Gumus, 2010; Lee et al., 2005). The injected fuel quantity, injection timing, and spray pattern can be affected by higher viscosity and specific gravity of biodiesel. Combustion and heat release rate (HRR) characteristics of biodiesel must be known in order to achieve the reduction of BSFC and emissions while keeping other engine performance parameters at an acceptable level. The differences in physical properties between diesel and biodiesel

fuels affect the combustion and heat release characteristics (Canakci, 2007; Canakci, Ozsezen, & Turkcan, 2009; Graboski & McCormick, 1998; Gumus, 2010; Ozsezen et al., 2008; Qi, Geng, et al., 2009). Numerous studies have been conducted on ignition delay (ID) and combustion behavior in diesel engines fuelled with biodiesel. The different varying parameters of these studies were fuel injection timing, injection pressure, engine load, and compression ratio. Results of the studies revealed that biodiesel has an early start of combustion (SOC), shorter ID and lower HRR.

2.7 LTC strategies: the diesel engine salvation

Automobile usage and production are exponentially increasing due to the rapid growth in the global population. Emission legislation has also become more stringent. The main mission for scientists, researchers, engineers and academicians is to discover solutions to minimize engine exhaust emissions and effectively utilize the energy. Over the last two decades, many automotive industries have introduced several modern automotive vehicles, mainly to increase fuel economy, minimize emissions, and to utilize different alternative fuels. In this regard, researchers and engineers have paid more attention towards advanced modes of LTC like HCCI, stratified charge compression ignition (SCCI), RCCI, and PCCI due to their superior thermal efficiencies and ultra-low emissions of NO_x and soot (Flowers et al., 2000; Wu et al., 2011; Yamada et al., 2005; Zhang, Pan, et al., 2011). Engines operating in LTC mode have a potential to meet the stringent emission standards (EURO VI) and CO₂ emission standards. Figure 2.2 shows the comparison of SI, CI and HCCI operations. In LTC strategies such as HCCI, a lean homogeneous flammable mixture (fuel–air equivalence ratio $\Phi < 1$) is prepared prior to the start of ignition and auto ignited as a consequence of temperature rise in the compression stroke. The HCCI operation is similar to SI engine which utilizes the homogeneous charge for combustion and similar to CI engine that has the auto ignition of the mixture. Thus, HCCI is the hybrid nature of SI and CI combustion processes

(Saxena et al., 2012). In SI engines, there are three zones of combustion, namely the burnt zone, unburned zone and a thin flame reaction zone in-between for turbulent flame propagation through the cylinder. In CI engines, fuel is diffused into the cylinder and a definite diffusion flame travels within the cylinder. In HCCI engine combustion, spontaneous ignition of whole cylinder charge takes place without any diffusion flame or flame front propagation (Mack et al., 2016). The comparison of different parameters influencing the combustion processes in SI, CI, and HCCI are given in Table 2.2.

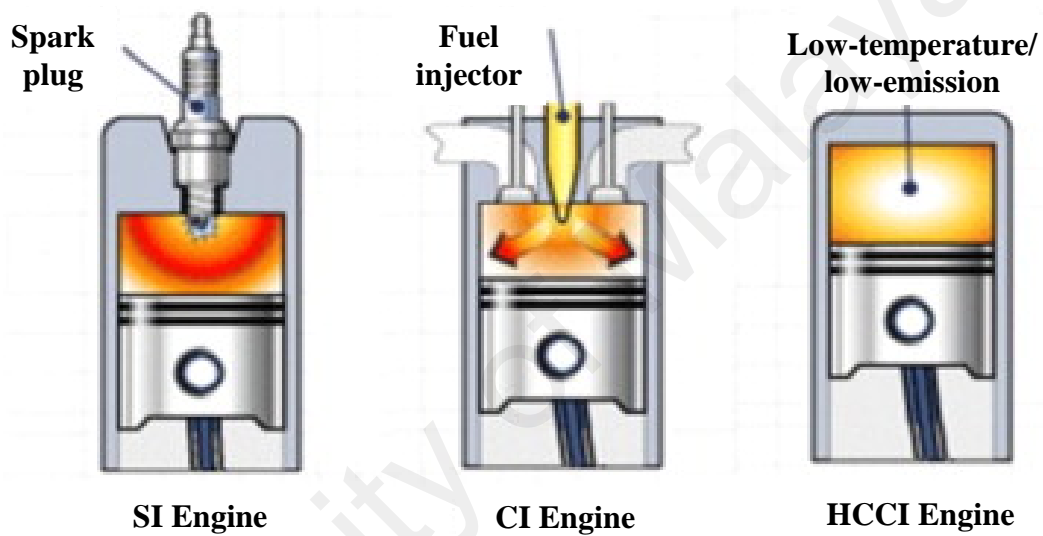


Figure 2.2: Comparison of SI, CI and HCCI engine (Clean combustion research centre, 2015).

Table 2.2: Comparison of SI, CI and HCCI combustion engines.

Engine type	SI	HCCI	CI
Ignition method	Spark ignition	Auto-ignition	
Charge	Premixed homogeneous before ignition		In-cylinder heterogeneous
Ignition point	Single	Multiple	Single
Throttle loss	Yes	No	
Compression ratio	Low	High	
Speed	High	Moderate	
Combustion flame	Flame propagation	Multi-point auto-ignition	Diffusive flame
Fuel economy	Good	Best	Better
Max. efficiency	30%	>40%	40%
Major emissions	HC, CO and NO _x	HC and CO Both port and direct injection	NO _x , PM and HC
Injection type	Port injection	Direct injection	Direct injection
Equivalence ratio	1	<1	
Fuel injection method	Indirect injection		

2.7.1 Homogeneous charge preparation strategies

The preparation of the homogeneous mixture is the main factor in reducing the particulate matter (soot) emissions, and local fuel rich regions to minimize NO_x. The local fuel-rich regions can be decreased by effective mixture preparation. However, the preparation of the homogeneous mixture for the cycle-to-cycle variation of speed and load is a difficult task due to less time availability for mixture preparation. The effective mixture preparation for the LTC includes both the fuel–air homogenization and temperature control over combustion. The strategies for mixture preparation are either in-cylinder direct injection, or external mixture, which are shown in Figure 2.3. Both preparation methods have their own disadvantages that the external mixture has a low volumetric efficiency and in-cylinder mixture is prone to oil dilution. Table 2.3 presents the various terminologies of LTC which are available in the literature.

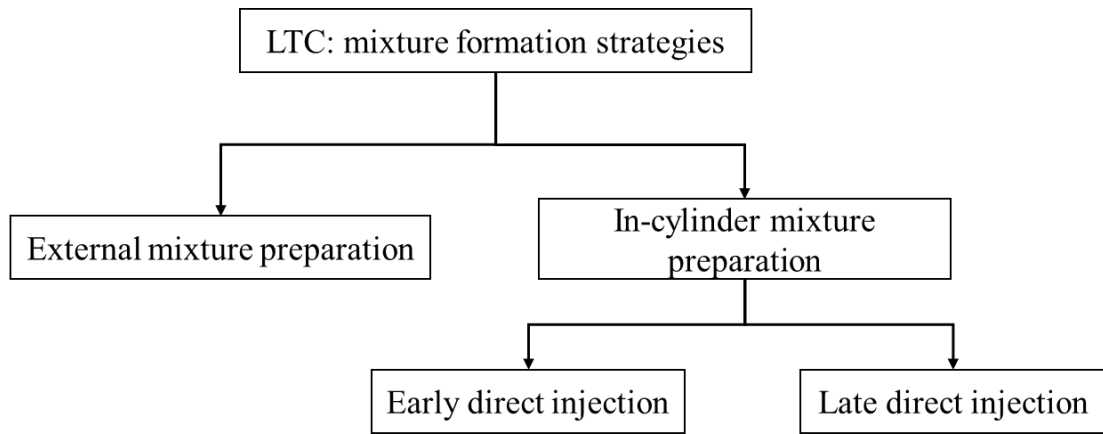


Figure 2.3: Mixture preparation strategies.

Table 2.3: Overview of LTC acronyms from literature.

Reference	Acronym	Meaning	Origin
(Onishi et al., 1979)	ATAC	Active thermo-atmosphere combustion	Nippon Clean Engine Research Institute
(Noguchi et al., 1979)	TS	Toyota-Soken combustion	Toyota/Soken
(Thring, 1989)	HCCI	Homogeneous charge compression ignition	Southwest Research Institute (SwRI)
(Ishibashi & Asai, 1996)	ARC	Active radical combustion	Honda
(Gatellier et al., 2001)	NADI™	Narrow Angle Direct Injection	Institut Français Du Pétrole (IFP)
(Kimura et al., 1999)	MK combustion	Modulated kinetics combustion	Nissan
(Takeda et al., 1996)	PREDIC	Premixed diesel combustion	New ACE
(Hashizume et al., 1998)	MULDIC	Multiple stage diesel combustion	New ACE
(Yokota et al., 1997)	HiMICS	Homogeneous charge intelligent multiple injection combustion system	Hino
(Hasegawa & Yanagihara, 2003)	UNIBUS	Uniform bulky combustion system	Toyota
(Iwabuchi et al., 1999)	PCI	Premixed compression ignited combustion	Mitsubishi
(Aoyama et al., 1996)	PCCI	Premixed Charge Compression Ignition	Toyota

2.7.1.1 External mixture preparation

The homogeneous mixture which is externally prepared is the most effective due to more mixing time availability prior to the start of combustion. This method is very suitable for high volatile fuels like gasoline and alcohols. The mixture preparation strategies are port fuel injection (PFI), manifold induction, fumigation, and wide-open throttle (WOT)

carburetion. However, low volatile fuel like diesel can also be used by using fuel vaporizer. The gaseous fuels are ready to mix with the air and preparation of homogeneous mixture externally is very simple, but the engine may suffer with lower volumetric efficiency if the calorific value of the gas is low. The gaseous fuels are mixed mostly in the intake manifold and some early implementations are acetylene (Lakshmanan & Nagarajan, 2011; Swami Nathan et al., 2010a), biogas (Sudheesh & Mallikarjuna, 2010; Swami Nathan et al., 2010b), and hydrogen (Ibrahim & Ramesh, 2013; Saravanan & Nagarajan, 2010; Saravanan et al., 2007). Figure 2.4 illustrates the different methods of external mixture preparation.

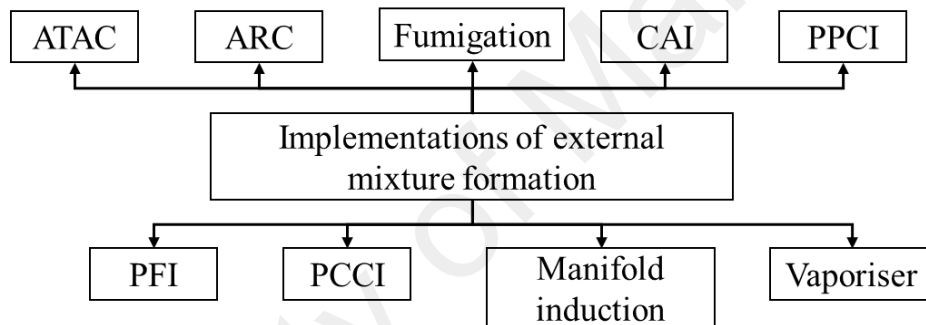


Figure 2.4: Early implementations of external mixture formation.

A first study on the LTC process has been performed on two stroke engines by Onishi et al. in 1979 (Onishi et al., 1979). There is no flame propagation, as in a conventional SI engine. Instead, the whole mixture burns slowly at the same time. They called it active-thermo atmosphere combustion (ATAC) (Iida, 1997). The same combustion was demonstrated by Toyota Motor Co. Ltd. and named as “Toyota-Soken (TS) combustion” (Noguchi et al., 1979). Noguchi et al. (Noguchi et al., 1979) demonstrated the same combustion process in an opposed-piston two stroke engine. Later, Honda R&D Co. Ltd. investigated activated radical combustion (ARC) on two stroke gasoline engines (Ishibashi & Asai, 1996; Ishibashi & Asai, 1998; Ishibashi & Sakuyama, 2004) by winning the fifth place in the Granada-Dakar rally competition. The PCCI engine

developed by Toyota Central Research (Aoyama et al., 1996) in which the combustion of premixed lean mixture arises from a multi-point ignition is very promising and necessary for achieving both higher efficiency and lower NO_x emission. The PCCI engine operation is stable in the air–fuel ratio range of 33–44 and ignition occurs spontaneously at unspecified points as it does in diesel engines. Table 2.4 shows the external mixture preparation strategies used in LTC engines.

Table 2.4: Overview of external mixture preparation strategy implemented in gasoline-fuelled LTC engines.

Reference	LTC acronym	Key features	Advantages	Disadvantages
(Onishi et al., 1979)	ATAC	Uniform mixing between residuals and fresh charge. No flame propagation as in the case of SI engines. High EGR rates are used to achieve auto-ignition of gasoline.	Remarkable reduction in emissions and high fuel efficiency.	Limited to part load operation.
(Noguchi et al., 1979)	TS	Stable spontaneous auto-ignition with port fuelling in presence of active radicals.	Smooth combustion with low HC emissions and improved fuel consumption.	Limited to part load operation.
(Thring, 1989)	HCCI	The operating regime was function of air/fuel equivalence ratio and external EGR rates.	High fuel efficiency and low emissions.	Restricted to part load operation and control of auto-ignition timing is problematic.
(Ishibashi & Asai, 1996)	ARC	Active radicals in the exhaust gases were controlled by changing the exhaust valve axis movement.	Two-stage auto-ignition combustion is observed at lower load. Fuel economy was improved by 57% while HC emission reduction by 60%.	Idling with auto-ignition was not possible with AR combustion.
(Aoyama et al., 1996)	PCCI	Spontaneous ignition occurred at unspecified points as it does in diesel engines. The flame then developed rapidly throughout the combustion chamber.	Low NO _x emission was noticed than in diesel engines.	Intake air heating and supercharging were necessary to extend the range of stable combustion.

Some researchers introduced an electronically controlled fuel vaporizer for low volatile and high boiling point fuels such as diesel (Ganesh & Nagarajan, 2010; Ganesh et al., 2008; Singh & Agarwal, 2012). The diesel vaporizer formed a very light and dispersed aerosol with a very fast evaporation due to a very high surface to volume ratio. The smoke

emissions were reported to be negligible and the EGR was used for combustion control and NO_x emissions. The operation temperature of the vaporizer is above the boiling point of fuel for successful external mixture preparation (Ganesan et al., 2012). Some researchers used a high intake air temperature (Bahri et al., 2013; Kim & Lee, 2006; Liu et al., 2011; Liu et al., 2012) to vaporize the fuel in the intake manifold. The common disadvantage reported by them is the electric power consumption for the vaporisation of diesel. Another study was reported by the researchers on the effect of premixed ratio in diesel engine with the partially premixed charge compression ignition (PPCI) combustion using diesel fuel (Padala, Woo, et al., 2013; Soloiu et al., 2013).

The PFI is the simplest method of external mixture preparation, in which the injector is mounted in the intake manifold very close to the intake valve. This system improves the volumetric efficiency and fuel distribution over carburetion. The mixture enters into the cylinder during engine suction and the turbulence created by intake flow improves further homogenization. This method of mixture formation has been reported to be successful with gasoline and alcohol fuels (Li et al., 2013; Padala, Le, et al., 2013; Saxena et al., 2012; Wu et al., 2014). The main drawback of this strategy is that injection timing cannot influence the start of ignition. Furthermore, heavy fuels with lower volatility of PFI result in poor vaporisation with increased wall impingements.

2.7.1.2 In-cylinder mixture preparation

The demerits associated with diesel-fuelled by the port fuel injection with an internal mixture formation has been widely investigated. Generally, there are two strategies that have been widely adopted: (i) early direct injection and (ii) late direct injection for in-cylinder mixture formation. The injection timing for early direct injection was set during compression stroke. For late direct injection it was set after TDC. Besides, high injection

pressures with a large number of small nozzle holes was typically adopted in this strategy to increase the spray disintegration which forms homogeneous mixture.

(a) Early direct injection

The fuel injection process in the LTC is charge homogeneity, which is influenced by injection timing. The early injection method is the most used method of achieving LTC diesel combustion. Early injection allows a longer ignition delay along with low temperatures to homogenize the diesel–air mixture. Unlike conventional diesel, direct in-cylinder injection and coupled with multiple injection strategy is used. The total amount of fuel per cycle is injected in many pulses as shown in Figure 2.5. The early in-cylinder implementations used in diesel-fuelled vehicles are PREDIC, MULDIC, HiMICS, UNIBUS and MULINBUMP. Figure 2.6 represents various direct in-cylinder strategies used in recent years.

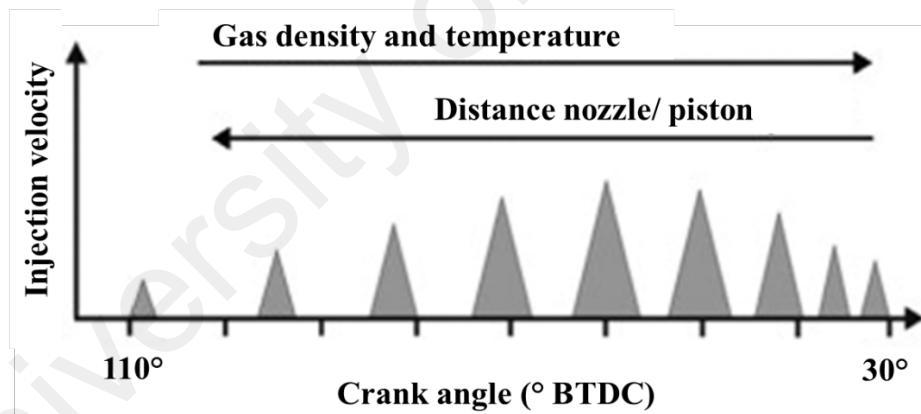


Figure 2.5: Pulsed injection strategy for early in-cylinder injection (Baumgarten, 2006).

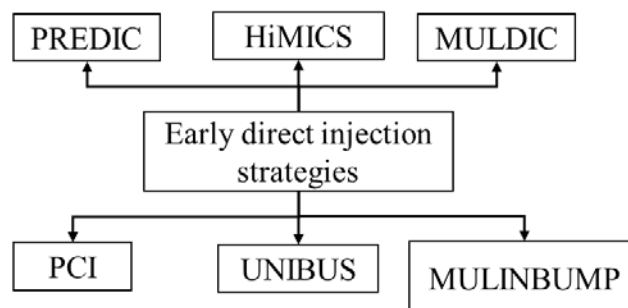


Figure 2.6: Early in-cylinder diesel direct injection strategies.

(b) Late direct injection

The development of diesel-fuelled late DI LTC system is the modulated kinetics (MK) combustion system developed by Nissan Motor Co., Ltd. (Kawashima et al., 1998; Kimura et al., 1999). A schematic diagram of the Nissan MK-concept is shown in Figure 2.7 (Kimura et al., 2001). This system combines two mutually independent intake ports, one of which is a helical port for generating an ultra-high swirl ratio and the other is a tangential port for generating a low swirl ratio. The tangential port incorporates a swirl control valve that controls the swirl ratio (3.5–10) by varying the flow rate. To achieve the premixed combustion, the fuel–air mixture homogeneity before ignition is required in MK combustion that can be achieved by increasing the ignition delay longer and rapid mixing with a high swirl. In the MK system, there are three features: (i) late fuel injection timing starts from 7° BTDC to 3° ATDC; (ii) high levels of EGR; and (iii) high swirl ratio. The formation of NO_x emissions can be suppressed by high EGR rates (reduces oxygen concentration from 21% to 15%) and low temperature combustion. The ignition delay was lengthened by lowering the compression ratio to 16:1.

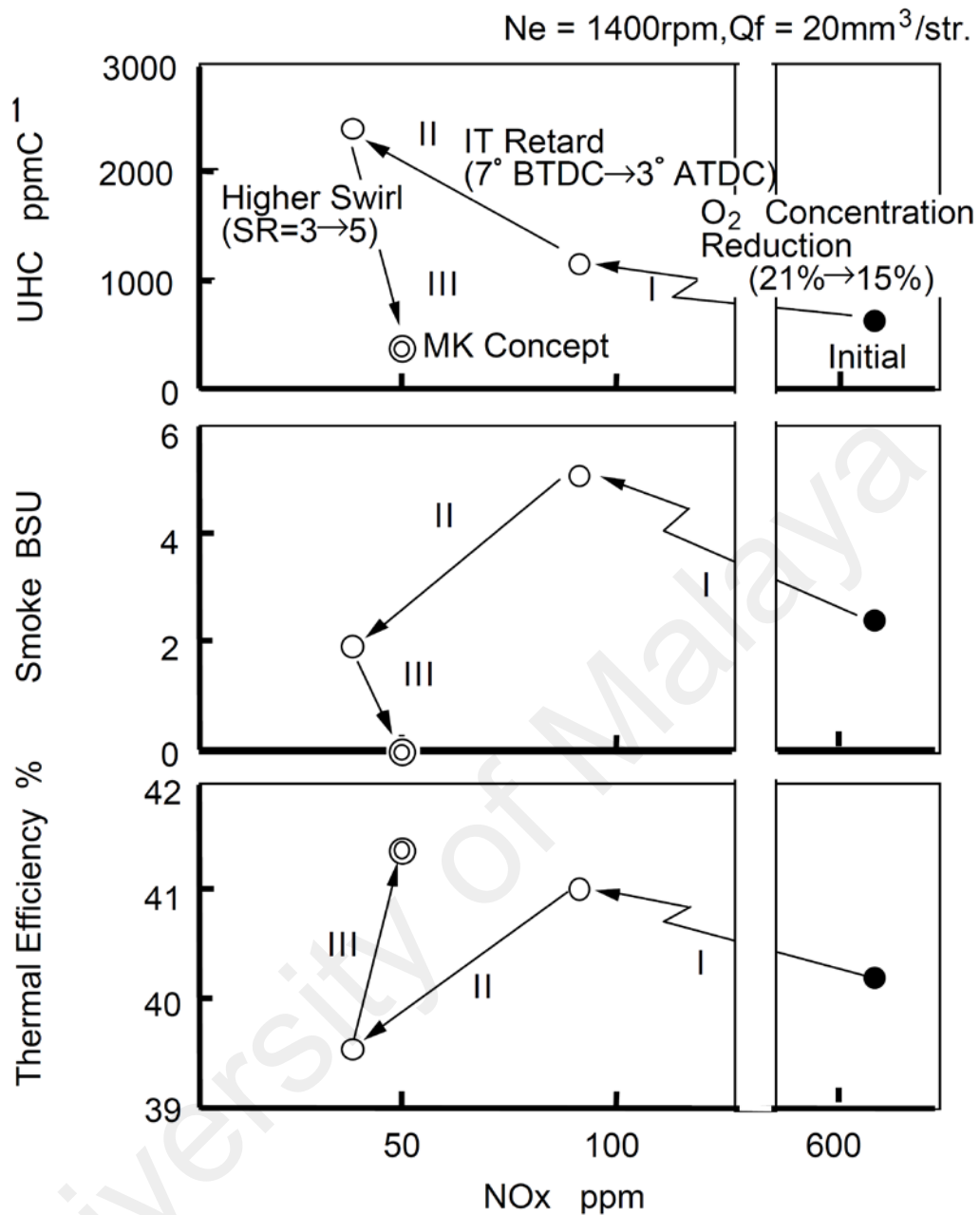


Figure 2.7: Nissan MK-concept: effects of EGR, retarded injection timing (IT) and increased swirl on exhaust emissions and thermal efficiency (Kimura et al., 2001).

Kawamoto et al. (Kawamoto et al., 2004) found that a low compression ratio was more effective in expanding the MK combustion region on the high-load side. The basic concept of MK combustion is explained schematically in Figure 2.8 (Kimura et al., 2002). Kimura et al. (Kimura et al., 1992) investigated the effects of combustion chamber insulation on both the heat rejection and thermal efficiency. The combustion chamber was insulated by using a silicon nitride piston cavity that was shrink-fitted into a titanium alloy

crown. The application of heat insulation reduced the angular velocity of the flame in the combustion chamber by about 10~20%. This reduction in the angular velocity of the flame was found to be one cause of combustion deterioration when the heat insulation was applied to the combustion chamber. The main advantage of the late direct injection system is combustion control by the injection timing over both the port fuel injection and the early direct injection systems.

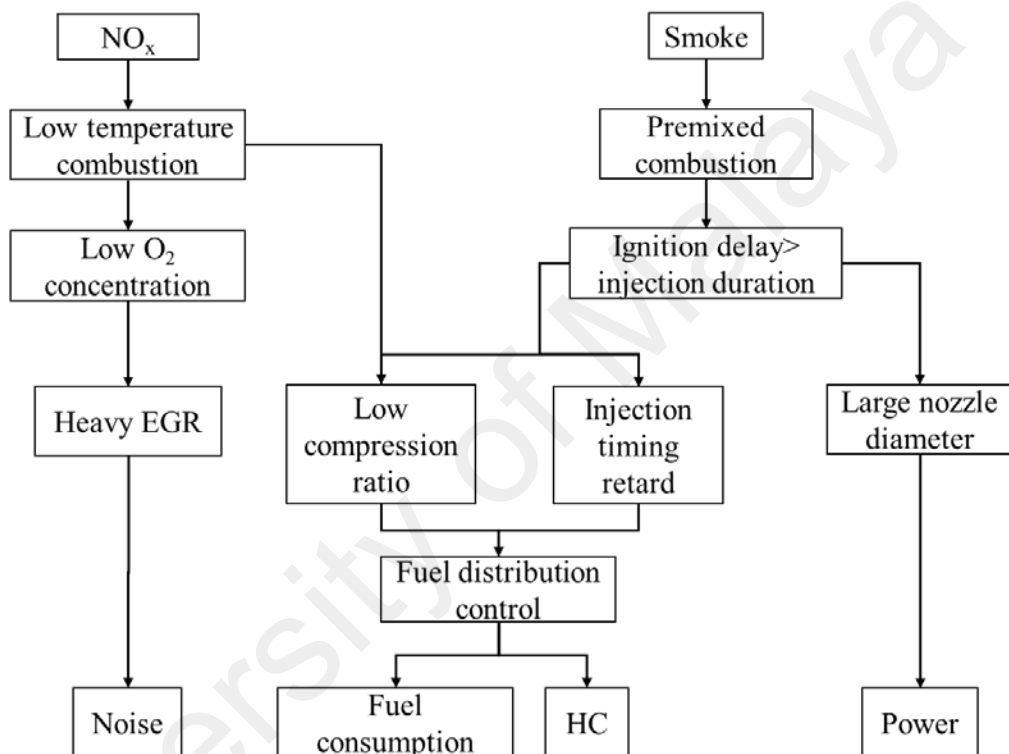


Figure 2.8: Schematic of the MK combustion concept (Kimura et al., 2002).

(c) **Narrow angle direct injection NADI™**

The angle between the spray must be reduced in order to avoid fuel deposition on the cold cylinder liner. The concept of narrow angle direct-injection (NADI) was suggested by Walter and Gatellier (Gatellier et al., 2001; Walter & Gatellier, 2003) to keep the fuel target within the piston bowl and avoid the interaction of the spray with the liner at advanced injection timing. The results indicated that the liquid fuel impingement on the bowl wall leads to fuel film combustion which is called “pool fire”. Because of the rich

air–fuel mixture and low temperature on the wall surface, the pool fire results in incomplete combustion and high soot formation for all early injection cases.

Kim and Lee (Kim & Lee, 2007) examined this strategy with a narrow fuel spray angle and dual injection. The fuel injection angle was narrowed from 156° of a conventional diesel engine to 60° , while the compression ratio was reduced from 17.8:1 to 15:1 to prevent the early ignition of the mixture. The results revealed that the NO_x emissions were greatly reduced as the injection timing was advanced beyond 30° BTDC and the IMEP indicated a modest decrease although the injection timing advanced to $50\text{--}60^\circ$ BTDC in the case of narrow spray angle configuration. Figure 2.9 graphically illustrates the narrow spray adoption in early in-cylinder direct injection. In early in-cylinder fuel injection, the spray direction adaption is important because the volume between the injector nozzle and piston is large. However, the main challenges facing NADITM engines are its limited operational range (Reveille et al., 2006) and increased NO_x emissions with increased injection pressures (Fang et al., 2008) as reported in some applications.

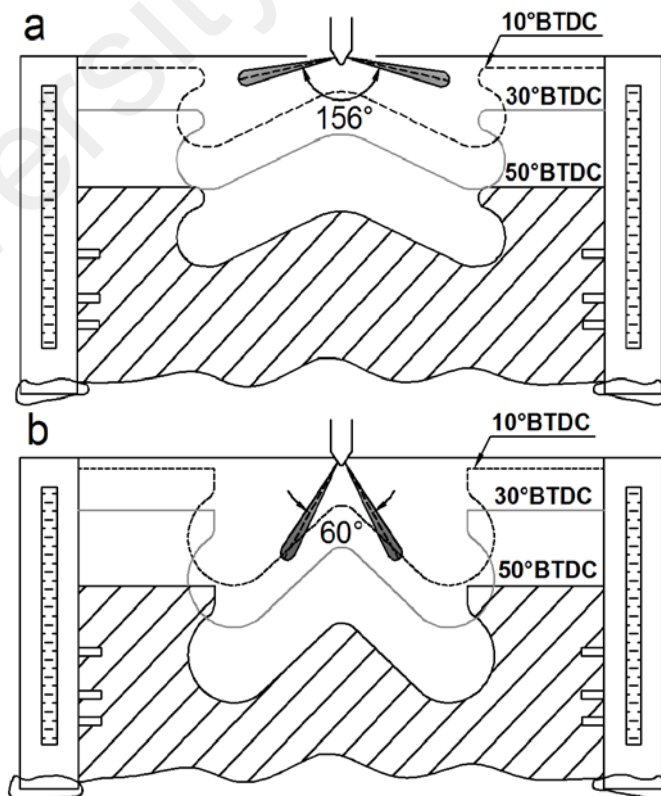


Figure 2.9: Schematic diagrams of the (a) conventional diesel engine. (b) NADITM for an early injection.

2.8 LTC control strategies

The combustion phase in LTC engines can be controlled either by altering time temperature history or by altering the mixture reactivity (Stanglmaier & Roberts, 1999). Figure 2.10 illustrates the methods of controlling LTC. The first group indicates the purpose of which is to alter the time–temperature history of the mixture. It includes fuel injection timing, variation of intake air temperature, variation of compression ratio (VCR) and variable valve timing (VVT). The second group attempts to control the reactivity of the charge by varying the properties of the fuel, the fuel–air ratio or the amount of oxygen by EGR. However, the homogeneous mixture preparation, prior to the start of ignition, is the primary goal of LTC which can be controlled (a) by increasing the degree of homogeneity; and (b) delaying auto-ignition.

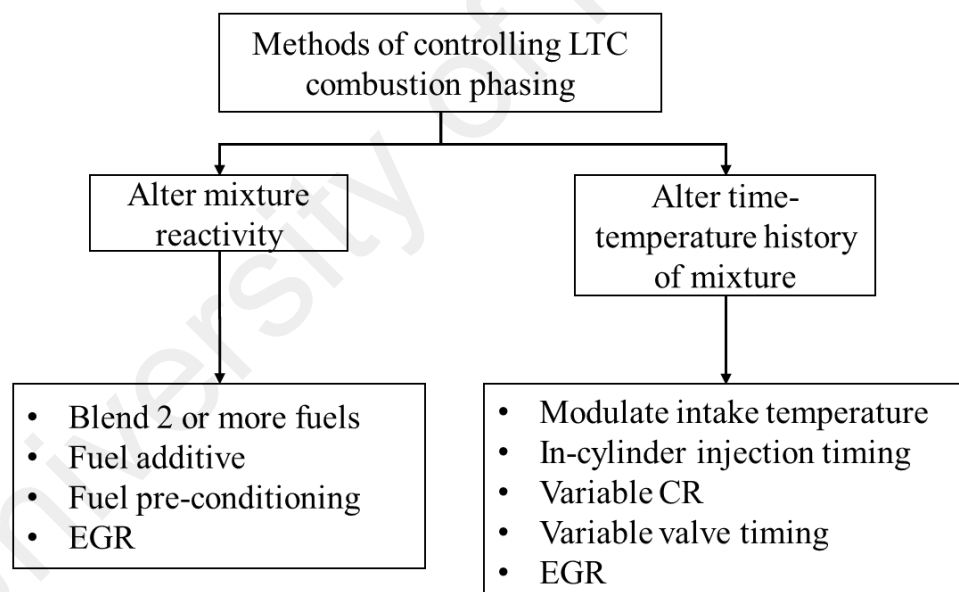


Figure 2.10: Methods for controlling LTC phasing (Stanglmaier & Roberts, 1999).

2.8.1 Exhaust gas recirculation (EGR)

EGR technology is widely used in LTC due to its high potential of controlling the auto-ignition of time–temperature history and enhancement of NO_x emission reduction (Nakano et al., 2000). The EGR can be categorized into internal and external EGR.

Internal EGR is achieved by the exhaust gas trap using the negative valve overlap (NVO) and VVT methods. The most practical means to delay the auto-ignition in LTC engine is through the addition of high levels of EGR into the intake. The inert gases present in the EGR can be used to control the heat release rate due to its impact on chemical reaction rate, which can delay the auto-ignition timing. Hence, EGR reduces the heat release rate, and thus lowers the peak cylinder temperature due to the constituents of EGR (mainly CO₂ and H₂O) having higher specific heat capacities. Although some studies have been carried out on LTC engines, as shown above, LTC has had no practical application to internal combustion engines. The biggest problem is the difficulty of the ignition timing control. Spontaneous combustion is dominated by the chemical reaction of the mixture which starts long before the auto-ignition occurs. The effects of EGR and water injection on the LTC were studied by Christensen and Johansson (Christensen & Johansson, 1998, 1999) using HCCI engine. Their results indicate that the ignition timing in a HCCI engine is delayed by these methods.

2.8.2 Fuel modification

The auto-ignition characteristics of the fuel–air mixture can be controlled with fuel blending or/and additives. For LTC engines, the volatility and auto-ignition characteristics of the fuel are important (Epping et al., 2002). Fuel requirements for HCCI engine operation by Rayn and Matheaus (Ryan & Matheaus, 2003) on constant volume combustion bomb experiments shows that the primary properties of fuel relate to the distillation characteristics and the ignition characteristics. Research octane number (RON) is a measure of fuel resistance to knock while motor octane number (MON) is a measure of how the fuel behaves when under load. Kalghatgi (Kalghatgi et al., 2003; Kalghatgi, 2005) developed an Octane Index (OI) (function of MON and RON) for measuring the auto-ignition or anti-knock quality of a practical fuel at different operating conditions. Kalghatgi's lower OI shows earlier combustion phasing. Shibata et al.

(Shibata et al., 2004, 2005) showed a relationship between RON and low temperature heat release (LTHR) which has a strong impact on high temperature heat release (HTHR). They studied 12 hydrocarbon constituents for LTC in which olefins and aromatics (except benzene) have a function to retard combustion phasing of LTHR while iso-paraffins and n-paraffins have a function to advance combustion of HTHR. The effects of cetane number (CN) on LTC performance, auto-ignition, and emissions were investigated by a number of researchers (Hosseini et al., 2011; Ickes et al., 2009; Li et al., 2006; Risberg et al., 2005; Szybist & Bunting, 2005). Aroonsrisopon et al. (Aroonsrisopon et al., 2002) found that LTC is a strong function of fuel composition and cannot be predicted by octane number. Shibata et al. (Shibata et al., 2004) demonstrated that the fuel chemistry directly affected by LTHR and the subsequent main combustion stage of HTHR. Bunting et al. (Bunting, Wildman, et al., 2007; Bunting, Crawford, et al., 2007) found high cetane fuels have stronger LTHR behaviour and do not require high intake temperature for auto-ignition. They concluded that low cetane fuels are more desirable for pure HCCI combustion (Bunting et al., 2009). The LTC of high octane fuel (iso-octane) shows single stage ignition while fuel blends shows two-stage ignition (Sjöberg & Dec, 2007). Figure 2.11 shows the single and two-stage heat release rates for iso-octane and PRF80.

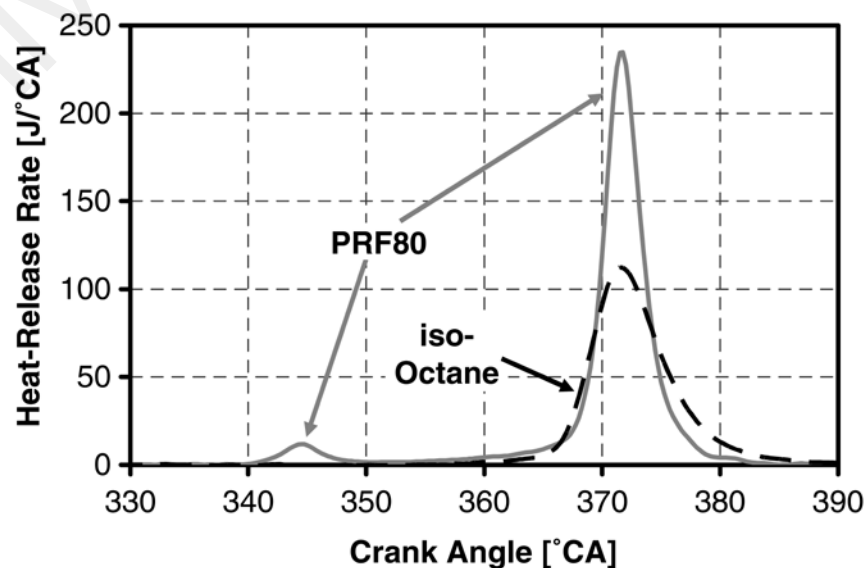


Figure 2.11: Heat-release traces for iso-octane and PRF80 (Sjöberg & Dec, 2007).

Experiments conducted by Bessonette et al. (Bessonette et al., 2007) suggested that the best fuel for HCCI-type operation may have auto-ignition qualities between those of diesel fuel and gasoline. Gasoline's resistance to auto-ignition can be exploited to extend the pre-combustion mixing time, but at low load poor auto-ignition qualities of gasoline can make it difficult to achieve combustion. Conversely, diesel fuel has better auto-ignition qualities, but requires high levels of EGR for appropriate combustion phasing as the engine load increases.

Inagaki et al. (Inagaki et al., 2006) investigated dual-fuel (premixed iso-octane and direct injected diesel) premixed compression ignition (PCI) operation with the goal of reducing the EGR requirements of PCI strategies. In that investigation, they were able to operate up to 12 bar IMEP in the PCI mode. From these studies, it can be concluded that different fuel blends could be required at different operating conditions, i.e. a high cetane fuel at light load and a low cetane fuel at high load. Thus, it is desirable to have the capability to operate with fuel blends covering the spectrum from neat gasoline to neat diesel fuel, depending on the operating regime. Accordingly, one strategy proposes the injection of low CN fuel (low reactivity fuel) in the intake port, and early cycle DI of high cetane number fuel (high reactivity fuel). This has been called RCCI by Kokjohn et al. (Kokjohn et al., 2009). The key feature of the dual fuel approach is the ability to control the combustion process by optimizing the reactivity of the blended fuels. This led to the terminology “reactivity controlled compression ignition” or RCCI, to differentiate the combustion process from HCCI or PCCI.

2.9 Diesel engine fuel delivery system

The conventional fuel injection system has some limitations such as injection pressure that depends on engine speed, maximum fuel pressure limitation, and difficulties in introduction of pilot fuel injection. These problems were resolved after the introduction

of the common-rail fuel injection system. Generally, there are two kinds of common-rail fuel injection systems in use today. One is the common-rail system that pressurizes the fuel and injects it directly into the cylinders. The world leading manufacturer of common-rail system such as DENSO, Robert Bosch, Siemens, and Delphi are the major suppliers of modern common-rail systems (Wikipedia, 2015). This system, which is undergoing further development, has been adopted in passenger car applications. The other system is the Hydraulic Electric Unit Injection (HEUI) system, developed by Caterpillar in the United States. This system uses pressurized engine oil to pressurize the fuel by actuating the piston of the nozzle (injector) through which the pressurized fuel is injected (Denso Corporation, 2007).

The development of the maximum injection pressure of heavy-duty engines over the last 30 years is presented in Figure 2.12. On an average, the pressure was increased from 800 (inline pump) to 2000 bar (high pressure fuel injection systems) in only three decades (Mahr, 2004). The fuel that is injected from the nozzle turns into finer particles as the fuel injection pressure increases. This enhances combustion and reduces the amount of smoke contained in the exhaust gases. As can be seen in Figure 2.13, initially the maximum injection pressure of the in-line pump (A type) and the distributor pump (VE type) was 60 MPa. Due to advancement in high-pressure applications, there are some recently developed fuel injection systems that inject fuel at a pressure of 100 MPa or higher. The second-generation common-rail system used in this study injects fuel at a considerably higher pressure of 180 MPa.

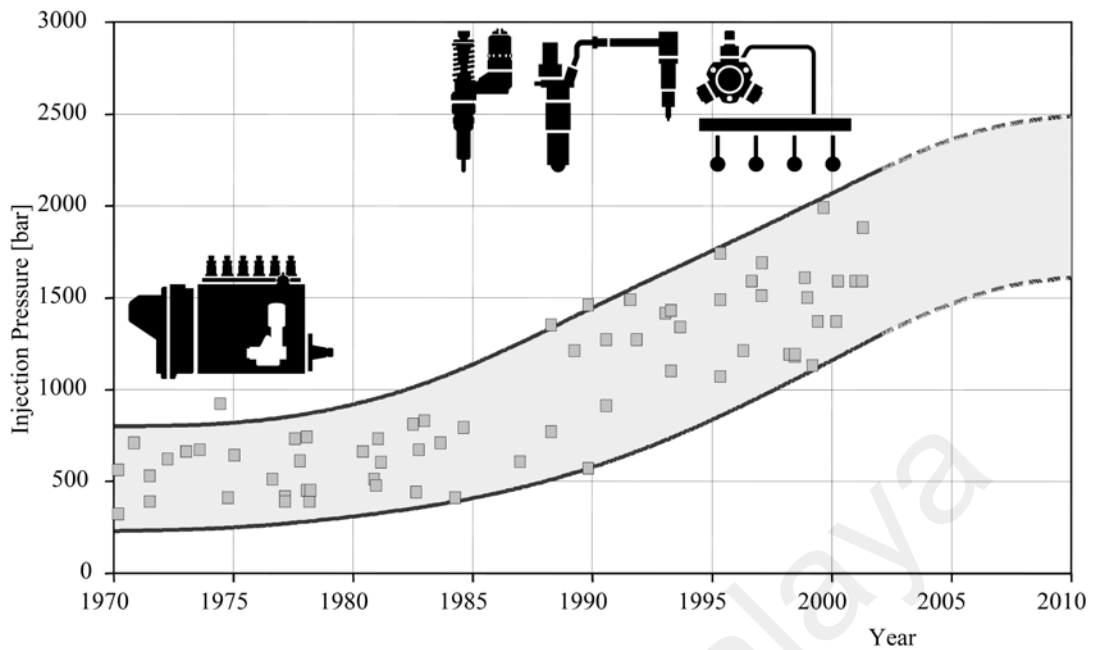


Figure 2.12: Development of injection pressure of diesel engine (Mahr, 2004).

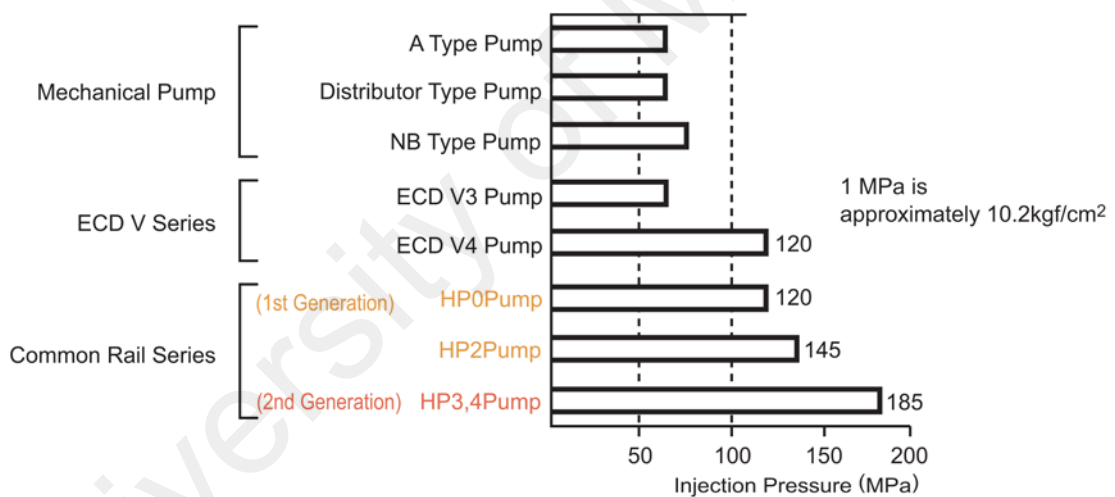


Figure 2.13: Comparison of injection pressures (Denso Corporation, 2007).

The specification for all diesel engines is increasingly restricted with regard to exhaust gas limits, fuel consumption, noise and costs, accompanied by increasing demands on drivability, lifetime, power output, service and diagnosis (see Figure 2.14). When applying EGR or increased rated speed to a heavy-duty diesel engine, higher maximum injection pressures are essential. Additionally, a lower Sulphur diesel fuel is necessary to achieve future more stringent exhaust gas limits. The flexible diesel fuel injection system is assisting this development with the measures multiple injection, rate shaping of the

main injection and an increased maximum injection pressure. Furthermore, high efficiency of the injection system itself is important. New developments on actuators (new solenoid and piezo technique), nozzle design, ECU control strategies and exhaust gas after treatment are key factors for future diesel engine technology.

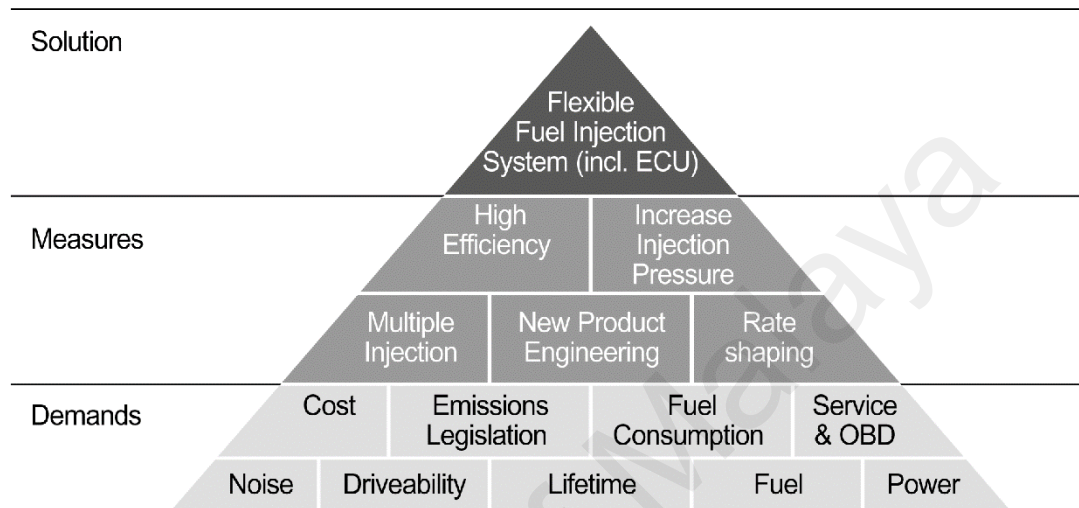


Figure 2.14: Key factors for diesel fuel injection system development (Mahr, 2004).

2.10 Diesel fuel injection system conversion

The problems of the conventional mechanical type pump-line-nozzle injection system with fixed injection timing are well known, with their low combustion efficiency and high exhaust emissions. The conventional injection system leaves little room for engine performance optimization to be tailored to biodiesel fuels since the injection process, controlled by the camshaft, is dependent on the engine speed. In a DI diesel engine, the fuel injection system (including the injection nozzles and pump) plays a vital role because it directly affects the performance of the engine. Several desired demands are: higher injection pressure, optimized injection rate, higher precision of injection timing control, and higher precision of injection quantity control, which could significantly affect the mixture formation and combustion quality of the diesel engine. In fact, all of these injection system parameters must be controllable especially for alternative fuel research

studies. In general, commercially available single-cylinder engines are equipped with a mechanical fuel injection system and most of the injection parameters cannot be readily changed. Utilizing electronically controlled fuel injection through a common-rail injection system instead of the conventional mechanical injection permits continuous control of injection timing and injection quantity to a high level of precision. This technology also offers the highest levels of flexibility for the control of both the injection timing and injection amount, while still yielding significantly better results than any conventional injection system. Some of the key features that differentiates the common-rail system from the conventional mechanical pump-line-nozzle system are shown in Table 2.5. It is evident that the common-rail injection technology brings more advantages than disadvantages to a DI diesel engine. These merits are applicable for both the single and multi-cylinder engines applications, due to its capability of enhanced combustion process on an individual cylinder basis. In fact, single-cylinder engines have many attractive attributes for use in research, due to their low cost, flexibility, and easy access for instrumentation.

For engines equipped with common-rail injection technology, the fuel injectors are typically ECU controlled. There are various studies focused on the conversion of mechanically controlled fuel injection systems to an electronic common-rail system and efforts are being made in the design of the engine controller unit. In the study by Ergenç and Koca (Ergenç & Koca, 2014), the test engine which was initially equipped with mechanical injection, has been modified and converted into a test engine with a common-rail injection system. All injectors (LPG and diesel) in their study were also controlled by programmable logic controllers (PLC) which served as an ECU for control applications. Likewise, in another study performed by Goldwine (Goldwine, 2008), a dedicated common-rail injection single-cylinder air-cooled diesel engine was converted from a mechanical injection design, and most of the parts of the injection system were adopted

from regular diesel engine parts. A piezoelectric type injector was employed in their study and multiple data acquisition/control cards were used as an ECU for the control of fuel injection, injection pressure and engine load. The software was written in LabVIEW and the algorithm implemented closed loop control for the engine speed (through load regulation) and fuel pressure. The piezoelectric injector used in their study has the ability to implement up to six injections per cycle with various lengths and dwell times.

Table 2.5: Comparison of the common-rail fuel injection system with the conventional mechanical pump-line-nozzle system.

Type of fuel injection system	Advantages	Disadvantages
Common-rail system	<ol style="list-style-type: none"> 1. Fuel pressure available on demand and independent of engine speed and load conditions. 2. Provide higher injection pressure and finer atomization of fuel. 3. Lower fuel pump peak torque requirements. 4. Flexibility in controlling injection timing and injection rate. 5. Improves the air fuel mixture formation. 6. Delivers a more controlled quantity of atomized fuel, which leads to higher performance, better fuel economy, reduction of overall exhaust emissions and particulate emissions, lower levels of noise and vibration. 7. Multiple injections per cylinder combustion are possible. 	<ol style="list-style-type: none"> 1. The system and design setup is relatively expensive and would increase vehicle cost. 2. High degree of engine maintenance and costly spare parts.
Mechanical pump-line-nozzle system	<ol style="list-style-type: none"> 1. Lower cost compared to common-rail system. 	<ol style="list-style-type: none"> 1. Poor pressurization and atomization results. 2. Timing and rate control are limited and fixed in camshaft geometry.

CHAPTER 3: RESEARCH METHODOLOGY

3.1 Introduction

This chapter presents the research methodology and the experimental setup for achieving the four major objectives of the current research work. The detailed schematic of the research methodology is shown in Figure 3.1 and the test details including test conditions are tabulated in Table 3.1. As can be seen, the experimental setup, which consisted of test cell system setup, combustion analyzer system development, ECU system development, common-rail fuel supply system, EGR system development and port fuel injection system development, was established to accomplish the objectives of the research study. Besides, neat biodiesels, biodiesel blended fuels and baseline petroleum diesel fuel were used as a direct injected fuel. Whereas, gasoline fuel was used as the port injected fuel for dual-fuel combustion study. In addition, three types of NO_x reduction strategies, such as introduction of EGR, in-cylinder fuel injection timing variation, and dual-fuel low temperature combustion were considered in the present study. The engine-out-responses parameter analysis included the aspects of engine performance, emissions and combustion pressure.

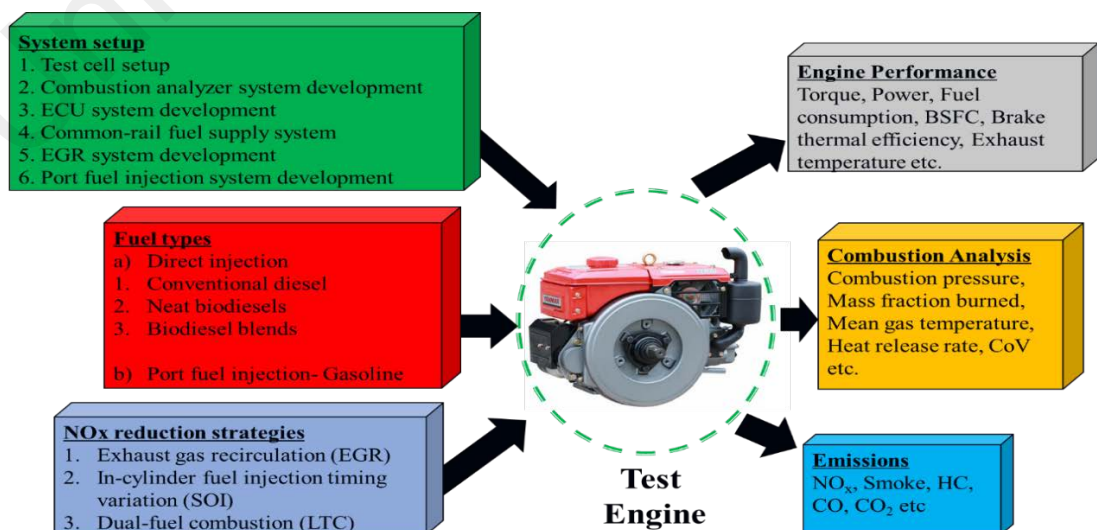


Figure 3.1: Schematic representation of the research methodology.

Table 3.1: Engine test details.

No.	Type of test	Fuel type	Load	Speed (rpm)	Fuel injection parameters	EGR setting	Measurement
1	Engine-out responses of the converted common-rail fuel injection system	Diesel	i. 25% ii. 50% iii. 75% of load	i. 1000 ii. 1500 iii. 2000	i. SOI timing variation from 0° BTDC to 22° BTDC, single injection, P=600 bar. ii. Rail pressure variation from 300 bar to 1800 bar, single injection, at optimal SOI timing, various speeds. iii. Single, double and triple injection strategies.	No EGR	i. Torque ii. BTE iii. Rail pressure response iv. NO _x , Smoke v. Combustion pressure
2	Effect of biodiesel blends on common-rail diesel engine	i. Diesel ii. JB10 iii. JB30 iv. JB50 v. JB100 vi. PB10 vii. PB30 viii. PB50 ix. PB100	i. 0.1 ii. 0.2 iii. 0.3 iv. 0.4 v. 0.5 vi. 0.6 MPa of BMEP	1500	i. SOI = 17° BTDC ii. Rail pressure = 600 bar	No EGR	i. BSFC ii. BTE iii. CO, NO _x , Smoke iv. Exhaust gas temperature (EGT) v. Combustion pressure vi. Engine vibration
3	Effect of fuel injection timing variation with biodiesel	i. Diesel ii. Neat PME	Constant BMEP of 0.4 MPa	1500	i. SOI timing variation from 0° BTDC to 25° BTDC ii. Rail pressure = 600 bar	No EGR	i. BSFC ii. BTE iii. NO _x , Smoke iv. EGT v. Combustion pressure

Table 3.1: Engine test details, continued.

No.	Type of test	Fuel type	Load	Speed (rpm)	Fuel injection parameters	EGR setting	Measurement
4	Effect of EGR variation with biodiesel	i. Diesel ii. Neat PME	Constant BMEP of 0.4 MPa	1500	i. SOI = 11° BTDC ii. Rail pressure = 600 bar	i. 0% ii. 10% iii. 20% iv. 30% v. 35% vi. 40% vii. 45% viii. 50%	i. BSFC ii. BTE iii. O ₂ , NO _x , Smoke iv. Intake and exhaust CO ₂ v. Combustion pressure
5	Effect of dual-fuel combustion with injection timing variation	i. Diesel/Gasoline ii. Neat PME/Gasoline	i. Constant equivalent fuel energy = 760 J ii. Premixed ratio = 0.6	1500	i. SOI timing variation from 5° BTDC to 95° BTDC ii. Rail pressure = 600 bar	30%	i. BSFC ii. BTE iii. NO _x , HC, CO iv. Combustion pressure
6	Effect of dual-fuel combustion with EGR variation	i. Diesel/Gasoline ii. Neat PME/Gasoline	i. Constant equivalent fuel energy = 760 J ii. Premixed ratio = 0.6	1500	i. SOI timing variation from 5° BTDC to 95° BTDC ii. Rail pressure = 600 bar	i. 30% ii. 35% iii. 40% iv. 45% v. 50%	i. ISFC ii. BTE iii. NO _x , HC, CO, Smoke iv. Combustion pressure

3.2 Biodiesel selection

In the present investigation, biodiesel selection was primarily made based on the ready availability of feedstock in Malaysia and their favorable fuel properties. The transesterification process, fuel blending and analysis of most of the fuel properties were carried out at the Department of Mechanical Engineering, University of Malaya.

Recently, the cost-effectiveness of biodiesel production has become a new topic for debate. From an economic point of view, the use of the most cost-effective biodiesel feedstock will pave the way for large-scale production of biodiesel. By far, the three most common available biodiesel feedstocks are palm oil (from Malaysia), soybean (from US) and rapeseed (from EU) and their production costs are USD \$ 684, \$751 and \$ 996 a tonne (Lam et al., 2009). Apparently, palm oil offers the most cost competitiveness and it is a viable biodiesel feedstock. Furthermore, palm oil has been cited as a high-yield source of biodiesel with an average yield of approximately 5,950 litres per hectare, which is nearly 13 times better than the yield of soybean oil (Ong et al., 2011).

Besides, the potential of using *Jatropha* as an alternative non-edible feedstock for biodiesel production has attracted a lot of attention recently. To minimize dependency on consuming a biodiesel fuel that is primarily sourced from crude palm oil, the biodiesel policy of the Malaysian government recommended the utilization of non-edible oils for the production of biodiesel. *Jatropha curcas* oil is one of the major non-edible, tree-borne feedstocks used for the large scale production of biodiesel in Malaysia and South East Asia; this is because it is well adapted to local climatic conditions and is available in surplus quantities across the region (Lim & Teong, 2010; Mofijur et al., 2012).

In consequence of the advantages above-mentioned, it is clear that biodiesel derived from palm and *Jatropha* oil are viable alternative options for petroleum diesel fuel. On this

basis, both have been selected in this study for testing in a common-rail injection diesel engine.

3.3 Test fuels

In this study, fossil diesel fuel, gasoline, palm oil and Jatropha oil were obtained in commercial form. There are numerous ways to convert vegetable oil into biodiesel fuel, such as pyrolysis, microemulsion, dilution, and transesterification. Of these different conversion methods, the transesterification process is the most popular method and has been extensively used to reduce the viscosity of crude vegetable oil and convert triglycerides into esters and glycerol. Figure 3.2 shows the transesterification reaction of triglycerides. A catalyst is typically employed to enhance the reaction rate and yield. As the reaction is reversible, excess alcohol is used to shift the equilibrium toward the product side (right side).

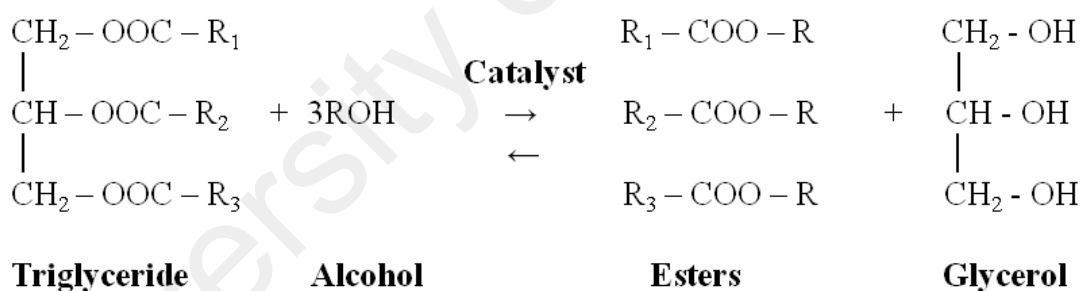


Figure 3.2: Transesterification of triglycerides with alcohol.

Biodiesel production in this study was conducted via transesterification process. Firstly, crude oil was transferred into a preheated reactor at a temperature of 60 °C. The oil was reacted with 25% (v/v oil) methanol and 1% by weight of alkali catalyst (KOH). The reaction mixture was maintained at 60 °C for 2 hours with stirring at the constant speed of 800 rpm. After the completion of the reaction, the produced methyl esters were poured into a separation funnel for 24 hours to separate the glycerol from the biodiesel. The lower layer, which consists of impurities and glycerin, was drawn off. Then, the methyl ester

was washed with warm distilled water and evaporated with a rotary evaporator at 65 °C for 30 minutes to remove residual methanol and water. Lastly, the methyl ester was dried using Na₂SO₄ and filtered using qualitative filter paper to collect the final product.

Upon completion of the transesterification process, the fuel properties of the produced methyl ester were examined and compared with the biodiesel standards. Table 3.2 contains a description of the key physicochemical properties of the converted neat palm methyl ester (PME), Jatropha methyl ester (JME) and biodiesel blends in comparison with the ASTM standard. The important properties of petroleum diesel and gasoline are also listed in this table. It can be observed that the physicochemical properties of the produced biodiesel were measured and benchmarked against the biodiesel standards based on ASTM D6751. It appears that all of the physicochemical properties of PME and JME are sufficient to meet the ASTM biodiesel standard. In particular, the kinematic viscosity of the transesterified palm and Jatropha oil was substantially improved, but it was slightly higher than that of petroleum diesel. In addition, the flash point for PME and JME was relatively higher than that of petroleum diesel and are suitable for use as transportation fuels. However, the calorific value of the PME and JME was lower than that of petroleum diesel.

Another key property that significantly influences engine performance, emissions, and combustion characteristics is the cetane number of fuel. It can be observed that PME and JME have a higher cetane number than petroleum diesel fuels. Further, the distillation characteristics also have important effects on engine combustion and performance. Typically, the distillation temperature is used as a quality check for fuel and the distribution range provides an insight into the volatility, flash point and fatty acid composition. Biodiesel tends to shift the distillation curve towards higher boiling points than petrol-diesel, especially in the T_{50} region (Alptekin & Canakci, 2009). In this study,

the full ranges of the distillation temperatures of the fuel samples T_x , where “ x ” stands for distillation temperatures corresponding to x vol % of the distilled and condensed liquid fuel were measured by a distillation temperature analyzer (Anton Paar ADU 5, Anton Paar Strasse 10, 8054 Graz, Austria). As can be seen, the distillation temperature of T_{50} for PME, JME and diesel fuel are 327.0 °C, 334.0 °C and 298.5 °C. A higher distillation temperature may shorten the ignition delay of the fuel, thus increasing the cetane number and decreasing the probability of the occurrence of knocking in diesel engines (Lin & Li, 2009b).

In addition, the fatty acid composition of PME and JME was measured by a gas chromatography/ flame ionization detector (GC/ FID). The GC/ FID operating conditions are given in Table 3.3. The analysis of fatty acids was based on AOAC 996.06 official methods. The results of the fatty acid composition of PME and JME fuel in comparison with other studies are shown in Table 3.4. It can be observed that PME contained a moderate level composition of saturated (44.87%) and unsaturated (55.14%) fatty acids, in which the level of saturated fatty acids is almost equal to that of the unsaturated fatty acids. On the other hand, the JME contains a saturation-unsaturation ratio of 23.27:76.73, in which the level of unsaturated fatty acids is about 3-fold higher than that of saturated fatty acids. In fact, the distribution of fatty acid compositions for PME (Ng et al., 2011) and JME (Atabani et al., 2013) from other study is found to be in very close agreement with this study.

Table 3.2: Fuel properties of petroleum diesel, gasoline, PME, JME and biodiesel blends.

Properties	Unit	Diesel fuel	Biodiesel			Gasoline	
			Limit (ASTM D6751)	Test method	PME		JME
Kinematic viscosity @ 40°C	mm ² /s	3.34	1.9-6.0	D445	4.4	4.42	0.567
Density @ 15°C	kg/L	0.8527	0.88	D4052	0.8773	0.8827	0.7423
Acid number	mg KOH/g	0.12	0.5 max	D664	0.2	0.37	-
Calorific value	MJ/kg	45.31	-	D240	39.98	39.9	43.5
Flash point	°C	71.5	130 min	D93	155.5	178.5	-36
Pour point	°C	-6	-	D97	9	3	-
Cloud point	°C	7	-	D2500	13	5	-
Carbon	% wt	86.1	-		76.3	76.5	78.3
Hydrogen	% wt	13.8	-	D5291	13.2	13.0	12.7
Nitrogen	% wt	<0.1	-		<0.1	<0.1	<0.1
Oxygen	% wt	0.1	-	calculation	10.5	10.4	9.0
Copper strip corrosion (3 Hrs @ 50°C)	-	1a	No. 3 max	D130	1a	1a	1a
Distillation, °C:							
Initial boiling point		165.5	N/S		296.5	125.0	36.0
5% recovery		220.0	N/S		323.5	324.0	52.5
10% recovery		240.0	N/S		324.0	329.0	58.0
20% recovery		262.5	N/S		324.5	331.0	66.0
30% recovery		276.5	N/S		325.5	332.0	74.5
40% recovery	°C	288.5	N/S	D86	326.0	333.0	84.0
50% recovery		298.5	N/S		327.0	334.0	95.5
60% recovery		309.0	N/S		328.0	335.0	108.0
70% recovery		320.0	N/S		329.5	337.0	120.0
80% recovery		333.0	N/S		331.5	340.0	134.5
90% recovery		351.0	360 max		336.5	345.0	154.0
Final boiling point		374.0	N/S		346.0	345.0	195.5
Oxidation stability @ 100°C	hours	>40	3 min	EN14112	15	6.5	-
Cetane number	-	52	47 min.	D6890	61	58	-

N/S= Not Specified

Table 3.2: Fuel properties of petroleum diesel, gasoline, PME, JME and biodiesel blends, continued.

Properties	Unit	Biodiesel blends							
		Limit ASTM D7467	Test method	JB10	JB30	JB50	PB10	PB30	PB50
Kinematic viscosity @ 40°C	mm ² /s	1.9-4.1	D445	3.62	3.73	3.90	3.66	3.68	3.98
Density @ 15°C	kg/L	0.858 max	D127	0.8582	0.8642	0.8713	0.8551	0.8598	0.8647
Acid number	mg KOH/g	0.3 max	D664	0.17	0.23	0.27	0.15	0.20	0.23
Calorific value	MJ/kg	35 min	D240	44.84	43.66	42.57	44.65	43.33	42.04
Flash point	°C	52 min	D93	87.5	96.5	103.5	74.5	79.5	85.5
Pour point	°C	N/S	D97	-6	-6	0	0	3	3
Cloud point	°C	N/S	D2500	6	6	7	8	5	4
Distillation, °C:									
Initial boiling point		N/S		158.5	161.0	180.0	167.5	173.5	181.5
5% recovery		N/S		222.0	235.0	232.0	220.0	236.5	254.5
10% recovery		N/S		244.0	256.5	265.0	245.0	258.5	276.0
20% recovery		N/S		266.5	280.0	293.0	267.5	280.0	295.5
30% recovery		N/S		281.5	294.5	308.0	282.5	294.0	307.0
40% recovery	°C	N/S	D86	293.5	307.0	316.0	294.0	305.5	315.0
50% recovery		N/S		304.1	315.5	322.0	304.5	314.0	321.0
60% recovery		N/S		314.0	323.0	327.0	314.0	321.0	324.5
70% recovery		N/S		323.5	329.5	332.0	323.5	327.0	328.5
80% recovery		N/S		333.0	335.5	336.0	333.5	333.5	333.0
90% recovery		343		347.0	345.0	342.0	347.5	344.0	341.5
Final boiling point		N/S		367.5	362.0	349.0	369.0	364.5	356.0
Cetane number	-	52 min	D6890	53.0	54.0	56.0	55.0	57.0	59.0
Oxidation stability @ 100°C	hours	6 min	EN14112	18.6	12.8	10.8	30.4	22.5	18.8

N/S = Not Specified

Table 3.3: GC/FID operating conditions.

Property	Specification
Carrier gas	Hydrogen
Flow rate of carrier gas	1 ml/min
Column	Agilent HP-88 (60m x 0.25 mm ID, 0.2mm)
Inlet temperature	250 °C
Initial temperature	120 °C
Initial holding time	1 minute
Oven ramp conditions	1 st ramp 10°C / min to 175°C (hold 10 min)
	2 nd ramp 5°C /min to 210°C (hold 5 min)
	3 rd ramp 5°C/min to 230°C (hold 5 min)
Type of detector	FID
Split ratio	50:1
FID detector temperature	260 °C
Injection volume	1 µL

Table 3.4: Fatty acid composition of neat PME and JME fuel.

Property	Formula	PME	PME (Ng et al., 2011)	JME	JME (Atabani et al., 2013)
Carbon chain length distribution (wt.%)					
Saturated fatty acid					
C4:0 (Butyric acid)	C ₄ H ₈ O ₂	0.15	N/D	0.19	N/D
C6:0 (Caproic acid)	C ₆ H ₁₂ O ₂	0.08	N/D	0.39	N/D
C8:0 (Caprylic acid)	C ₈ H ₁₆ O ₂	0.21	N/D	0.09	N/D
C10:0 (Capric acid)	C ₁₀ H ₂₀ O ₂	0.18	N/D	N/D	N/D
C12:0 (Lauric acid)	C ₁₂ H ₂₄ O ₂	1.56	0.2	0.13	N/D
C14:0 (Myristic acid)	C ₁₄ H ₂₈ O ₂	1.4	0.9	0.12	1.4
C15:0 (Pentadecanoic acid)	C ₁₅ H ₃₀ O ₂	0.05	N/D	N/D	N/D
C16:0 (Palmitic acid)	C ₁₆ H ₃₂ O ₂	36.74	43.7	15.25	15.6
C17:0 (Heptadecanoic acid)	C ₁₇ H ₃₄ O ₂	0.1	N/D	0.09	N/D
C18:0 (Stearic acid)	C ₁₈ H ₃₆ O ₂	4.23	4.5	7.01	9.7
C20:0 (Arachidic acid)	C ₂₀ H ₄₀ O ₂	0	0.3	N/D	0.4
C21:0 (Heneicosanoic acid)	C ₂₁ H ₄₂ O ₂	0.07	N/D	N/D	N/D
C24:0 (Lignoceric acid)	C ₂₄ H ₄₈ O ₂	0.1	N/D	N/D	N/D
Unsaturated fatty acid					
C16:1n7 (Palmitoleic acid)	C ₁₆ H ₃₀ O ₂	0.19	N/D	0.85	N/D
C18:1n9t (Elaidic acid)	C ₁₈ H ₃₄ O ₂	0.7	N/D	0.59	N/D
C18:1n9c (Oleic acid)	C ₁₈ H ₃₄ O ₂	41.9	39.7	40.66	40.8
C18:2n6c (Linoleic acid)	C ₁₈ H ₃₂ O ₂	10.03	10	32.78	32.1
C18:2n6t (Linolelaidic acid)	C ₁₈ H ₃₂ O ₂	0.31	N/D	N/D	N/D
C18:3n6 (γ -Linoleic acid)	C ₁₈ H ₃₀ O ₂	0.42	N/D	0.23	N/D
C18:3n3 (Linolenic acid)	C ₁₈ H ₃₀ O ₂	0.19	N/D	0.21	N/D
C20:1 (<i>cis</i> -11-Eicosenoic acid)	C ₂₀ H ₃₈ O ₂	0.19	N/D	0.14	N/D
C20:2 (<i>cis</i> -11,14-Eicosadienoic acid)	C ₂₀ H ₃₆ O ₂	1.13	N/D	0.93	N/D
C20:3n6 (<i>cis</i> -8,11,14-Eicosatrienoic acid)	C ₂₀ H ₃₄ O ₂	0.08	N/D	0.34	N/D
Fatty acid saturation /unsaturation ratio (wt.%/wt.%)		44.87/	49.6/	23.27/	27.1/
		55.14	49.7	76.73	72.9

N/D= Not detected

3.4 Engine operating conditions

Generally, the test program in this study comprises of four series of tests to assess for the following effects:

- i. Effect of the converted common-rail fuel injection system on engine-out responses;
- ii. Effect of biodiesels and its blends on the common-rail diesel engine;
- iii. Effect of fuel injection timing and EGR variation with biodiesel;
- iv. Effect of dual-fuel combustion with injection timing and EGR variation.

In the first test series, the test program is sub-divided into three series of tests to evaluate the performance of the developed fuel injection system control, including precise control of SOI timing and opening duration for pilot, main and post injections, as well as injection pressure control. In the first sub series, the effect of fuel injection timing (0° BTDC to 22° BTDC) on performance, emissions and combustion characteristics of the modified diesel engine was investigated. The experiments were conducted at different speed and load conditions, with single injection approach, and at a constant injection pressure of 600 bar. In the second sub series, the effect of injection pressure variation (300 – 1800 bar) on engine-out-responses was investigated. The experiments were conducted at various speed conditions, 50% load, with single injection approach, and at optimal SOI timing of 4° , 12° and 16° BTDC at 1000, 1500 and 2000 rpm, respectively. In the third sub series, the effect of injection strategies, including double injection of pilot and main, triple injection of pilot, main and post under various fuel injection pressures were studied. In this test scheme, the engine speed was set constantly at 1500 rpm with 50% load and at pilot, main, and post SOI of 30, 12, and -5° BTDC, respectively.

In the second test series, the experiment was conducted at a constant speed of 1500 rpm, with varying BMEP (i.e. 0.1, 0.2, 0.3, 0.4, 0.5, and 0.6 MPa), SOI of 17° BTDC, with single injection approach and injection pressure of 600 bar. These six test points were selected as the most representative of a wide variety of engine load ranges. Initially, diesel fuel was used as the baseline fuel for the basis of comparison. Following this, mixtures of diesel and methyl ester (PME and JME) with 10, 30, and 50% volumetric proportions, as well as neat biodiesels were tested. Consequently, a total of 54 runs experimental conditions, including baseline diesel were tested in this test series. When the engine was fuelled with neat methyl ester and its blended fuels, the engine ran satisfactorily throughout the entire test, which was performed at room temperature, and had no starting difficulties.

In the third test series, all experiments were conducted at a constant speed of 1500 rpm and injection pressure of 600 bar. This test program was further sub-divided into two series of tests to assess the effects of biodiesel fuel on engine performance, emissions and combustion characteristics. Firstly, the effect of fuel injection timing variation on the performance, emissions and combustion characteristics of the engine operating in conventional compression ignition mode was investigated. At constant BMEP of 0.4 MPa and without EGR, start-of-injection (SOI) timing was varied from 0° BTDC to 25° BTDC. In the later test series, the EGR rate was varied from 0% to 50% at a constant BMEP of 0.4 MPa and SOI of 11° BTDC. This SOI timing was confirmed based on the peak brake thermal efficiency as found in the previous test series. In each series of tests, diesel fuel was used as the baseline fuel for the basis of comparison. When the engine was fuelled with biodiesel fuel, the engine ran satisfactorily throughout the entire test, which was performed at room temperature, and had no starting difficulties.

In the fourth test series, the experiment was conducted at a constant speed of 1500 rpm and injection pressure of 600 bar. Two kinds of dual-fuel experiments, i.e. the DI diesel with PFI gasoline (diesel/gasoline) and DI PME fuel with PFI gasoline (PME/gasoline) are compared in terms of performance, emissions, and combustion characteristics. Gasoline was port fuel injected onto the opened intake valve at 360° BTDC. Experiments were performed at five EGRs, 30, 35, 40, 45 and 50%. At each EGR level, SOI timing was varied from 5° BTDC and advanced up to the point at which potential unstable combustion starts to occur. For each type of DI fuel, the injection quantity was set to 6.5 mg/stroke for baseline diesel fuel and 7.6 mg/stroke for PME fuel, respectively. Considering the lower calorific value of PME fuel compared to baseline diesel, higher injection quantity necessary to ensure equivalent fuel energy was injected for every cycle. In this study, the gasoline ratio was maintained at 0.6 for both direct injected diesel and PME dual-fuel combustion. In addition, the total supplied fuel energy is approximately 760 J/cycle. In each test, diesel fuel was used as the baseline fuel for comparison. When the engine was fuelled with biodiesel fuel, the engine ran satisfactorily throughout the entire test, which was performed at room temperature, and had no starting difficulties.

All tests as described above were performed under steady-state conditions with a sufficiently warmed exhaust gas and water coolant temperature. To enhance the accuracy of the study, each test point was repeated twice to produce average readings. The reproducibility of the data was matched over 95% for each test.

3.5 Test engine

The test engine used in this study was a modified water-cooled, single-cylinder, compression ignition diesel engine (YANMAR TF-120E) (shown in Figure 3.3). Originally, the engine was equipped with a regular fuel injection system consisting of a mechanical type of pressure fuel pump (200 bar) timed by the camshaft, and a mechanical fuel injector with an injection angle of 150° and four 0.26 mm diameter holes. The engine was naturally aspirated with a maximum output of 7.5 kW. The original fuel injection timing was constant and set to 17° BTDC. The engine was originally equipped with a mechanical governor to control the engine speed. The specifications of the test engine are listed in Table 3.5.

Table 3.5: Characteristics of single-cylinder engine.

Parameter		Units
Displacement	638	cm ³
Bore	92	mm
Stroke	96	mm
Compression ratio	17.7:1	
Rated power	7.8	kW
Rated speed	2400	rpm
D/H _{bowl}	2.81	
Combustion chamber	Re-entrant type	



Figure 3.3: Single cylinder diesel engine.

3.6 Common-rail fuel injection system conversion

The original mechanical type fuel injection system of the test engine was disassembled and a new common-rail injection system was retrofitted. The specifications of the retrofitted test engine are listed in Table 3.6 and the schematic diagram of the experimental setup is shown in Figure 3.4. The system was based on commercially available common-rail diesel engine components. The major components of a common-rail fuel injection system include:

- i. Fuel rail and supply pump
- ii. Engine controller unit (ECU)
- iii. Fuel injector

The design, development and system integration of the above mentioned components are described in the following sections.

Table 3.6: Specifications of the retrofitted test engine.

Parameter	Before Modification	After Modification
Model	YANMAR TF-120E	
Displacement	638 cm ³	
Bore x Stroke	92 mm x 96 mm	
Compression ratio	17.7:1	
Rated power	7.8 kW @ 2400 rpm	
Fuel injection system	Mechanical cam driven injection	Electronically common-rail injection
Nozzle holes	4	5
Nozzle diameter	0.26 mm	0.134 mm
Fuel pump mounting	Engine mechanically driven	Electrically driven
Injection timing	17 °BTDC (fixed)	180 °BTDC - 60 °ATDC (variable)
Number of injection per cycle	1	3 (Pilot, main, and post injection)
Injection pressure	200 bar (fixed)	200- 1800 bar (variable)

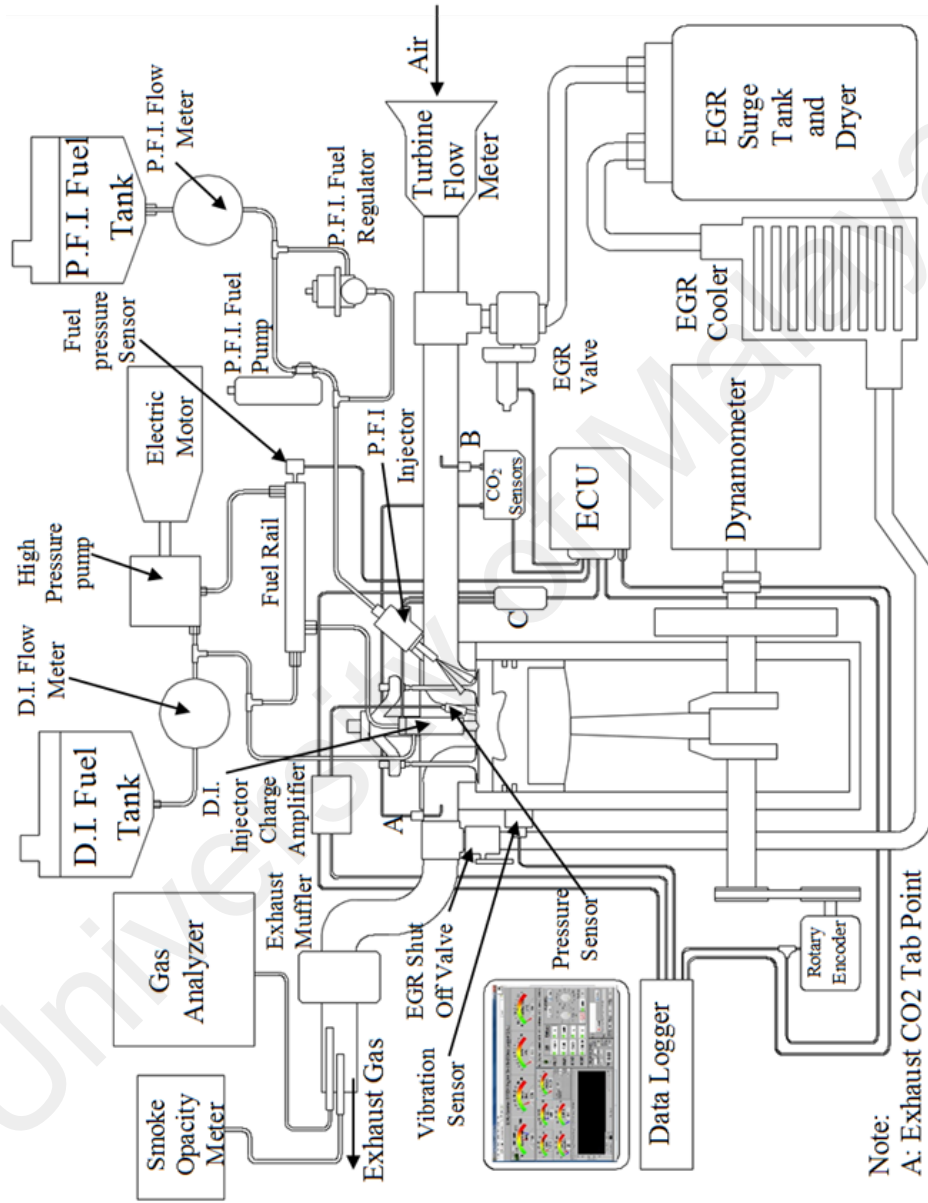


Figure 3.4: Schematic diagram of the experimental setup.

3.6.1 Fuel rail and supply pump

The fuel injection system in this investigation was based on the common-rail fuel injection concept and the fuel delivery setup is shown in Figure 3.5. This system is commonly used for direct injection diesel engines as it greatly provides flexibility regarding injection timing, fuel amount and injection events, which are fully controlled electronically. Figure 3.6 shows a schematic view of the injection system used for this study. Fuel from the tank is gravity fed through a filter to the high pressure pump. The high pressure pump is a production Denso HP 3 second-generation common-rail pump driven by a 2.2 kW electric motor. The specifications of the Denso HP3 supply pump and Denso high-pressure common-rail are both listed in Table 3.7 and Table 3.8, respectively. The rotational speed of the electric motor is controlled by the inverter and operates at a constant speed of 750 rpm to maintain the required high-pressure levels in the fuel rail and to ensure a stable line pressure with minimum fluctuation. The fuel is supplied to a Denso high pressure common-rail through a single thick-wall steel pipe. The Denso rail pressure sensor is fitted on the common-rail to control the injection pressure. It senses the fuel pressure in the rail and sends a signal to the rail pressure controller. This is a semiconductor sensor that uses the piezoelectric effect of the electrical resistance varying when pressure is applied to a silicon element. The common-rail has four outlets, three of which are blanked off and the remaining one connects the rail with the injector. The pressure level in the rail is fully controlled by Proportional-Integral-Derivative (PID) closed-loop regulation and it can be changed to pressure between 0 and 1800 bar.



Figure 3.5: Fuel delivery setup with pump driven by electric motor.

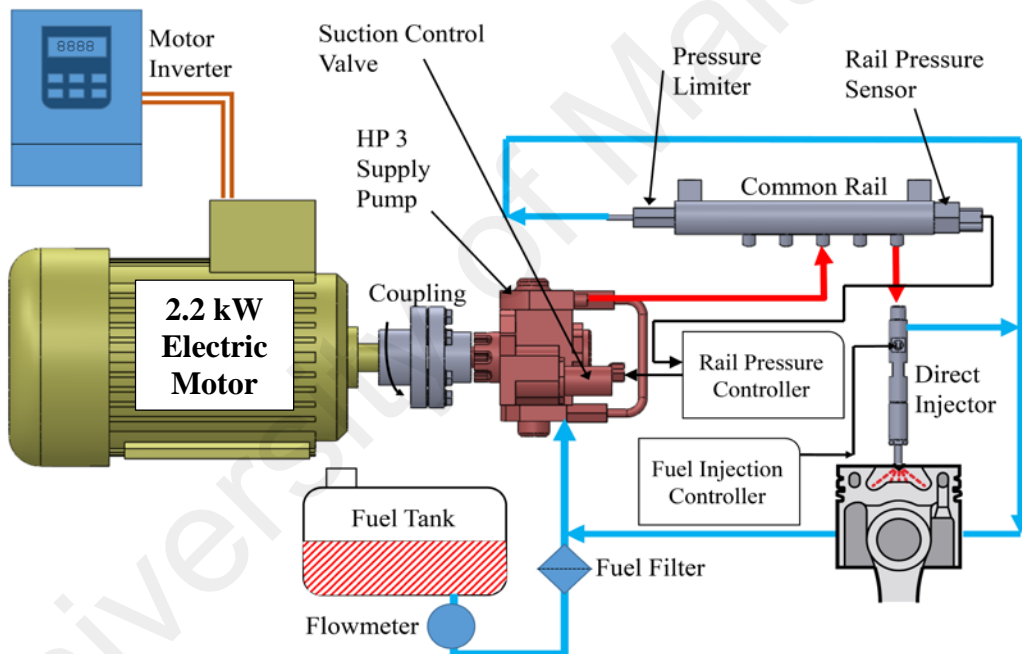


Figure 3.6: Schematic of the fuel system.

Table 3.7: Supply pump specifications.

Parameter		units
Fuel injection pump	Denso HP3 supply pump	-
Maximum outlet pressure	1800	bar
Low pressure pump	Build-in trochoid type feed pump	-
High pressure pump	Dual-plunger, high pressure rotary fuel pump	-
Total fuel flow	96	kg/hr
Max. fuel inlet temperature	75	°C
Fuel temperature rise, inlet to return	43	°C
Max. fuel inlet restriction	20	kPa
Weight	3.8	kg
Control signal for pressure regulator	12	V
Suction control valve type	Normally closed	-
Direction of rotation	Clockwise rotation	-
Cam shaft	Taper x ϕ 20	mm
Cam lift	8.8	mm
Discharge port	Rear discharge (Top)	-

Table 3.8: High-pressure common-rail specifications.

Parameter		units
Stored fuel pressure	0 - 2000	bar
Pressure limiter	Mechanical type, ball valve with spring preload	-
Valve opening pressure level	2000	bar
Valve closing pressure level after burst	500	bar
Rail pressure sensor	Resistance type (1.0V to 4.2V for 0 to 2000 bar)	-
Fuel volume held in rail	20	cm ³
Number of inlet port	1	-
Number of outlet port	4	-

The suction control valve equipped on the HP 3 supply pump uses a linear solenoid type electromagnetic valve to regulate the common-rail pressure. Figure 3.7 shows the external and internal views of the suction control valve. It is a normally closed type and the suction valve is closed when not energized. The fuel flow quantity supplied to the high-pressure plunger can be precisely controlled by varying the time (via duty cycle control) for which current is applied from the rail pressure microcontroller to the suction control valve. When current flows through (energized) the suction control valve, the armature within travels according to the duty ratio. The fuel flow quantity varies in accordance with the armature

operation, and is controlled in accordance with the size of the cylinder fuel passage opening. As a result, the intake fuel quantity is controlled to achieve the target rail pressure and the supply pump actuation load decreases. As shown in Figure 3.8, the rail pressure microcontroller is programmed to output square wave signals with a constant frequency (i.e. 500 Hz). The value of the current is the effective (average) value of these signals. As the effective value increases, the valve opening increases (rail pressure increases), and as the effective value decreases, the valve opening decreases (rail pressure decreases).

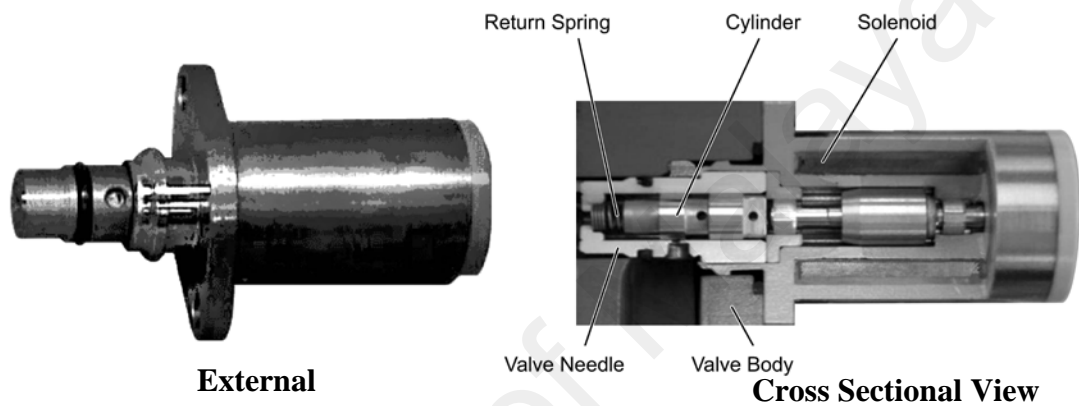


Figure 3.7: External and cross sectional views of the suction control valve (Denso Corporation, 2007).

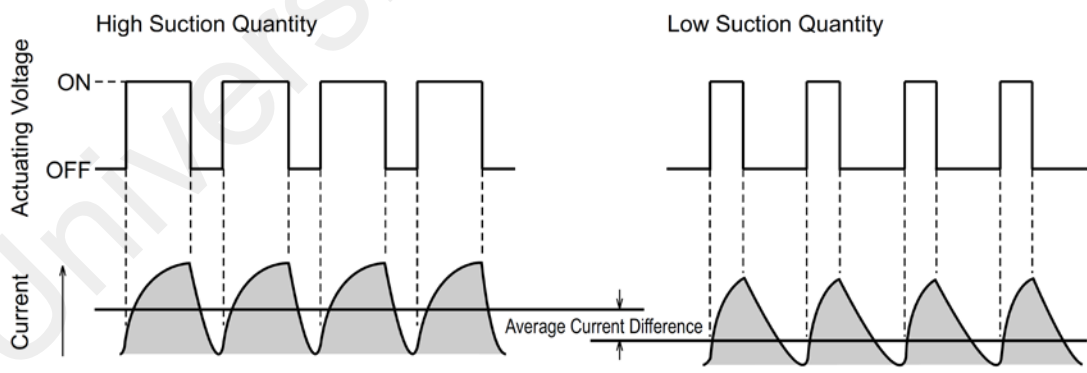


Figure 3.8: Intake fuel quantity variation via duty cycle control (Denso Corporation, 2007).

3.6.2 Engine controller unit (ECU)

In this research study, a fully flexible ECU that is capable of controlling multiple fuel injectors to accommodate advanced dual-fuel combustion modes was required. Previous research applications usually employed standard or modified ECUs, but they are found to

be unsuitable for this study. For this specific investigation, the original mechanical type fuel injection system was completely replaced with a common-rail injection system. Moreover, an engine operating with RCCI dual-fuel combustion strategy required the addition of a PFI system to the test engine. The PFI and common-rail injection system needed a fully flexible ECU to operate and control engine parameters. This has motivated the researcher to develop an ECU system based on the low-cost open-source Arduino Mega 2560 microcontroller (Arduino, 2015). Figure 3.9 illustrates the microcontroller board and the technical specifications are provided in Table 3.9. This microcontroller was adopted to support high-speed encoder pulse counting and high-resolution injector pulse-width control. For this research study, fuel injection control was performed with two Arduino Mega 2560 microcontrollers, one for the control of injection timing and the other one for the control of injection pulse-width. The first controller is called a start-of-injection control unit (SOICU), while the other is called a pulse-width control unit (PWCU).

The SOICU receives the timing signals from the incremental encoder (same encoder used in combustion analyzer system) and the pickup coil sensor. A timing belt pulley with 36-tooth was used and mounted on the starting shaft of the engine. This shaft rotates at the same speed as the engine camshaft, but at half the speed of the crankshaft. A simple hexagon head bolt was mounted on the circumference of the pulley to serve as the timing mark for cylinder stroke identification (TDC compression or TDC exhaust). As the timing mark approaches the pickup coil, the magnetic field around the pickup tip is disturbed and creates a voltage to trigger the SOICU. This has effectively identified the correct engine stroke in order to properly time the fuel injections for the test engine. To measure the angular position of the crankshaft of the test engine, an incremental encoder was fitted with 18-tooth timing belt pulley and coupled to the starting shaft by a timing belt. This will ensure that the incremental encoder spins at exactly twice the starting shaft/ camshaft

speed because the timing belt pulley for the encoder is half the diameter of the starting shaft pulley. The sensors setup is illustrated in Figure 3.10 and the outline diagram of the ECU interface with sensors and actuator is shown in Figure 3.11. On the microcontroller side, the SOICU uses three interrupt service routines (ISRs) to pick up the signal from the incremental encoder (one for index pulse and one for crank angle pulse) and pickup coil. The SOICU is responsible for instantaneously processing and calculating the timing signals received from the sensors. Based upon user-defined parameters such as SOI timing for port, pilot, main and post injections, the SOICU generates a total of four timing pulses for each complete engine cycle and sends the signals to the PWCU through the digital I/O pins. Upon receiving these signals, the PWCU outputs signals to the injector via an injector driver circuit. The PWCU is designed to control the injection quantity (via opening pulse-width) for port and direct fuel injectors. In addition, the PWCU is also responsible for the engine speed calculation and closed-loop engine speed control. When the engine PWCU is switched to AUTO mode via the LabVIEW program, the PID closed loop engine speed control scheme is enabled. The PWCU controls the engine speed by adjusting the main injection opening pulse width and the simplified cycle control process is illustrated in Figure 3.12. Clearly, an engine speed below the set point causes the PWCU to increase the main injection pulse-width. When the engine speed rises above the set point in response to the richer mixture, the PWCU reduces the injection pulse-width. The timing diagram of the pickup coil and encoder signals aligned with the SOICU, PWCU, port and direct fuel injection output signals is shown in Figure 3.13. The programming code was written with the open-source Arduino Software (IDE) and loaded to the boards via serial communication with the computer. Figure 3.14 and Figure 3.15 shows the programming flow chart for SOICU and PWCU, respectively.

A LabVIEW based graphical user interface (GUI) program was employed in this study in order to carry out real-time control and monitoring of the injection parameters such as

engine speed, start of injection (SOI) timing and opening pulse-width (PW) for port, pilot, main and post injection, closed-loop engine and speed control mode selection. The fuel injection interface program tab is shown in Figure 3.16. The injection timing parameters for generating a four-pulse injection event is shown in Figure 3.17. In this setup, the developed ECU is capable of controlling both the injection pulse-width and SOI timing down to $1 \mu\text{s}$ ($1/1000\ 000$ of a second) and 0.25°CA resolution, respectively.

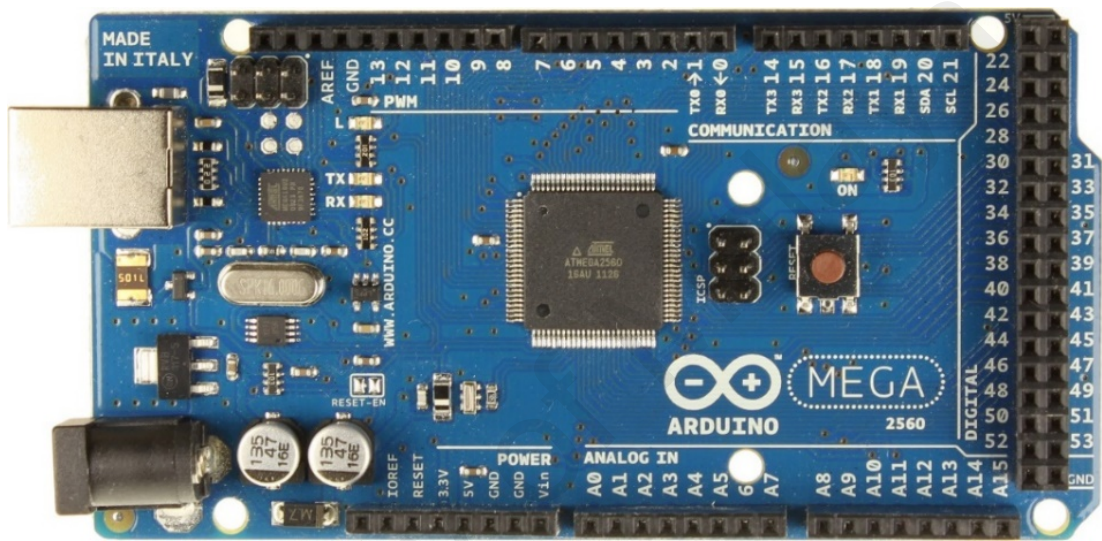


Figure 3.9: Arduino Mega 2560 microcontroller as ECU.

Table 3.9: Technical specifications of the Arduino Mega 2560 microcontroller.

Microcontroller	ATmega2560
Operating Voltage	5V
Input Voltage (recommended)	7 – 12V
Input Voltage (limits)	6 – 20V
Digital I/O Pins	54 (of which 14 provide PWM output)
Analogue Input Pins	16
DC Current per I/O Pin	40 mA
DC Current for 3.3V Pin	50 mA
Flash Memory	256 KB of which 8 KB used by bootloader
SRAM	8 KB
EEPROM	4 KB
Clock Speed	16 MHz

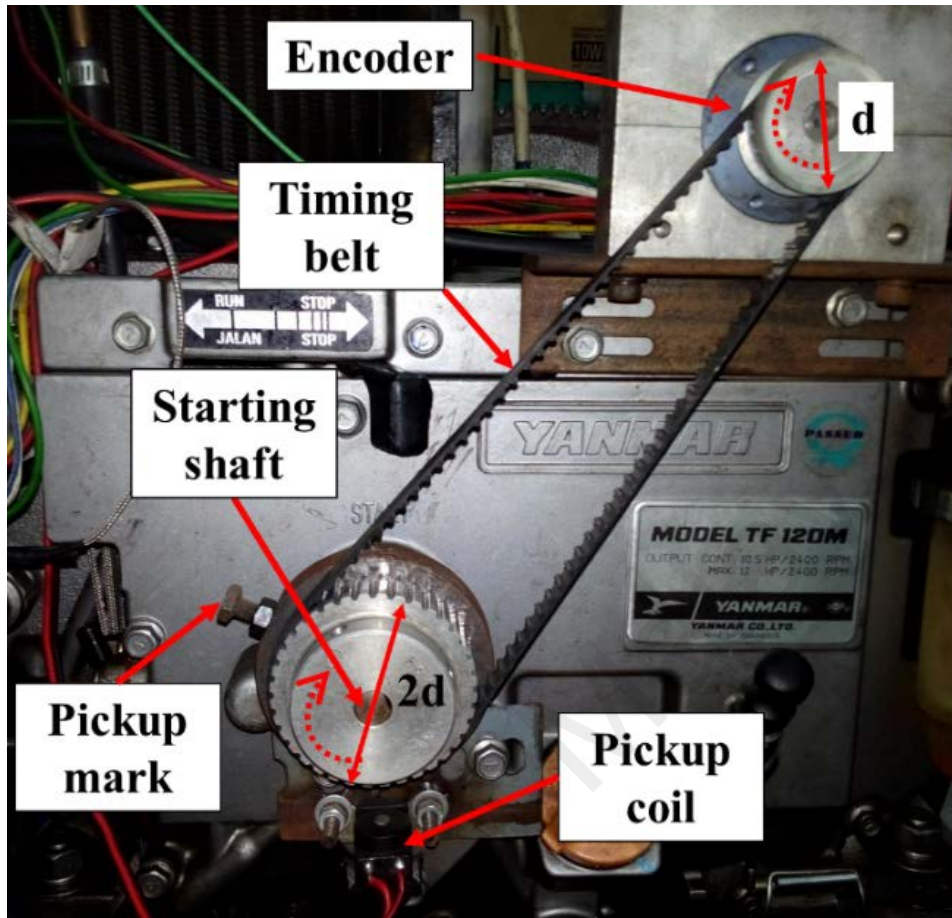


Figure 3.10: Sensors arrangement.

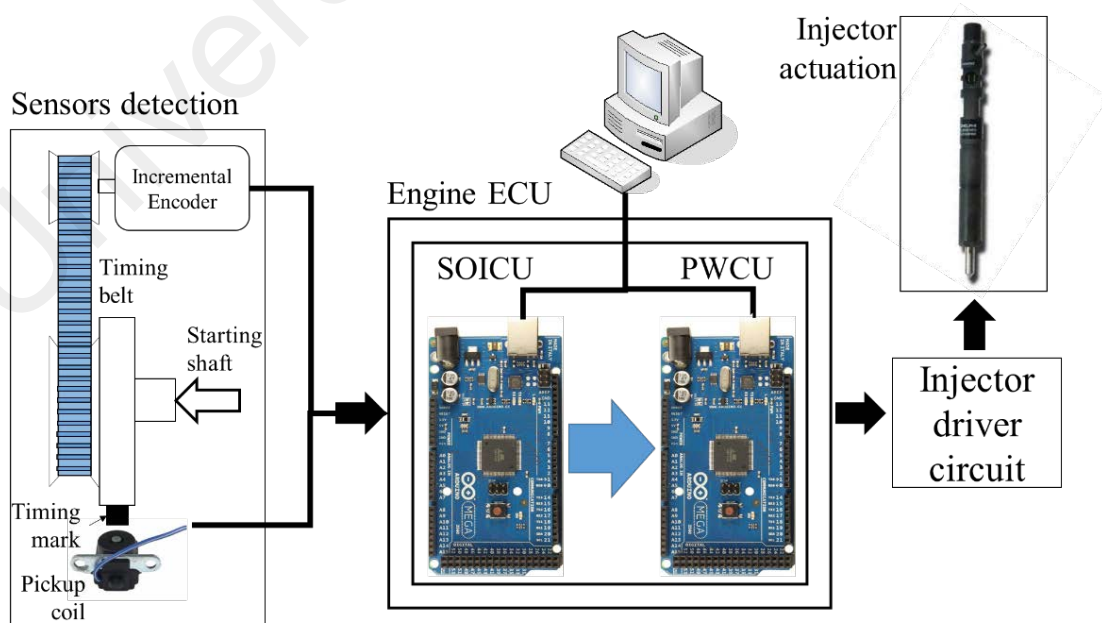


Figure 3.11: Outline diagram of the ECU interface with sensors and actuator.

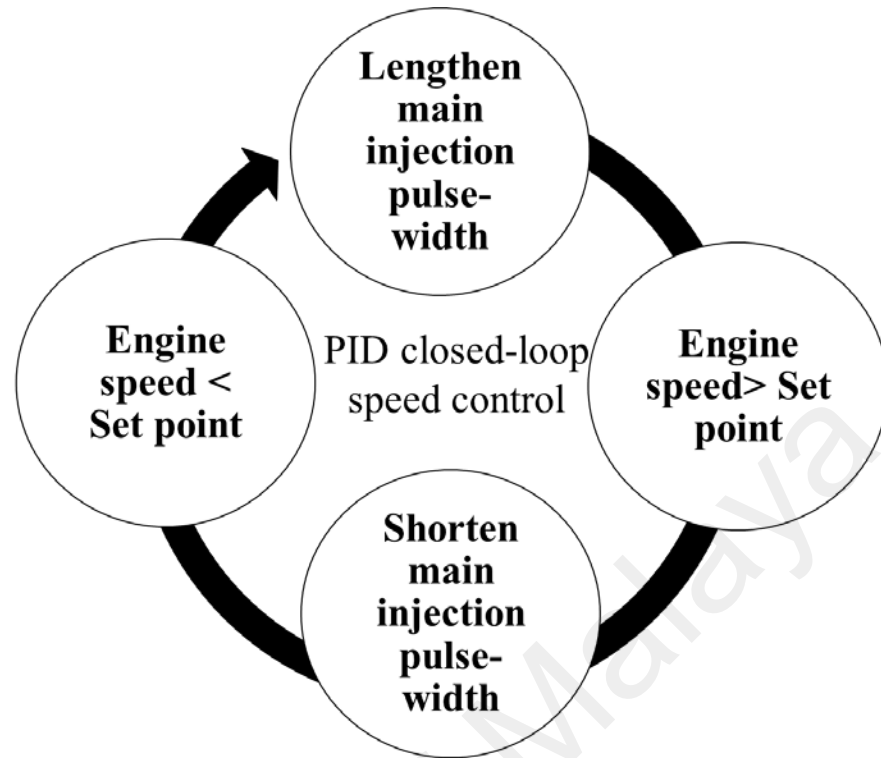


Figure 3.12: PID closed loop engine speed control scheme.

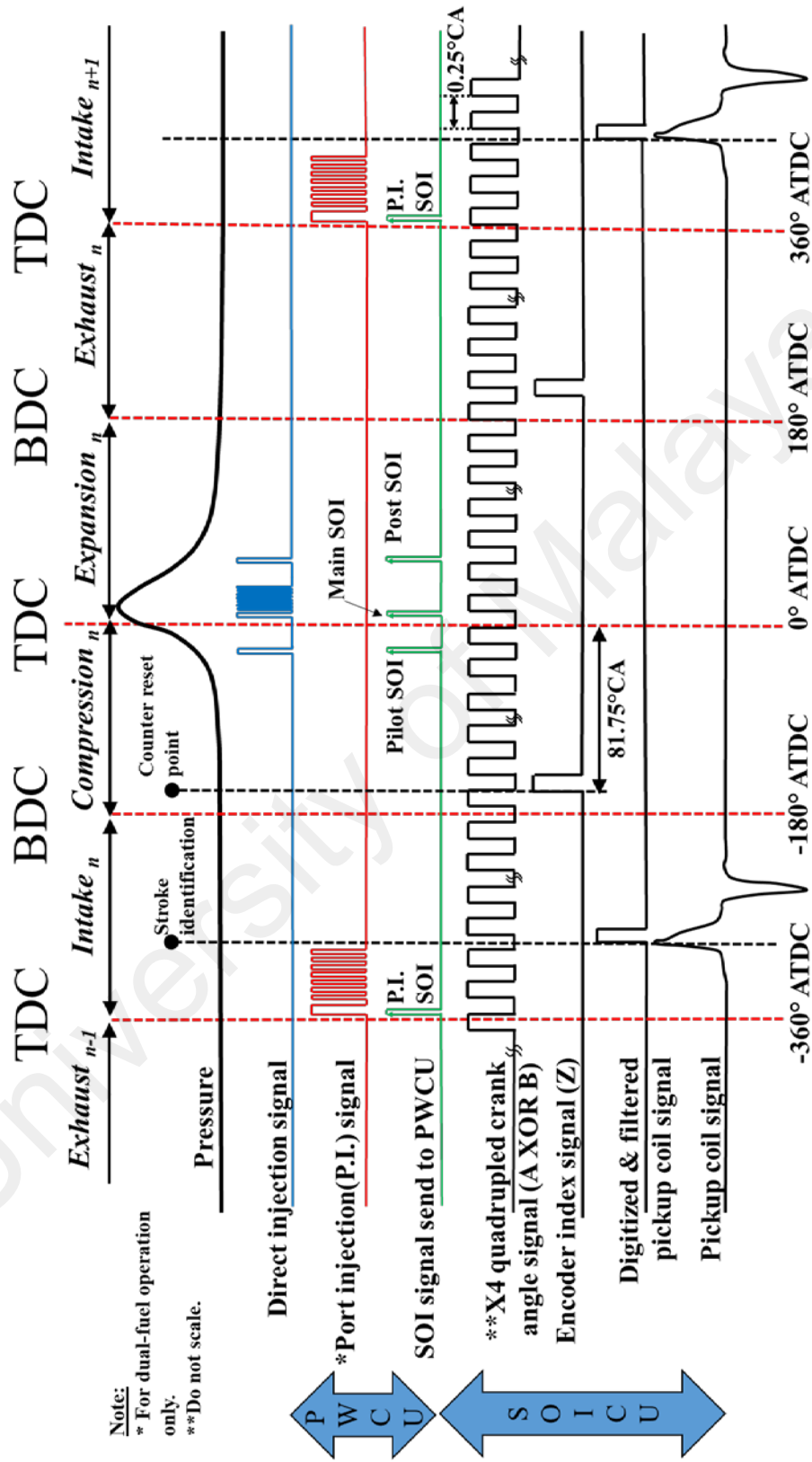


Figure 3.13: Timing diagram of the pickup coil and encoder signals aligned with the SOICU, PWCU, port and direct fuel injection output signals.

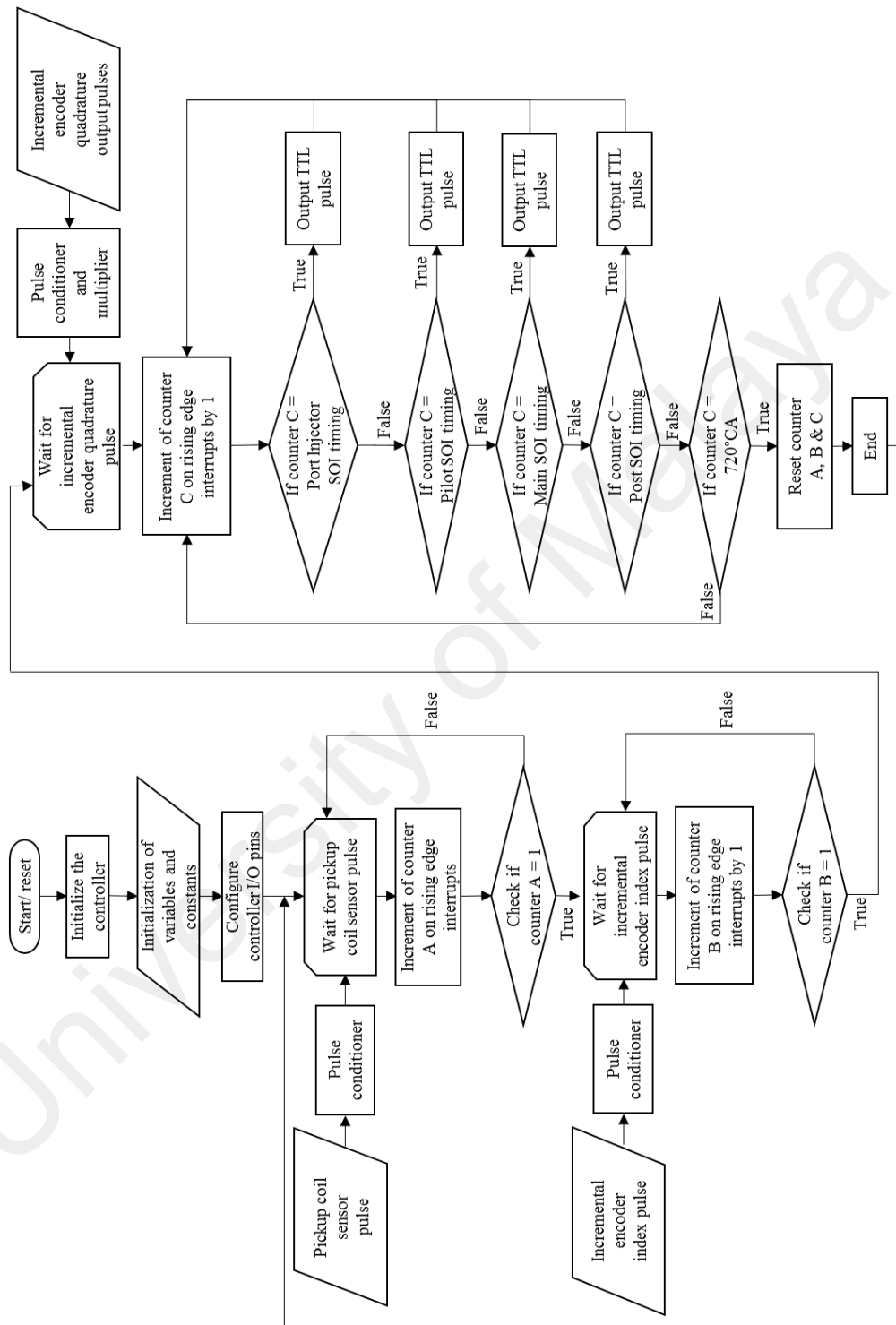


Figure 3.14: Programming flow chart for SOICU.

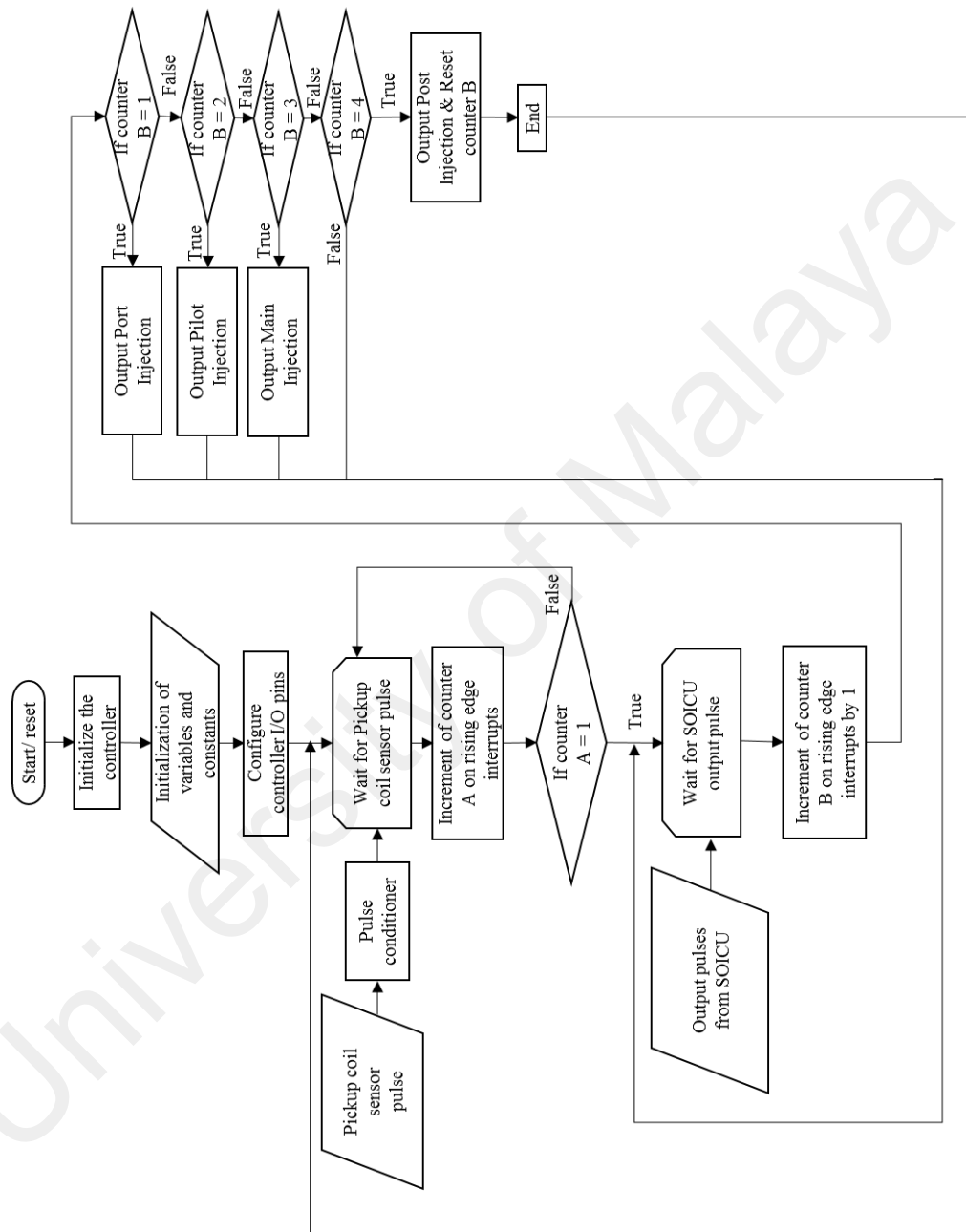


Figure 3.15: Programming flow chart for PWCU.

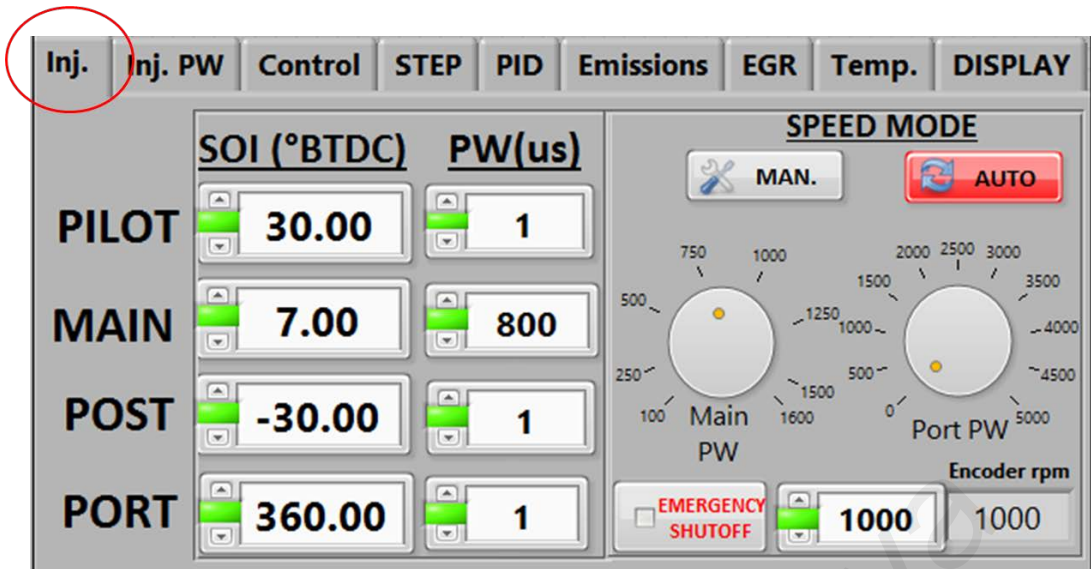


Figure 3.16: Fuel injection interface program tab.

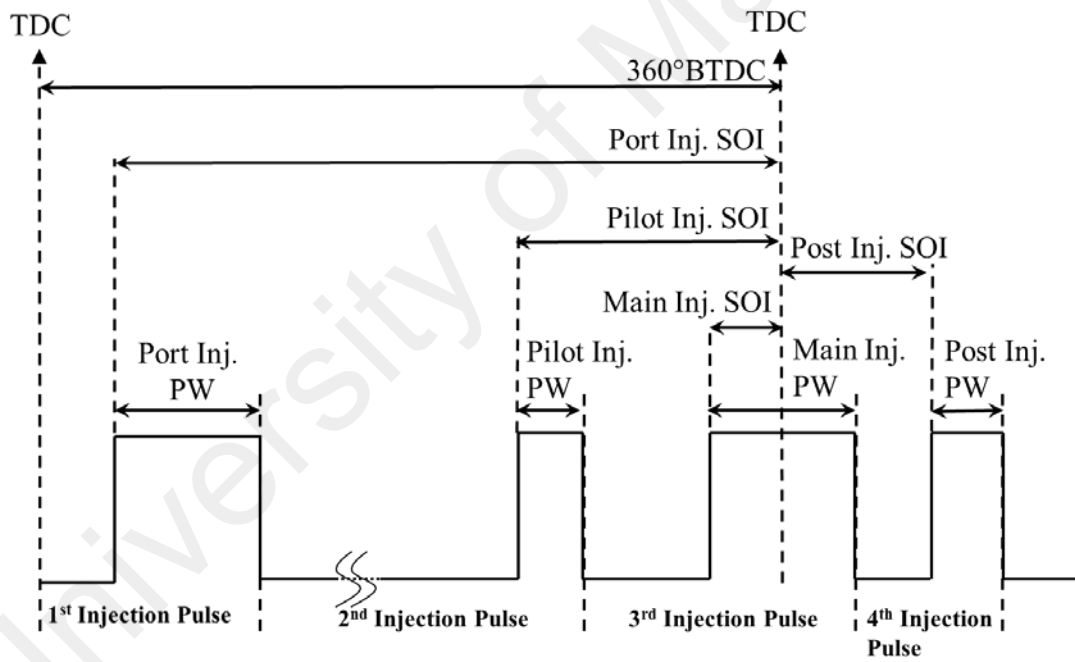


Figure 3.17: Fuel injection pulse train.

3.6.3 Fuel injector

Two injectors were used for the present study, one for common-rail direct injection and one for PFI. The first was a Delphi diesel common-rail injector as shown in Figure 3.18 while the other was a Denso gasoline port fuel injector as depicted in Figure 3.19. Both injectors are solenoid-actuated and design working with 12 volt battery voltage, thus boost voltage is not required, especially for the common-rail injector (Sealand Turbo-Diesel Asia Pte Ltd, 2015). This helps simplify the overall design of the ECU and eliminates the use of boost power supply. For the common-rail injector, this injector type was selected for its fast-acting response to close-coupled injection commands (O'Connor & Musculus, 2014). On the dynamic aspect of this injector, the opening/ closing time of the servo valve is relatively fast, ranging between 100-250 μs (Dober et al., 2008). As illustrated in Figure 3.20, the photo shows the common-rail injector mounted on the engine head. For this particular injector, information on the nozzle diameter was not available. Hence, the nozzle diameter was accurately measured using the Ducom CCD image acquisition system and the resultant images are shown in Figure 3.21. The camera system is connected with propriety software that is capable of measuring the major and minor axes and automatically computing the mean diameter. The measured nozzle diameter is found to be approximately 0.134 mm with five evenly spaced nozzle holes.

In dual-fuel operation mode, the engine required the installation of an additional port fuel injector. The injector is based on an automotive style gasoline port fuel injector. This injector is commonly used in the Toyota 2TR-FE 2.7L I4 gasoline engine. It is a 12-hole fuel injector with long nozzle (with an approximately 25.9 mm nozzle length), which greatly reduces droplet size and minimizes wall wetting. The injector was mounted just upstream of the intake valve and the location of the injector in the engine is presented in Figure 3.22. The SOI timing was controlled by the ECU and the injection was timed to

coincide with cylinder's intake stroke. The PFI fuel line pressure was maintained at 400 kPa using an automotive adjustable fuel pressure regulator.



Figure 3.18: Diesel solenoid injector (Delphi France SAS, 2007).



Figure 3.19: Denso port fuel injector.



Figure 3.20: Common-rail injector mounted on the engine cylinder head.

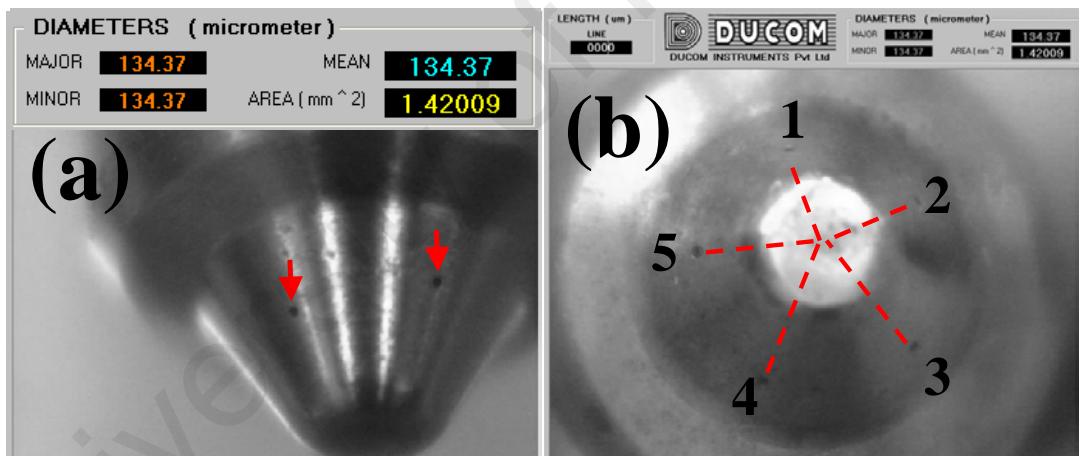


Figure 3.21: Images showing the Delphi injector (a) nozzle hole diameter, and (b) nozzle holes arrangement.

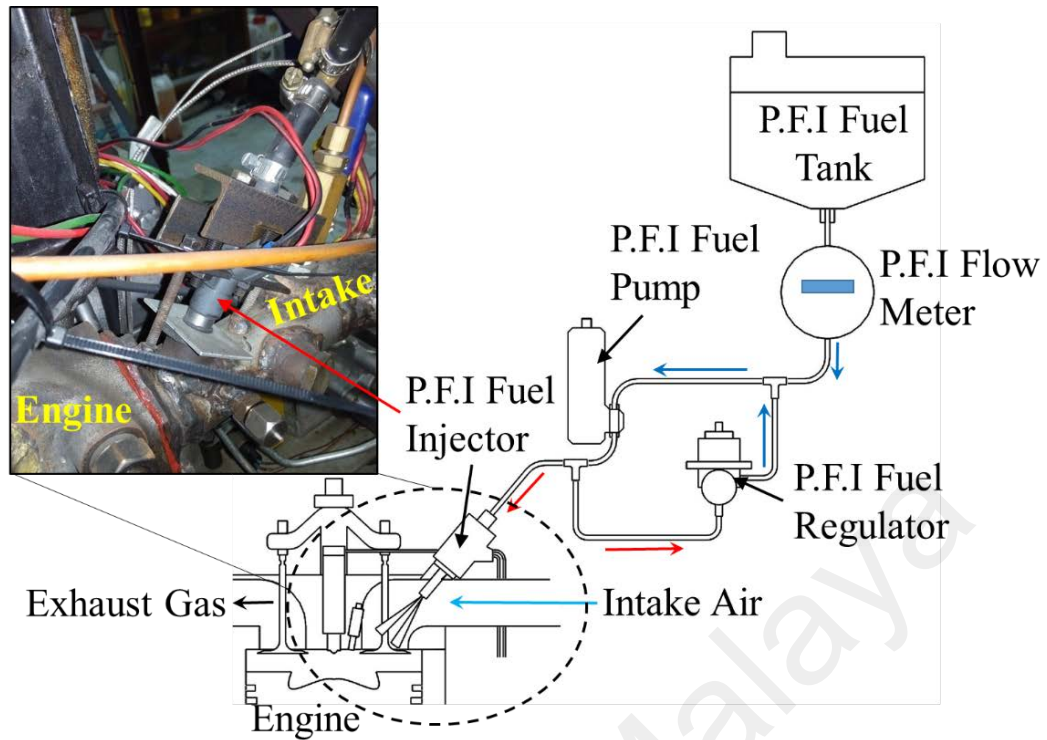


Figure 3.22: Schematic of the port fuel injection system.

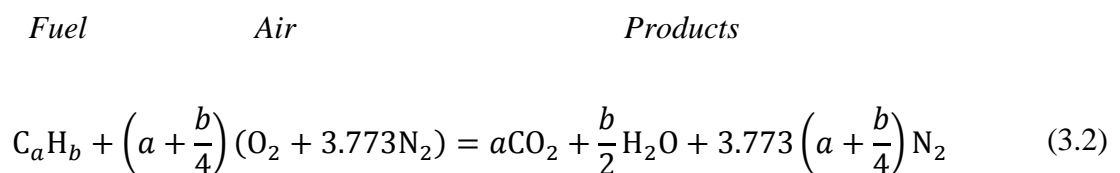
To ensure the injector is appropriately sized to the test engine, some initial calculations were performed to estimate the correct size in terms of flow rating. The approach is to obtain the fuel quantity required for stoichiometric combustion, assuming that the volumetric efficiency is 100% with air at atmospheric pressure. The fuel quantity for full load is then calculated as follows:

For an engine displacement of 638 cm^3 filled with air at 101 kPa and 30°C (303K),

$$\text{Mass of air} = m_a = \frac{PV}{RT} = \frac{101 \times 10^3 \text{ Pa} \times 638 \times 10^{-6} \text{ m}^3}{287 \frac{\text{J}}{\text{kg} \cdot \text{K}} \times 303\text{K}} \quad (3.1)$$

$$\text{Mass of air} = 7.41 \times 10^{-4} \text{ kg}$$

The overall complete combustion chemical equation is,



From Equation 3.2, the stoichiometric air/fuel ratio is,

$$\left(\frac{A}{F}\right)_s = \frac{\left(1 + \frac{y}{4}\right) (32 + (3.773 \times 28.16))}{12.011 + (y \times 1.008)} \quad (3.3)$$

where, $y = b/a$. The molecular weights of atmospheric nitrogen, oxygen, atomic carbon, and atomic hydrogen are, 28.16, 32, 12.011, and 1.008, respectively.

For diesel fuel, the analysis results (according to ASTM D5291) for carbon and hydrogen composition (by % weight) in the fuel gives 86.1% and 13.8%, respectively (ref. Table 3.2).

Thus, the gravimetric analysis of fuel gives,

$$y = \frac{b}{a} = \frac{13.8/1.008}{86.1/12.011} = 1.91 \quad (3.4)$$

By substituting Equation 3.4 into Equation 3.3, therefore the final expression for stoichiometric air/fuel ratio is equal to:

$$\left(\frac{A}{F}\right)_s = \frac{\left(1 + \frac{1.91}{4}\right) (32 + (3.773 \times 28.16))}{12.011 + (1.91 \times 1.008)} = 14.66 \quad (3.5)$$

As shown earlier, under stoichiometric conditions, the oxygen content in the air is completely consumed in the combustion process. However, in practice the diesel engines are operating with excess oxygen. In fact, the corresponding oxygen level in the exhaust may vary from 5% at full load to 20% during idling (Tan, 2014). This implied that only about 76% of the total amount of oxygen in the air is consumed at full load condition.

The following formula is used to obtain this value.

$$\% \text{ of air consumed} = \frac{\text{Ambient } O_2 \text{ level } (\%) - \text{Exhaust } O_2 \text{ level } (\%)}{\text{Ambient } O_2 \text{ level } (\%)} \times 100 \quad (3.6)$$

$$\% \text{ of air consumed} = \frac{20.9 - 5}{20.9} \times 100 = 76\%$$

Then the mass of fuel required per cycle at full load condition would be,

$$\text{Mass of fuel per stroke} = \frac{\text{mass of air} \times \% \text{ of air consumed}}{\left(\frac{A}{F}\right)_s} \quad (3.7)$$

$$\text{Mass of fuel per stroke} = \frac{7.41 \times 10^{-4} \text{ kg} \times \frac{76}{100}}{14.66} = 3.84 \times 10^{-5} \text{ kg} = 38.4 \text{ mg}$$

Thus, about 38.4 mg of diesel fuel per injection is required at full load condition.

In the next section, the flow test on both the common-rail and port fuel injector is detailed. The bench test was conducted with the same ECU developed for this engine by varying the injection pulse-width to measure the amount of fuel collected. The flow rate was evaluated according to the following procedure:

- i. Set the rail pressure (fixed at 400 kPa for port fuel injector);
- ii. Pulse the injector for a known pulse-width (in microsecond, μs);
- iii. Count the number of injection events (i.e. 2000 injections);
- iv. Weigh the fuel collected in a collection vessel with a weighing scale sensitive to ± 0.0001 g; and
- v. Calculate the fuel mass injected per stroke.

The calibration step for each point was repeated twice to produce average readings. The repeatability was matched over 95% for each run. The flow characteristics of the port and common-rail fuel injector are shown in Figure 3.23 and Figure 3.24, respectively. As visible, the amount of fuel injected is proportional to the injection pulse-width (for both injectors) and rail pressure (for common-rail injector). The bench test results also indicate that the opening time for port and common-rail fuel injector were found approximately equal to 1500 μs and 250 μs , respectively. This is the duration required to energize the

solenoid and open the injector before any fuel is released. Further, the common-rail injector was found to be capable of delivering up to 40 mg/stroke (>38.4 mg/stroke) of fuel at injection pulse-width of 1560 μs and rail pressure of 1400 bar. Therefore, this common-rail injector is suitable for use to operate the engine over most of the load range.

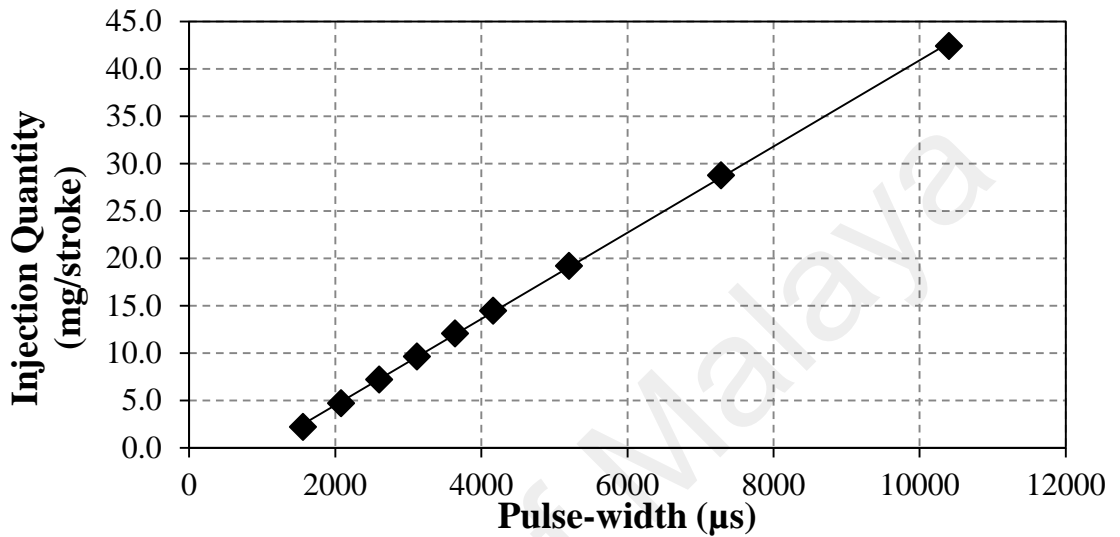


Figure 3.23: Port fuel injector injection quantity versus pulse-width at constant pressure of 400 kPa (Calibration fluid: Gasoline).

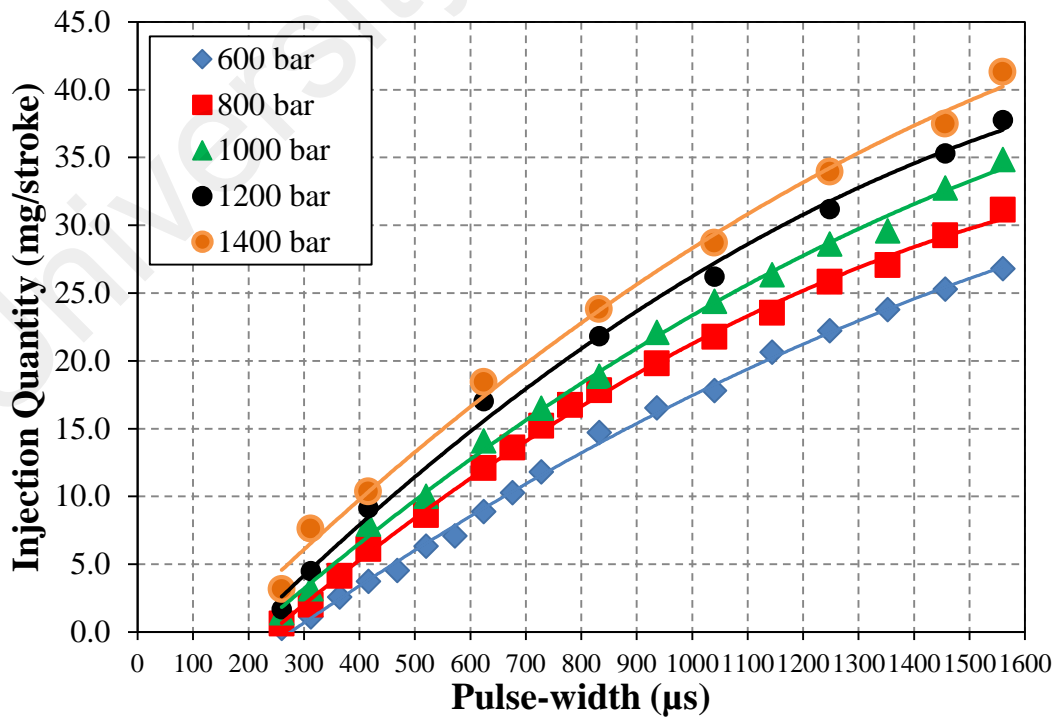


Figure 3.24: Direct injector injection quantity versus pulse-width under different rail pressure (Calibration fluid: Diesel).

In the following section, the configuration of current profile management for the common-rail injector is detailed. Generally, a wide range of solenoid fuel injectors are available and they can be classified depending on their flow rate and coil winding impedance. Injector solenoid impedance describes the electrical resistance of the windings and, essentially, they are divided into low and high impedance injectors. The common-rail diesel injector employed in this study is a low impedance injector and has a solenoid resistance of 0.3 ohms. The main benefit of a low impedance injector is a shorter triggering time, which provides precise control of fuel delivery, especially at very short pulse durations. However, this low impedance injector will consume 40 or more amperes of current if connected directly to a 12V power supply with no current-limiting driver (Ohm's law: $I=V/R$; $I=12/0.3= 40$ A), and this will cause the solenoid to overheat very rapidly and may cause permanent damage to the injector. Another issue is that the high current flow could also potentially cause the driving circuit to overheat and destruct. Therefore, a programmable peak and hold pulse-width-modulation (PWM) injection output function has been specially built into the ECU as a current-limiting driver for the injector.

Figure 3.25 illustrates the ECU's output signal along with the current waveform for the solenoid coil of the common-rail injector. As can be seen, at point A, the injector is initially in OFF state. At point B (also known as Start of Injection, SOI timing), the ECU triggers the injector ON by pulling the injector coil to ground via the transistor, hence the current flow across the injector coil rises exponentially. It is worth mentioning here that the SOI timing throughout this study is referred to as the ECU commands the fuel injector to open instead of the hydraulic SOI timing of the injector. In addition, starting at point B marked the beginning of Boost phase. During the Boost phase, the low coil impedance causes the current to flow rapidly across the injector coil. Generally, the higher the current slew rate, the shorter the fuel injector opening time and faster the injector opening

response. This high current has created a strong magnetic field around the coil to overcome the internal spring pre-loading force, thus lifting the valve to open. In this study, it takes about 230 μs to fully open the common-rail injector and this duration is commonly referred to as the injector opening time. During this period, the amount of fuel delivered to the combustion chamber is relatively insignificant. In fact, incorrectly setting the engine to operate at or below the minimal injector opening time may skew the fuel atomization and contribute to high exhaust emissions and rough idle quality (i.e. inconsistent cycle-to-cycle fuel supply). Thus, this duration should be properly configured to achieve the optimal peak current required to open the injector valve consistently. The Boost phase can be defined to sustain for a fixed time (T_{boost}) prior to the execution of the next phase. Following this is the Bypass phase (region C to D) where the ECU turns the injector OFF via the transistor and this is split between the Boost phase and the Hold phase. The injector coil current quickly decays through a flyback diode current path around the fuel injector as shown in Figure 3.26. The flyback diode provides a current route for the inductive current in the solenoid when the transistor switches OFF the injector, and protects the injector from the high voltage spike generated from the collapsing magnetic field around the injector coil. This phase is specially inserted for the purpose of releasing the electromagnetic force to a hold level. This strategy is simply based on the fact that the current (and hence the electromagnetic force) required to open a solenoid valve is several times greater than the current necessary to merely hold it open. This is because during the Hold phase, with the reduced working air-gap of about 30 μm (the distance between coil and valve) therefore the electromagnetic force to be applied to the valve can thus be reduced. Another reason is that it is no longer necessary to overcome valve inertia of the injector (Delphi France SAS, 2007). In this study, the optimal interval required for the strength of the magnetic field to be dropped to a lower hold level was empirically determined by experiment and confirmed based on engine performance and

the injector current profile. The Bypass phase can be programmed for a fixed duration (T_{bypass}), then only follow by the Hold phase. From the diagram, point D marked the beginning of the Hold phase. During the Hold phase, the ECU generates a high frequency (i.e. 31 kHz) pulse-width-modulation (PWM) signal, in the form of a square wave with a configurable duty cycle, to switch the injector driver transistor ON and OFF very rapidly (in about 0.0000323 seconds). This switching frequency is quicker than the injector valve can respond, so capable to keep the valve needle floats in an open position throughout the Hold phase. Besides, the configurable duty cycle (usually expressed as a percentage, 100% being fully on) of the PWM signal enabled the control of current waveform during the Hold phase, thus effectively improving the injector performance and reducing the injector temperature. From the current waveform, it demonstrates that the peak current and hold current for this injector are nominally 17.8 A and 9.5 A, respectively. In the last stage, when the overall pulse-width duration is reached, the ECU turns the injector OFF at point E, so the injector coil current returns to zero. To access and real-time configure the current profile of the injector such as Boost duration (T_{boost}), Bypass duration (T_{bypass}) and PWM duty cycle (PWM%), a LabVIEW based graphical user interface (GUI) program was employed in this study. The common-rail fuel injector current profile management interface program tab can be seen in Figure 3.27. Further, the injection current profile key parameters for the common-rail injector employed in this study are tabulated in Table 3.10.

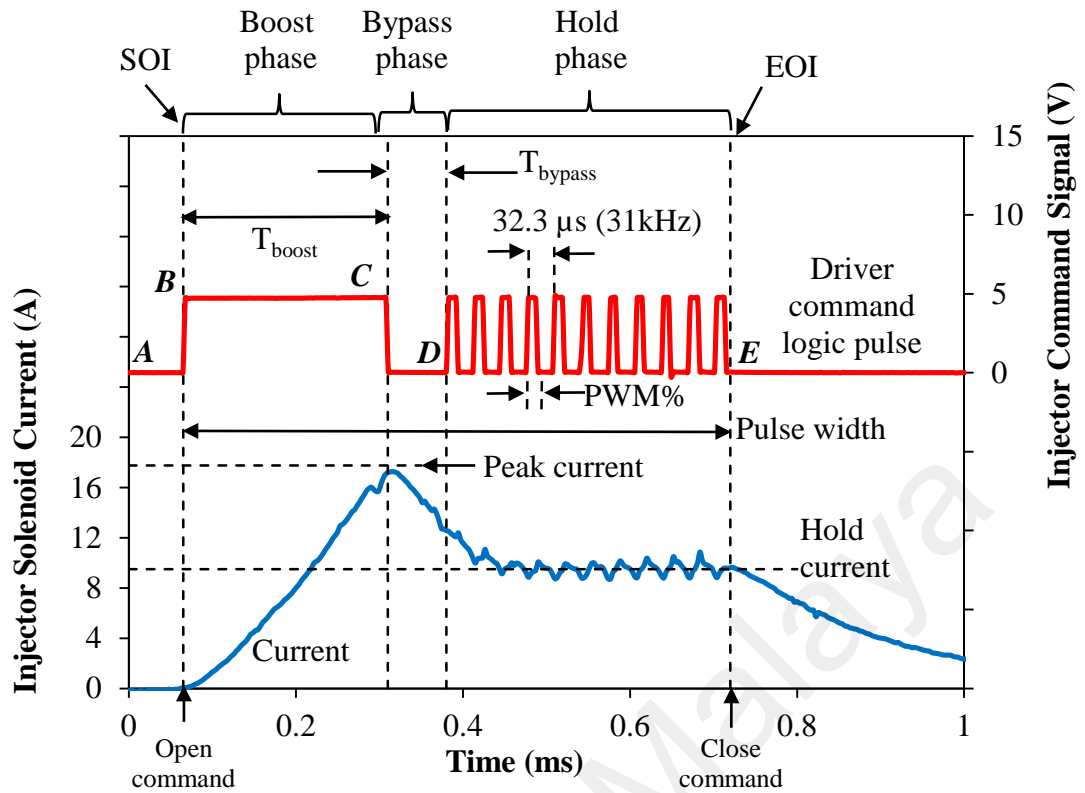


Figure 3.25: Common-rail fuel injector driver control logic pulse signal and current across solenoid coil with PWM.

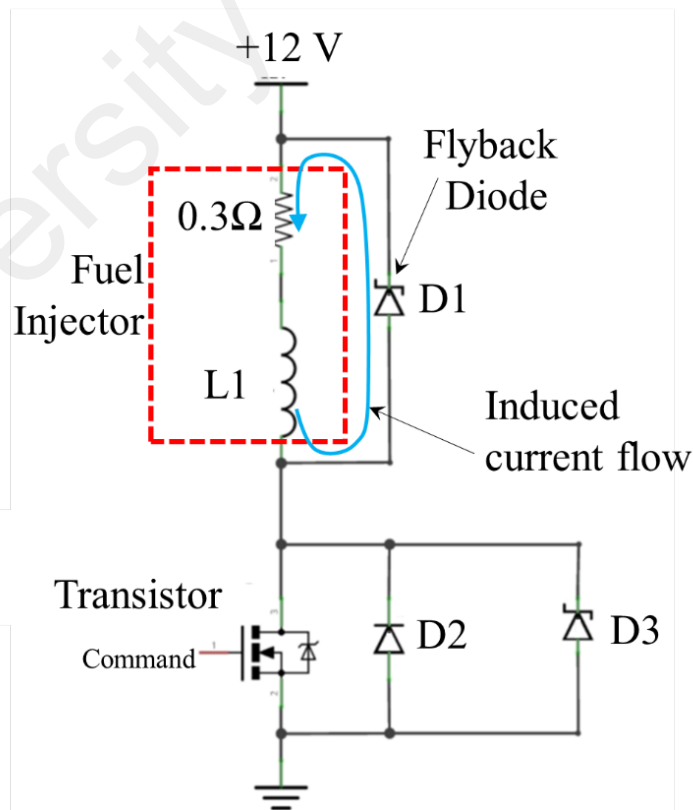


Figure 3.26: Flyback diode across the coil of common-rail injector.

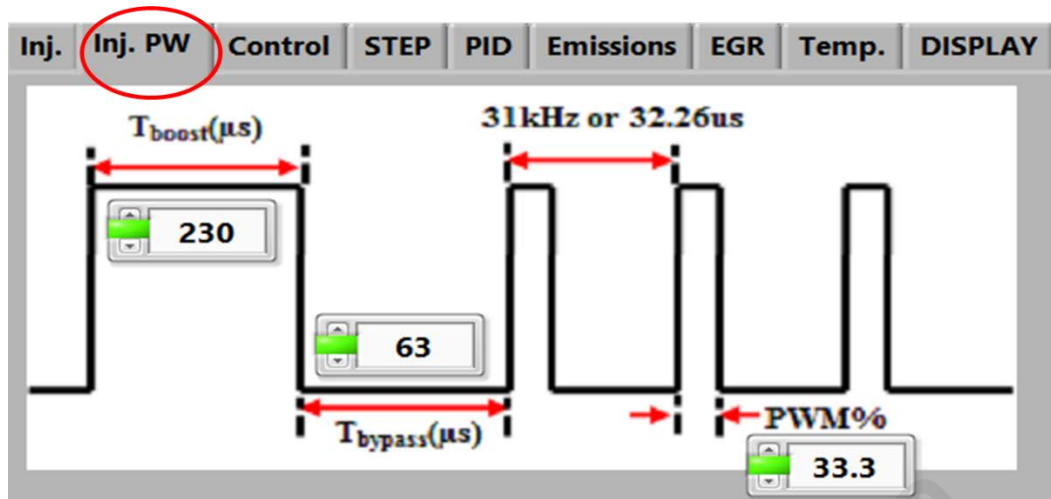


Figure 3.27: Common-rail fuel injector current profile management interface program tab.

Table 3.10: Injection current profile key parameters for common-rail injector.

Parameter name	Description	Value
T_{boost}	Fixed time for Boost phase	230 μ s
T_{bypass}	Fixed time for Bypass phase	63 μ s
PWM%	PWM duty cycle	33.3%

3.7 Engine test bed setup

This study required the design and installation of a single-cylinder engine test bed system to carry out engine performance testing. The design was constructed using commercially available computer aided design (CAD) software. In particular, this involved the installation of Focus Applied Technologies's model DC2AP dynamometer controller. This dynamometer controller enables the user to control the dynamometer in various modes: Torque, Manual, Speed and Road Load; which of these modes to use depends on the user requirement. For instance, the user may select the simple loading of an engine with the Manual Control mode. For operation at constant torque (with varying speed) and constant speed (with varying torque), the user may select the Torque Control and Speed Control mode, respectively. The engine load absorber was based on the ST-7.5 model

7.5kW A.C. synchronous dynamometer. It is used to provide loading to the engine and to maintain the engine speed.

To measure the intake airflow rate, a 4" turbine type SuperFlow™ airflow meter with 2 to 70 litres per second (L/s) measuring range and accuracy of $\pm 0.5\%$ full scale was installed, as shown in Figure 3.28. The air turbine is a volumetric airflow measurement device. When air flows through the housing, an internal fan rotates. The fan is connected to a turbine which outputs a frequency signal as it spins. The frequency output is directly proportional to volumetric airflow in the rated flow range of the turbine and is independent of air density. The calibration is performed on a SuperFlow™ flowbench and the flow rate is calculated by using an interpolation based on the values from the calibration sheet (as shown in Table 3.11).

When using an air turbine in conjunction with exhaust emissions measurement and fuel flow readings to determine the emissions on mass basis, the air flow reading must be in mass flow (kg/min). The exhaust flow can be obtained from the following equation according to SAE J177:

$$\text{Mass Exhaust (kg/min)} = (\text{Mass Inlet Air, kg/min}) \times (1 + F/A) \quad (3.8)$$

To monitor the exhaust gas temperature, a type K thermocouple was used and mounted in the exhaust stream as shown in Figure 3.29. The fuel flow rate for direct injection and the port fuel injection system was measured separately with a Kobold DOM-A05 HR11H00 positive displacement gear wheel flow meter with measuring range of 0.5- 36 L/hr, which interfaced with a Kobold ZOD-Z3KS2F300 flow rate counter. The calibration is performed by Kobold Messring GmbH and the calibrated flowmeter "K" factor is 2,790 pulses per litre. The operational principle of the flow meter is shown in Figure 3.30. As can be seen, when liquid flows through this flow meter, two oval geared rotors measure a constant volume per rotation within a precisely machined measuring

chamber. With each rotation, a constant volume of liquid is measured. The rotation of the oval gears is sensed via magnets embedded within the rotors. These magnets transmit a high resolution pulse output. The output signal is processed externally via the Kobold flow rate counter. To remotely log the reading, a microcontroller is used to measure the elapsed time during a single cycle pulse output (transistor-transistor logic- TTL) and the processed data passes between the computer and the microcontroller through a serial USB cable. All related microcontroller boards were connected to the central computer via a serial USB for data acquisition. The data acquisition system is responsible for collecting signal, rectifying, filtering and converting the signal to the data to be read. The user can monitor, control and analyse the data using a LabVIEW based GUI program and the interface program can be seen in Figure 3.31. All data could be logged simultaneously by clicking the record button and at the rate of 5 Hz.

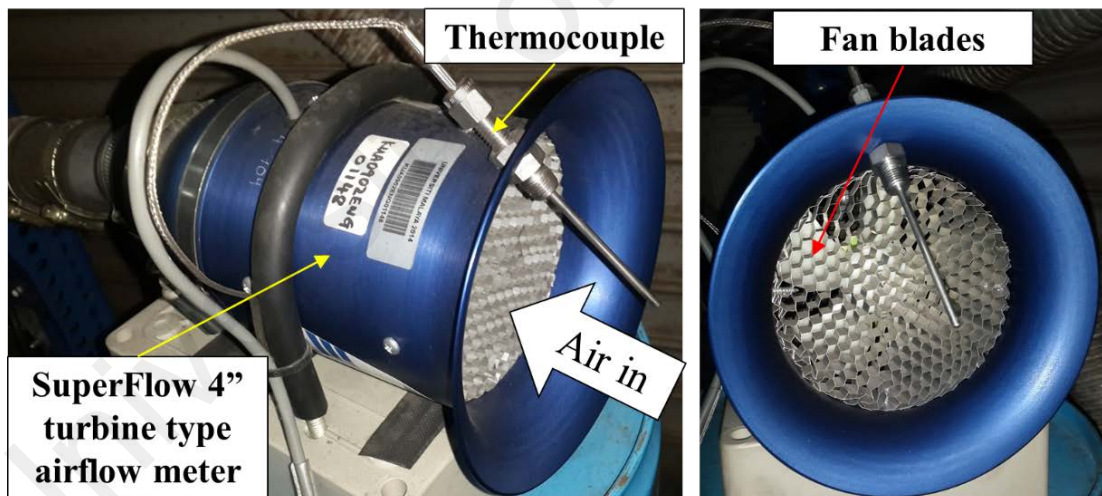


Figure 3.28: SuperFlow™ 4” turbine type airflow meter. Note that the fan blades are clearly visible in the photo on the right.

Table 3.11: SuperFlow™ airflow meter calibration data.

Frequency (HZ)	24	87	178	400	654	825
Air flow rate (L/s)	3.7	11.6	24.0	50.5	80.3	101.2

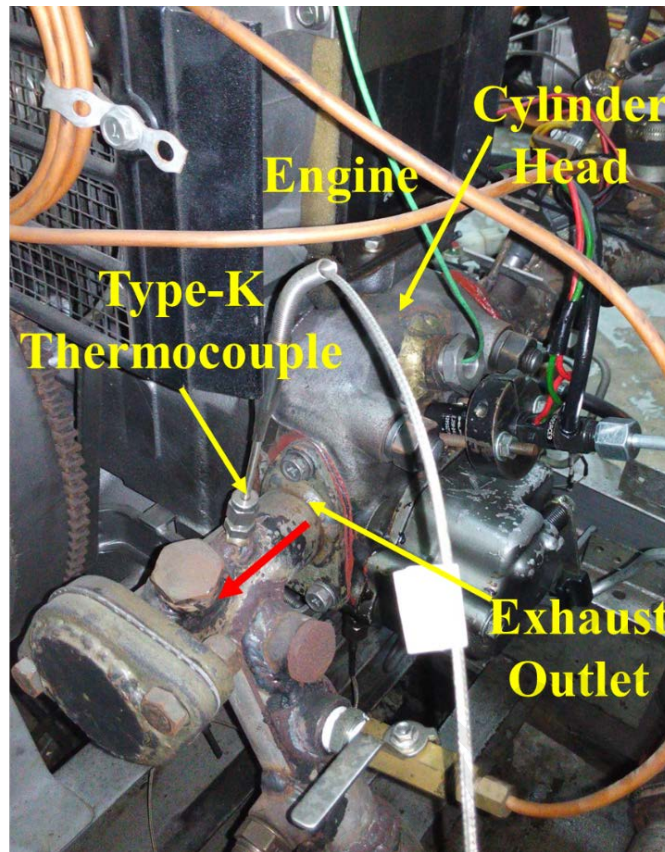


Figure 3.29: Type-K thermocouple mounted in the exhaust stream.

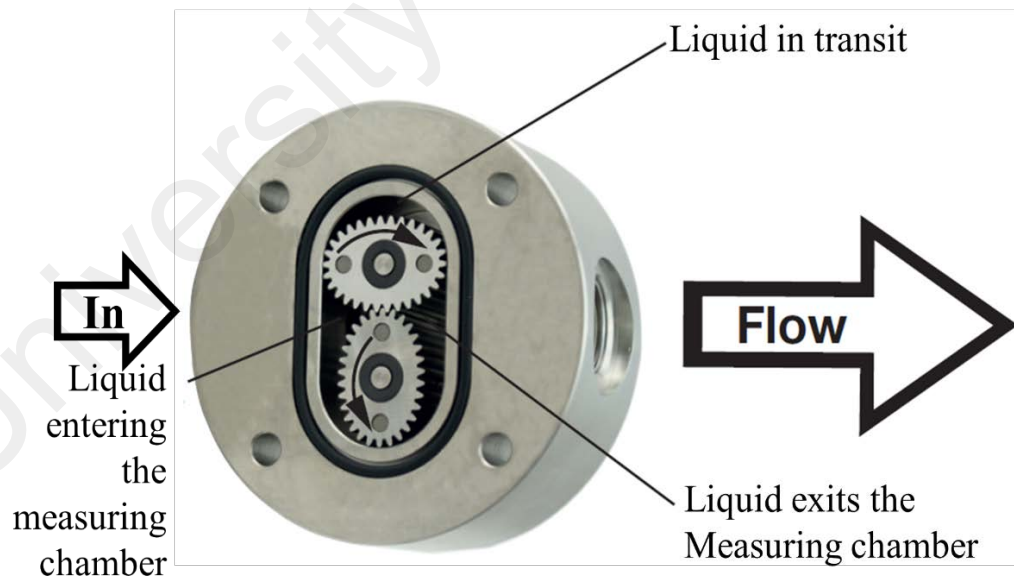


Figure 3.30: Operation principle of Kobold positive displacement gear wheel flow meter.

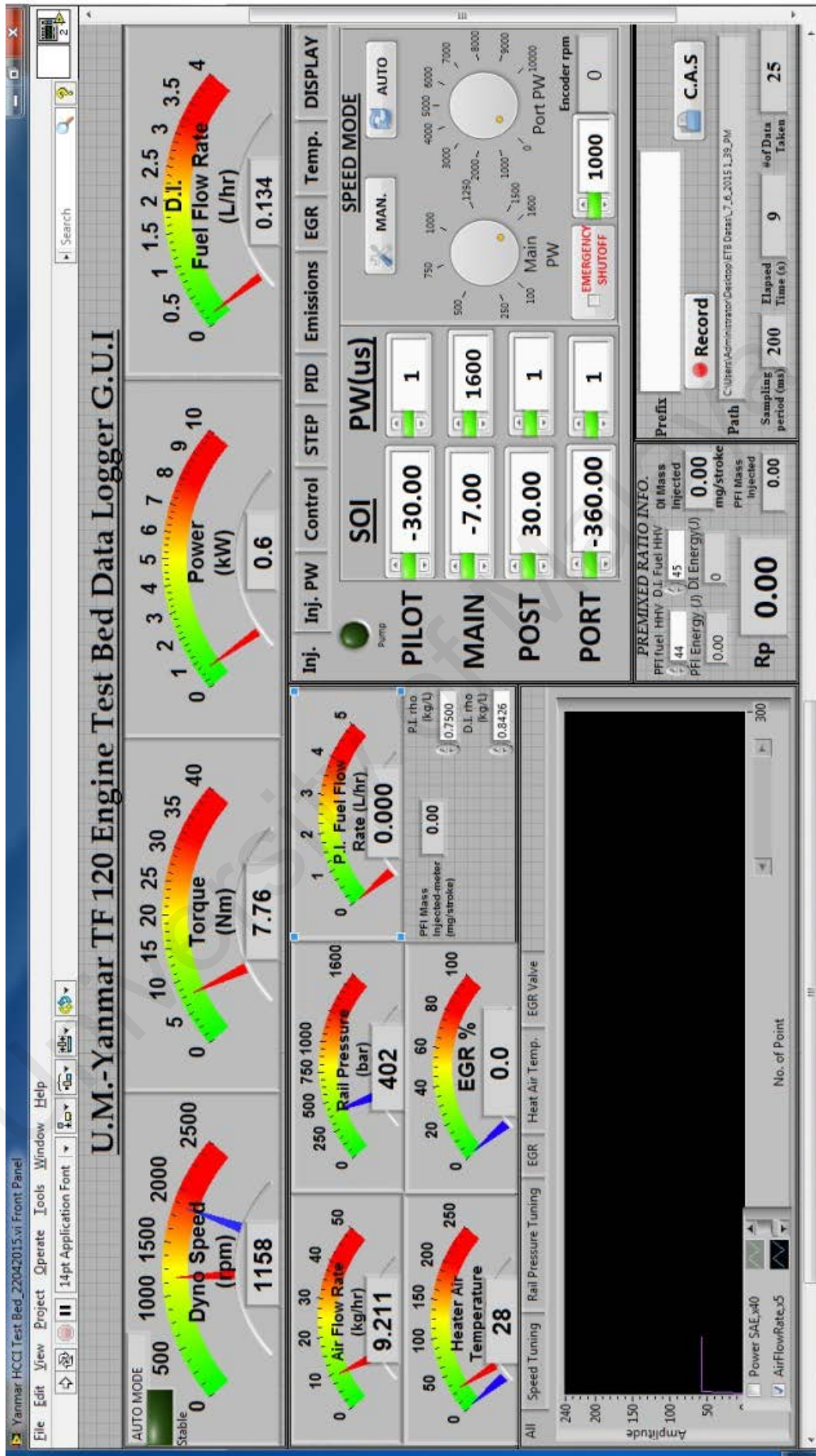


Figure 3.31: LabVIEW software user interface screen shot.

For the exhaust emission measurement, an AVL DICOM 4000 5-gas analyser was used to measure the concentrations of HC, CO, CO₂, and NO_x. Opacity of smoke was measured using AVL DiSmoke 4000. All emissions were measured during steady-state engine operation. The measurement range and resolution of both of the instruments are provided in Table 3.12. The HC, CO and NO_x emissions were converted into brake specific emissions by using the following equations according to SAE J177:

$$\text{BSHC} \left(\frac{g}{kWhr} \right) = \frac{0.0287 \times \text{HC}(ppm) \times \text{Exhaust mass flow rate} \left(\frac{kg}{min} \right)}{\text{Brake power} (kW)} \quad (3.9)$$

$$\text{BSCO} \left(\frac{g}{kWhr} \right) = \frac{0.0580 \times \text{CO} (ppm) \times \text{Exhaust mass flow rate} \left(\frac{kg}{min} \right)}{\text{Brake power} (kW)} \quad (3.10)$$

$$\text{BSNO}_x \left(\frac{g}{kWhr} \right) = \frac{0.0952 \times \text{NO}_x (ppm) \times \text{Exhaust mass flow rate} \left(\frac{kg}{min} \right)}{\text{Brake power} (kW)} \quad (3.11)$$

Table 3.12: Measuring components, ranges and resolution of the AVL DICOM 4000 gas analyzer and DiSmoke 4000 smoke analyzer.

Equipment	Measurement principle	Component	Measurement range	Resolution
Gas analyzer	Non-dispersive infrared	Unburned hydrocarbon (HC)	0-20,000ppm	1 ppm
	Non-dispersive infrared	Carbon monoxide (CO)	0-10% Vol.	0.01% Vol.
	Non-dispersive infrared	Carbon dioxide (CO ₂)	0-20% Vol.	0.1% Vol.
	Electrochemical	Nitrogen oxides (NO _x)	0-5,000 ppm	1 ppm
	Calculation	Relative air-fuel ratio (λ)	0-9,999	0.001
Smoke opacimeter	Photodiode detector	Opacity (%)	0-100%	0.10%

3.8 Combustion analyzer system setup

The test system was installed with necessary sensors for the combustion analysis and fuel injection timing identification as shown in Figure 3.32. In-cylinder gas pressure was measured using a Kistler 6125B type pressure sensor. The charge signal output of the pressure sensor was converted to a low-impedance voltage signal using a PCB model 422E53 in-line charge converter; this unit was powered using a PCB model 480B21 3-

channel ICP signal conditioner. To acquire the top dead centre (TDC) position and crank angle signal for every engine rotation, an incremental quadrature rotary shaft angle encoder with 0.125°CA resolution (X4 encoding) was used. To determine and verify the SOI timing and injection duration for both of the injectors, the injector current signal was measured with a hall effect current sensor. To perform engine vibration measurements, an accelerometer (PCB model 603C01) with calibrated sensitivity to a 95 mV/g and 50 g measurement range was used. This rugged accelerometer is capable of performing over a wide frequency range of 0.5–10000 Hz. Engine vibration motion in the lateral (y) axis (or perpendicular to cylinder axis) was chosen for monitoring vibrations. To sense the magnitude of vibration in this direction, the accelerometer was mounted on the engine body with an adhesive mounting base. The output signal from the sensor was connected to the same signal conditioner (PCB model 480B21) with unity gain. In each test, engine-block vibration signals for a total of 100 consecutive combustion cycles at 0.125° CA resolution were recorded and the averaged RMS was calculated according to the following equation:

$$a_{rms} = \frac{1}{n} \left[\sum_{j=1}^n \left(\sqrt{\left(\sum_{i=1}^N a_i \right) / N} \right)_j \right] \quad (3.12)$$

where, a_{rms} is the average RMS value for the acceleration signal, n is the total of the engine combustion cycles, j is the number of combustion cycles, a_i is the instantaneous acceleration value in the angle domain signal at point i and N is the total sample number within one cycle.

To simultaneously acquire the cylinder pressure signal, injector current signal, vibration signal and encoder signal, a computer equipped with a high-speed ADLINK DAQ-2010 simultaneous sampling data acquisition card, which has 14 bits resolution, 2 MS/s

sampling rate, and four analog input channels, was used. The ADLINK DAQ-MTLB v1.5 software for MATLAB™ was installed on the computer to integrate ADLINK DAQ-2010 card with MATLAB™ Data Acquisition Toolbox 2.15. This software driver enables the user to directly control the DAQ card from MATLAB™ R2009b environment. MATLAB™ version R2009b was chosen for the purpose of this investigation due to their wide application in research study. For each test point, several data acquisitions were performed by loading the command file (m file) in the MATLAB™ command window. Usually, each acquisition generates a daq extension (.daq) file with a data size of 60 MB per acquisition. The data processing and analysis tasks uses computationally intensive code written in MATLAB™ to analyze and generate result files. In each acquisition, 100 consecutive combustion cycles of pressure data were collected and an average was calculated. To reduce noise effects, smooths data using SPAN as the number of points used to compute each element was applied to the sampled cylinder pressure data. Combustion parameters, such as peak pressure magnitude, peak pressure location, heat release rate, peak heat release rate location, and ID, were all computed using MATLAB™ software.

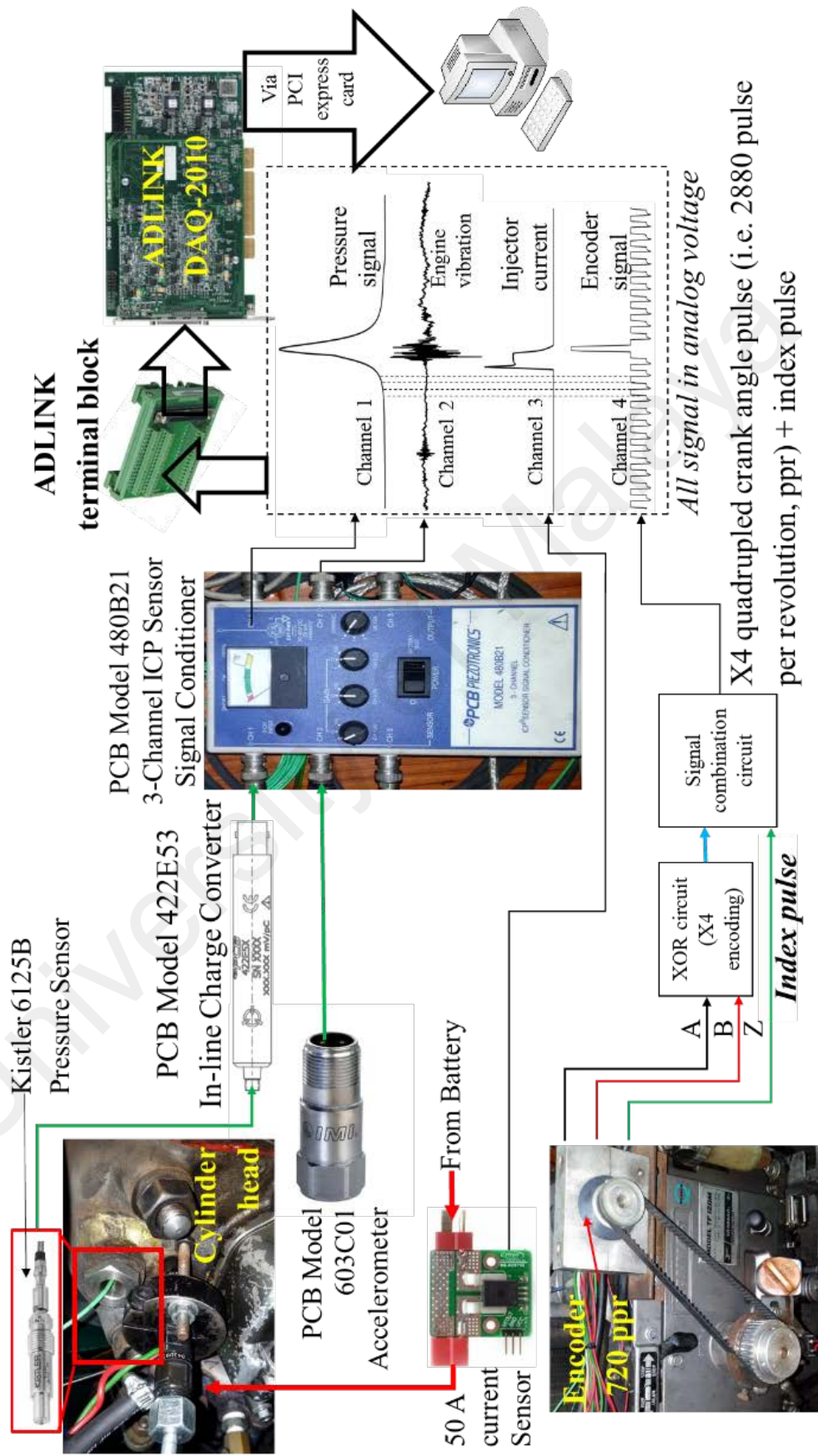


Figure 3.32: High-speed data acquisition system setup and integration with combustion analyzer system.

3.9 Exhaust gas recirculation (EGR) setup

In diesel engines, EGR is usually adopted to moderate the heat release rate (HRR) and combustion timing phasing. Moreover, EGR is a proven approach for the reduction of NO_x emissions. Typically, this method is obtained by mixing a portion of the higher specific heat gases (made up of nitrogen, carbon dioxide etc.) from the exhaust gas with fresh air. Hence, EGR increases the specific heat of the intake charge, which helps to reduce the flame temperature of combustion. The introduction of EGR in naturally aspirated diesel engines is very straightforward because the exhaust line backpressure is usually higher than the intake pressure (Zheng et al., 2004). To establish EGR, the flow passage between the exhaust and the intake manifolds need to be devised and controlled with a throttle valve as shown in Figure 3.33. The generated pressure difference between these two lines is generally sufficient to drive the EGR flow at a desire rate.

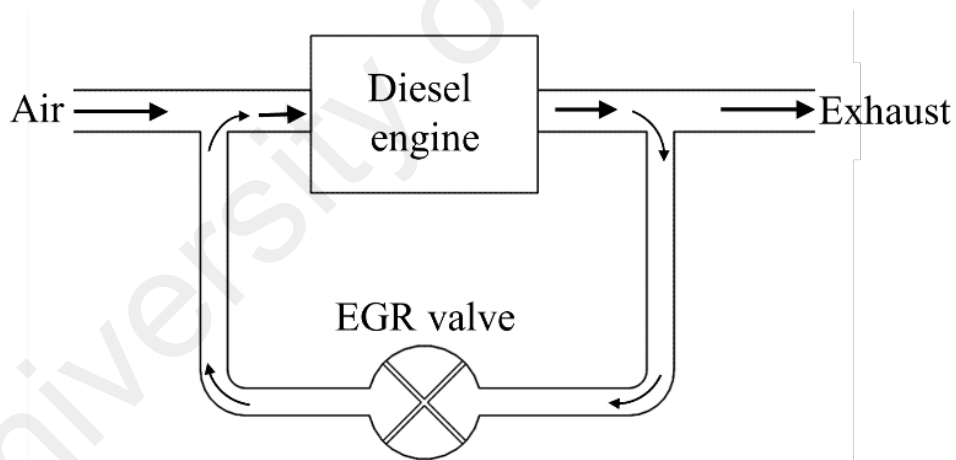


Figure 3.33: Exhaust gas recirculation.

For this research study, the engine operation required the design and installation of a cooled EGR system for integration with the single-cylinder test bed system. In particular, this involved the installation of an EGR valve, EGR cooler, EGR surge tank and two identical CO_2 sensors. EGR cooling enhances the air density and, therefore, the intake air mass flow rate. Cooled EGR was achieved by using an inter-cooler heat exchanger, with ambient air as the cooling medium (air-cooled). To improve its cooling effectiveness, an

automotive type 12-V electric cooling radiator fan was used to draw ambient air through the inter-cooler heat exchanger. The recirculated exhaust gas temperature was maintained under 35°C by controlling the electric cooling radiator fan. However, the exhaust gas has a high water content and cooling of the EGR gas can cause water condensation in the EGR line. To address this problem, the moisture was treated and removed by using silica gel (SiO₂) as an absorbent. The silica gel (about 3 kg) is placed at the bottom of the EGR surge tank to allow heavier exhaust constituents to settle to the bottom of the tank. To ensure that the recirculated gas stream is in contact with the silica gel, the inlet into the surge tank was extended to the bottom to direct the flow to the bottom of the tank. The EGR system setup and the schematic of the EGR system indicating the sensors location is shown in Figure 3.34 and Figure 3.35, respectively.

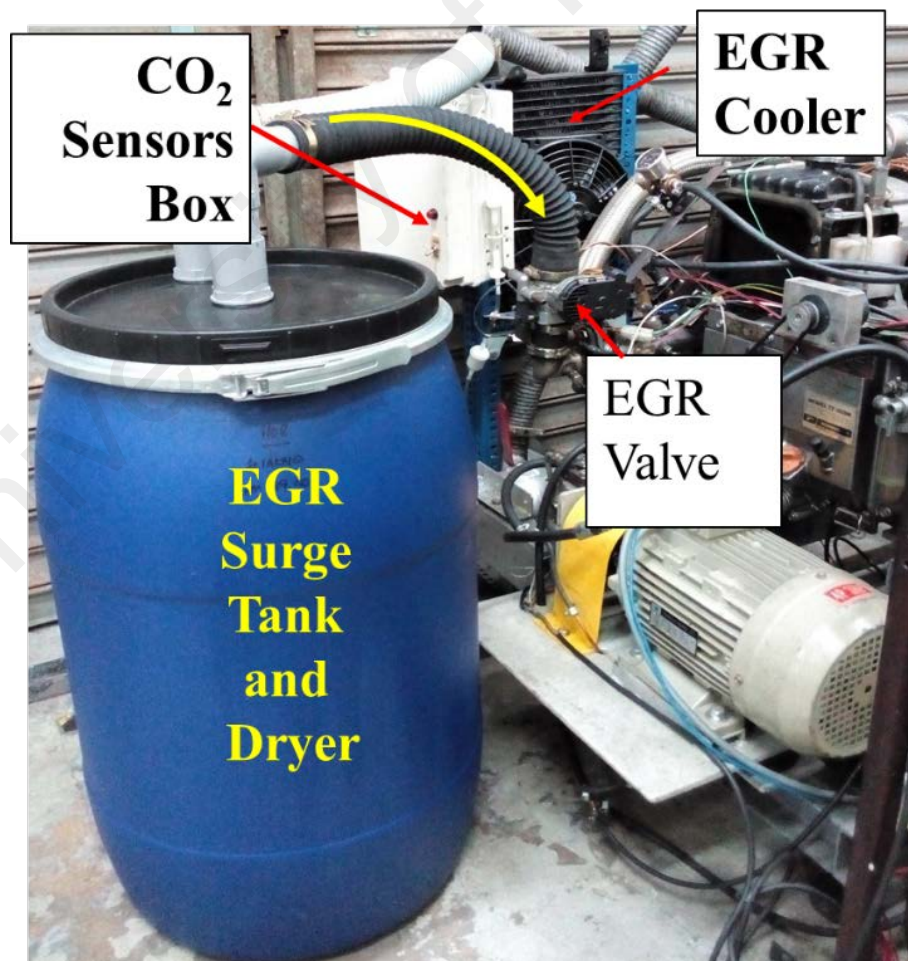


Figure 3.34: EGR system setup.

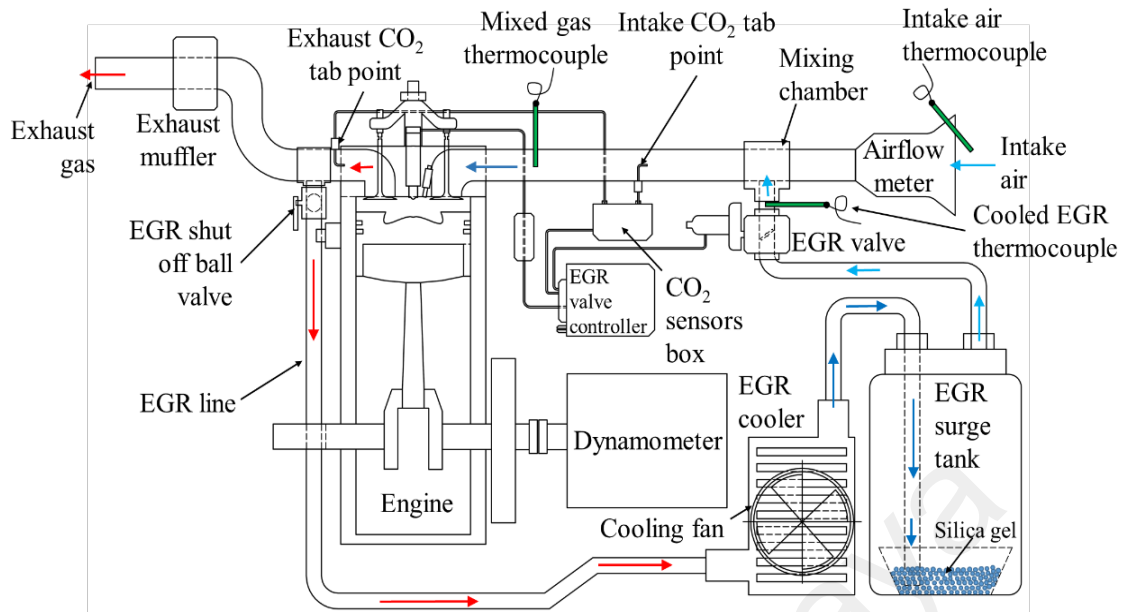


Figure 3.35: Schematic of the EGR system.

Two identical low cost K-33 ICB 30% CO₂ sensors were used for the measurement of the amount of exhaust gas recirculating to the intake and the technical specifications of the sensor are shown in Table 3.13. The first sensor samples the CO₂ concentration of the exhaust gas exiting the engine. The second CO₂ sensor was employed to sample the mixed air before it enters the engine.

Table 3.13: Technical specifications of K-33 ICB 30% CO₂ sensor.

Measurement range	0 – 300,000 ppm (0-30%)
CO ₂ measurement	non-dispersive infrared (NDIR)
Accuracy	± 0.5% vol. CO ₂ ± 3% of measured value
Resolution	0.01% / 100ppm
Measurement rate	30 measurements/ min
Sampling method	tube draw
Sensor life expectancy	> 15 years
Maintenance interval	no maintenance required
Self-diagnostics	complete function checks of the sensor module
Communication option	I ² C

Under steady-state conditions, the EGR rate (Chen et al., 2013; Rajesh kumar & Saravanan, 2015) can be measured on a molar basis by comparing the ratio of the CO₂ level in the intake to the exhaust as follows:

$$\text{EGR (\%)} = \frac{[\text{Intake CO}_2]}{[\text{Exhaust CO}_2]} \times 100 \quad (3.13)$$

It is indeed important to ensure that the sampled gas is clean before entering the CO₂ sensor because the untreated gas might foul the sensor. For each of the exhaust gas and mixed air sampling line, gas is drawn through a 150-micron particulate filter, water trap and finally a 0.20-micron hydrophobic filter for cleaning and to remove excess moisture in the gas. For each of the sampling train, a micro diaphragm pump with a constant flow of 0.5 L/min is used to pull the gas from the sample line and push the gas across a CO₂ sensor. The setup employs an Arduino Mega 2560 microcontroller to initiate data collection with K-33 CO₂ sensors via Inter-Integrated Circuit (I²C) pins. To carry out a basic reading of the CO₂ value from the sensors, the Arduino IDE is used to write the program and load to the microcontroller board via serial communication with the computer. The exhaust and intake air sampling trains system arrangement with the sensors connected to the Arduino Mega 2560 microcontroller is shown in Figure 3.36.

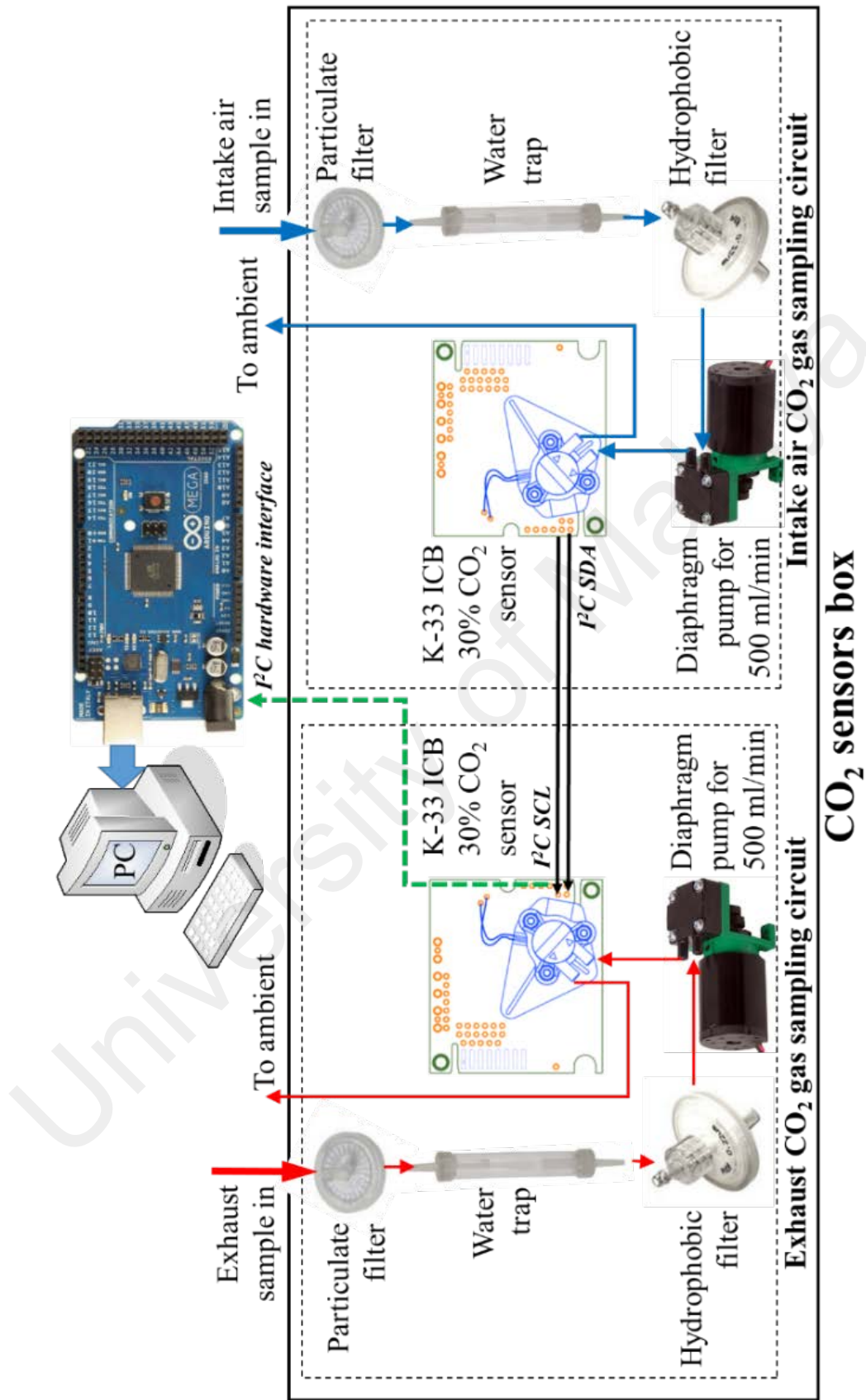


Figure 3.36: Exhaust and intake air sampling trains with sensors connected to the Arduino Mega 2560 microcontroller.

Alternatively, the EGR rate can also be defined volumetrically by calculating the percentage reduction in the volume flow rate of intake air under a fixed operating condition:

$$\text{EGR (\%)} = \frac{\dot{V}_o - \dot{V}_e}{\dot{V}_o} \times 100 \quad (3.14)$$

where \dot{V}_o = volume flow rate of intake air without EGR

\dot{V}_e = volume flow rate of intake air with EGR.

The derivation of Equation 3.14 is based upon a volume balance in the mixing section of intake fresh air and exhaust gases. The step for developing this equation is discussed further below. The volume flow rate of intake air entering the cylinder for both with and without EGR was measured by using the turbine type airflow meter as previously discussed in section 3.7. In Figure 3.37, the point where intake fresh air and exhaust gases mixed is shown. Assuming that the volume of charge entering the engine cylinder remains constant irrespective of the mixtures gas properties and temperature, hence the comparison of two operating conditions can be made: one without and one with EGR. The volume of EGR admitting the engine cylinder, \dot{V}_3 can then be determined according to Figure 3.38. Also, note that the assumption of constant volumetric efficiency was also made for the calculation of EGR. This has led to the following derivation and the variables defined as shown in Figure 3.37:

Based upon a volume balance, thus $\dot{V}_2 = \dot{V}_1 + \dot{V}_3$

Consider for the case of without EGR, thus $\dot{V}_3 = 0$.

Therefore,

$$\dot{V}_2 = \dot{V}_1 = \dot{V}_o = \text{volume flow rate of air without EGR} \quad (3.15)$$

Now consider with EGR and with a constant volumetric efficiency, hence the volume flow rate of EGR admitting the engine cylinder, \dot{V}_3 is calculated through:

$$\dot{V}_3 = \dot{V}_2 - \dot{V}_1$$

\dot{V}_3 = volume flow rate of air without EGR – volume flow rate of air with EGR

$$\dot{V}_3 = \dot{V}_o - \dot{V}_e \quad (3.16)$$

The EGR rate on a volume basis is written as:

$$\text{EGR (\%)}_{\text{volume basis}} = \frac{\dot{V}_3}{\dot{V}_2} \times 100 \quad (3.17)$$

By substituting Equation 3.15 and 3.16 into 3.17, therefore the final expression for EGR

(%) volume basis is equal to Equation 3.14.

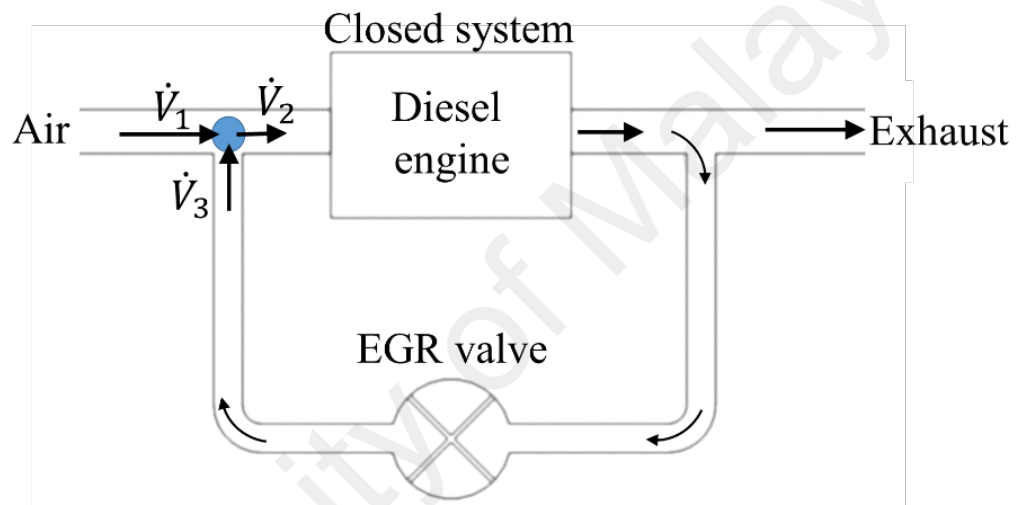


Figure 3.37: Schematic diagram of the mixing point of intake fresh air and exhaust gas.

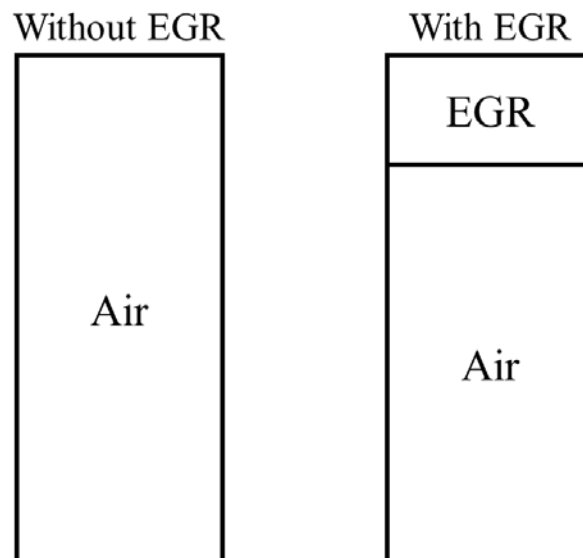


Figure 3.38: Visualization of the intake charge content with and without use of EGR.

The Horiba MEXA-700λ air-to-fuel ratio analyzer as shown in Figure 3.39 was employed to measure the concentration of excess oxygen in the exhaust gas. The excess oxygen in the exhaust gas can also serve as a useful parameter in the monitoring of EGR in diesel engines. With an increasing EGR rate at a fixed operating condition, the excess oxygen available in exhaust gas is expected to reduce due to a decreased oxygen concentration in the fresh charge. Besides, this analyzer uses a wideband zirconia (ZrO_2) sensor to sense the concentration of oxygen in the exhaust gas. This sensor is also known as a UEGO (Universal Exhaust Gas Oxygen) sensor. The analyzer output is transferred via analog output (0 to 5 V DC) and RS-232C serial communication to a PC and data collection was performed with the LabVIEW program (the interface program tab is shown in Figure 3.40).



Figure 3.39: Horiba MEXA-700λ air-to-fuel ratio analyzer and the UEGO sensor.



Figure 3.40: MEXA-700λ O₂ reading interface program tab.

In addition, the EGR setup required the installation of an EGR valve to control the amount of EGR admitting the engine cylinder. The EGR valve opening position and, hence, EGR rate is controlled by adjusting the duty cycle of a pulse-width modulated (PWM) EGR valve. This requires a microcontroller for controlling the EGR valve opening position in order to regulate the EGR rate. In this study, the EGR valve was based on the commercially available Bosch electronic drive-by-wire butterfly valve throttle body. The throttle body is actuated by a motor coil that turn the throttle plate against the tension of a spring. To drive the throttle plate, the microcontroller is programmed to continuously generate a PWM output to the throttle body motor coil via the driver circuit. In addition, the microcontroller also received analog signals from the EGR valve position sensor and performed PID closed-loop throttle opening control. The plot of EGR throttle position opening (%) versus EGR valve position sensor voltage (V) is shown in Figure 3.41. Note that the sensor reading varies from 0.9 volts at closed throttle to 4.8 volts when fully opened. This signal is used by the microcontroller to control throttle valve opening by adjusting the duty cycle of the PWM. The outline diagram of the microcontroller interface with the EGR valve is illustrated in Figure 3.42. In this study, the NI LabVIEW program was used to interface the Arduino microcontroller to PC via a USB serial port. A LabVIEW based GUI program was employed in this study in order to real-time control and monitor EGR parameters such as intake and exhaust CO₂ concentration, the resulted EGR rate using airflow rate and CO₂ measurement method, EGR valve opening set point, and PWM duty cycle. The EGR interface program tab is shown in Figure 3.43.

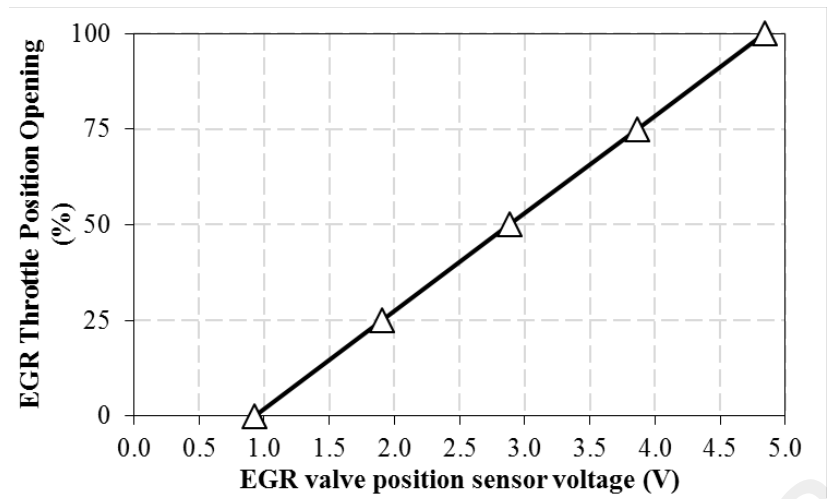


Figure 3.41: EGR valve position sensor chart.

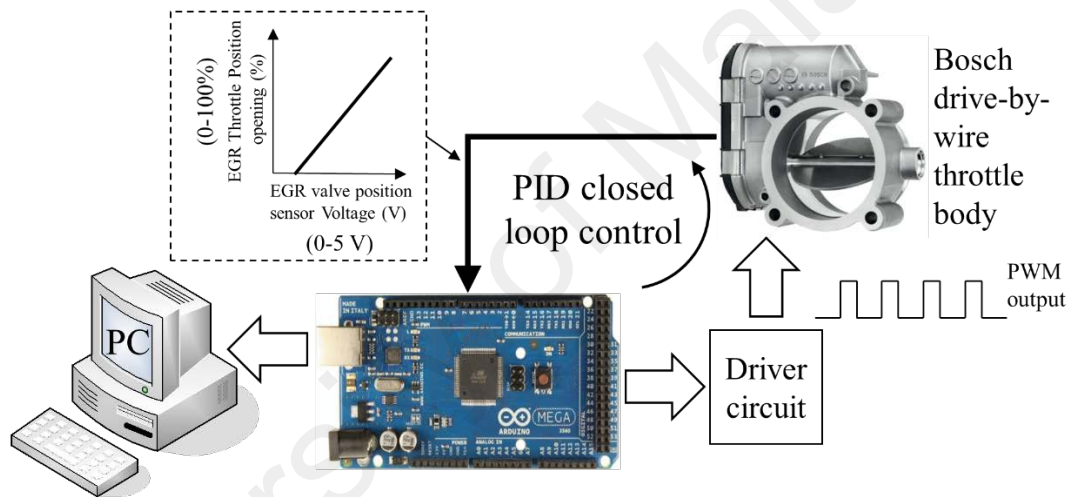


Figure 3.42: Outline diagram of the microcontroller interface with EGR valve.

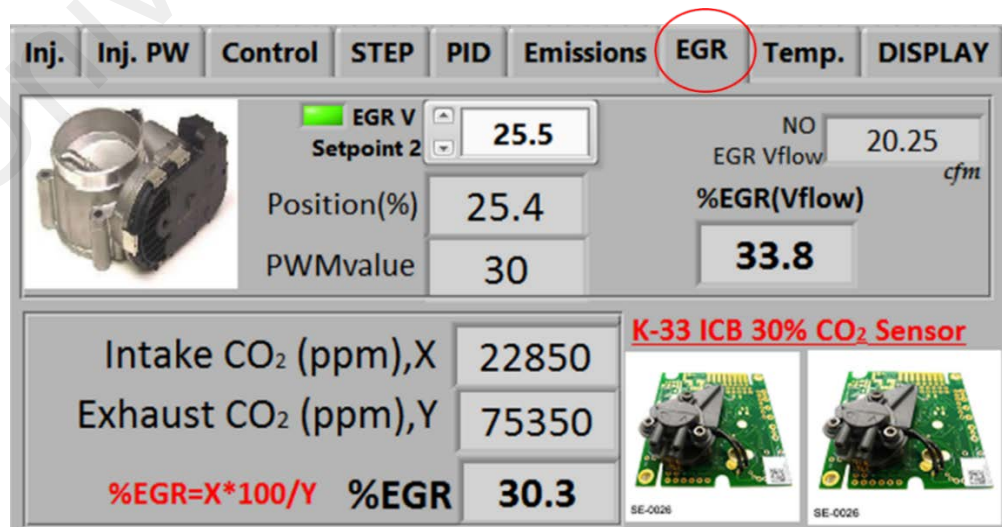


Figure 3.43: EGR interface program tab.

After the EGR valve installations were completed, tests were carried out to characterize the EGR rate in response to the valve opening position. The characteristic curve can be determined by measuring the EGR rate at various valve opening positions. During the tests, the EGR valve was re-positioned at 5% increments and EGR rate measurements were performed. Measured EGR rates using both the CO₂ method and the volume flow rate of intake air method, as well as the result of exhaust gas excess O₂ concentration, in response to the valve opening position are depicted in Figure 3.44. Note that measurements were performed at an engine speed of 1000 rpm with partial load of 0.2 MPa. As visible, the measured EGR rate based on volume flow rate method is simply proportional to the valve opening position. As for the measured EGR rate based on the CO₂ method, the EGR rate variation was highly linear from 10% to 40% of valve opening position. Besides, the amount of excess oxygen present in the exhaust stream decreased systematically as the valve opening position was increased. This implies that EGR reduces the available oxygen in the cylinder, thus lowering the amount of NO_x formed during the combustion process. Overall, the EGR rate calculation based on a molar basis by using Equation 3.13 was considered in this study since this method is usually employed in research on internal combustion engines (Chen et al., 2013; Lattimore et al., 2016; Rajesh kumar & Saravanan, 2015).

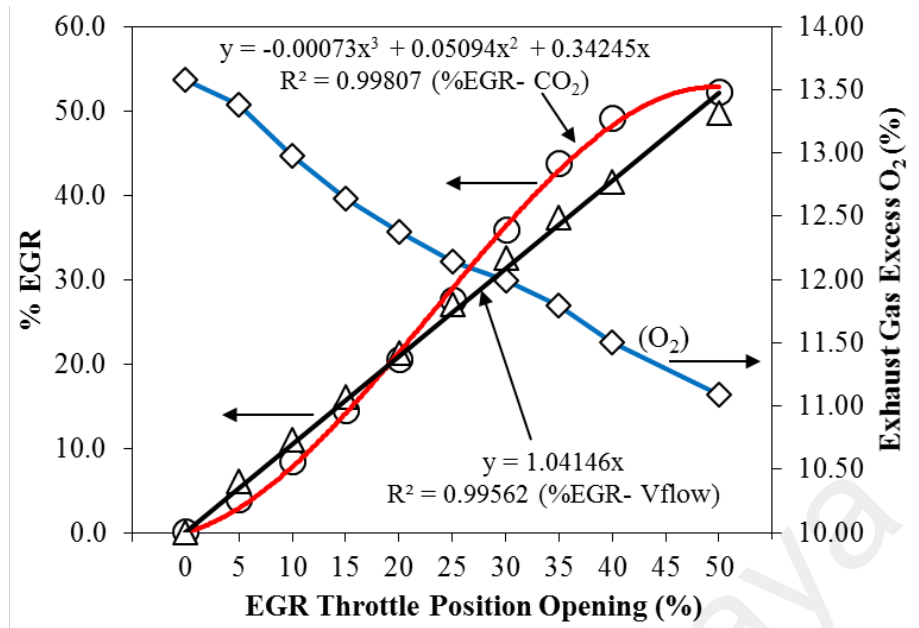


Figure 3.44: EGR valve characteristic curve.

3.10 Calculation methods

3.10.1 Engine performance

The engine performance in this work was evaluated based on the BSFC and BTE. The BSFC and BTE were determined and calculated according to the following equations:

$$\text{BSFC} \left(\frac{g}{kW\text{hr}} \right) = \frac{\text{Fuel Consumption} \left(\frac{g}{\text{hr}} \right)}{\text{Brake Power} (kW)} \quad (3.18)$$

$$\text{BTE} (\%)$$

$$= \frac{\text{Brake Power} (kW) \times 360}{\text{Calorific Value} \left(\frac{MJ}{kg} \right) \times \text{Fuel Consumption} \left(\frac{L}{\text{hr}} \right) \times \text{Density} \left(\frac{kg}{L} \right)} \quad (3.19)$$

3.10.2 Combustion analysis

HRR analysis is a useful approach to assess the effects of the fuel injection system, fuel type, engine design changes, and engine operating conditions on the combustion process and engine performance (Ghojel & Honnery, 2005). Given the plot of HRR *versus* crank angle, it is easy to identify the SOC timing, the fraction of fuel burned in the premixed

mode, and differences in the combustion rates of fuels (Canakci, Ozsezen, & Turkcan, 2009). In this study, different fuels were used in an identical compression ignition engine; hence, the HRR information is an important parameter in interpreting the engine performance and exhaust emissions. In this study, the averaged in-cylinder pressure data of 100 successive cycles, acquired with a 0.125° crank angle resolution, were used to compute the HRR. The HRR, given by $\frac{dQ}{d\theta}$, at each crank angle was obtained from the first law of thermodynamics, and it can be calculated by the following formula:

$$\frac{dQ}{d\theta} = \frac{\gamma}{\gamma - 1} P \frac{dV}{d\theta} + \frac{1}{\gamma - 1} V \frac{dP}{d\theta} \quad (3.20)$$

where, γ = specific heat ratio, P = instantaneous cylinder pressure (Pa), and V = instantaneous cylinder volume (m³).

3.11 Statistical and equipment uncertainty analysis

Experimental errors and uncertainties can arise from instrument selection, condition, calibration, environment, observation, reading, and test procedures. The measurement range, accuracy, and percentage uncertainties associated with the instruments used in this experiment are listed in Table 3.14. Uncertainty analysis is necessary to verify the accuracy of the experiments. Percentage uncertainties of various parameters, such as BSFC, BTE, BSHC, BSCO, and BSNO_x were determined using the percentage uncertainties of various instruments employed in the experiment. To compute the overall percentage uncertainty due to the combined effect of the uncertainties of various variables, the principle of propagation of errors is considered and can be estimated as $\pm 4.3\%$. The overall experimental uncertainty was computed as follows:

$$\begin{aligned} \text{Overall experimental uncertainty} &= \text{Square root of } [(\text{uncertainty of Fuel Flow Rate})^2 + \\ &(\text{uncertainty of BSFC})^2 + (\text{uncertainty of BTE})^2 + (\text{uncertainty of BSCO})^2 + (\text{uncertainty} \\ &\text{of BSNO}_x)^2 + (\text{uncertainty of exhaust gas temperature, EGT})^2 + (\text{uncertainty of Smoke})^2 \\ &+ (\text{uncertainty of Pressure sensor})^2 + (\text{uncertainty of Crank angle encoder})^2] \\ &= \text{Square root of } [(2)^2 + (1.95)^2 + (1.74)^2 + (2.22)^2 + (0.73)^2 + (0.15)^2 + (1)^2 + (1)^2 + \\ &(0.03)^2] = \pm 4.3\% \end{aligned}$$

Table 3.14: List of measurement accuracy and percentage uncertainties.

Measurement	Measurement range	Accuracy	Measurement techniques	% Uncertainty
Load	±120 Nm	±0.1 Nm	Strain gauge type load cell	±1
Speed	60-10,000 rpm	±1 rpm	Magnetic pick up type	±0.1
Time	-	±0.1s	-	±0.2
Fuel flow measurement	0.5-36 L/hr	±0.01 L/hr	Positive displacement gear wheel flow meter	±2
Air flow measurement	2-70L/s	±0.04L/s	Turbine flow meter	±0.5
CO	0-10% by vol.	±0.001%	Non-dispersive infrared	±1
NO _x	0-5,000 ppm	±1ppm	Electrochemical	±1.3
Smoke	0-100%	±0.1%	Photodiode detector	±1
EGT sensor	0-1200°C	±0.3°C	Type K thermocouple	±0.15
Pressure sensor	0-25,000 kPa	±12.5 kPa	Piezoelectric crystal type	±1
Crank angle encoder	0-12,000 rpm	±0.125°	Incremental optical encoder	±0.03
Computed				
BSFC	-	±7.8 g/kWhr	-	±1.95
BTE	-	±0.5 %	-	±1.74
BSCO	-	±0.1 g/kWhr	-	±2.22
BSNO _x	-	±0.1 g/kWhr	-	±0.73

CHAPTER 4: RESULTS AND DISCUSSION

4.1 Introduction

This chapter presents the experimental results of the engine performance, exhaust emissions, vibration and combustion characteristics of the converted diesel engine using conventional diesel fuel as baseline fuel, neat biodiesels of PME and JME, and its biodiesel-diesel blends. Firstly, the effect of injection timing variation, injection pressure variation and injection strategies on engine performance, emissions and combustion characteristics of the converted common-rail diesel engine are discussed. Secondly, the impact of neat palm biodiesel, Jatropha biodiesel and their respective fuel blends, and diesel fuel in an engine equipped with high-pressure common-rail injection system is analyzed and discussed. Thirdly, parametric studies dealing with injection timing variation using neat palm biodiesel in common-rail engine are compared with baseline diesel. Fourthly, the effect of EGR on the performance, emissions and combustion of the baseline diesel and PME fuelled engines are discussed. Lastly, a more comprehensive study which involved operating the engine in dual-fuel combustion mode is investigated.

Section 4.2: Shows the effect of the converted common-rail fuel injection system on engine-out responses.

Section 4.3: Shows the effect of biodiesels and its blends on the common-rail diesel engine.

Section 4.4: Shows the effect of fuel injection timing variation with biodiesel.

Section 4.5: Shows the effect of EGR variation with biodiesel.

Section 4.6: Shows the effect of dual-fuel combustion with injection timing variation and EGR variation.

4.2 Engine-out responses of the converted common-rail fuel injection system

Upon completion of the engine conversion to common-rail injection system, three series of tests were conducted to evaluate the performance of the developed fuel injection system control. The effect of injection timing variation, injection pressure variation and injection strategies on engine performance, emissions and combustion characteristics of the modified diesel engine are discussed in the following sub-sections.

4.2.1 Effect of injection timing variation

The SOI timing is a crucial parameter that determines engine performance. Thus the effective control SOI of fuel into the cylinder is key to improved engine performance and emissions in diesel engines. Figure 4.1 illustrates the resulting effect of SOI timing on engine torque under various speed and load conditions. Note that the term “load” in this context represents a constant injected fuel mass (via a fixed injection pulse width) which applied throughout the SOI variation for a certain engine load condition. With a fixed amount of fuel injected, changing of SOI timing will alter the combustion process, thus affecting the engine output torque. Generally, a total of nine operating conditions were selected to cover a wide range of engine operating parameters. From the results, it was observed that more advanced SOI timing (as much as 12°CA for low to high speed) is generally required at higher engine speed to attain the maximum brake torque at each loading condition. Also, the SOI timing is necessary to advance slightly (as much as 4°CA for low to high load) as the engine load rises at each engine speed condition. The optimal SOI timing that translates to maximum brake torque is marked with a circle at each operating condition. Apparently, non-optimized SOI timings may result in lower engine efficiency caused by the incomplete combustion of fuel and early buildup of cylinder pressure for too late and too early of SOI timing cases, respectively. This was most easily realized with the common-rail system that allows greater flexibility in the timing control

of the fuel injection event for minimal emissions, efficiency, and maximum torque generation.

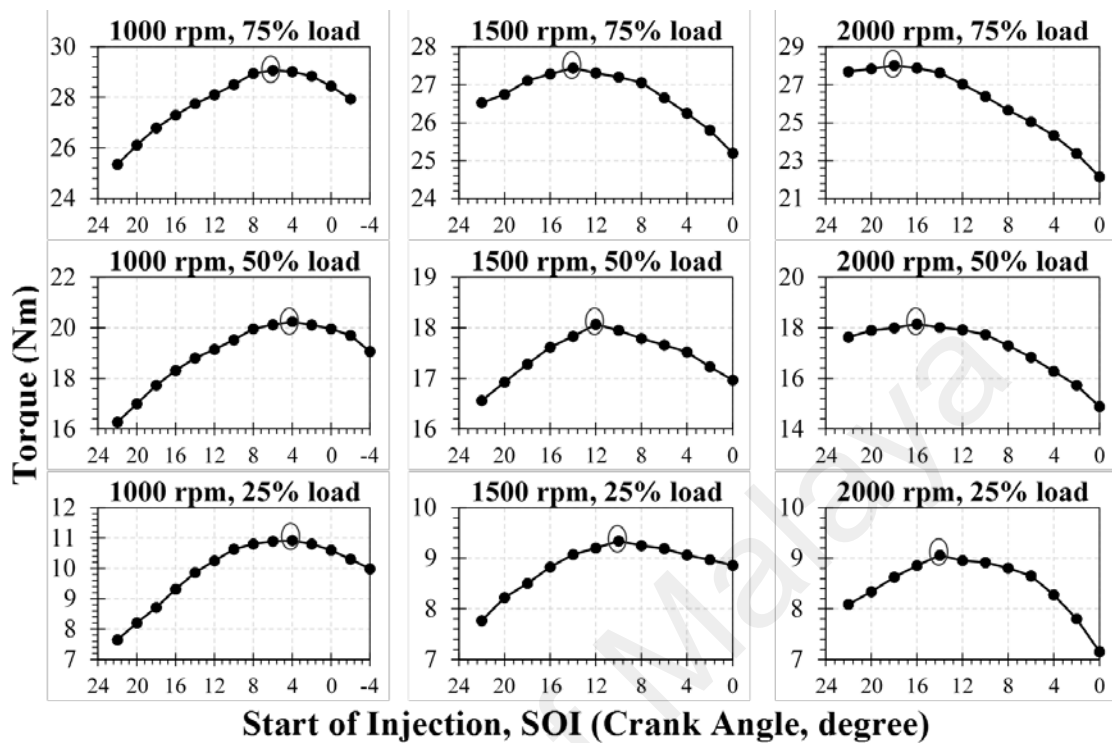


Figure 4.1: Effect of SOI timing on engine torque under various engine speed and load conditions under a constant injection pressure of 600 bar, without EGR and diesel fuel with compression ignition (maximum torque as indicated with circle).

Figure 4.2 shows the variation of combustion pressure and heat release rate (HRR) with respect to the crank angle at different SOI timings for the engine operated at 1500 rpm and 50% load. Generally, the combustion pressure peak consistently increases and shifted earlier toward the TDC position with advancing SOI timing. The resultant higher and more effective pressure was utilized to perform useful work and thus improve the brake torque. However, further advance in SOI timing beyond 12° BTDC caused combustion pressure to build up rapidly in the compression stroke, thus beginning to oppose the upward movement of the piston and causing deterioration in efficiency. This indicates that too high in peak pressure does not necessary lead to higher engine torque. The HRR curves have similar patterns, as the combustion pressure trend where the HRR peak that is associated with premixed combustion was shifted earlier toward the compression stroke with advanced SOI timing. When SOI was advanced toward the TDC in the expansion

stroke, the maximum HRR associated with the premixed combustion became initially lower and remained unchanged. However, further advances in SOI timing beyond 12° BTDC have led to significant increases in the maximum HRR. This was due to a longer ignition delay, which tends to promote more premixed combustion and increases both the maximum combustion pressure and HRR as shown in Figure 4.3. In addition, the results from Figure 4.3 reveal that as the SOI is advanced, the initial temperature and pressure are lower and thus result in longer ignition delay. Longer ignition delay permits better mixing of fuel and air prior to initiation of the combustion process, thus resulting in a higher first HRR peak. In fact, the magnitude of the first HRR peak correlates well with the ignition delay. As more fuel is consumed during the premixed phase, less heat is released in the mixing-controlled phase as evidenced by the lower second HRR peak beyond the SOI of 12° BTDC. It is worth noting that the HRR process can be precisely controlled by the SOI timing by using this custom-build common-rail diesel injection system.

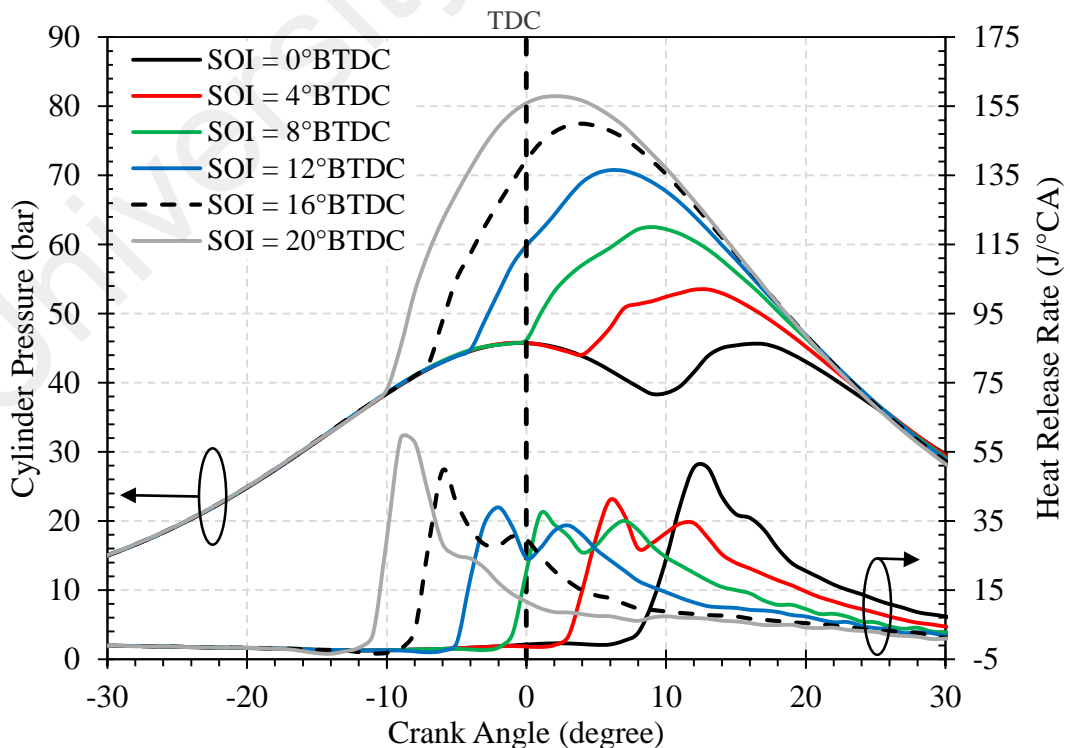


Figure 4.2: Combustion pressure and HRR curves at various SOI timings under 1500 rpm, 50% load and under a constant injection pressure of 600 bar and without EGR.

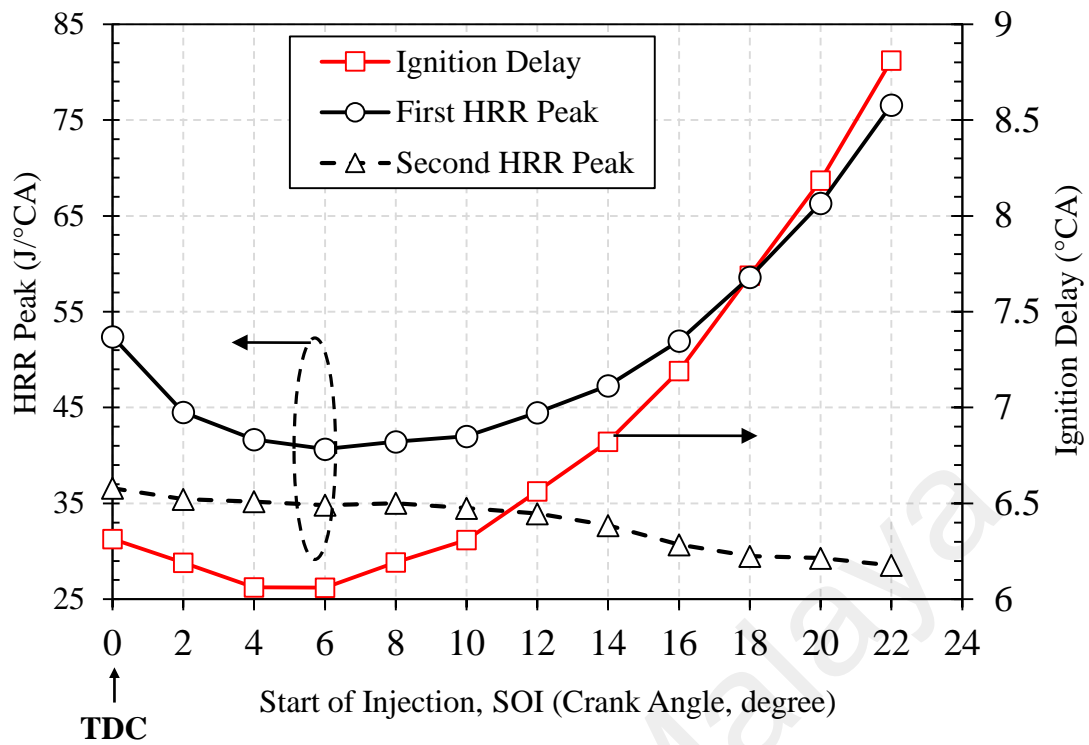


Figure 4.3: Effect of SOI timing on the first and second HRR peaks and ignition delay at 1500 rpm, 50% load and under a constant injection pressure of 600 bar and without EGR.

The variation of NO_x and smoke emissions at various SOI timings at 1500rpm and 50% load is illustrated in Figure 4.4. In general, the results show that advancement of the SOI timing resulted in increased NO_x emissions. The increasing trend in NO_x emissions suggested that with advanced SOI timing, the mixture ignites and burns earlier, hence resulting in early occurrence of peak pressure near TDC. This leads to a higher combustion temperature and promotes the thermal or Zeldovich NO_x formation mechanism. It can also be seen that the smoke emission level decreased with advanced SOI timings. This is due to cylinder operating temperatures being higher for advanced SOI timings, which improved the reaction between fuel and oxygen and resulted in lower smoke emissions. From the results of the SOI timing effect on NO_x and smoke emissions, an optimal trade-off between NO_x and smoke emissions can be achieved with SOI of 12° BTDC, with no adverse effect on engine performance.

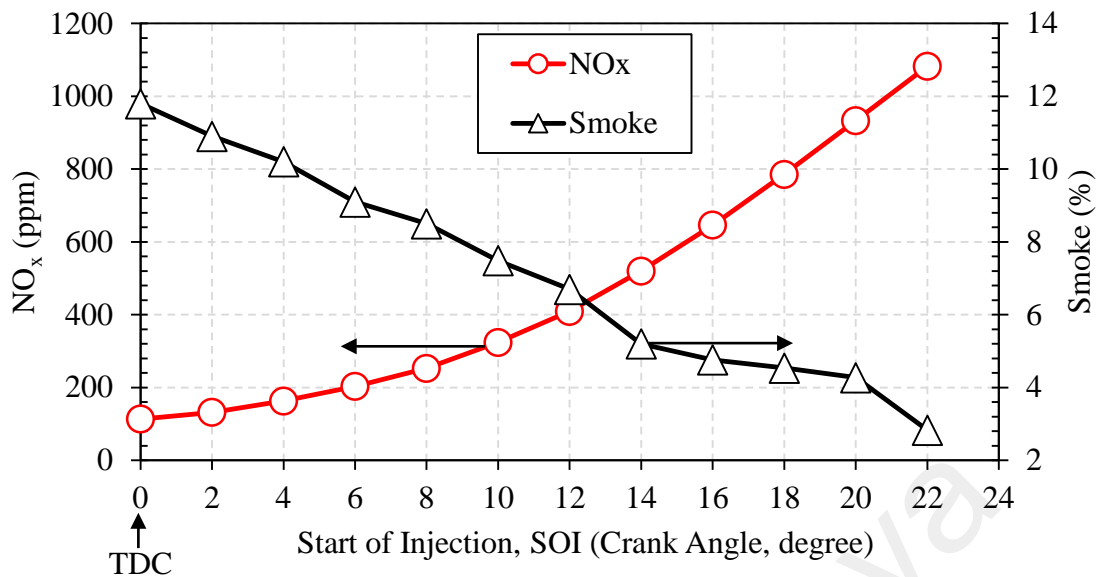
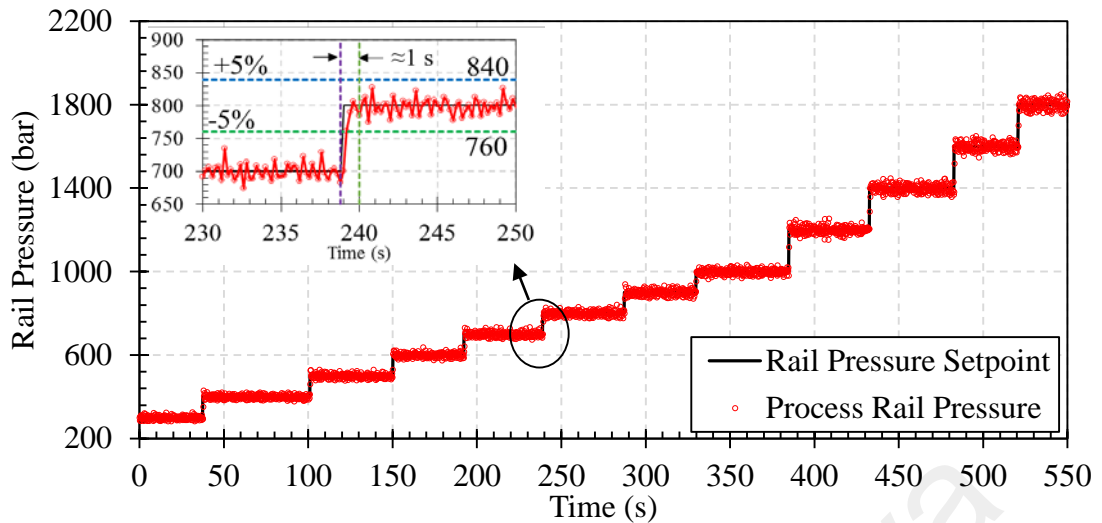


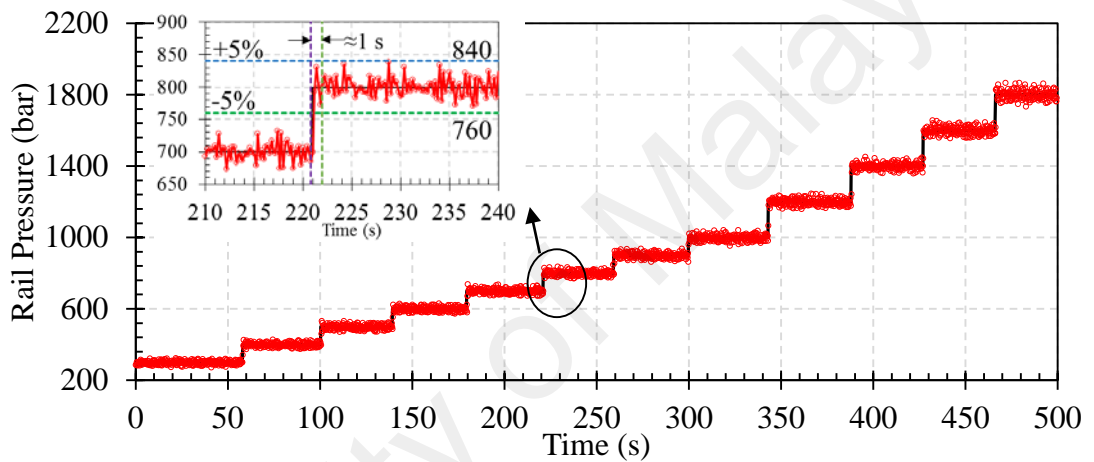
Figure 4.4: NO_x and smoke emission with various SOI timing at 1500 rpm, 50% load and under a constant injection pressure of 600 bar and without EGR.

4.2.2 Effect of injection pressure variation

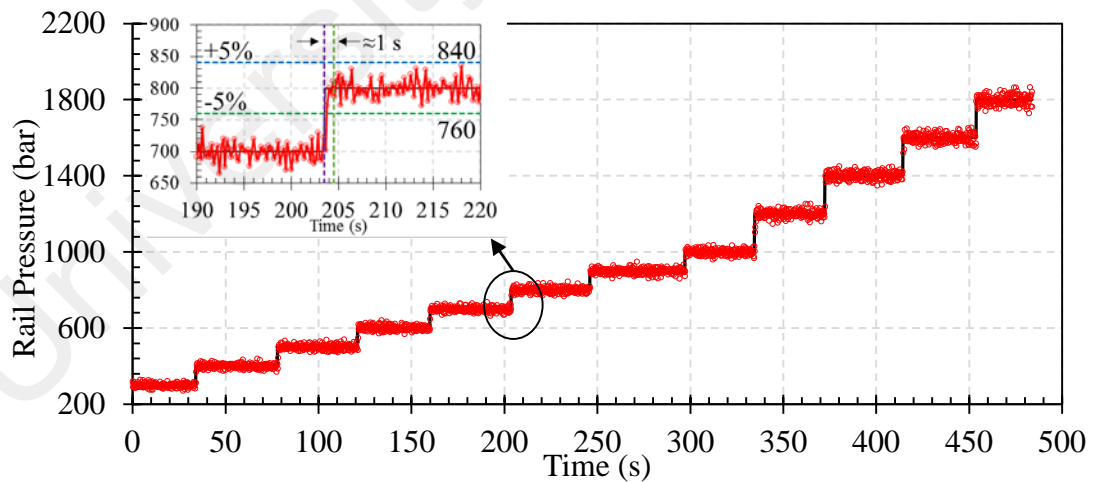
The level of rail pressure can be precisely controlled by varying the duty cycle for which current is applied from the controller to the suction control valve. The control system is based on closed-loop feedback control scheme for regulation of rail pressure with the engine test. The feedback section is a PID controller and the control gains are tuned to suit a wide variety of engine operating conditions. For this specific common-rail system, the rated rail pressure is 1800 bar. Figure 4.5 shows the control results of the rail pressure during the step change at engine speeds of (a) 1000 rpm, (b) 1500 rpm, and (c) 2000 rpm. Generally, the results reveal that the rising time is less than one second and the steady state error is less than 5% in tracking the targeted rail pressure. Additionally, in a PID control loop tuning strategy, the test duration of around 50 s is sufficient for the observation of the steady state behavior of the system under each of the pressure step change.



(a) 1000 rpm



(b) 1500 rpm



(c) 2000 rpm

Figure 4.5: Closed-loop response of the rail pressure with 100 bar (for 300-1000 bar) and 200 bar (for 1000-1800 bar) step change at various engine speed of (a) 1000 rpm, (b) 1500 rpm, and (c) 2000 rpm, 50% load. All tests were conducted without EGR.

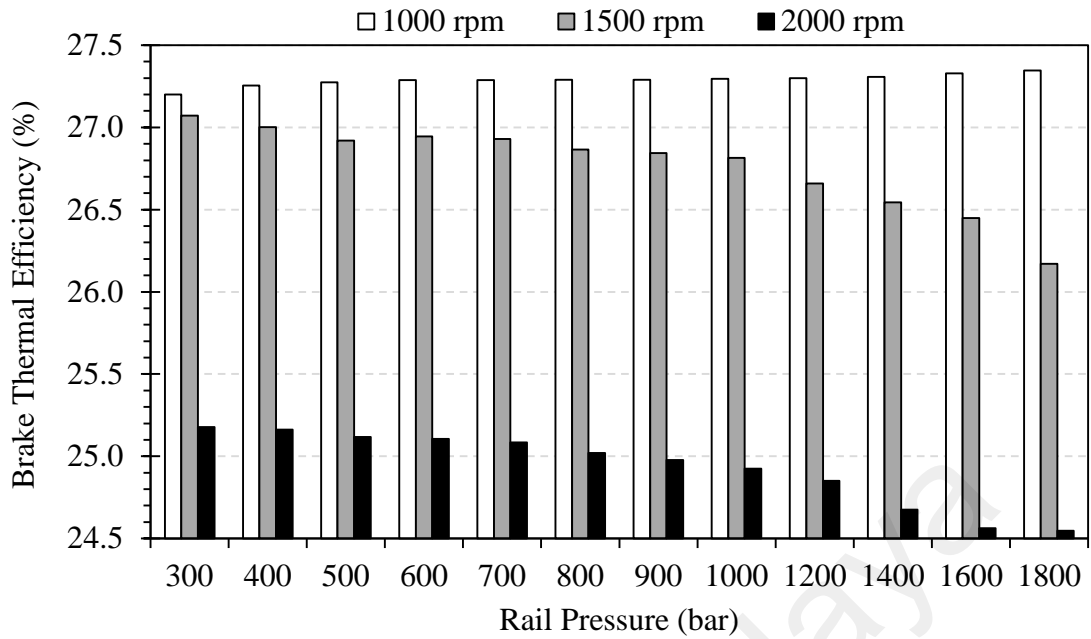


Figure 4.6: Engine BTE for varying rail pressure and engine speed (SOI_{1000 rpm} = 4° BTDC, SOI_{1500 rpm} = 12° BTDC, and SOI_{2000 rpm} = 16° BTDC). All tests were conducted without EGR and at 50% load.

In this study, fuel rail pressure was controlled using an in-house built ECU controller, which has flexibility for user defined control of fuel rail pressure at a wide range of pressure levels. Experiments were performed in order to analyze BTE, NO_x and smoke emissions at 12 rail pressure levels (300 – 1800 bar) and three different engine speeds. Figure 4.6 shows that the BTE decreased with increasing rail pressure setting at engine speeds of 1500 rpm and 2000 rpm, but hardly varied at the lower engine speed of 1000 rpm. The lower BTE is due to relatively inferior combustion characteristics, which led to lower energy conversion efficiency at higher injection pressure. Besides, the BTE was seen to be significantly lower at very high fuel injection pressures of beyond 1000 bars for engine speeds of 1500 and 2000 rpm. In addition, NO_x emissions (Figure 4.7) increased significantly with increasing fuel injection pressure due to higher HRR during the premixed combustion phase. It is observed that for an engine speed of 1500 rpm, a drastic NO_x increment of 430% at very high injection pressure of 1800 bar was obtained compared with a lower injection pressure of 300 bar. Again, this indicates that inappropriate adjustment of injection pressure may result in lower engine efficiency and

higher exhaust emissions. Figure 4.8 shows the variation of smoke emissions at different rail pressures, at 1000, 1500 and 2000 rpm. Generally, higher fuel injection pressure resulted in lower smoke emissions due to relatively superior fuel-air mixing for all engine speed conditions. However, this effect is found diminished by the adverse effect of spray-wall interaction issue, especially for lower engine speed of 1000 and 1500 rpm. Raising fuel injection pressure under both of the engine speeds were found to be less effective for smoke reduction as compared with higher engine speed of 2000 rpm. This is mainly due to the increased in penetration length of the fuel spray and caused fuel spray impingement on the relatively slow moving piston surfaces (i.e. low engine speed) and on the combustion chamber walls, thus resulted in improper combustion of some of the injected fuels and higher in smoke. Figure 4.9 shows that the HRR peak associated with the premixed combustion phase increased with greater fuel injection pressure because of the enhanced fuel atomization at higher injection pressure, which promoted mixing and led to a lower ignition delay. Further, the combustion duration decreased with increasing fuel injection pressure due to significantly higher HRR. Besides, the results indicate that the value of HRR peak associated with the premixed combustion phase is increased with greater fuel injection pressure. Higher fuel injection pressure has led to a longer spray tip penetration and larger spray area as compared to lower fuel injection pressure, which improve the mixing of air and fuel, thus results in significant portion of heat released during the premixed combustion phase. Figure 4.10 shows the cylinder pressure and HRR curves for varying injection pressures at various engine speeds. Generally, one can notice the combustion pressure peak consistently increases and shifted earlier toward the compression stroke with higher injection pressure. For a low engine speed of 1000 rpm, the resultant higher and more effective combustion pressure was utilized to perform useful work and thus improve the brake thermal efficiency. Ironically, for 1500 and 2000 rpm cases, the combustion pressure which built up rapidly in the compression stroke

begins to oppose the upward movement of the piston, causing deterioration in efficiency. The HRR curves have similar patterns, as the combustion pressure trend where the HRR peak that is associated with premixed combustion was shifted earlier toward the compression stroke with higher injection pressure. This shift is clearly visible at engine speeds of 1500 and 2000 rpm.

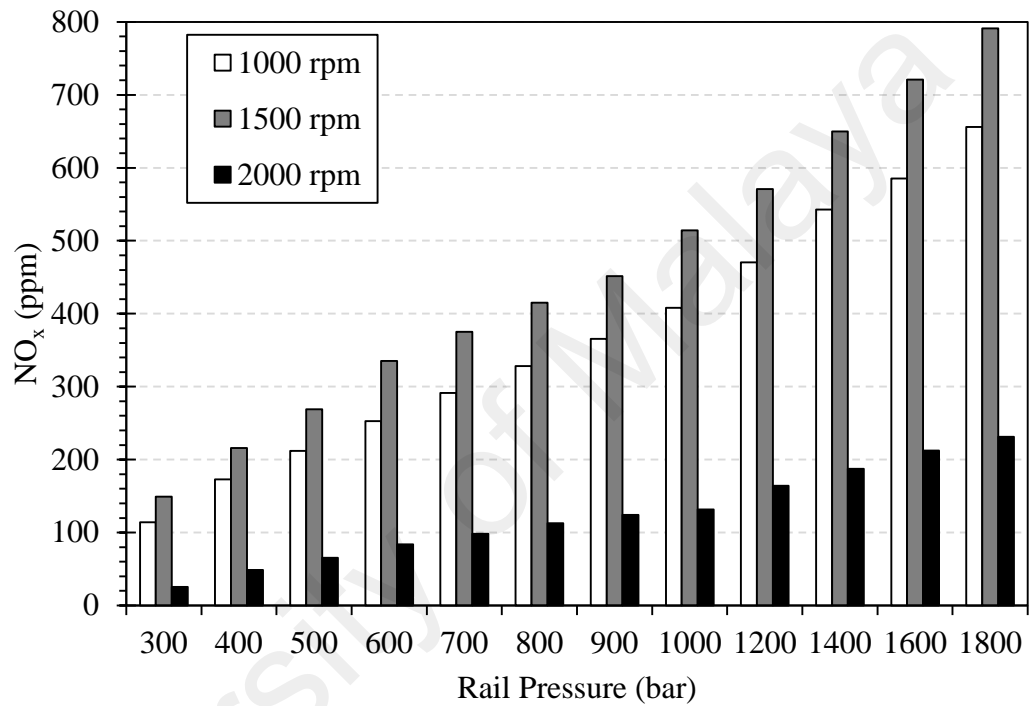


Figure 4.7: NO_x emission for varying rail pressure and engine speed (SOI_{1000 rpm} = 4° BTDC, SOI_{1500 rpm} = 12° BTDC, and SOI_{2000 rpm} = 16° BTDC). All tests were conducted without EGR and at 50% load.

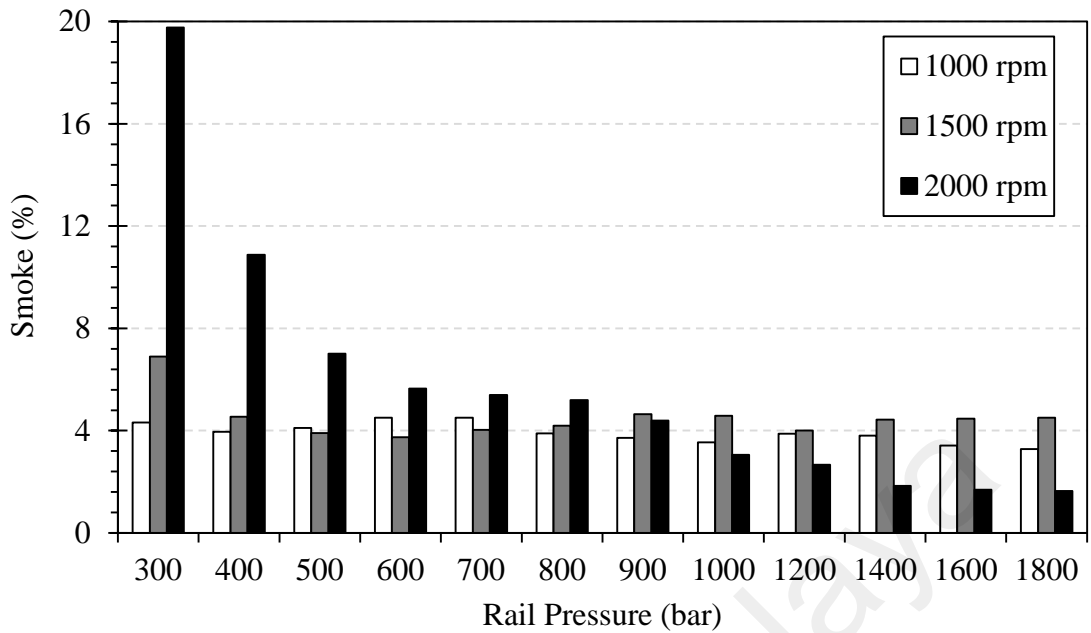


Figure 4.8: Smoke emission for varying rail pressure and engine speed ($SOI_{1000\text{ rpm}} = 4^\circ$ BTDC, $SOI_{1500\text{ rpm}} = 12^\circ$ BTDC, and $SOI_{2000\text{ rpm}} = 16^\circ$ BTDC). All tests were conducted without EGR and at 50% load.

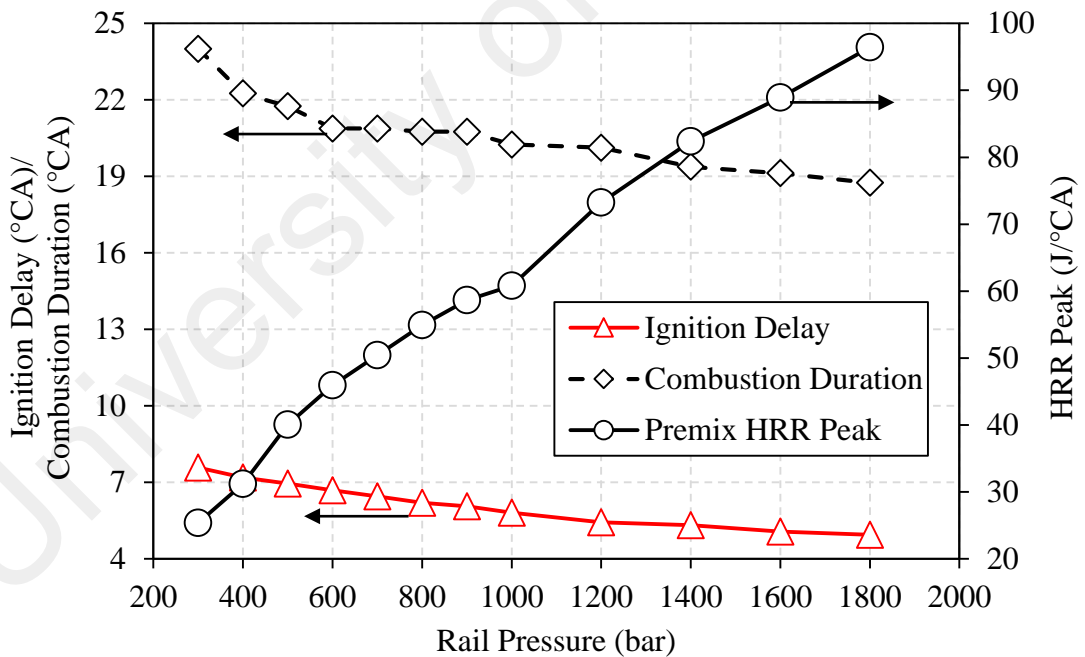
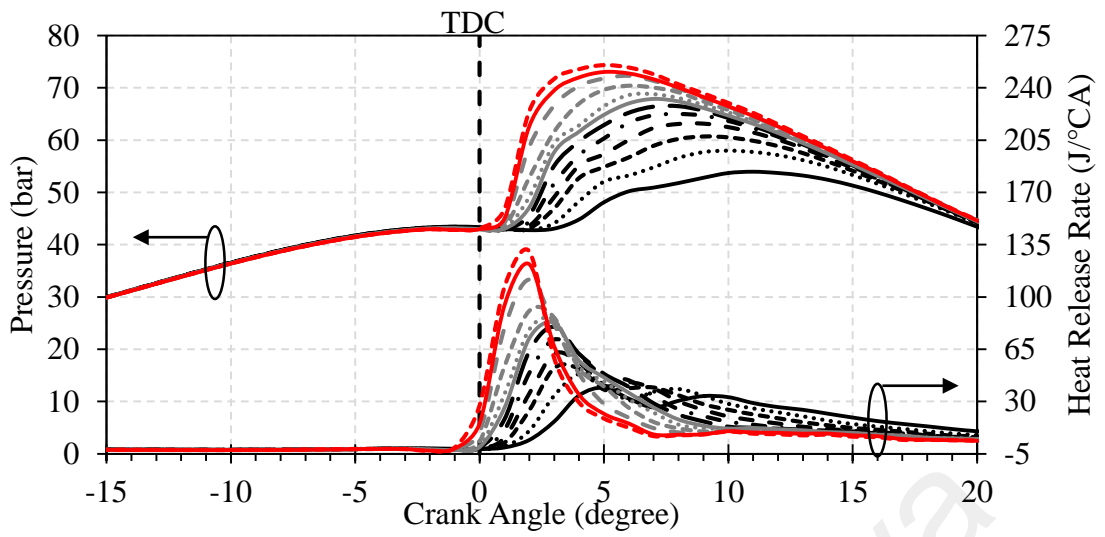
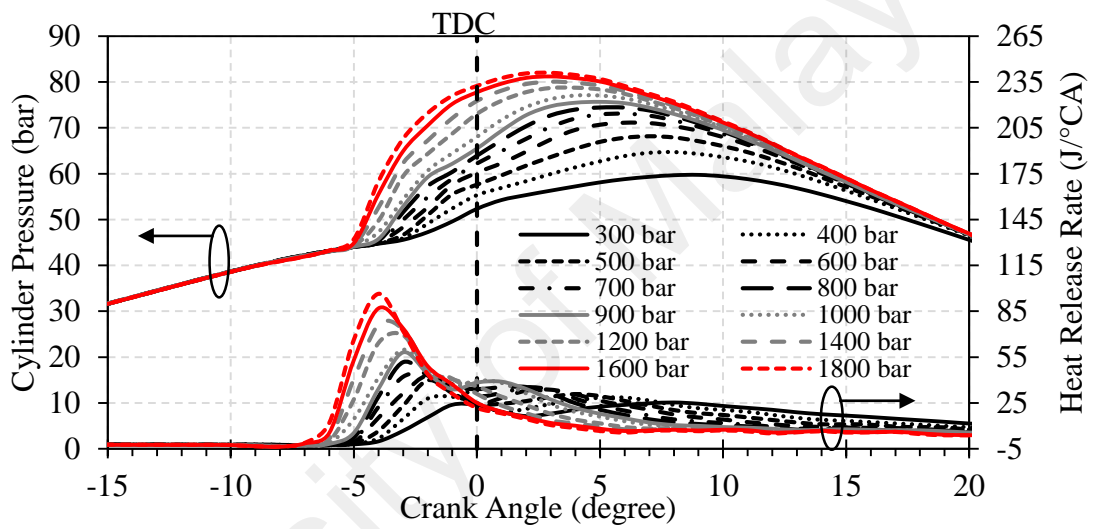


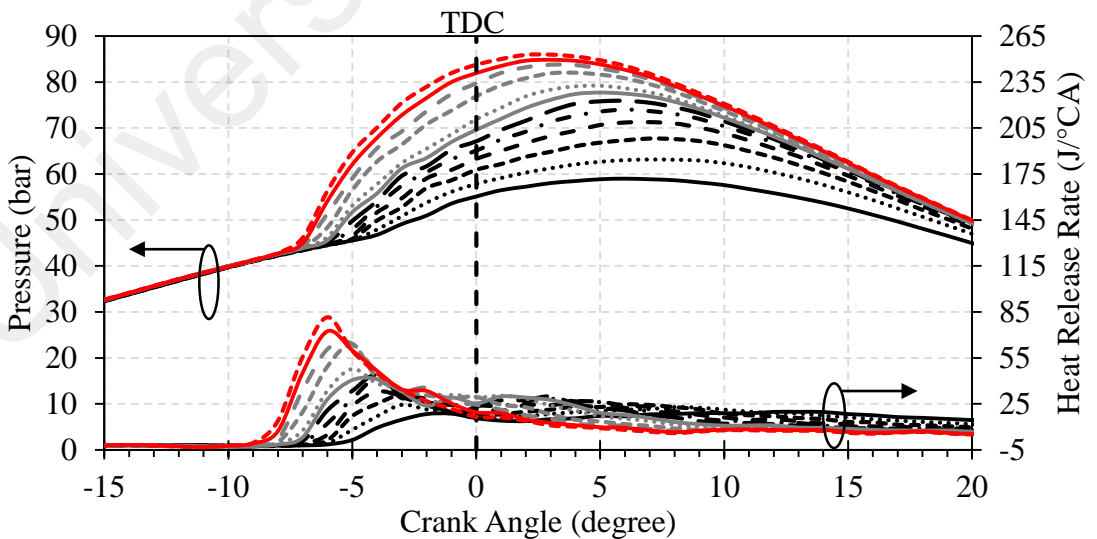
Figure 4.9: Effect of injection pressure on HRR peak, ignition delay and combustion duration at 1500 rpm, 50% load setting ($SOI_{1500\text{ rpm}} = 12^\circ$ BTDC). All tests were conducted without EGR.



(a) 1000 rpm



(b) 1500 rpm



(c) 2000 rpm

Figure 4.10: Combustion pressure and HRR curves at various fuel injection pressure under (a) 1000 rpm, (b) 1500 rpm, and (c) 2000 rpm, 50% load ($SOI_{1000\text{ rpm}} = 4^\circ$ BTDC, $SOI_{1500\text{ rpm}} = 12^\circ$ BTDC, and $SOI_{2000\text{ rpm}} = 16^\circ$ BTDC). All tests were conducted without EGR.

4.2.3 Effect of injection strategies

Multiple injections, including pilot injections and post-injections, are widely used to control PM and NO_x emissions, noise and to manage exhaust after treatment devices. Figure 4.11 shows the result of BTE, smoke, NO_x and pressure rise rate for engines operating with various injection strategies such as single main injection, double injection of pilot and main, and triple injection of pilot, main and post under various fuel injection pressures. In this test scheme, the engine speed is set constantly at 1500 rpm with 50% load and at SOI of 12°BTDC. From the Figure 4.11 (a), the results showed BTE for double injection strategy being consistently lower than that of single injection for all injection pressure. This is due to the early buildup of cylinder pressure in the compression stroke beginning to oppose the upward movement of the piston and causing deterioration of the efficiency as shown in Figure 4.12. Besides, the introduction of triple injection has slightly increased in BTE at a lower injection pressure of 400 bar, but decreased with greater injection pressure as compared to the single injection strategy. From the emissions aspect, smoke is decreased with the introduction of double and triple fuel injection strategies with respect to single strategy across all injection pressures as shown in Figure 4.11 (b). This indicates the effectiveness of post injection in soot oxidation, thus further reducing smoke emissions. However, the engine with double injection produced more NO_x emission compared with the single injection strategy across all injection pressures as shown in Figure 4.11 (c). This can be attributed to higher combustion temperatures near the cylinder TDC as a result of pilot combustion. However, the triple injection approach is found to generally produce less NO_x emissions, which can be associated to the lower HRR peak during the main combustion phase. This phenomenon can be clearly seen from the combustion results shown in Figure 4.12. The variations in peak pressure rise rate for various injection approaches under various injection pressures are presented in Figure 4.11 (d). It is noted that the peak pressure rise rate for all injection approaches

consistently increased with higher injection pressure. Besides, the introduction of pilot fuel in double and triple injection strategies smoothed the combustion process, thus helping to reduce the pressure rise rate and for quieter engine operation (How et al., 2013).

University of Malaya

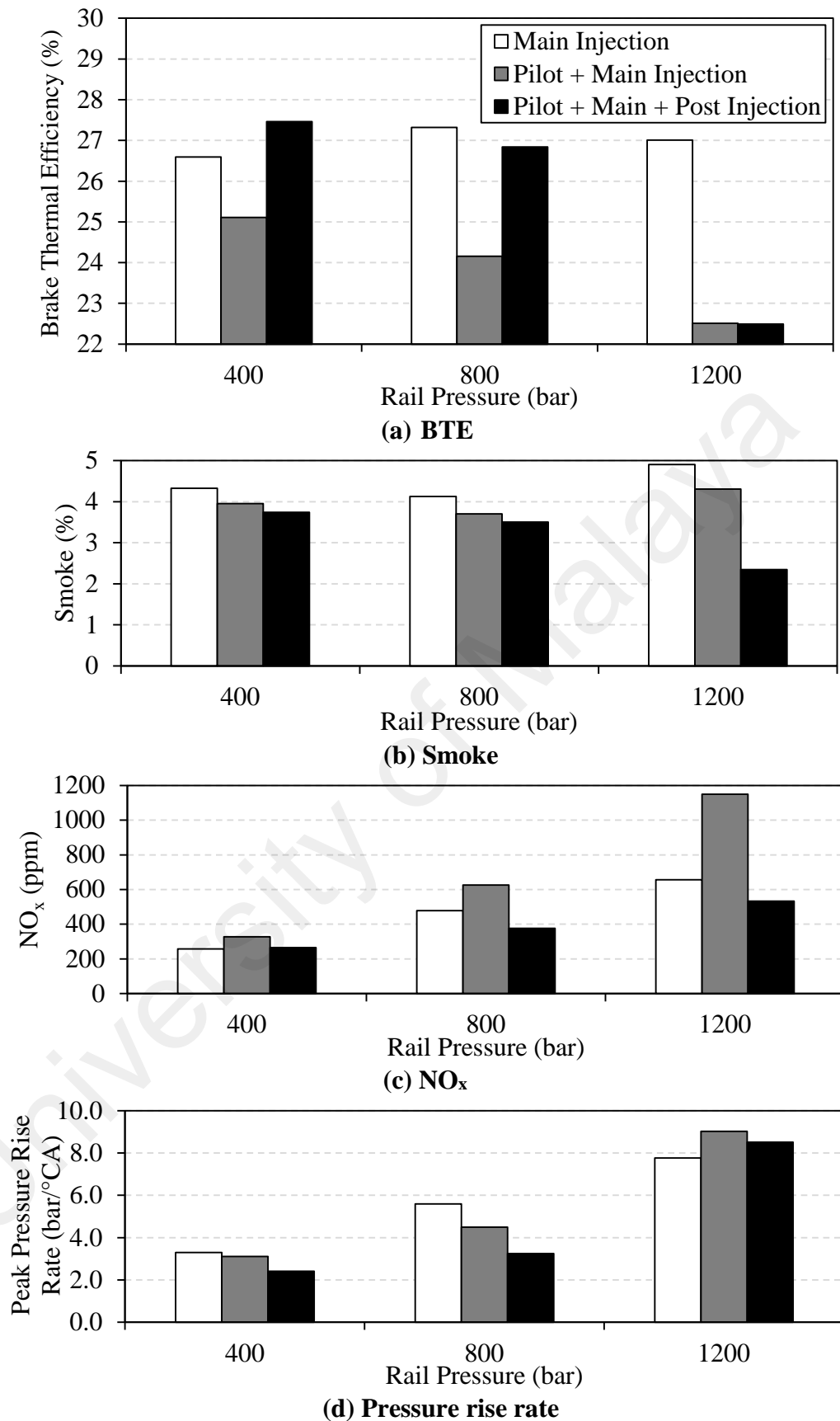


Figure 4.11: Effect of fuel injection strategies on (a) BTE, (b) smoke, (c) NO_x emissions, and (d) peak pressure rise rate at various fuel injection pressures, under 1500 rpm, 50% load, SOI_{Pilot} = 30° BTDC, SOI_{Main} = 12° BTDC, and SOI_{Post} = -5° BTDC. All tests were conducted without EGR.

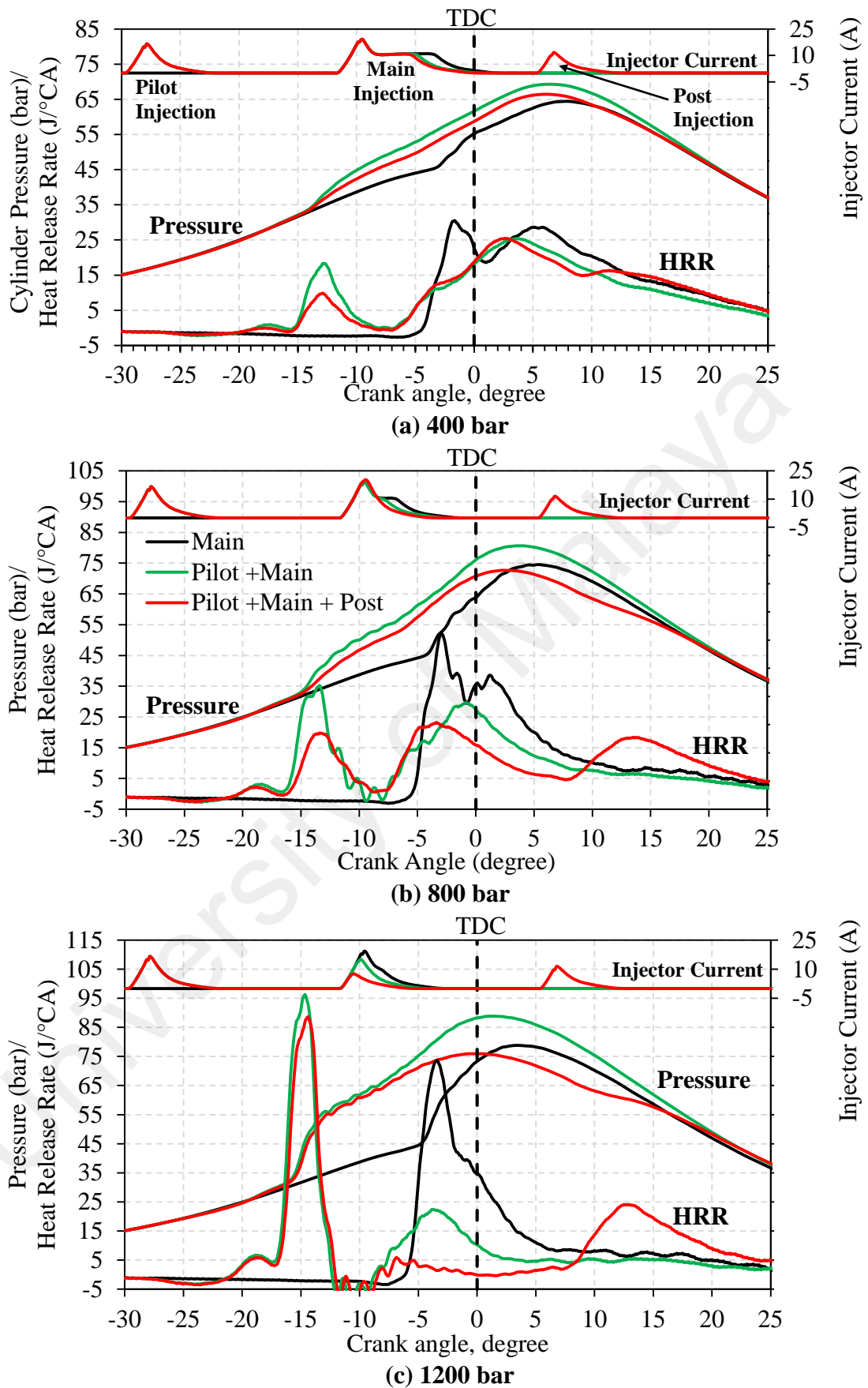


Figure 4.12: Combustion pressure and HRR curves at various fuel injection strategies under (a) 400 bar, (b) 800 bar, and (c) 1200 bar, at engine speed of 1500 rpm, 50% load, $SOI_{Pilot} = 30^\circ$ BTDC, $SOI_{Main} = 12^\circ$ BTDC, and $SOI_{Post} = -5^\circ$ BTDC. All tests were conducted without EGR.

4.2.4 Summary

In this test series, the converted single-cylinder common-rail diesel engine operated with petroleum diesel fuel and controlled using the in-house developed ECU was able to precisely control the SOI timing and opening duration for pilot, main and post injections, as well as injection pressure control. The following main findings can be drawn from this test series:

1. Experimental results indicated that the combustion process can be precisely controlled by the injection timing. It was observed that more advanced SOI timing (as much as 12°CA for low to high speed) is generally required at higher engine speed to attain the maximum brake torque at each loading condition. Also, the SOI timing is necessary to advance slightly (as much as 4°CA for low to high load) as the engine load rises at each engine speed condition.
2. The rising time response for rail pressure control is less than one second and the steady state error is less than 5% in tracking the targeted rail pressure.
3. The introduction of pilot fuel in double and triple injection strategies smoothed the combustion process, thus helping to reduce the pressure rise rate and for quieter engine operation.

Lastly, the custom-built common-rail injection system is capable of providing a higher degree of flexibility in varying the injection parameters for achieving optimal performance and reduced engine-out emissions.

4.3 Effect of biodiesel blends on common-rail diesel engine

The impact of neat palm biodiesel, Jatropha biodiesel and their respective fuel blends, and diesel fuel in an engine equipped with high-pressure common-rail injection system was analyzed. This series of experiments were performed at six different BMEP (i.e. 0.1, 0.2, 0.3, 0.4, 0.5, and 0.6 MPa), SOI of 17° BTDC, with single injection approach and at a rated engine speed of 1500 rpm. Parameters including BSFC, BTE, BSCO, BSNO_x, EGT, smoke opacity, peak pressure, peak of heat release, and vibration analysis are discussed in the following sub-sections.

4.3.1 Performance analysis

Figure 4.13 and Figure 4.14 illustrates the BSFC of the Jatropha biodiesel blends and palm biodiesel blends, respectively, with respect to various BMEPs. BSFC is defined as the ratio of the fuel consumption rate to the brake power output and as described by using Equation 3.18. From the results for Jatropha biodiesel, it is observed that, at the BMEP of 0.6 MPa, baseline diesel shows the lowest BSFC of 273.1 g/kWhr, followed by 275.8 g/kWhr, 280.2 g/kWhr, 288.7 g/kWhr, and 313.0 g/kWhr for the JB10, JB30, JB50 and JB100 fuels, respectively. Likewise, it is observed that the results for palm biodiesel followed a similar trend, with baseline diesel being the lowest, followed by 275.3 g/kWhr, 282.6 g/kWhr, 293.1 g/kWhr, and 313.7 g/kWhr for the PB10, PB30, PB50 and PB100 fuels, respectively. The higher BSFC of neat biodiesel fuel (B100) means that more fuel is consumed to develop the same amount of power. This was expected because of the relatively low calorific value of neat biodiesel fuels in comparison with diesel, which is approximately 12% less than that of diesel fuel (ref. Table 3.2). These results are in agreement with those reported by (Kivevele et al., 2011).

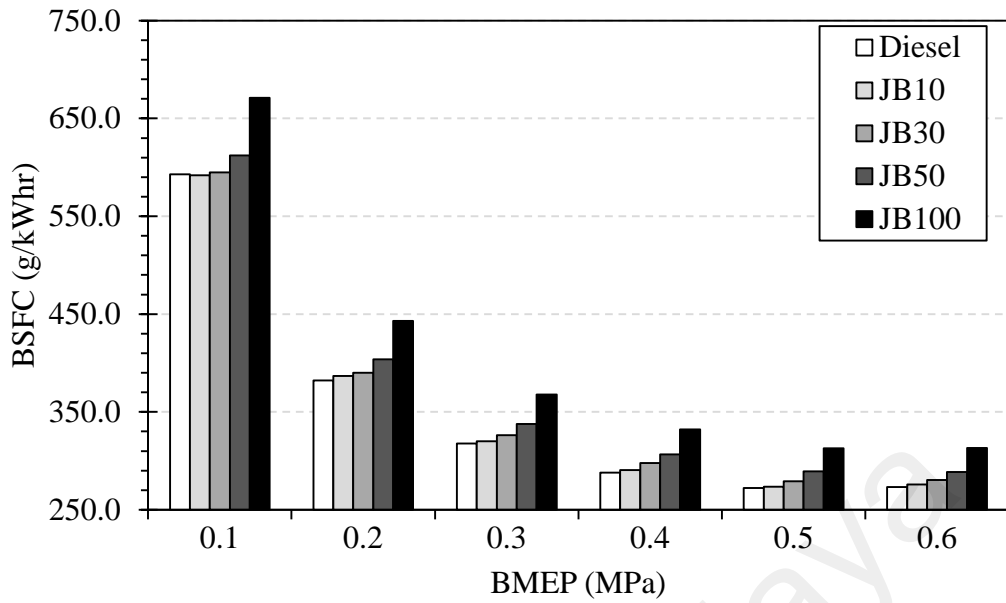


Figure 4.13: BSFC with Jatropha biodiesel blends compared with diesel fuel at various BMEP. All tests were conducted without EGR.

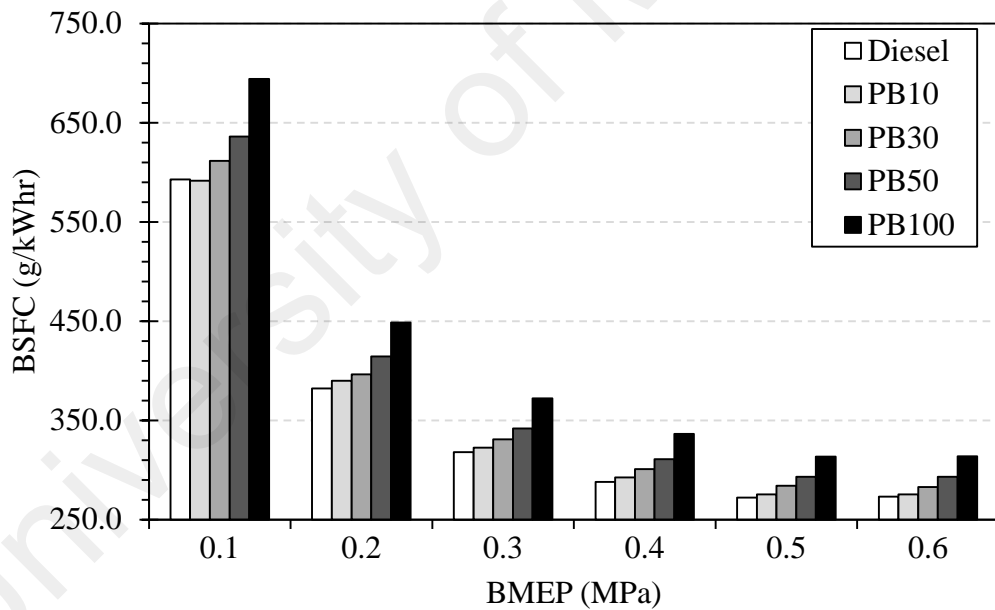


Figure 4.14: BSFC with palm biodiesel blends compared with diesel fuel at various BMEP. All tests were conducted without EGR.

Engine BTE is a product of two important efficiencies, namely, the mechanical efficiency and the net indicated thermal efficiency. Alternatively, it can be calculated by dividing the brake power output by the total energy input delivered to the system and as described by using Equation 3.19. Owing to the effect of various loss mechanisms, such as combustion inefficiency, exhaust blow down, heat transfer, flow, and mechanical friction, the BTE of a real operating diesel cycle is usually under 50%, and is often far lower (Heywood, 1988). Of these loss mechanisms, the magnitude of heat transfer losses constitutes a major fraction, and it varies with the mean piston speed as well as the combustion characteristics of the fuel. The variation of BTE versus BMEP for Jatropha and palm biodiesel fuels is recorded in Figure 4.15 and Figure 4.16, respectively. In general, it is observed that BTE for all tested fuels increased with an increase in BMEP. This is attributed to the twin effects of increased brake power and reduced wall heat loss at higher engine loads (Canakci, Ozsezen, Arcaklioglu, et al., 2009; Chauhan et al., 2012). Additionally, it is observed that with the addition of biodiesel in the blend, the BTE is slightly improved and is higher than that of diesel fuel across all BMEPs, except for neat biodiesels of JB100 and PB100. The largest improvement of 3.4% and 1.7% in BTE are observed with JB30 and PB10, respectively, at 0.1 MPa. This may be attributed to the early initiation of combustion and increase in peak pressures, therefore results in higher BTE.

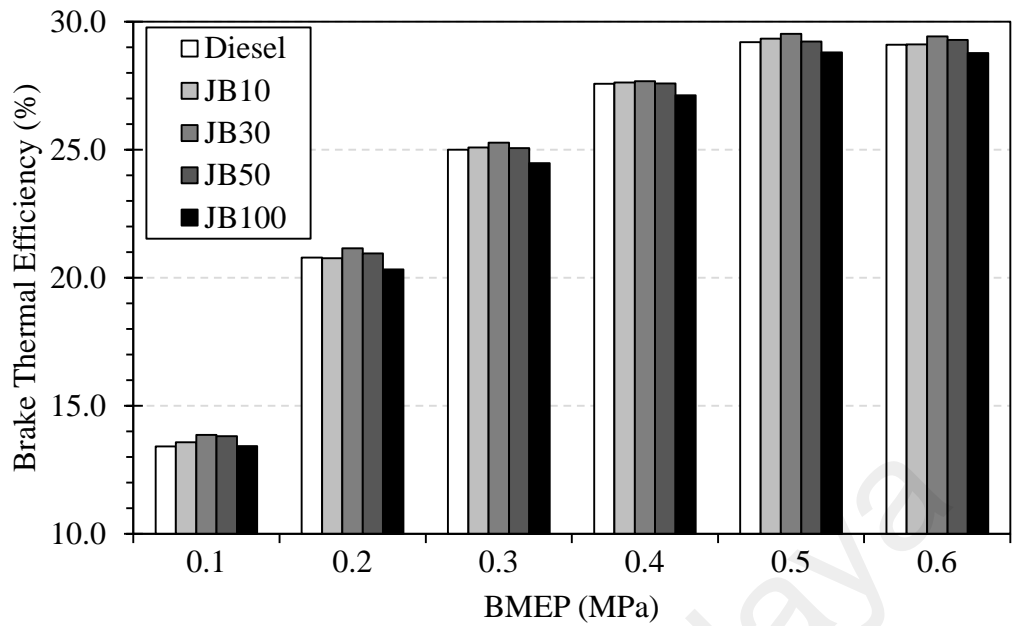


Figure 4.15: Brake thermal efficiency (BTE) with Jatropha biodiesel blends compared with diesel fuel at various BMEP. All tests were conducted without EGR.

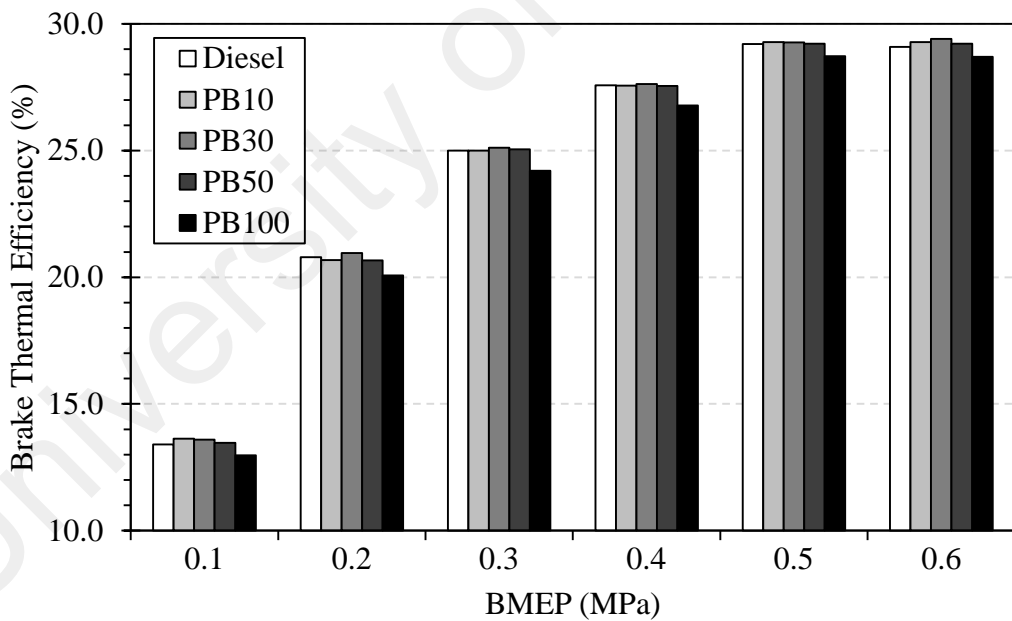


Figure 4.16: Brake thermal efficiency (BTE) with palm biodiesel blends compared with diesel fuel at various BMEP. All tests were conducted without EGR.

4.3.2 Emissions analysis

During combustion, CO emissions appear when the available oxygen is insufficient to fully oxidize all of the carbon in the fuel to carbon dioxide. The use of oxygenated fuel, such as methyl ester, would be expected to improve the combustion quality, especially in fuel-rich regions, consequently reducing CO emissions. The variation in BSCO emissions of the engine with different engine loads and fuel types is illustrated in Figure 4.17 and Figure 4.18. The results suggest that the magnitude of BSCO emissions is significantly governed by the engine load setting and biodiesel blending ratio. High fuel-borne oxygen content in biodiesel fuel plays a key role in reducing CO emissions. In general, it is observed that the reductions in BSCO emissions are obtained with the use of methyl ester in the blend. In fact, it consistently decreased with an increase in the biodiesel blending ratio. This is mainly due to the oxygen content in biodiesel promoting more complete combustion in the engine (Buyukkaya et al., 2013; Carraretto et al., 2004). In comparison with the diesel fuel, the BSCO emissions for *Jatropha* biodiesel fuels at a high engine load of 0.6 MPa decreased by 1.1, 28.0, 45.5, and 70.0% for JB10, JB30, JB50, and JB100, respectively. Similarly, in comparison with the diesel fuel, the BSCO emissions for palm biodiesel fuels at a high engine load of 0.6 MPa decreased by 9.9, 5.6, 48.2, and 63.8% for PB10, PB30, PB50, and PB100, respectively. Another observation is that the BSCO emissions at low load conditions are generally higher than high load conditions, regardless of the fuel used. This is largely owing to the better air-fuel mixing process, as a result of higher fuel injection pressure at higher engine loads, resulting from the use of the converted common-rail system, and consequently, decreasing the BSCO emissions. An alternative explanation is that this occurred owing to the fact that the air-fuel ratio is too lean for complete combustion at low load conditions, leading to higher BSCO emissions (How et al., 2014). The relative air-fuel ratio (λ) for various engine loads and fuel types is illustrated in Figure 4.19 and Figure 4.20. In short, λ is defined as the ratio

of the actual air-fuel ratio to that of the stoichiometric air-fuel ratio required to completely burn the fuel delivered. The air-fuel ratio of the mixture affects the combustion phenomenon and the completeness of combustion, especially at the fuel lean zone. In fact, the general trend indicates that the variations in BSCO emissions are very similar to the variation in λ values. In addition, it appears that even under high load conditions (i.e. 0.6 MPa of engine load), the λ values are still above unity, indicating a lean combustion process. Further, the addition of methyl ester in the blend creates a slightly rich (lower λ value) combustion process. Consequently, the ID becomes shorter, combustion duration increases, and combustion gets completed properly, leading to a further decrease in CO emissions.

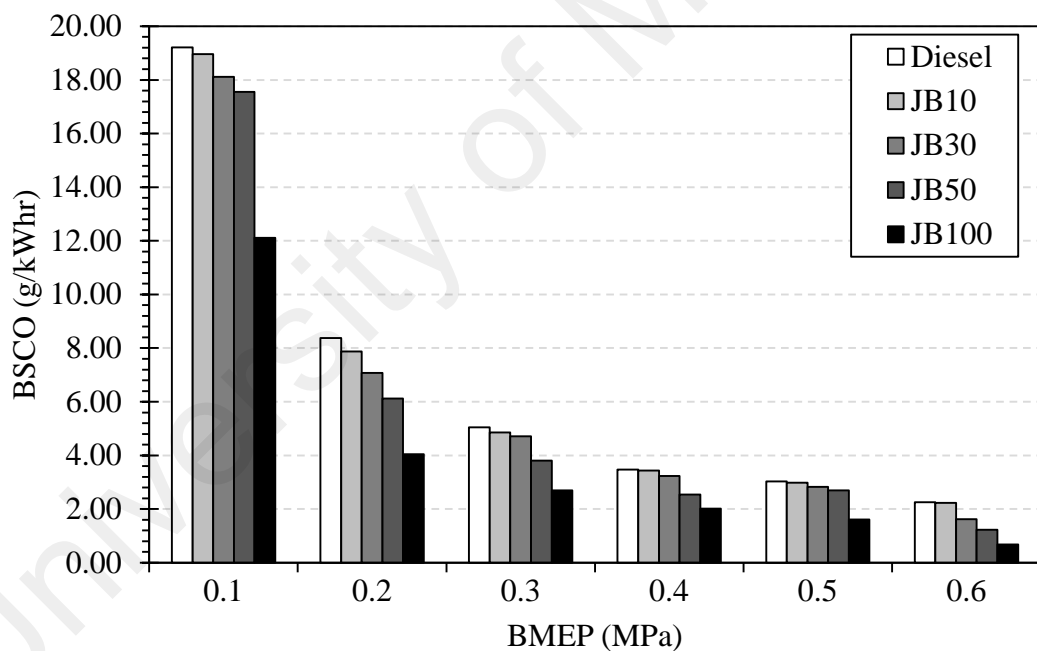


Figure 4.17: BSCO with Jatropha biodiesel blends compared with diesel fuel at various BMEP. All tests were conducted without EGR.

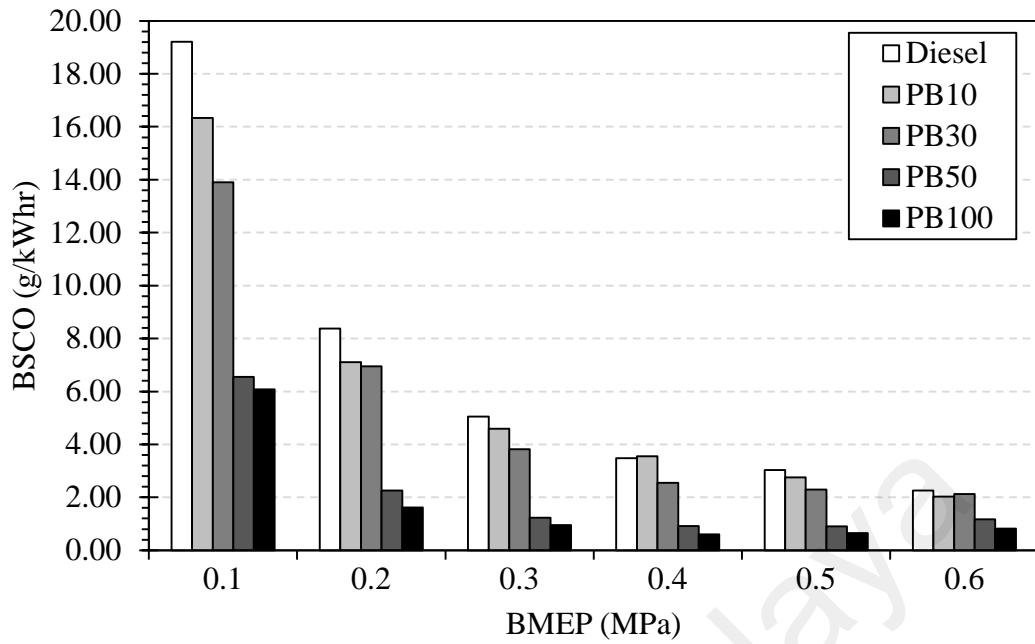


Figure 4.18: BSCO with palm biodiesel blends compared with diesel fuel at various BMEP. All tests were conducted without EGR.

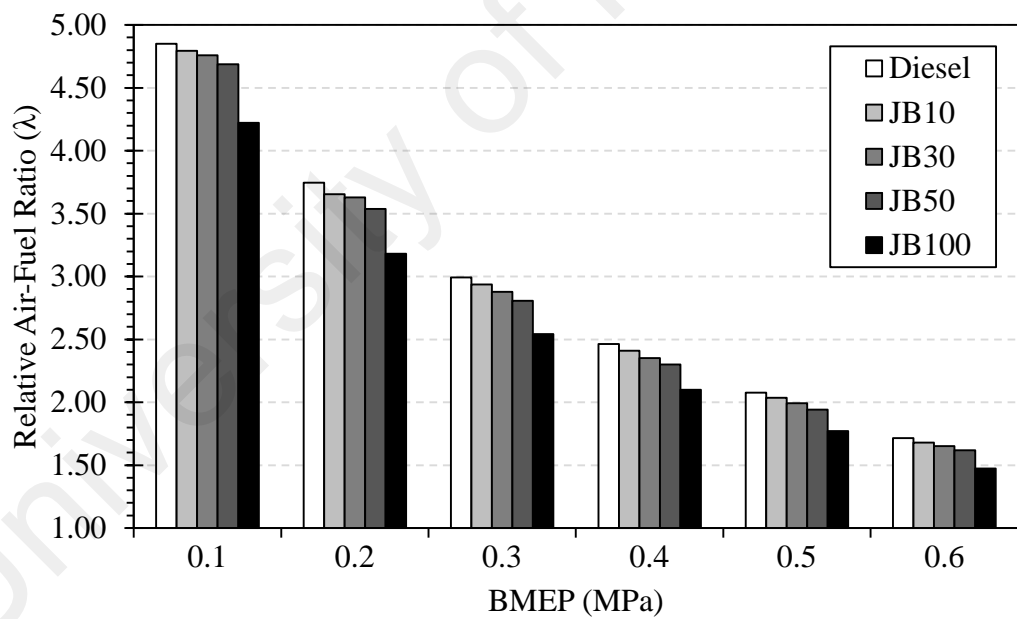


Figure 4.19: Relative air-fuel ratio with Jatropa biodiesel blends compared with diesel fuel at various BMEP. All tests were conducted without EGR.

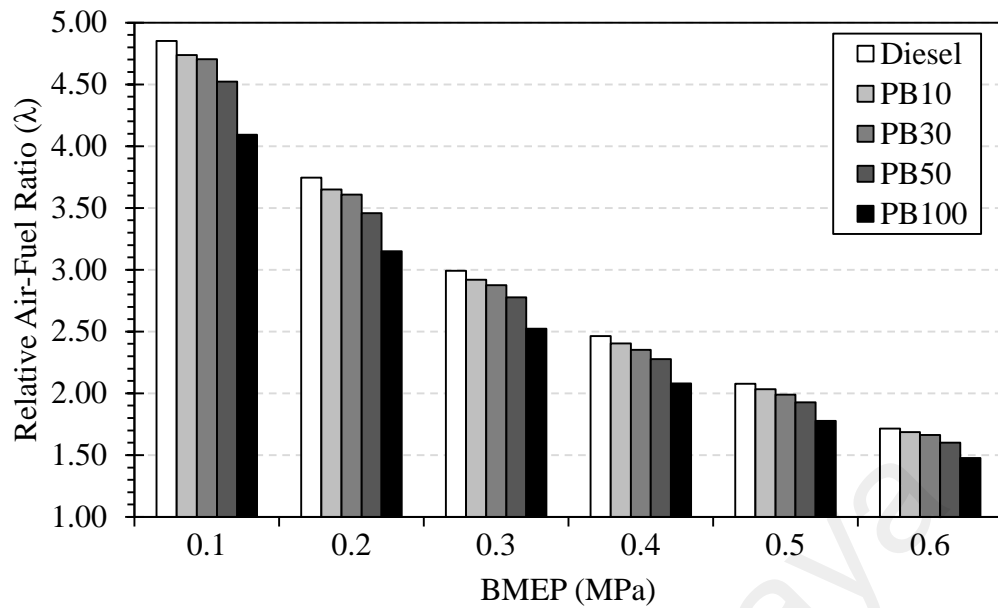


Figure 4.20: Relative air-fuel ratio with palm biodiesel blends compared with diesel fuel at various BMEP. All tests were conducted without EGR.

As discussed previously, fuel injection technology in biodiesel engines has significant effects on NO_x emissions. Unlike the conventional mechanical pump-line-nozzle injection system, the modified common-rail injection system utilized in this study eliminated the common issue of advanced injection timing owing to the relatively higher viscosity of biodiesel. Hence, the correlation of other effects on the variation of NO_x emissions when using biodiesel can be analysed more comprehensively. In automotive exhaust emissions, the formation of NO_x depends on the fuel type, fuel properties, and engine operating conditions (Szybist et al., 2005). In the literature, most researchers have reported an increase in NO_x emissions with the use of methyl ester blended fuel (Kwanchareon et al., 2007; Saravanan et al., 2010; Tan et al., 2012). The explanations given are primarily based on the higher oxygen content, which results in a higher combustion temperature that promotes a thermal NO_x formation pathway. However, some researchers have reported the opposite trend, with lower NO_x emissions when using methyl ester blended fuel (Dorado et al., 2003; Peterson & Reece, 1996). This is in good agreement with the results obtained throughout this study. As illustrated in Figure 4.21 and Figure 4.22, the presence of methyl ester in the blend decreased the BSNO_x relative

to baseline diesel, but it did not decrease further as the degree of blending of respective JME and PME increased. The largest recorded reduction in BSNO_x is approximately 16% for the PB 50 blend at a BMEP of 0.6 MPa. This can be attributed to the relatively lower calorific value of the methyl ester fuels being used and, consequently, reduced HRR in the premixed combustion region and lower peak combustion temperature (Huang et al., 2010). Additionally, the results also suggest that further increases in the methyl ester concentration to JB100 and PB100 resulted in an increase in BSNO_x across all engine loads. A similar result has been observed by Mueller et al. (Mueller et al., 2009) who reported that the higher cetane number of neat biodiesels relative to diesel causes ignition to occur earlier in the cycle. This allows the combustion products to have a longer residence time at high temperatures, which increases NO_x emissions. Another possible reason may be associated with the reduction in the heat dissipation by radiation as a consequence of the large reductions of soot emitted with the use of biodiesel (ref. Figure 4.25 and Figure 4.26), resulting in an increase in BSNO_x emissions (Cheng et al., 2006).

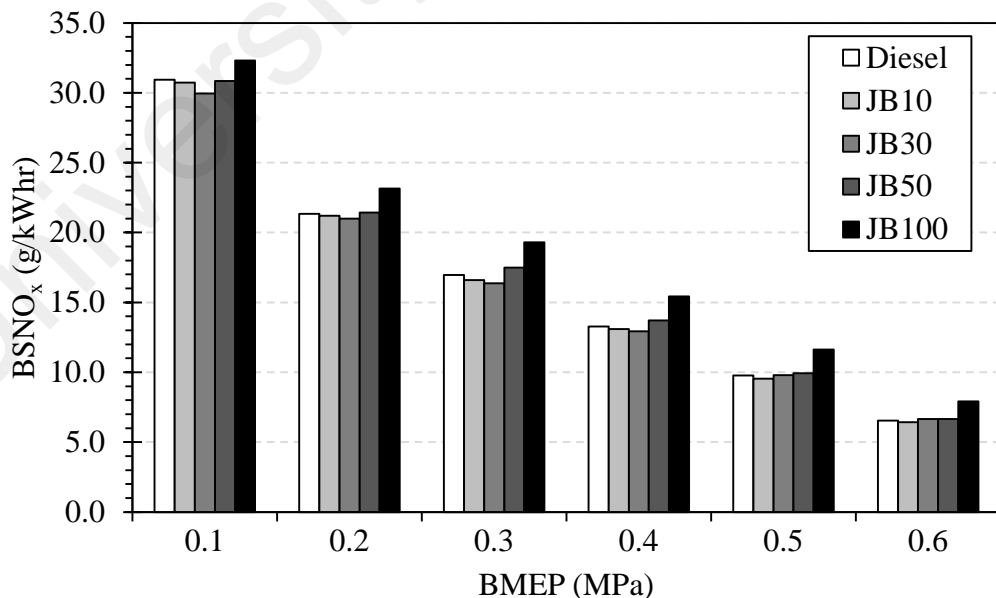


Figure 4.21: Variations in BSNO_x emissions with different engine loads and fuel types for Jatropha biodiesel fuels. All tests were conducted without EGR.

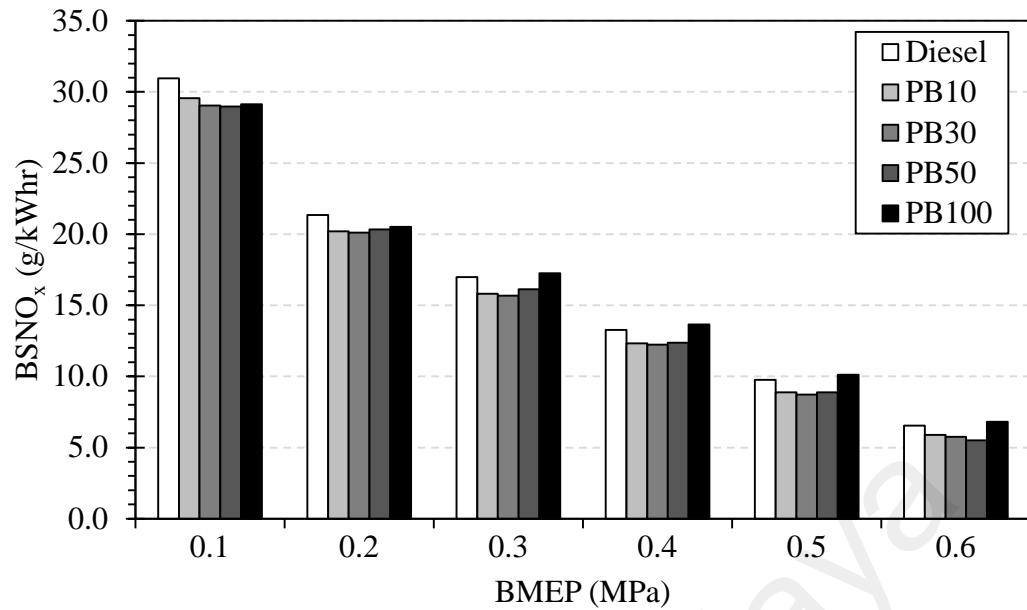


Figure 4.22: Variations in BSNO_x emissions with different engine loads and fuel types for palm biodiesel fuels. All tests were conducted without EGR.

Owing to the lean operation and higher expansion ratio of the diesel engine, the exhaust gas temperature (EGT) is typically lower than for a petrol engine. A higher EGT is unfavorable as this will deteriorate engine fuel economy by discharging some of the useful energy into waste exhaust thermal energy, as well as causing thermal damage to piston components. As illustrated in Figure 4.23 and Figure 4.24, in general, the EGT increased with an increase in the BMEP for all of the fuels tested in this study. Additionally, the presence of JME slightly increased the EGT relative to that for baseline diesel, but it did not increase further as the degree of biodiesel blending rose to JB100. However, the EGT for palm biodiesel blends is hardly varied relative to that for baseline diesel, except at higher engine load of 0.6 MPa. The highest achievable EGT for JB50, baseline diesel, JB30, JB10, and JB100 at a BMEP of 0.6 MPa is 445.3°C, 439.7°C, 439.4°C, 437.6°C, and 433.9°C, respectively. Additionally, the EGT is lower for higher blends of both JB100 and PB100 because of the improved combustion provided by the biodiesels under all engine loading conditions. In fact, many researchers have also reported that the EGT is lower with the engine fuelled with biodiesel fuel compared to the baseline diesel (An et al., 2012; Enweremadu & Rutto, 2010; Lin & Li, 2009a; Özener

et al., 2014). In general, this phenomenon is caused primarily by the lower calorific value and the existence of chemically bound oxygen in biodiesel blends, which reduces the total energy that is released and improves combustion. The EGT thereafter decreased.

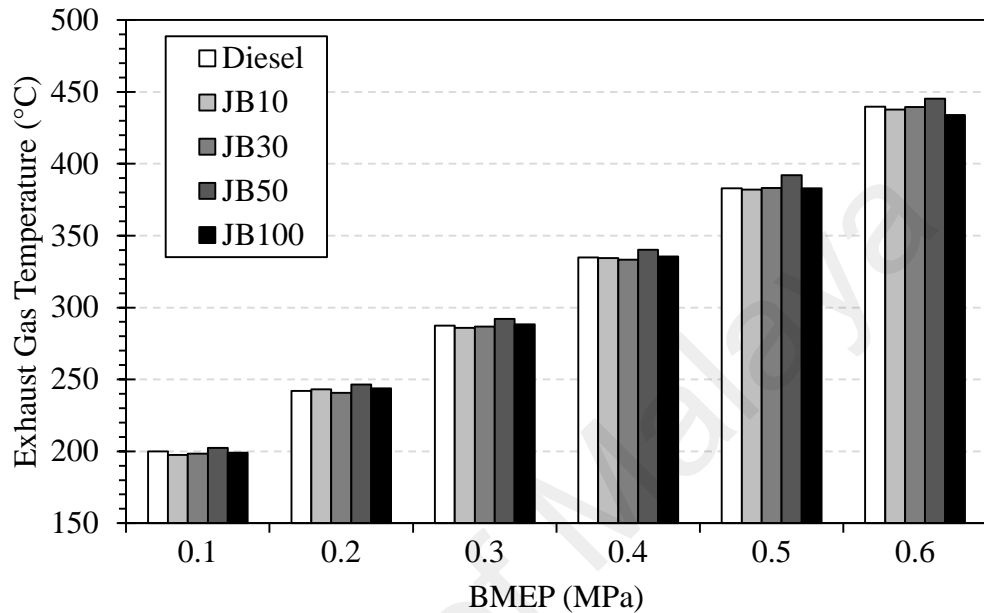


Figure 4.23: EGT with Jatropha biodiesel blends compared with diesel fuel at various BMEP. All tests were conducted without EGR.

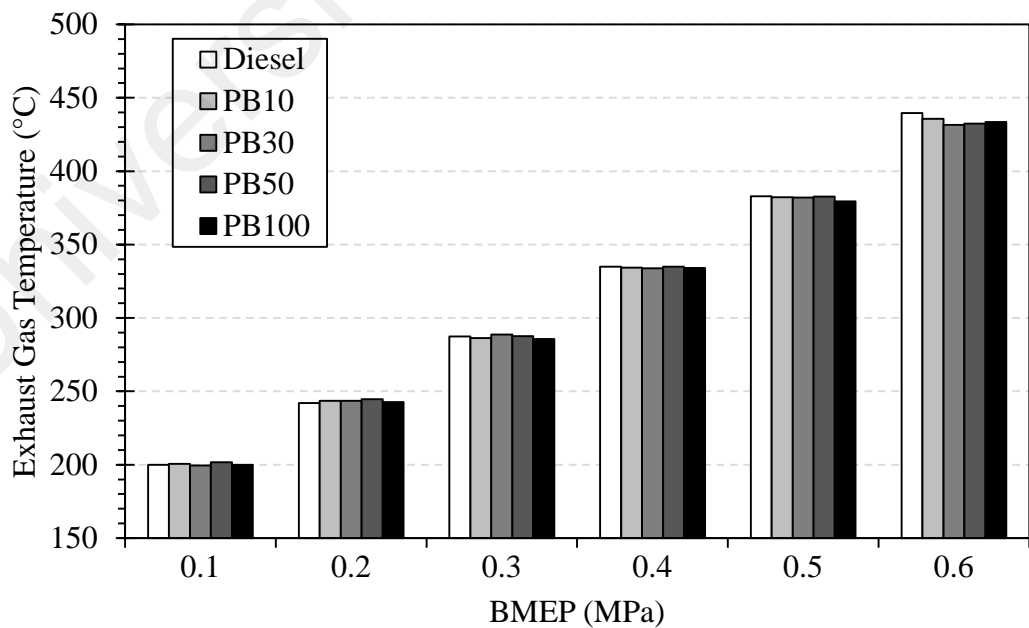


Figure 4.24: EGT with palm biodiesel blends compared with diesel fuel at various BMEP. All tests were conducted without EGR.

Smoke is an unwanted by-product of combustion in compression ignition diesel engines, which is primarily formed through the incomplete combustion of hydrocarbon fuel. In general, the smoke from the exhaust tailpipe is emitted visibly in the form of dark black smoke. The composition of smoke highly depends on the type of fuel, engine operating conditions, and carbon residue of the fuel. The emission of smoke opacity is demonstrated in Figure 4.25 and Figure 4.26 for different Jatropha and palm biodiesel fuel blends, respectively. In relation to the effect of biodiesel content on the smoke opacity, it is observed that smoke opacity generally tends to decrease as the blending ratio of biodiesel in the fuel blend is increased. At a BMEP of 0.1 MPa, it is observed that the maximum reduction is 90% and 88.5% with JB100 and PB100, respectively, compared with that of baseline diesel. The combined effects of lower impurities, higher oxygen, and lower sulphur content of methyl ester fuels are believed to be responsible for the decreased smoke opacity level (Canakci, Ozsezen, Arcaklioglu, et al., 2009).

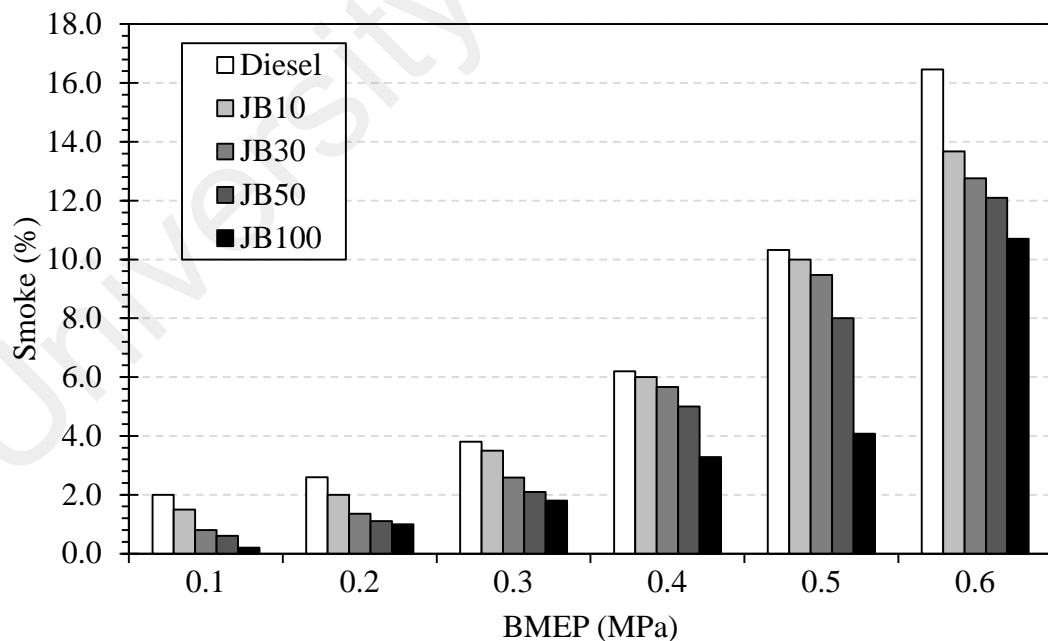


Figure 4.25: Smoke level with Jatropha biodiesel blends compared with diesel fuel at various BMEP. All tests were conducted without EGR.

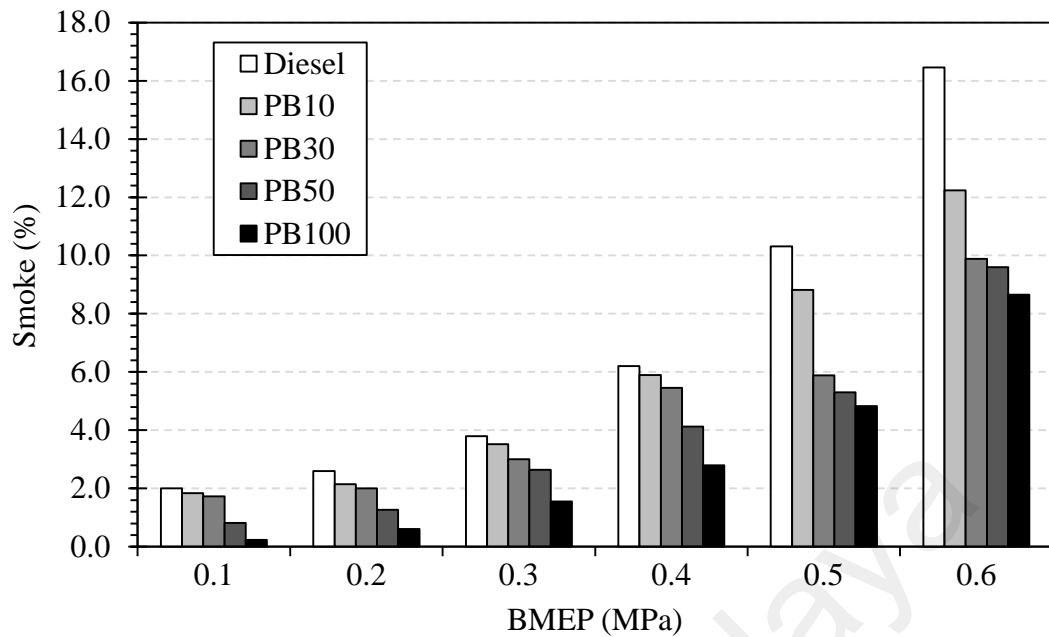


Figure 4.26: Smoke level with palm biodiesel blends compared with diesel fuel at various BMEP. All tests were conducted without EGR.

4.3.3 Combustion analysis

To evaluate the effect of the biodiesel blending ratio on the combustion characteristics, the cylinder pressures for 100 consecutive combustion cycles were recorded and compared at various loads and at a constant engine speed of 1500 rpm. The in-cylinder pressure, HRR and injector current traces at a BMEP of 0.1 MPa (low load) and 0.6 MPa (high load) for *Jatropha* and palm biodiesel fuels are illustrated in Figure 4.27 and Figure 4.28, respectively. As can be observed, the variation of engine load and biodiesel blending ratio has the greatest effect on the combustion characteristics for both types of biodiesels. Under low load conditions, the premixed combustion process dominated. Conversely, the diffusion flame combustion process dominated at high load conditions. In the case of lower engine load, the cylinder pressure profiles for all of the tested fuels are comparable with the baseline diesel. Additionally, the shift in the SOC timing is consistent with the change of biodiesel concentration in the blend. In fact, the combustion is shifted earlier towards TDC as the biodiesel concentration is increased. A small increment in peak pressure in the range of 0.6 – 1.5 bar is observed for the operation with both type of

biodiesel blend fuels. For instance, it is observed that PB100 achieved the highest peak pressure of 68.09 bar followed by PB50 (67.80 bar), PB30 (67.44 bar), PB10 (67.42 bar) and diesel (66.76 bar). The results suggest that adding biodiesel in the blend caused increases in the peak pressure and shifted the location of occurrence earlier toward the TDC point. This can be attributed to the prominent advance in SOC timing, which caused the earlier rise of the HRR and thus increased the in-cylinder gas pressure. In the case of higher engine load, less significant variations in terms of peak pressure are observed among all biodiesel blends and baseline diesel fuel.

Another interesting observation that can be made from the HRR diagram is the variations in ignition delay (ID). Mathematically, ID is defined as the crank angle interval measured from the start of fuel injection timing to the start of combustion timing; this is typically determined from the fuel injector signal and HRR data, respectively. As summarized in Table 4.1 and Table 4.2, it is found that, in general, regardless of the engine load, most of the biodiesel blends exhibited shorter ID than baseline diesel owing to their relatively higher cetane number. Similar trends of shorter IDs with biodiesel blends were also reported by Ozsezen and Canakci (Ozsezen & Canakci, 2011). As illustrated in Figure 4.29 and Figure 4.30, lines indicating the mass fraction burned of 10% (CA10), 50% (CA50), and 90% (CA90) are marked. Empirically, 10% and 90% lines marked the start and end of the main combustion duration, respectively. The period between CA10 and CA90 is defined as the combustion duration and this is typically measured in the unit of crank angle. From the results presented in Table 4.1 and Table 4.2, it can be seen that the general trend indicates that a shorter combustion duration is obtained with the addition of biodiesel in the blends for both fuel types and at all engine loads. In fact, in comparison with the corresponding baseline diesel, the JB10 promoted a faster combustion duration by 2° CA and 1.5° CA at engine load of 0.1 MPa and 0.6 MPa, respectively. The oxygen enrichment and improved combustion process of the JB10 blend are postulated to be the

reason for the shorter combustion duration. Additionally, it can be observed that the CA50 is hardly varied by the change of biodiesel concentrations for both types of biodiesel fuels. Typically, CA50 is used as a parameter that affected the ensemble heat release profile, and it is applied widely in the simulation of engine performance when the Wiebe function was employed (Wang et al., 2013). In this study, it can be observed that the CA50 timing occurred slightly earlier with both types of biodiesel blended fuels under all operating conditions. In fact, the largest shift in CA50 is found to be an advance of 0.75° CA for JB100 and PB100 in comparison with that of baseline diesel at higher load of 0.6 MPa and 0.5 MPa, respectively.

University of Malaya

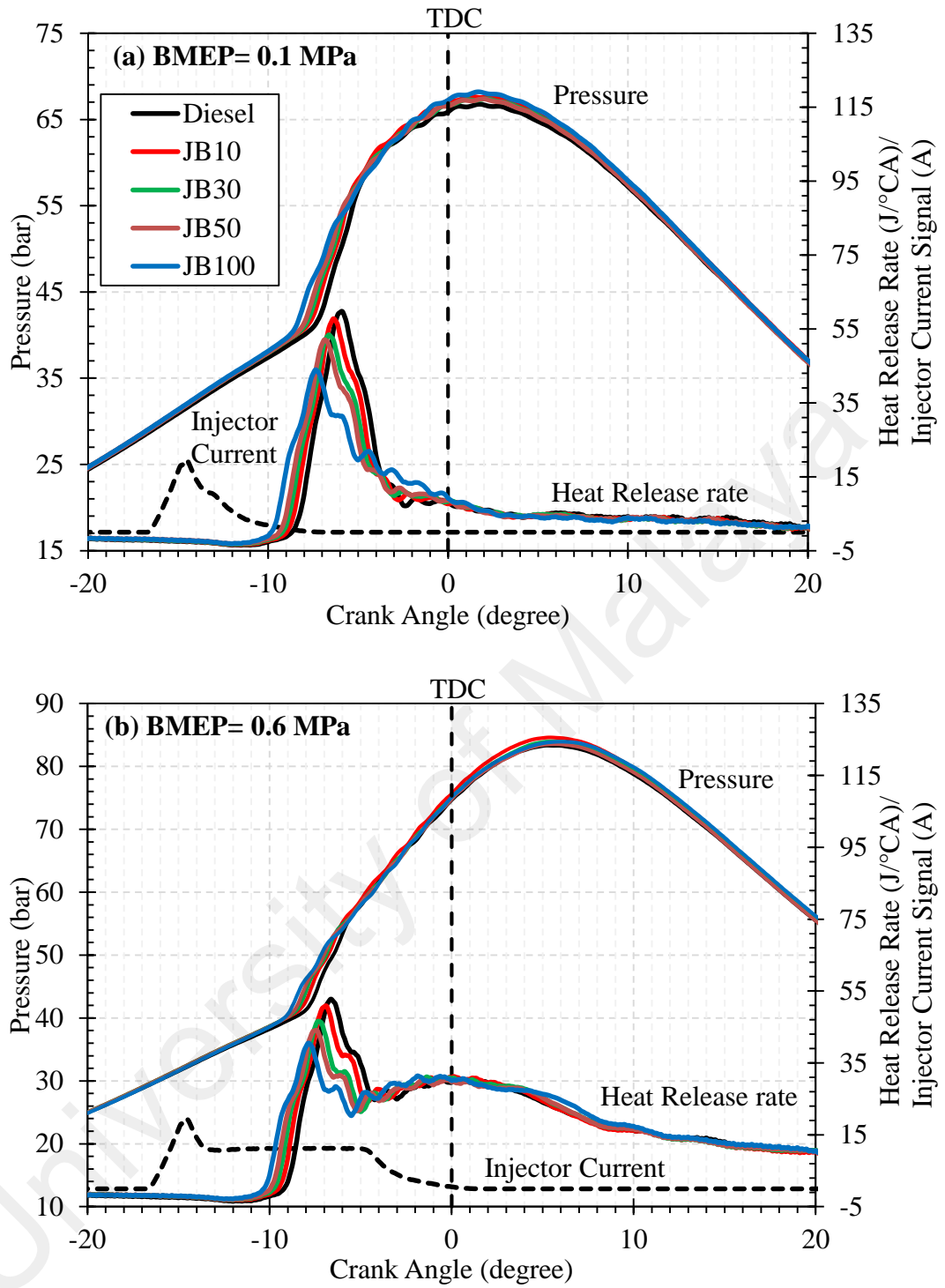


Figure 4.27: In-cylinder pressure and HRR versus crank angle for Jatropha biodiesel blends at a BMEP of (a) 0.1 MPa and (b) 0.6 MPa. All tests were conducted without EGR.

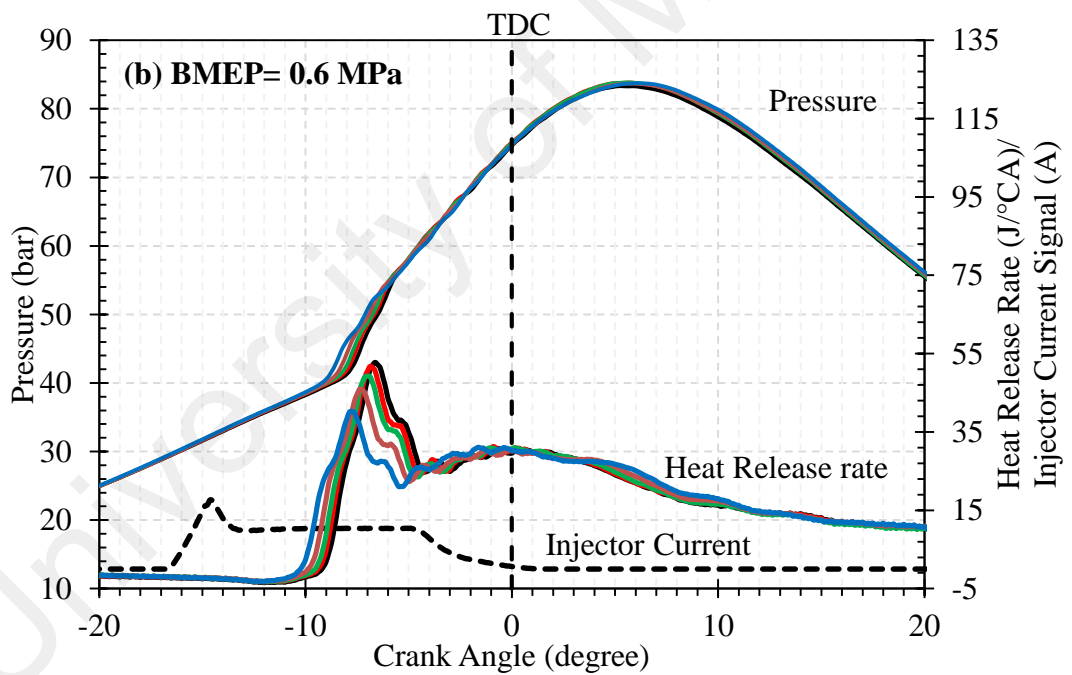
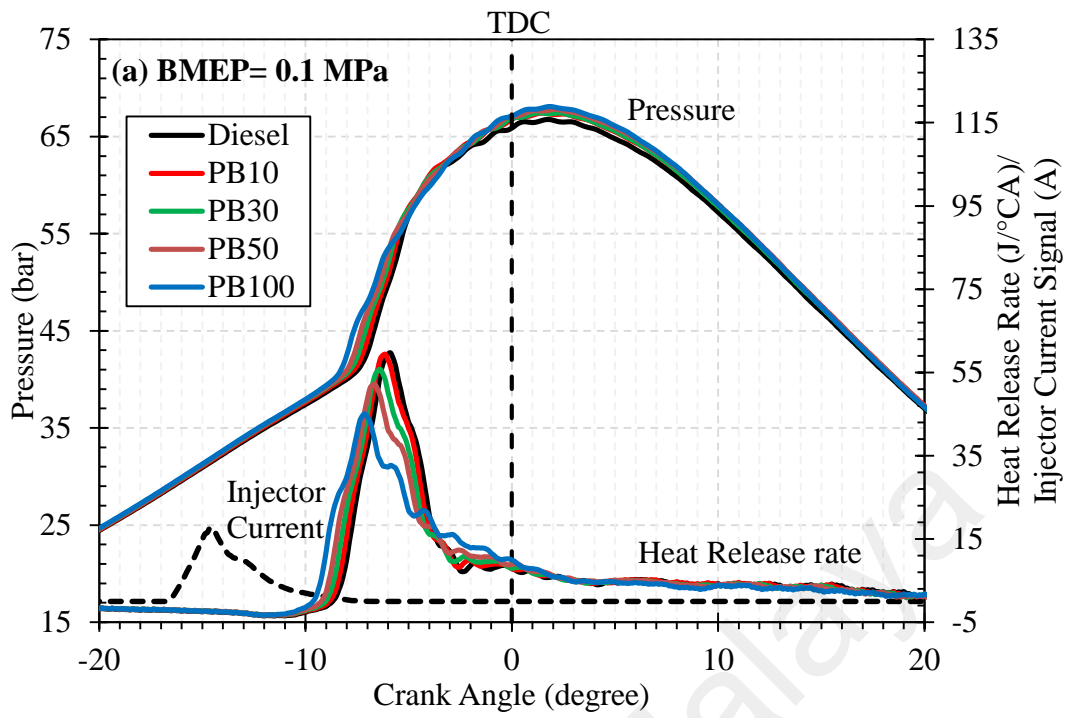


Figure 4.28: In-cylinder pressure and HRR versus crank angle for palm biodiesel blends at a BMEP of (a) 0.1 MPa and (b) 0.6 MPa. All tests were conducted without EGR.

Table 4.1: Crank angle position corresponding to certain percent mass fraction burned for all Jatropha biodiesel blends under various BMEPs.

BMEP (MPa)	Fuel type	Start of injection, SOI (°BTDC)	Start of combustion, SOC (°BTDC)	ID (°CA)	Crank angle for certain percent mass fraction burned (°BTDC)			Combustion duration (°CA)
					10%	50%	90%	
0.1	Diesel	17.000	8.625	8.375	7.000	4.500	-13.250	20.250
	JB10	17.000	8.875	8.125	7.250	4.875	-11.000	18.250
	JB30	17.000	9.125	7.875	7.500	4.875	-11.375	18.875
	JB50	17.000	9.375	7.625	7.625	5.000	-11.625	19.250
	JB100	17.000	9.750	7.250	8.125	4.500	-11.000	19.125
0.2	Diesel	17.000	8.750	8.250	6.875	3.125	-14.625	21.500
	JB10	17.000	9.000	8.000	7.250	3.375	-12.750	20.000
	JB30	17.000	9.375	7.625	7.375	3.125	-12.875	20.250
	JB50	17.000	9.375	7.625	7.500	3.000	-13.375	20.875
	JB100	17.000	9.875	7.125	8.000	2.750	-13.250	21.250
0.3	Diesel	17.000	9.000	8.000	6.875	1.375	-16.750	23.625
	JB10	17.000	9.250	7.750	7.250	1.750	-15.000	22.250
	JB30	17.000	9.500	7.500	7.375	1.500	-15.250	22.625
	JB50	17.000	9.625	7.375	7.500	1.625	-15.625	23.125
	JB100	17.000	10.125	6.875	7.875	1.375	-15.375	23.250
0.4	Diesel	17.000	9.125	7.875	6.875	0.125	-19.000	25.875
	JB10	17.000	9.375	7.625	7.125	0.250	-17.250	24.375
	JB30	17.000	9.625	7.375	7.250	0.000	-17.625	24.875
	JB50	17.000	9.750	7.250	7.375	0.000	-17.500	24.875
	JB100	17.000	10.125	6.875	7.750	0.000	-17.000	24.750
0.5	Diesel	17.000	9.250	7.750	6.750	-1.625	-21.875	28.625
	JB10	17.000	9.500	7.500	7.000	-1.125	-20.000	27.000
	JB30	17.000	9.750	7.250	7.125	-1.500	-20.500	27.625
	JB50	17.000	9.875	7.125	7.375	-1.500	-20.625	28.000
	JB100	17.000	10.250	6.750	7.500	-1.500	-19.625	27.125
0.6	Diesel	17.000	9.125	7.875	6.500	-3.625	-24.875	31.375
	JB10	17.000	9.500	7.500	6.875	-3.000	-23.000	29.875
	JB30	17.000	9.750	7.250	7.000	-3.375	-23.375	30.375
	JB50	17.000	9.875	7.125	7.125	-3.500	-23.375	30.500
	JB100	17.000	10.250	6.750	7.250	-3.500	-22.750	30.000

Table 4.2: Crank angle position corresponding to certain percent mass fraction burned for palm biodiesel blends under various BMEPs.

BMEP (MPa)	Fuel type	Start of injection, SOI (°BTDC)	Start of combustion, SOC (°BTDC)	ID (°CA)	Crank angle for certain percent mass fraction burned (°BTDC)			Combustion duration (°CA)
					10%	50%	90%	
0.1	Diesel	17.000	8.625	8.375	7.000	4.500	-13.250	20.250
	PB10	17.000	8.750	8.250	7.125	4.625	-12.375	19.500
	PB30	17.000	9.000	8.000	7.375	4.750	-11.750	19.125
	PB50	17.000	9.125	7.875	7.500	4.625	-11.500	19.000
	PB100	17.000	9.625	7.375	7.875	4.375	-11.375	19.250
0.2	Diesel	17.000	8.750	8.250	6.875	3.125	-14.625	21.500
	PB10	17.000	8.875	8.125	7.000	3.125	-13.875	20.875
	PB30	17.000	9.125	7.875	7.250	3.000	-13.625	20.875
	PB50	17.000	9.375	7.625	7.500	2.875	-13.250	20.750
	PB100	17.000	9.750	7.250	7.875	2.750	-13.250	21.125
0.3	Diesel	17.000	9.000	8.000	6.875	1.375	-16.750	23.625
	PB10	17.000	9.125	7.875	7.000	1.500	-15.625	22.625
	PB30	17.000	9.375	7.625	7.250	1.500	-15.500	22.750
	PB50	17.000	9.625	7.375	7.500	1.375	-15.500	23.000
	PB100	17.000	10.000	7.000	7.750	1.250	-15.500	23.250
0.4	Diesel	17.000	9.125	7.875	6.875	-0.125	-19.000	25.875
	PB10	17.000	9.250	7.750	7.000	-0.125	-18.375	25.375
	PB30	17.000	9.375	7.625	7.125	0.000	-17.625	24.750
	PB50	17.000	9.750	7.250	7.375	-0.125	-17.750	25.125
	PB100	17.000	10.125	6.875	7.625	-0.125	-17.250	24.875
0.5	Diesel	17.000	9.250	7.750	6.750	-1.625	-21.875	28.625
	PB10	17.000	9.375	7.625	6.875	-1.625	-20.625	27.500
	PB30	17.000	9.500	7.500	7.000	-1.500	-20.250	27.250
	PB50	17.000	9.750	7.250	7.250	-1.625	-20.250	27.500
	PB100	17.000	10.125	6.875	7.500	-1.750	-19.875	27.375
0.6	Diesel	17.000	9.125	7.875	6.500	-3.625	-24.875	31.375
	PB10	17.000	9.375	7.625	6.625	-3.375	-23.625	30.250
	PB30	17.000	9.500	7.500	6.750	-3.250	-23.250	30.000
	PB50	17.000	9.875	7.125	7.000	-3.625	-23.375	30.375
	PB100	17.000	10.125	6.875	7.125	-3.625	-22.875	30.000

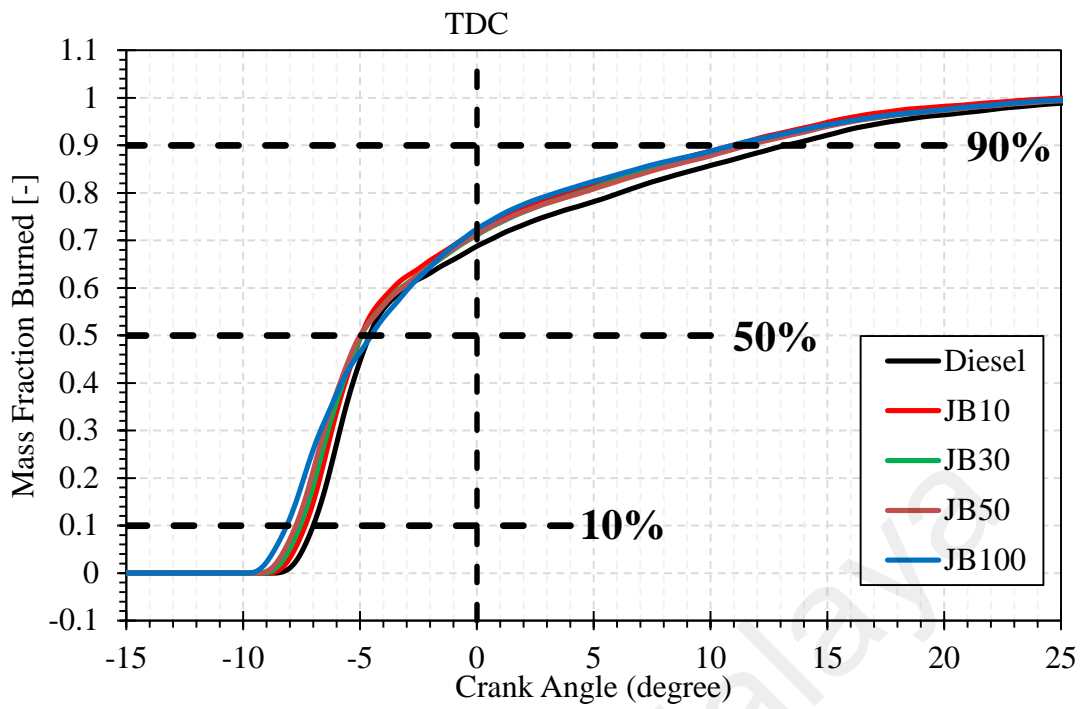


Figure 4.29: Variations in mass fraction burned for diesel and Jatropha biodiesel blends at a BMEP of 0.1 MPa and without EGR.

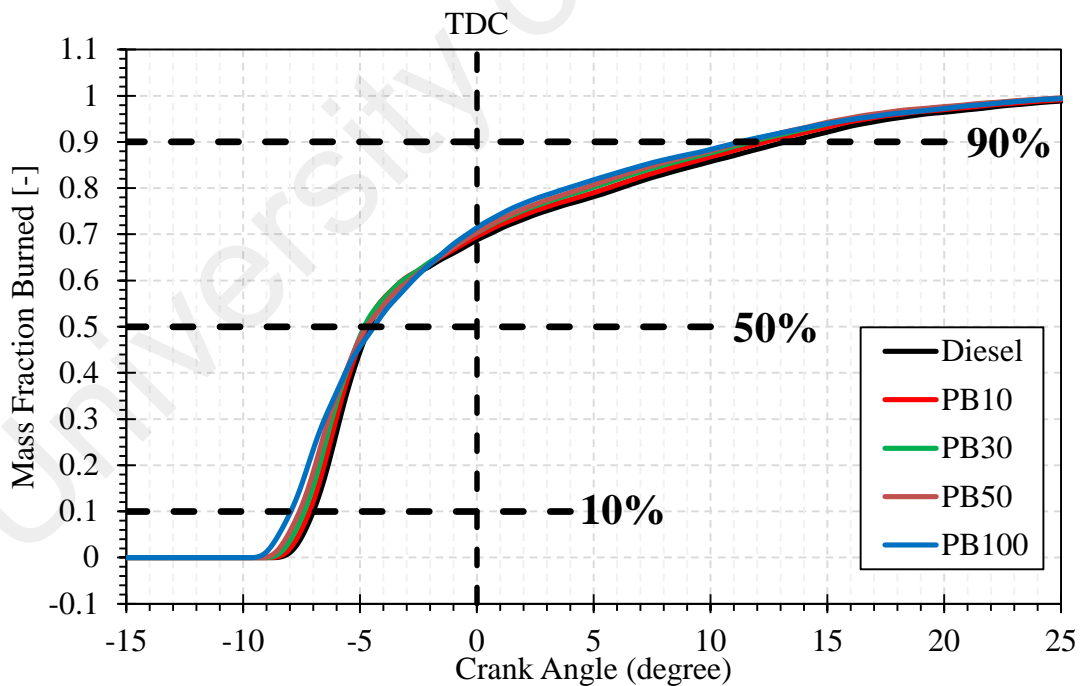


Figure 4.30: Variations in mass fraction burned for diesel and palm biodiesel blends at a BMEP of 0.1 MPa and without EGR.

4.3.4 Vibration analysis

Vibration signals in an internal combustion engine are usually used as a diagnostic tool. They allow engine bearings to be monitored for wear and overall engine knock detection. There are many sources of vibration in an engine, including piston slap, faults in valves, knocking, burning pressure oscillation, torsional vibration, and the rotation of other engine accessories. This vibration is transmitted via a variety of paths and then ultimately radiated acoustically to the surroundings. Exposure to excess vibration can accelerate the wear and tear of mechanical components and have an adverse impact on human comfort. The combustion process in a diesel engine has an effect on the engine vibration. The methyl ester fuel blends influenced the combustion process and consequently the noise and vibration. Figure 4.31 and Figure 4.32 shows the illustration of RMS of the vibration acceleration signals for both type of biodiesel fuels, which was calculated according to Equation 3.12. For each test, the average RMS of the acceleration signal for 100 successive engine combustion cycles was considered. As can be seen, the magnitude of the resultant vibration acceleration signal (i.e. $< 50 \text{ m/s}^2$) are in agreement with those reported by other sources (How et al., 2014; Taghizadeh-Alisaraei et al., 2012). The general trend indicates that the variations in RMS of acceleration are decreased with engine load. Additionally, the results also indicate that the RMS of acceleration is affected by biodiesel fuel blends. It is observed that neat biodiesel for both fuel types consistently resulted in the lowest RMS of accelerations in comparison with the baseline diesel under all loading conditions. It is interesting to note that the largest reduction of approximately 19% in RMS of acceleration is obtained with JB100 and PB100 at engine load of 0.6 MPa in comparison with the baseline diesel. The major factor in reducing vibration in the engine is the smoother in combustion process. From the combustion analysis, the variations in peak pressure rise rate for Jatropha biodiesel fuels and palm biodiesel fuels in comparison with diesel are presented in Figure 4.33 and Figure 4.34, respectively. The

range of the peak pressure rise rate for all the tested fuels is in the range of 4.9 to 6.7 bar/°CA. In fact, it is noted that the peak pressure rise rate for biodiesel blends is consistently lower than that of baseline diesel at all loading conditions. In addition, the general trend reveals that the variations in RMS of acceleration are very similar with the variation in peak pressure rise rate.

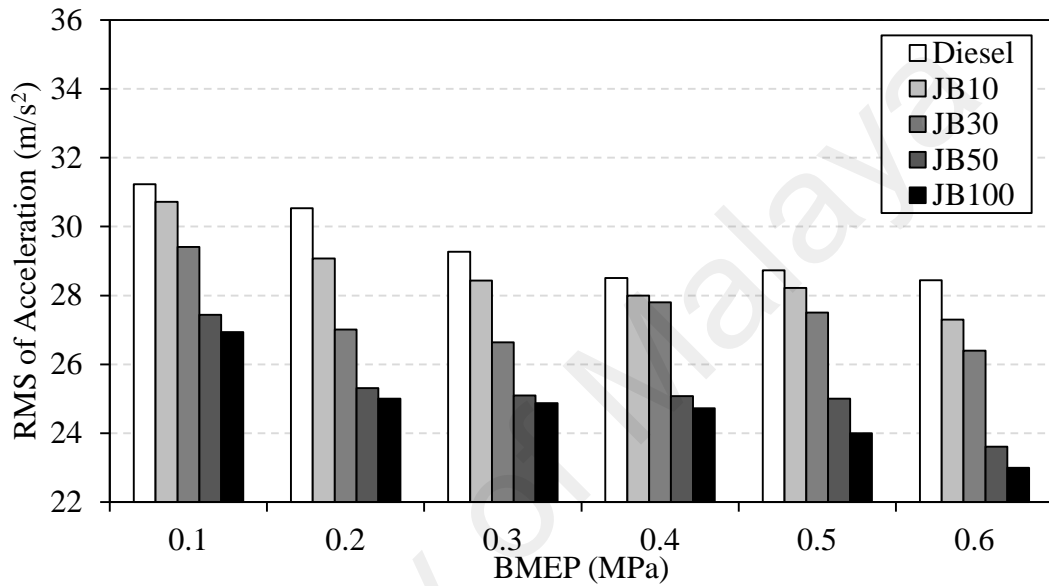


Figure 4.31: Variations in RMS of acceleration for diesel and Jatropha biodiesel blends at different engine loads and without EGR.

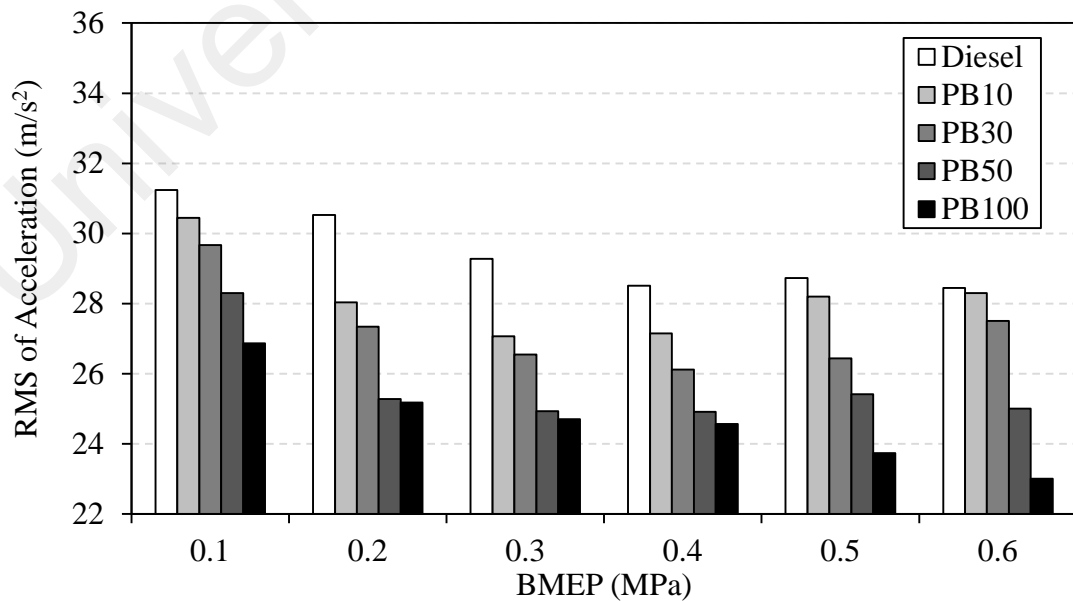


Figure 4.32: Variations in RMS of acceleration for diesel and palm biodiesel blends at different engine loads and without EGR.

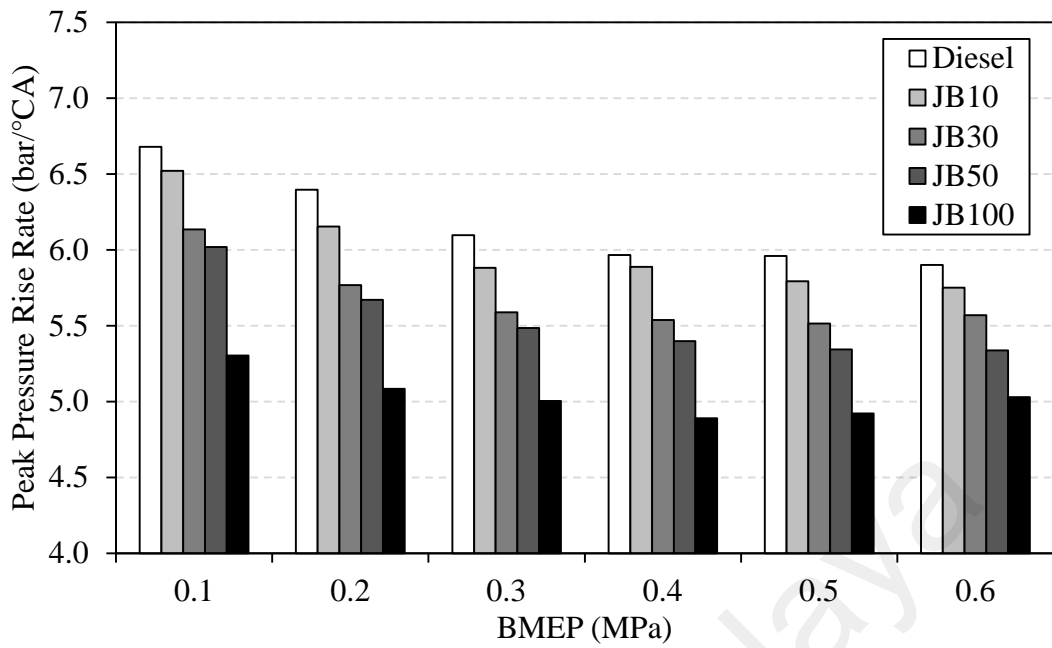


Figure 4.33: Variations in peak pressure rise rate for diesel and Jatropha biodiesel blends at different engine loads and without EGR.

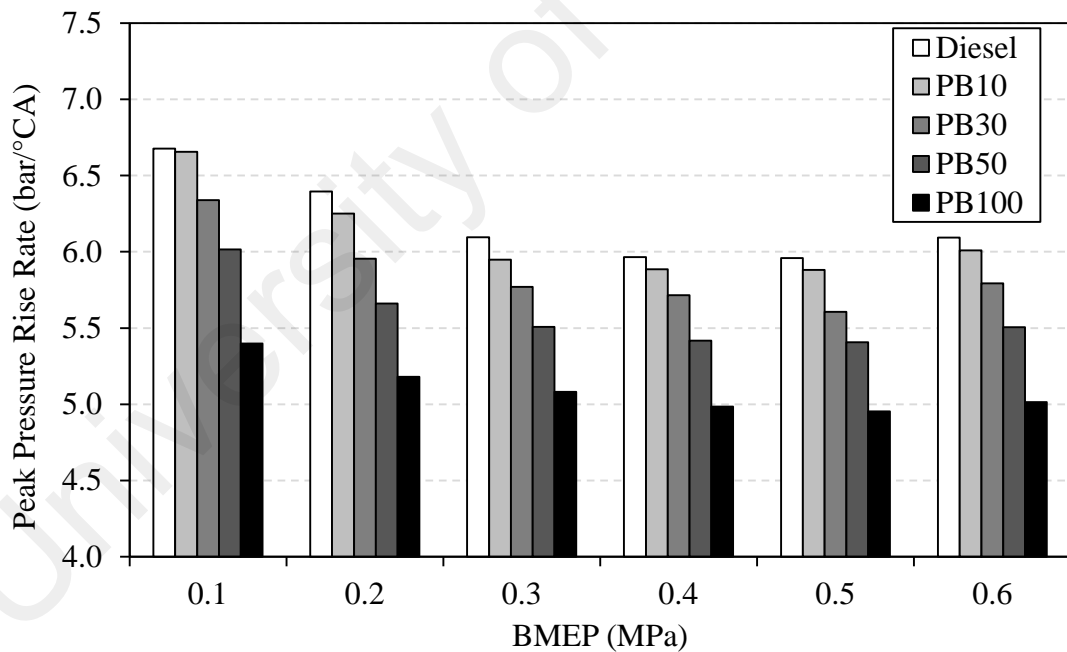


Figure 4.34: Variations in peak pressure rise rate for diesel and palm biodiesel blends at different engine loads and without EGR.

4.3.5 Summary

In this test series, the performance, emissions, combustion and vibration characteristics of an engine fuelled with diesel fuels, neat palm biodiesel, neat Jatropha biodiesel, as well as their respective fuel blends were investigated at engine loads of 0.1, 0.2, 0.3, 0.4, 0.5, and 0.6 MPa. The following main findings can be drawn from this test series:

1. All biodiesel fuels showed a prominent increase in BSFC at all load conditions. Additionally, JB30 and PB10 blends showed a marginal improvement of 3.4% and 1.7%, respectively, in BTE at an engine load of 0.1 MPa.
2. The engine load showed the greatest effect on BSCO emissions variation. The BSCO emissions decreased with the increasing biodiesel blend ratio and engine load. Additionally, the BSNO_x emissions decreased with increase in engine load and biodiesel blending ratio. The presence of methyl ester in the blend decreased the BSNO_x relative to the baseline diesel, but the BSNO_x did not decrease further as the degree of blending of their respective JME and PME increased. In addition, both the JME and PME blended fuels showed lower smoke emissions than baseline diesel across all the engine loading conditions.
3. It was found that, at a lower engine load of 0.1 MPa, most of the biodiesel blends showed higher peak pressure in the range of 0.6–1.5 bar in comparison with the baseline diesel. The location of occurrence of these peaks has shifted earlier towards the TDC point. In the case of the higher engine load, less significant variations in terms of peak pressure were observed among all biodiesel blends and baseline diesel fuel. Furthermore, the JME and PME biodiesel blended fuels consistently showed lower peak HRR in comparison with baseline diesel. In addition, the JME and PME biodiesel blended fuels showed a slightly shorter ID and shorter combustion duration in comparison with baseline diesel across the engine load operations.

4. The JME and PME biodiesel blended fuels showed direct correlation with RMS of acceleration. JB100 and PB100 showed the largest reduction of 19% in the RMS of acceleration in comparison with the baseline diesel at engine load of 0.6 MPa. In addition, the variations in RMS of acceleration showed a very similar trend with the variation in peak pressure rise rate for all fuel types and engine loading conditions.

4.4 Effect of Injection timing

In this test series, the experiments were conducted at a constant speed of 1500 rpm and an injection pressure of 600 bar. Parametric studies dealing with injection timing variation using neat palm biodiesel in common-rail engine were performed and compared with baseline diesel. The start of injection (SOI) timing was varied from TDC to 25° BTDC to acquire the optimum injection timing for the corresponding baseline diesel and biodiesel fuel. The effects of biodiesel fuel and injection timing variation on engine performance, emissions, and combustion characteristics are discussed in the following sub-sections.

4.4.1 Performance analysis

Figure 4.35 illustrates the resulting effect of SOI timing on the BSFC of the engine fuelled with PME biodiesel fuel and baseline diesel. Generally, the BSFC is a measure of the amount of fuel required to generate one-kilowatt of power per hour. From the results, it is observed that the BSFC for PME biodiesel fuel is consistently higher than that of baseline diesel across all SOI timings. The higher BSFC of PME means that a greater amount of fuel is required to attain the same amount of power. This was expected because of the low calorific value of PME in comparison with diesel, which is about 12% lower than that of baseline diesel fuel. Additionally, it can be observed that the variation in injection timing also has a significant effect on the variation of the BSFC. As the SOI timing is advanced from the top dead center (TDC) point, the BSFC dropped for all fuels. This reduction in the BSFC can be explained by the fact that as the SOI timing is

advanced, there would continuous enhancement in the combustion efficiency and quality. With a constant amount of brake power output, the decreased effect of the BSFC means less fuel is being supplied to undergo a more efficient combustion process. This is particularly for the case of advanced SOI timing. However, it is observed that a further advance in SOI timing beyond 11° BTDC causes penalties in the BSFC as the combustion pressure build up begins to resist the upward movement of the piston. Based on the BSFC results, the optimum SOI timing for PME and diesel operations is found to be 11° BTDC and this setting will be used for the following EGR test series.

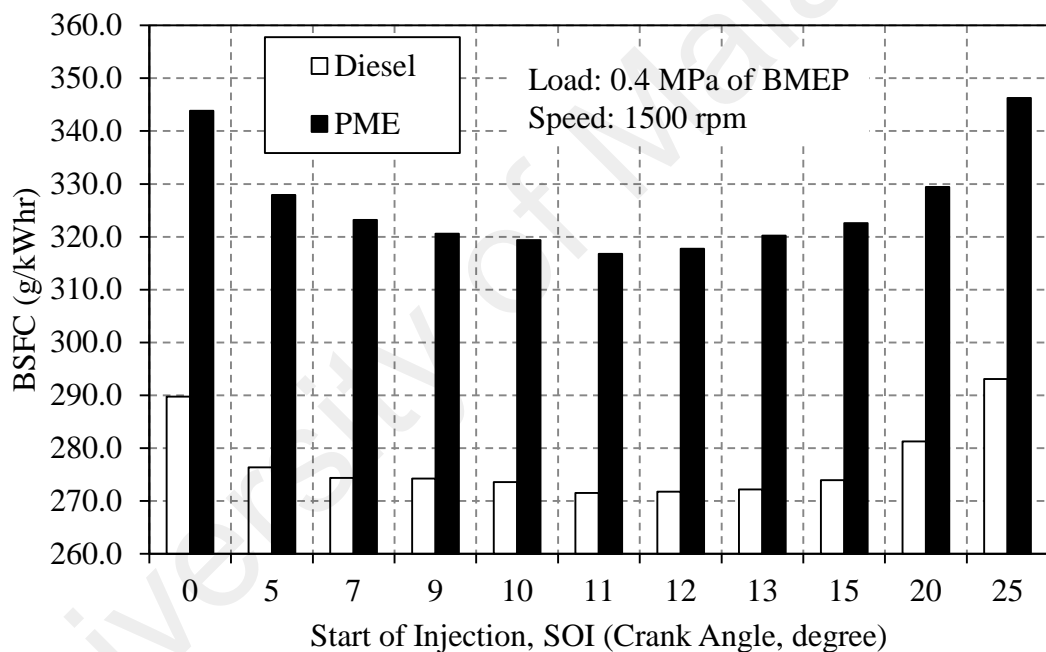


Figure 4.35: BSFC with PME compared with diesel fuel at various SOI timings and without EGR.

Engine BTE is commonly used to express the efficiency of an engine to convert fuel chemical energy to mechanical energy. BTE can be calculated by dividing the brake power output by the total energy input delivered to the system. Figure 4.36 illustrates the variations in BTE with different SOI timings of the engine fuelled with PME biodiesel fuel and baseline diesel. The BTE of baseline diesel is found to be consistently higher than that of PME across all SOI timings. In fact, it can be observed that the peak BTE for baseline diesel and PME is 29.5% and 28.6%, respectively, at an SOI timing of 11

$^{\circ}$ BTDC. In addition, the results also indicate that the BTE is significantly affected by the variation in SOI timing. There is an improvement in the BTE for all the test fuels with advanced SOI timings, except for the case of SOI timings beyond 11° BTDC. The incremental effect is due to the longer ignition delay (physical delay) leading to better mixing, which results in better combustion and a higher BTE. Another reason is that at advanced injection timing, the engine reaches the peak pressure closer to TDC and is therefore able to produce higher effective pressure to perform useful work (Bari et al., 2004). However, there is a continuous deterioration of the BTE in the case of further advances in SOI timing beyond 11° BTDC for both fuel operations. It may be due to the decrease in the delay period, which reduces the power output because a larger amount of fuel burns during expansion and the cylinder pressure rises only when the cylinder volume is expanding rapidly, and as a result lower effective pressure is produced (Bari et al., 2004; Shivakumar et al., 2011).

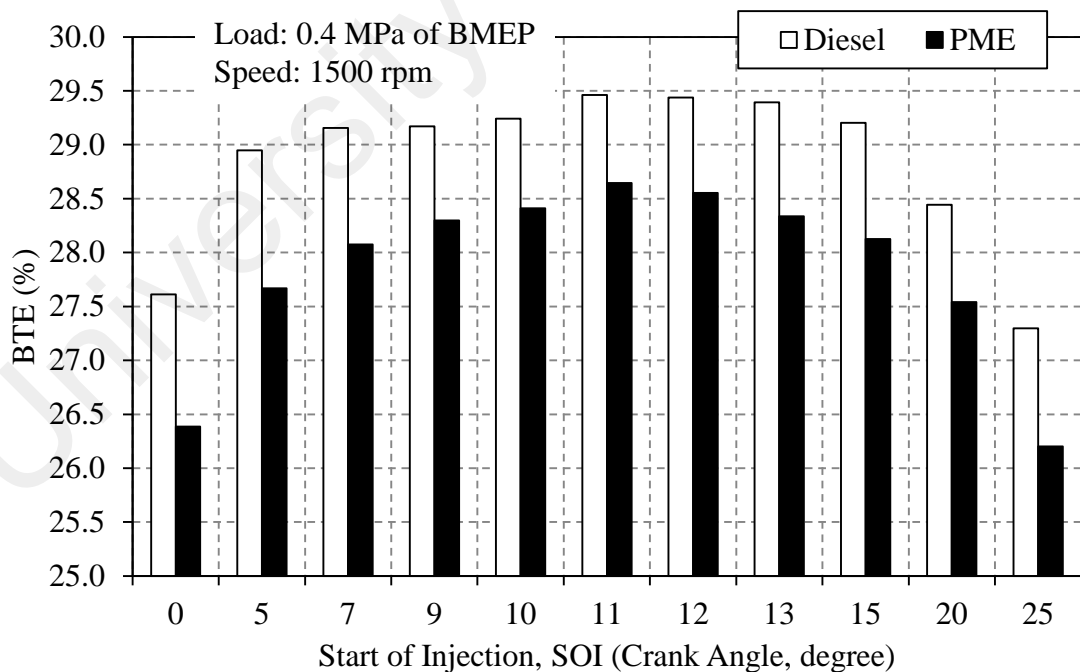


Figure 4.36: Brake thermal efficiency at different SOI timing conditions and without EGR.

4.4.2 Emissions analysis

NO_x is a hazardous and undesirable emission product that has a wide variety of human health and environmental impacts. Literature studies indicate that there is no absolute trend in NO_x emissions when biodiesel fuels are used in CI engines. Researchers from all over the world have reported higher NO_x emissions with biodiesel-fuelled engines (Karavalakis et al., 2011; Tan et al., 2012; Wu et al., 2009), and others found lower NO_x emissions when using methyl ester fuels (Choudhury & Bose, 2008; Huang et al., 2010). Typically, the NO_x formation depends on the fuel properties, fuel type, type of engine and engine operation conditions (Szybist et al., 2005; Xue et al., 2011). The variation of BSNO_x emissions of the test fuels at various SOI timings is illustrated in Figure 4.37. The result shows that advancement of the SOI timing resulted in increased BSNO_x emissions for all the test fuels. The increasing trend in BSNO_x emissions suggested that with advanced SOI timing, the mixture ignites and burns earlier, hence resulting in early occurrence of peak pressure near TDC. This leads to a higher combustion temperature and promotes the thermal or Zeldovich NO_x formation mechanism. The results also show that PME fuel tends to lower the BSNO_x emissions across all the SOI timings. This can be attributed to the relatively higher cetane number and lower heating value of the PME compared with baseline diesel, which consequently lowers the heat release rate at the premixed combustion stage and reduces the peak combustion temperature. This finding is further reinforced by the similar trend of the in-cylinder mean gas temperature, as shown in Figure 4.38.

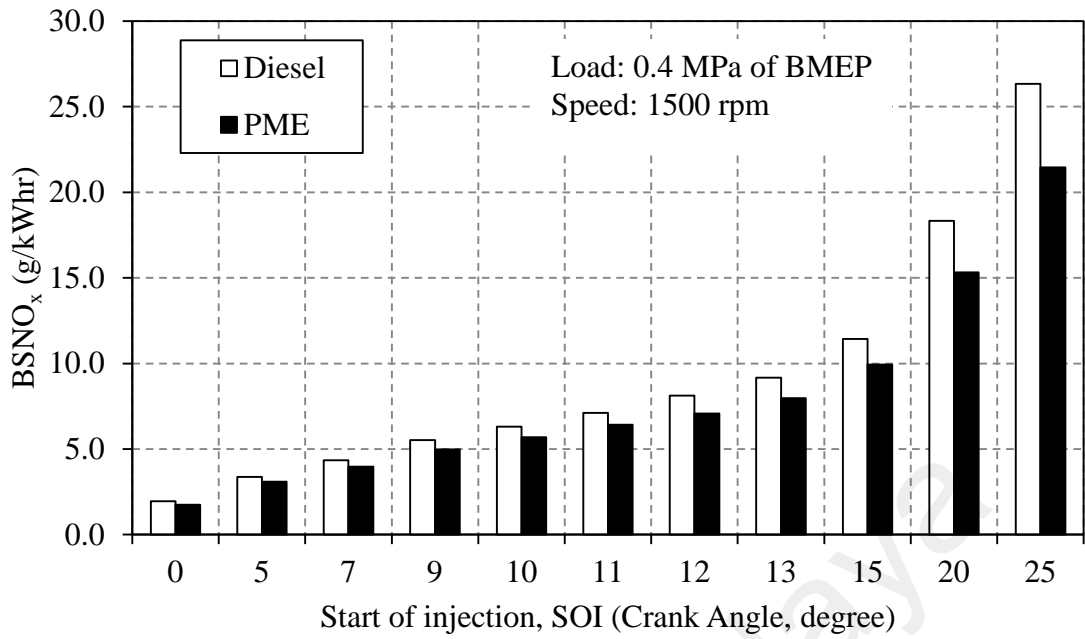


Figure 4.37: BSNO_x emissions at different SOI timing conditions and without EGR.

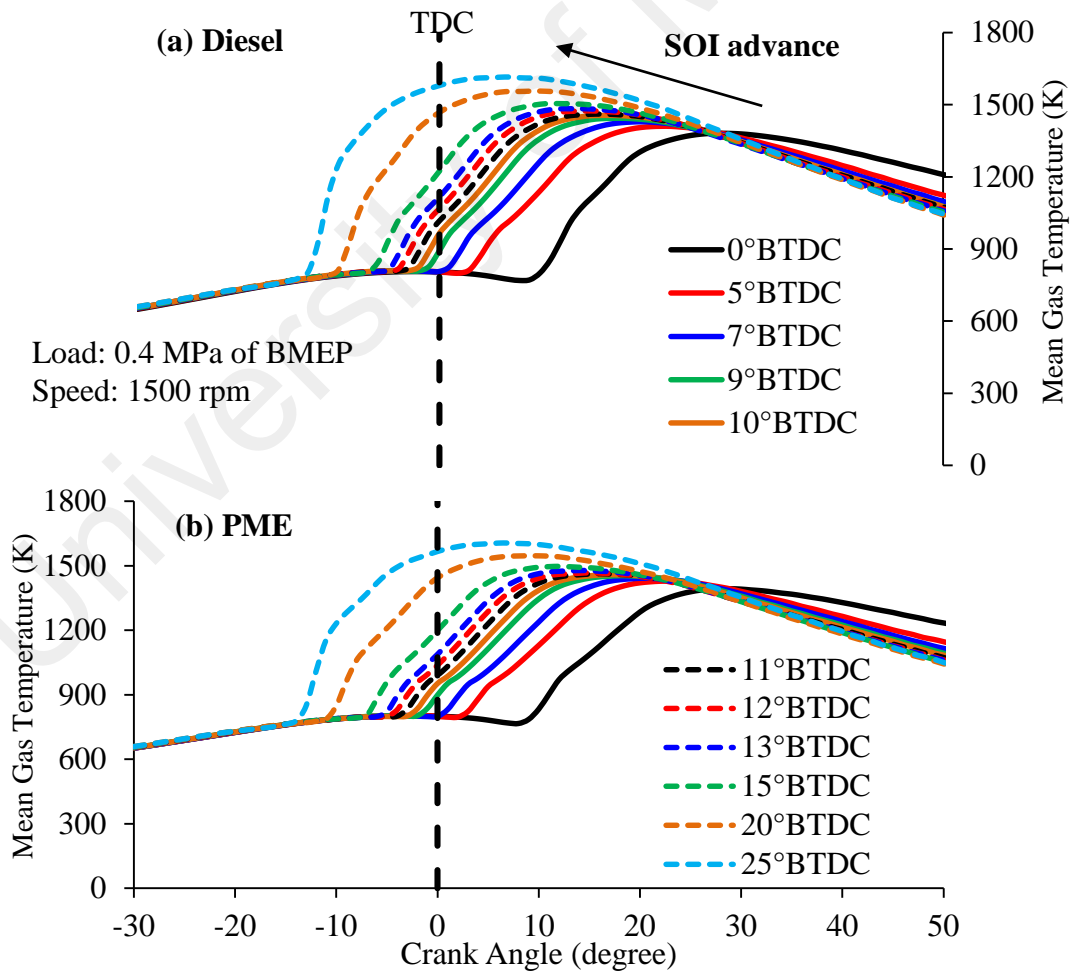


Figure 4.38: In-cylinder mean gas temperature curves for (a) baseline diesel, (b) PME at various SOI timings and without EGR.

The smoke formation results from the incomplete combustion of the hydrocarbon fuel and partial reaction of the carbon content in the liquid fuel. The variation of smoke emissions of the test fuels at various SOI timings is presented in Figure 4.39. Generally, it can be seen that the smoke emission level decreased with PME at all SOI timings. Lower smoke emissions are observed than in diesel fuel across all SOI timings, largely because of higher fuel-borne oxygen, lower carbon content, and the absence or lower amount of aromatics in PME fuel (Gumus et al., 2012). The results also indicate that smoke emissions are reduced with advanced SOI timings. This is due to cylinder operating temperatures being higher for advanced SOI timings, which improved the reaction between fuel and oxygen and resulted in lower smoke emissions (Shivakumar et al., 2011). Another reason may be due to the availability of sufficient time for the fuel to evaporate and mix with the air, leading to better mixing and combustion (Ganapathy et al., 2011).

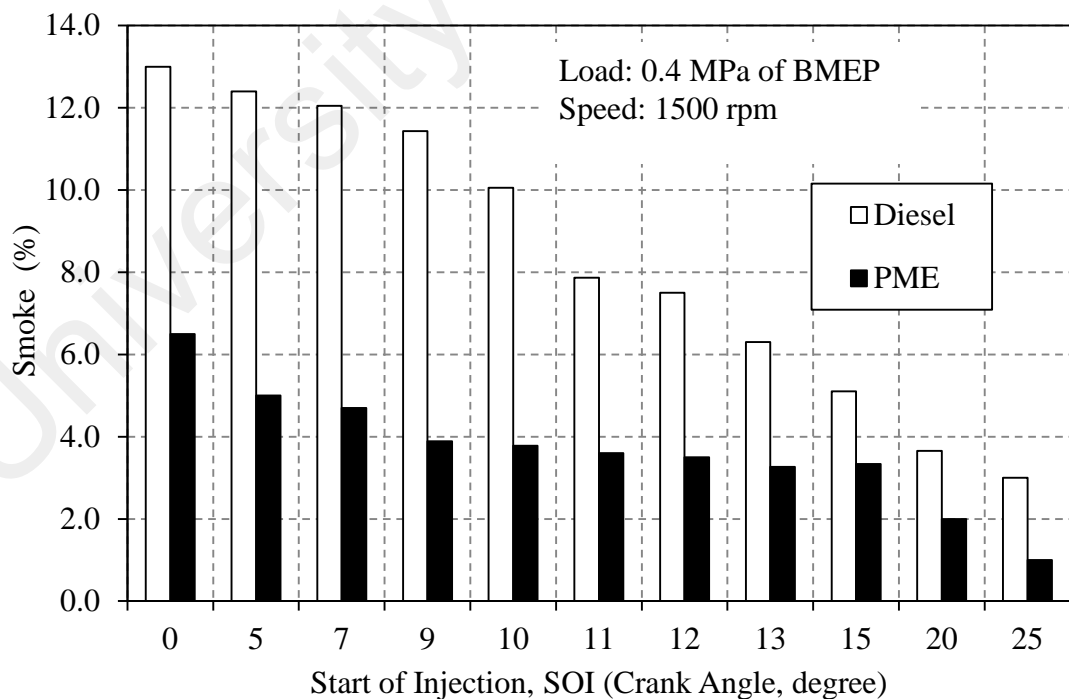


Figure 4.39: Smoke emissions at different SOI timing conditions and without EGR.

Due to the overall lean operation and higher expansion ratio of the diesel engine, the exhaust gas temperature (EGT) is typically lower than that of the gasoline engine. A higher EGT is unfavorable as this will deteriorate the engine fuel economy by discharging some of the useful energy into waste exhaust thermal energy, and may also cause thermal damage to piston components. The variation of exhaust gas temperature of the test fuels at various SOI timings is shown in Figure 4.40. Generally, it can be seen that the variation in exhaust gas temperature follows a similar trend to the BSFC with advanced SOI timing. In fact, running on PME fuel exhibits a higher EGT when compared to diesel fuel across all SOI timings. The increment may be due to the lower calorific value of PME fuel. Thus, the increased fuel quantity injected for attaining the same amount of power has caused an increase in-cylinder bulk-gas-averaged temperatures. On an average, EGT for PME fuel across all SOI timings are increased by 11.5 °C compared to baseline diesel. The highest increment of EGT is 15 °C for SOI of 5° BTDC with respect to baseline diesel. Another interesting observation is that as the SOI timing is advanced, EGT reduced for all fuels. This is due to greater heat release occurring closer to TDC in the expansion stroke, which offered sufficient time for the hot combustion products to expand and cool down prior to the exhaust valve being opened. This enhances the heat utilization and allows better cooling of combustion gases, thus lowering the exhaust gas temperature. Further advances in SOI timing beyond 13° BTDC has caused the increase in EGT because of the increase in BSFC.

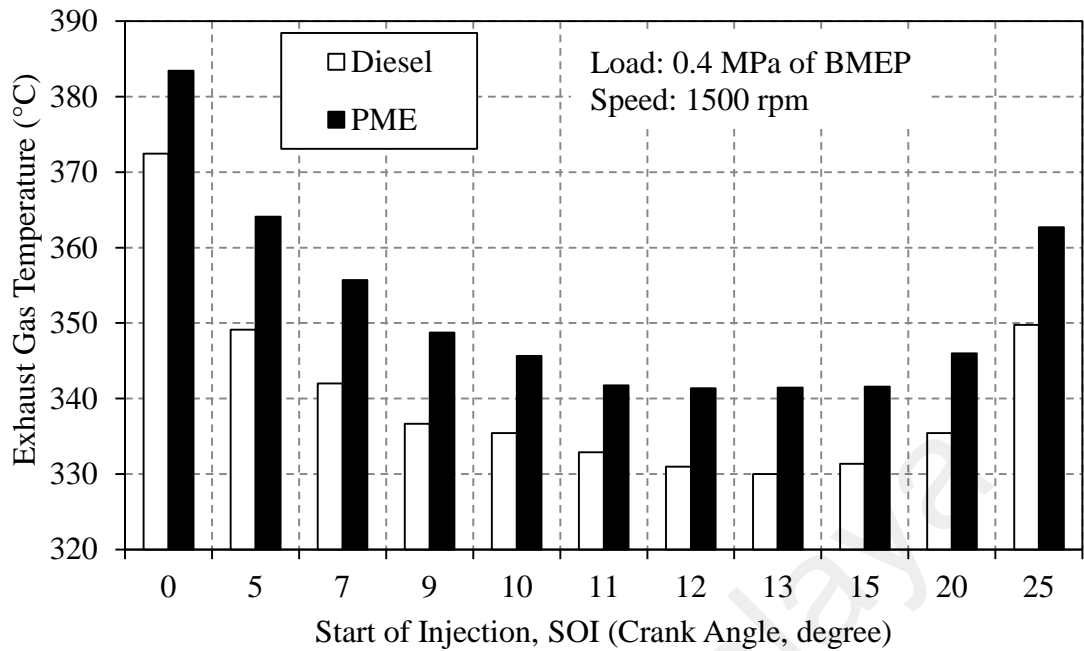


Figure 4.40: Exhaust gas temperature variation at different SOI timing conditions and without EGR.

4.4.3 Combustion analysis

To study the effect of biodiesel fuel on combustion, the cylinder pressures for 100 consecutive combustion cycles were recorded, averaged, and compared. Figure 4.41 shows the plot of combustion pressure, HRR and injector current profile of the engine operated with baseline diesel and PME fuels at optimum SOI timing of 11° BTDC. As can be observed, the engine operated with PME fuel had little effect on the combustion characteristics, and the pattern is comparable with the baseline diesel. The pressure peak is shifted later toward the expansion stroke with PME fuel although the location of SOC timing for PME occurred 0.25° CA earlier than that of baseline diesel. In addition, a small reduction in the pressure peak in the range of 0.6 bar is observed for the PME fuel operation. Two prominent peaks of HRR are observed for both fuels. The first and second peak of HRR correspond to the premixed and mixing controlled combustion phases respectively. Also, it can be clearly observed that the location of occurrence of the first and second peak of HRR for the PME fuel is shifted earlier (by 0.25° CA) and later (by 0.875° CA) from the TDC point, respectively, compared to baseline diesel. The primary

reason for the early occurrence of the first HRR peak can be attributed to the advance in SOC timing, which caused the earlier rise of the HRR. On the other hand, slow burning rate and thus longer combustion duration of PME fuel has caused the second HRR peak to occur later in the expansion stroke as compared to that of baseline diesel. The total burning angles for PME fuel with respect to baseline diesel are shown in Figure 4.42. The total burning angle in this study is defined as the period between 10% and 90% mass burnt. The longer combustion duration of PME fuel means that it has a slower burn rate than baseline diesel, especially during the mixing controlled combustion phase. This may be due to the slightly higher viscosity of PME fuel compared to baseline diesel, hence delaying the mixing time required for diffusive burning. Another explanation may be due to the lower calorific value of the PME fuel, thus resulting in an increase in fuel quantity injected for attaining the same amount of power. As more fuel is being injected, a richer mixture is thus formed inside the cylinder chamber, which burns more rapidly in the early stages of combustion (premixed combustion phase) and the remaining fuel burns in the later stages (mixing controlled combustion phase) and requires a longer duration.

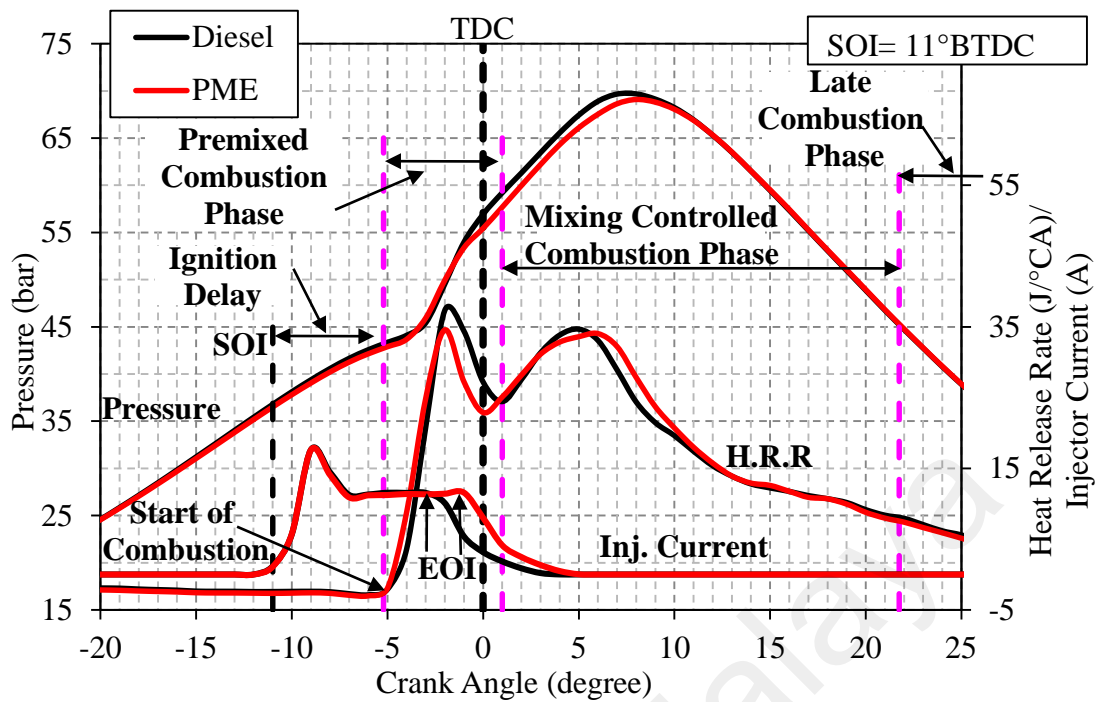


Figure 4.41: Combustion pressure, heat release rate and injector current profiles for diesel and PME fuel at SOI of 11° BTDC and without EGR.

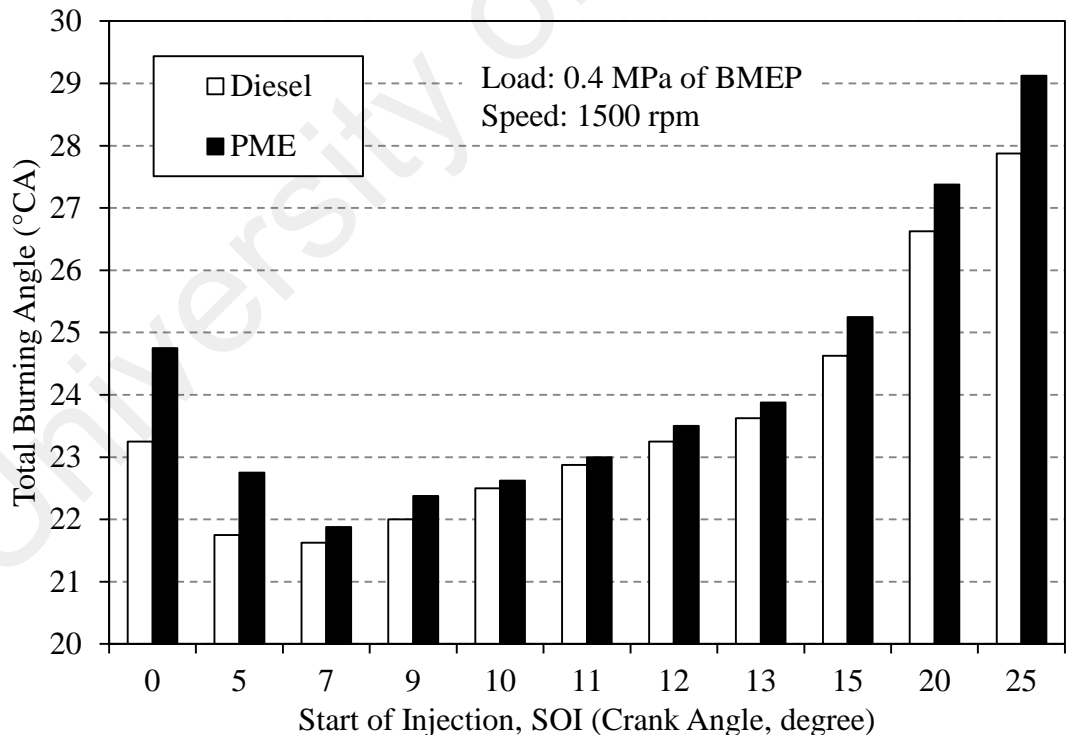


Figure 4.42: Total burning angle as a function of SOI timing for diesel and PME fuel and without EGR.

Figure 4.43 shows the variation of combustion pressure and HRR with respect to the crank angle at different SOI timings for the engine operated with baseline diesel and PME fuel. Generally, the combustion pressure peak consistently increases and shift earlier toward the TDC position with advancing SOI timing for both the fuels. The resultant higher and more effective pressure is utilized to perform useful work and thus improve the BSFC and BTE. However, further advance in SOI timing beyond 11° BTDC caused combustion pressure to build up rapidly in the compression stroke, thus beginning to oppose the upward movement of the piston and causing deterioration of the BSFC. On an average, it is found that PME produces 0.77 bar lower maximum combustion pressure compared to baseline diesel at all SOI timings. The HRR curves show similar patterns, as the combustion pressure trend where the HRR peak that is associated with premixed combustion is shifted earlier toward the compression stroke with advanced SOI timing, for both of the tested fuels. When SOI is advanced toward the TDC in the expansion stroke, the maximum HRR associated with the premixed combustion became initially lower and remained unchanged. However, further advances in SOI timing beyond 15° BTDC have led to significant increases in the maximum HRR. This is due to a longer ignition delay, which tends to promote more premixed combustion and increase both the maximum combustion pressure and HRR. With the PME fuel, the HRR is similar to baseline diesel, however it can noticed that a higher fuel fraction is burned in the mixing controlled combustion phase (i.e. a wider plateau region after the first HRR peak). This phenomenon is clearly visible for the retarded SOI cases (i.e. SOI = 0° BTDC) as compared to earlier SOI conditions. This is mainly due to higher cetane number of PME fuel compared to baseline diesel, thereby resulting in a shorter ignition delay and a lower pressure peak. In fact, the peak of the pressure curve also shifted away from the TDC point in the expansion stroke as compared to baseline diesel for the corresponding SOI

timing. On an average, it is found that PME produces $5.7 \text{ J/}^\circ\text{CA}$ lower in maximum HRR compared to baseline diesel across all SOI timings.

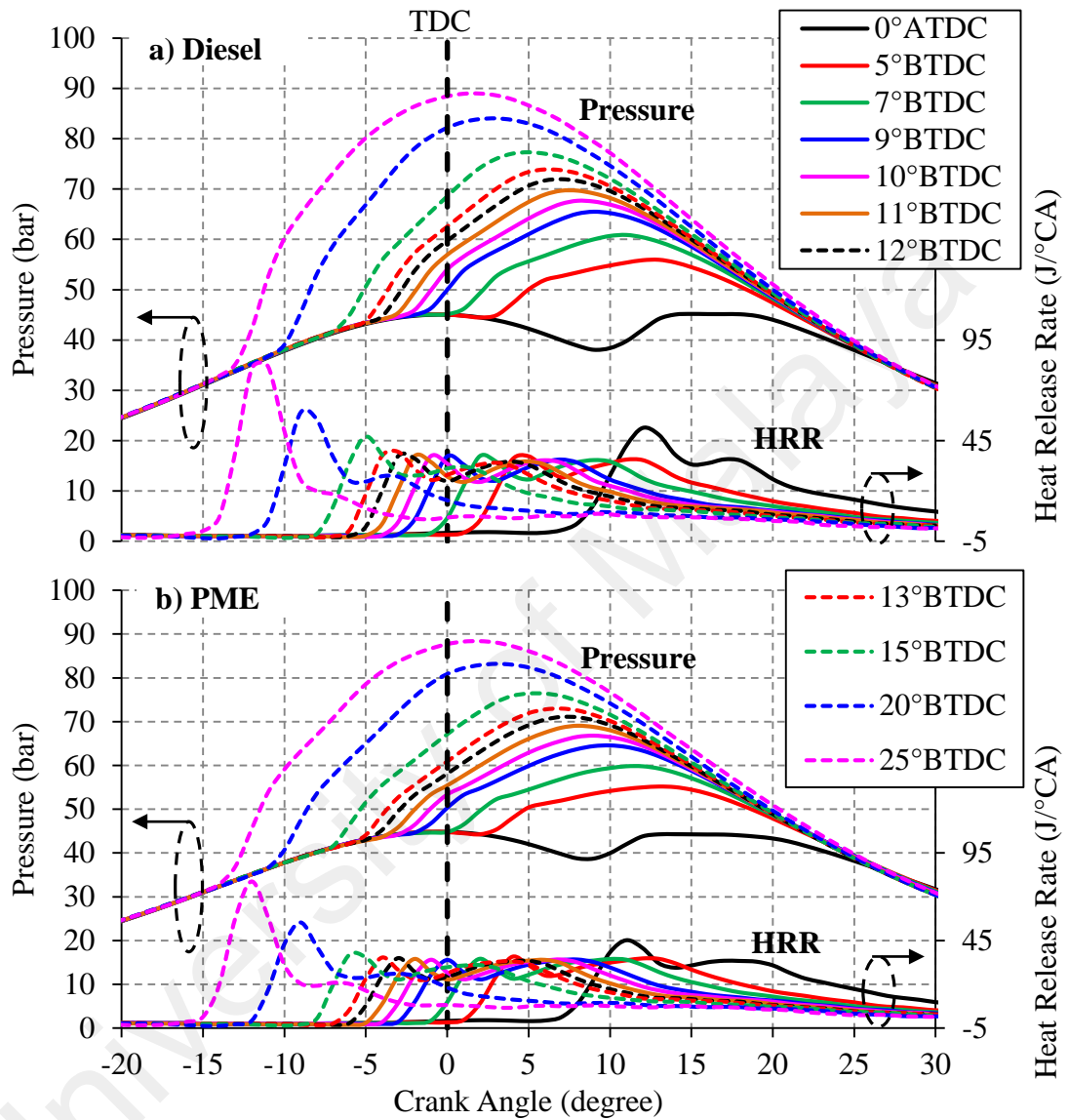


Figure 4.43: Combustion pressure curves for (a) baseline diesel and (b) PME at various SOI timings and without EGR.

4.4.4 Summary

In this test series, the effect of SOI timing variation on engine performance, emission and combustion characteristics of neat palm biodiesel and diesel fuel have been experimentally investigated in a high-pressure common-rail DI diesel engine. The engine was operated at a constant speed of 1500 rpm and a BMEP of 0.4 MPa. The following main findings can be drawn from this test series.

1. Based on the highest BTE and the reasonable NO_x level, the optimum injection timing is found to be 11° BTDC for both the baseline diesel and biodiesel operations.
2. The advancement of the SOI timing increased the BSNO_x emissions for both the test fuels. In fact, the PME fuel tends to lower the BSNO_x emissions across all the SOI timings.
3. With PME fuel operation, lower smoke emissions were observed than in diesel fuel across all SOI timings. Besides, the smoke emissions were reduced with advanced SOI timings for all tested fuels.
4. At optimum SOI timing of 11° BTDC, it was found that the PME fuel had little effect on the combustion characteristics, and the pattern is comparable with the baseline diesel.
5. The combustion pressure peak consistently increases and shifted earlier toward the TDC position with advancing SOI timing for both the fuels. With the PME fuel, the HRR was found similar to baseline diesel, however it can be noticed that a higher fuel fraction was burned in the mixing controlled combustion phase. This phenomenon became more visible for the retarded SOI cases as compared to earlier SOI conditions.

4.5 Effect of EGR

EGR is one of the most promising strategies to reduce NO_x emissions in diesel engines by controlling the oxygen density and combustion peak temperature (Agarwal, Singh, et al., 2011; Gomma et al., 2011). However, the trade-off between NO_x and soot emissions must be analyzed carefully with EGR and the biodiesel fuelled engine. In this section, the effect of EGR on the performance, emissions and combustion of the baseline diesel and PME fuelled engines are discussed. The SOI timing was kept at an optimum of 11° BTDC as found in the previous test series and EGR rates were varied (i.e. 0 to 50%).

4.5.1 Performance analysis

The variations in the BSFC with respect to the EGR rate for the engine operated with PME biodiesel fuel and baseline diesel is shown in Figure 4.44. Generally, it can be seen that the BSFC for PME biodiesel fuel is consistently higher than that of baseline diesel across all EGR rates. This is mainly due to the lower calorific value of PME, thus the BSFC is higher than that of baseline diesel at all EGR rates. It can also be observed that the variation in the EGR rate also has a small effect on the BSFC. As the EGR rate increased, the BSFC dropped for all fuels, compared to without EGR. However, at EGR rate higher than 30% and 35% for baseline diesel and PME fuel, respectively, the BSFC begins to increase gradually. At higher EGR rates, the oxygen available for combustion is reduced. Thus, the air–fuel ratio is altered and this raises the BSFC. This is evident by the decrease in excess oxygen available in the exhaust tailpipe as shown in Figure 4.45. Besides, the results also indicate that the BSFC dropped as the EGR rate increases from 0 to 30% and 35% for baseline diesel and PME fuel, respectively. The possible factor may be re-burning of hydrocarbons that enter the combustion chamber with the re-circulated exhaust gas. This phenomenon has been reported in other investigations of EGR in diesel engine (Agarwal, Singh, et al., 2011; Pradeep & Sharma, 2007; Selim, 2003).

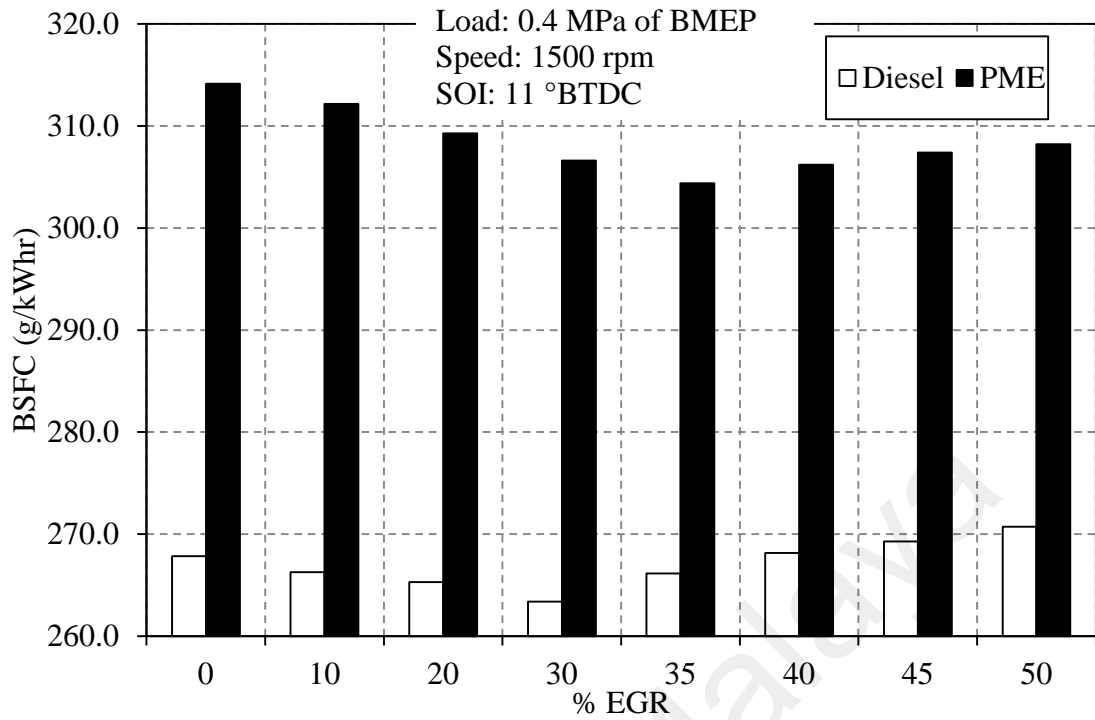


Figure 4.44: BSFC with PME compared with diesel fuel at various EGR rates.

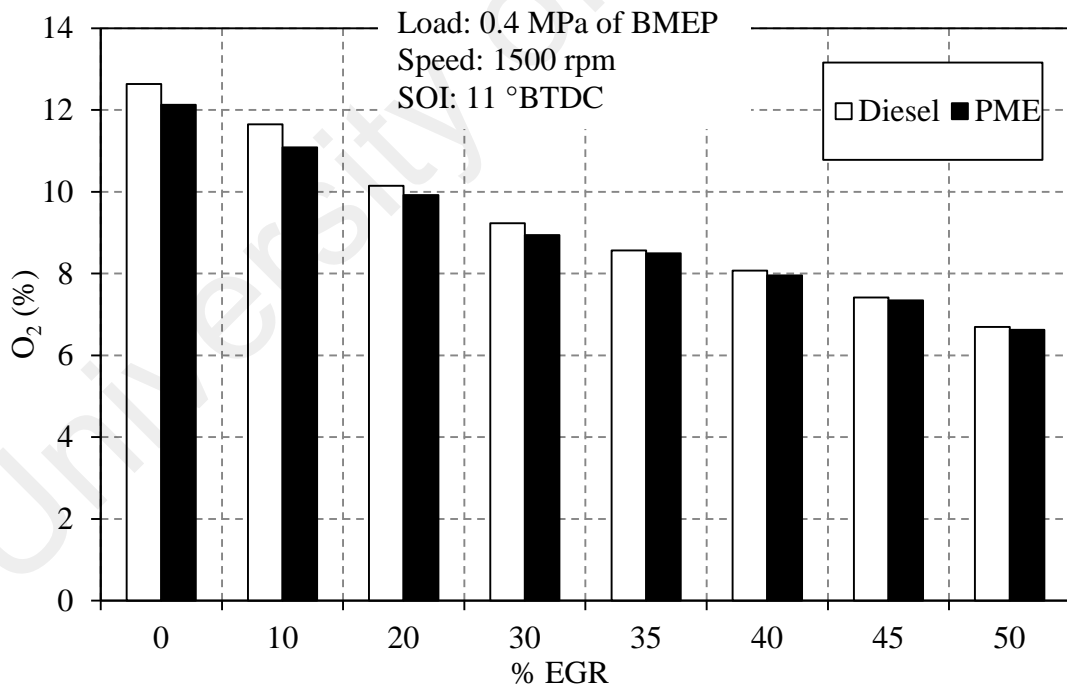


Figure 4.45: Exhaust gas O₂ concentration with PME compared with diesel fuel at various EGR rates.

Figure 4.46 shows the comparison of the BTE for the engine operated with PME biodiesel and baseline diesel. It is evident that the BTE for PME fuel is always lower than that of

baseline diesel regardless of the EGR rate. The lower calorific value of the PME fuel could be the reason for this. Subsequently, the BTE is found to slightly increase with a moderate EGR rate for both the tested fuels. At moderate EGR rates, the burned gas temperature is decreased significantly, thus reducing heat loss via the combustion chamber surfaces, leaving more heat available for conversion to mechanical work during the expansion stroke. Another possible reason may be due to the reduced pumping work as the EGR rate is increased at a constant brake load. On the other hand, lower oxygen exhaust gas feeds into the intake at higher EGR rates, thus resulting in poor air utilization and this leads to a reduction of BTE. Also, the decrease in BTE for the PME at EGR rate of more than 35% is less prominent compared to baseline diesel. This can be credited to the higher oxygen content in PME fuel which aids in better combustion efficiency.

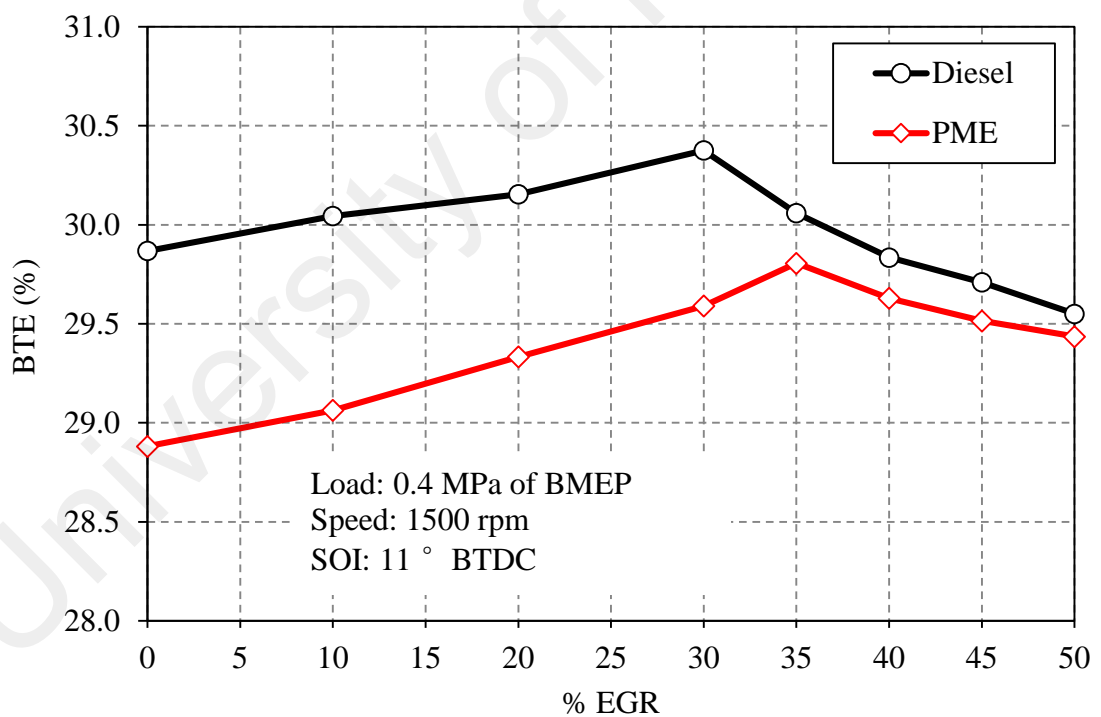


Figure 4.46: BTE with PME compared with diesel fuel at various EGR rates.

4.5.2 Emissions analysis

Figure 4.47 shows the variation of BSNO_x emission and smoke of PME and baseline diesel with various EGR rates. The overall trend indicates that the BSNO_x emissions for both the tested fuels tend to decrease as the EGR rate increases. The BSNO_x emission is reduced with increasing EGR rate due to lower burned gas temperature with dilution. Compared to baseline diesel, the BSNO_x emissions of PME are lower across all EGR rates. It is observed that for both the fuels, a drastic BSNO_x reduction in the range of 23.8–97% at 10–50% EGR rate is obtained compared with the corresponding engine operation without EGR. In fact, on an average the addition of EGR in reducing BSNO_x emissions for PME is about 0.5% more effective than baseline diesel. As discussed above, a lower heat release rate during the premixed combustion phase and a lower peak combustion temperature for PME results in lower BSNO_x emissions. In addition to this, re-entering of more water vapor and CO₂ into the combustion chamber due to the increase in the specific fuel consumption of PME fuel compared with the operation of baseline diesel also may lead to a greater BSNO_x reduction. This is evident by the increase in the CO₂ concentration in intake air as shown in Figure 4.48. The plots also indicate that PME fuel emitted a higher exhaust CO₂ than baseline diesel across all EGR rates. This may be due to the combined effects of lower calorific value and the extra oxygen content of PME fuel altering the combustion process which eventually results in higher exhaust CO₂. At above 45% EGR, the BSNO_x emission is less than 0.4 g kW⁻¹ h⁻¹ for both fuels, which is the EURO VI emission standard. On the other hand, the effects of EGR on the smoke emission for baseline diesel and PME revealed an increasing trend with higher EGR rates. It is evident that as compared to baseline diesel, the smoke emissions are lower for PME fuel and tend to increase at a much slower rate with higher EGR rates. It is the oxygen content in the PME fuel that plays a vital part in the combustion process which eventually causes a reduction in the smoke emissions. Moreover, the smoke formation rate increased

sharply as the EGR rate rose over 35% for both fuels. When the engine is fuelled with PME, an increase of the smoke emissions of 186% is observed with 35% EGR. Further increase in the EGR rate to 50% rapidly increased the smoke emission by 620% when compared with the engine operation without EGR. Under high EGR conditions, the exhaust gases re-circulated into the intake result in a reduction of the oxygen available for combustion. The in-cylinder soot formation and oxidation processes are strongly governed by the engine operation on gradually richer mixtures due to the reduction in oxygen content by EGR. Hence, the reduction in oxygen availability for fuel combustion and lower combustion temperature reduces the soot oxidation process which leads to higher smoke emissions. Another interesting topic that can be further discussed is the trade-off between BSNO_x, smoke and the EGR rates. From the results of the EGR effect on BSNO_x and the smoke emissions of the PME, an optimal trade-off between BSNO_x and smoke emissions can be achieved with EGR in the range of 10–30%, without a significant adverse effect on engine performance. It was realized that with PME fuel, an engine operating with 30% EGR resulted in an optimal trade-off between BSNO_x and smoke emissions. At this EGR rate, the BSNO_x emissions have effectively decreased by 80.7%, but the smoke emissions have increased by 167.3% compared to the engine operation without EGR. However, compared to diesel operation with 30% EGR, the PME fuel effectively reduced smoke emissions by 50%. Therefore, by considering both the positive effect of the reduction in BSNO_x and the smoke emissions, it is acceptable to operate an engine using PME with 30% EGR.

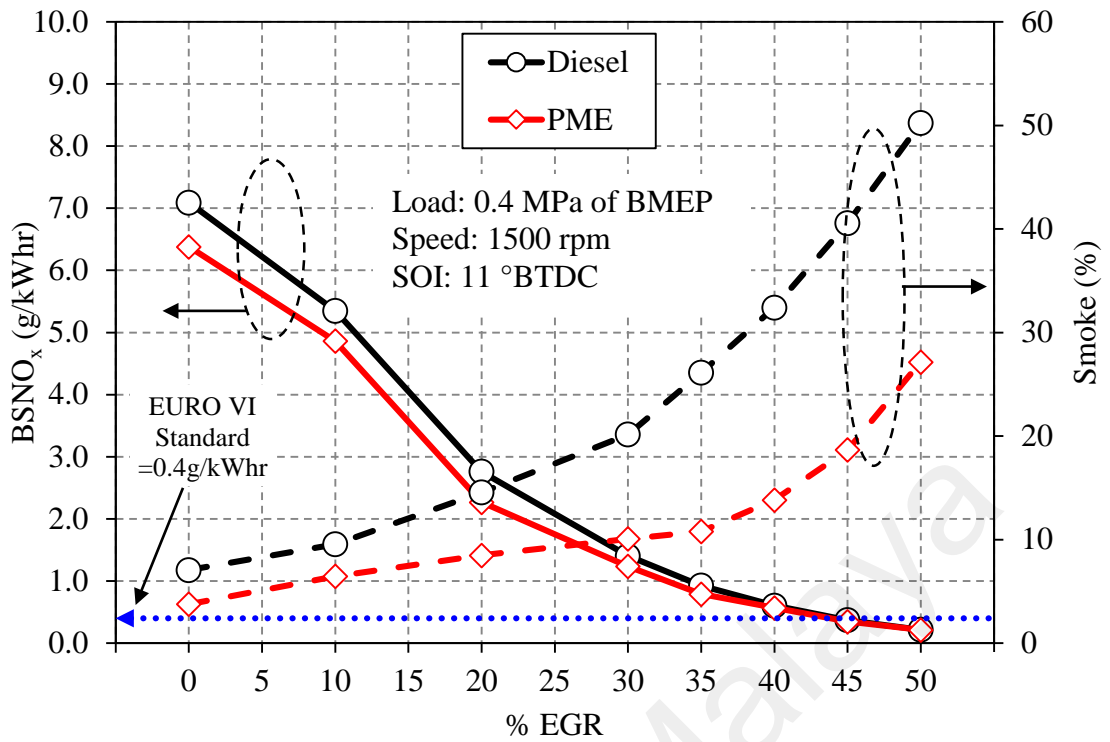


Figure 4.47: BSNO_x and smoke emission with various EGR rates.

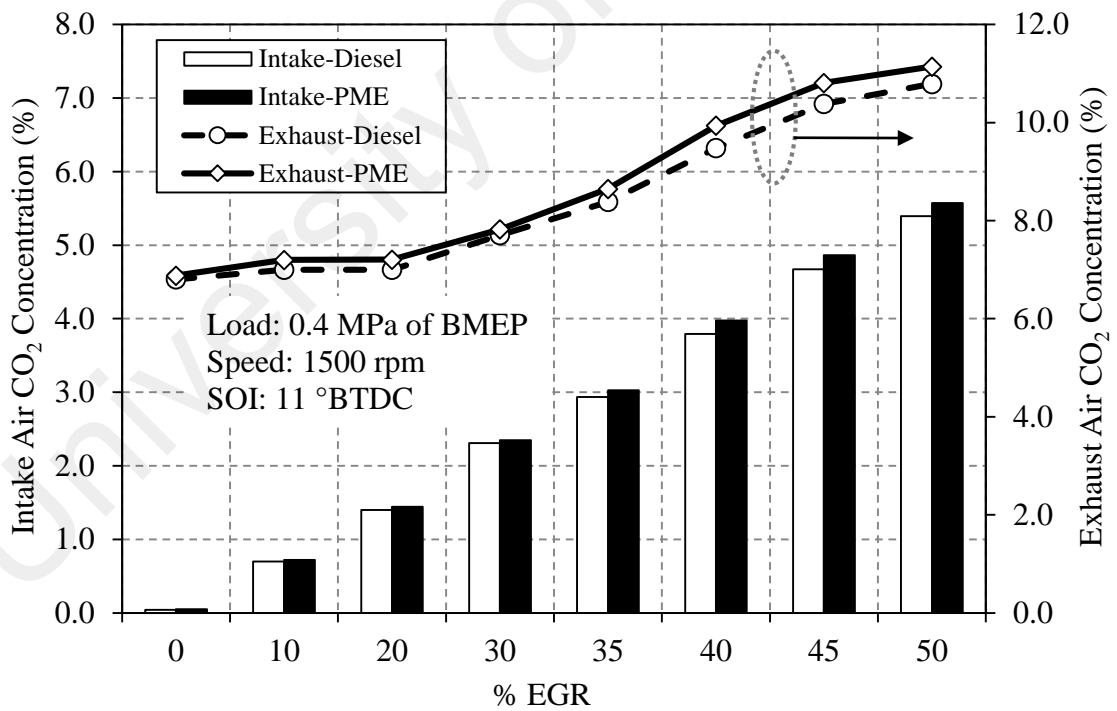


Figure 4.48: Intake and exhaust air CO₂ concentration with PME compared with diesel fuel at various EGR rates.

4.5.3 Combustion analysis

To evaluate the effect of the EGR variation using PME and baseline diesel on the combustion characteristics, the in-cylinder combustion pressures for 100 consecutive combustion cycles were recorded and compared with various EGR rates (0–50%) and at a fixed engine speed of 1500 rpm and a BMEP of 0.4 MPa. The in-cylinder pressure, HRR and injector current profiles for the engine using PME and baseline diesel are illustrated in Figure 4.49. As can be seen, the variation of EGR rate shows the greatest effect on the combustion characteristics for both the tested fuels. According to the HRR results, both fuels produced double peaks of HRR: the first peak reflects the premixed combustion process, and the second peak corresponds to the mixing controlled combustion phase. However, the transition from premixed combustion into mixing controlled combustion became less explicit with an increasing EGR rate for both fuels. In addition, the HRR results indicate that an increasing EGR rate caused a progressive increase in the peak HRR during the premixed burn fraction and shifted the location of the occurrence later toward the expansion stroke. This shift in heat release revealed a delay of the combustion processes due to the prolonged ignition delay. In the present study, the timing difference between the SOI and start of combustion is defined as the ignition delay. The SOI was confirmed from the injector current signal trace and the start of combustion by analyzing the first appearance of positive heat release. As can be seen in Figure 4.50, the plot of ignition delay versus EGR rate evidently shows that the increase in the EGR rate caused a progressive increase in the ignition delay for both fuels. In fact, in comparison with the corresponding baseline diesel, the use of the PME fuel resulted in a shorter ignition delay by an average of 0.3° CA. This is credited to the higher cetane number of the PME fuel compared to baseline diesel, thereby resulting in better ignition quality. Subsequently, the effect of prolonging the ignition delay also caused a progressive increase in the peak HRR with a higher EGR rate. As the EGR increases, the

in-cylinder fuel air mixture becomes more homogeneous due to a longer ignition delay, which could have allowed a larger fraction of fuel air mixture to burn during the premixed combustion phase. This effect also explains the phenomenon of the premixed combustion process dominating at a high EGR setting. Related to the EGR effects on NO_x emissions, the prolonged ignition delay retards the combustion events toward the expansion stroke, thus promoting more combustible mixtures to burn at a lower temperature. As a result, NO_x formation via the thermal or Zeldovich mechanism can be greatly reduced. Compared to baseline diesel, the peak HRR at the premix combustion stage is found to be consistently lower with PME fuel across all EGR rates. This explains the lower BSNO_x emissions of the PME fuel with respect to baseline diesel at all EGR rates. In addition, the steepness of the HRR curves during the premixed combustion phase decreased with increasing EGR. Again, this is an evidence of reduced reaction rates and decreased BSNO_x with increasing EGR for baseline diesel and the PME fuels.

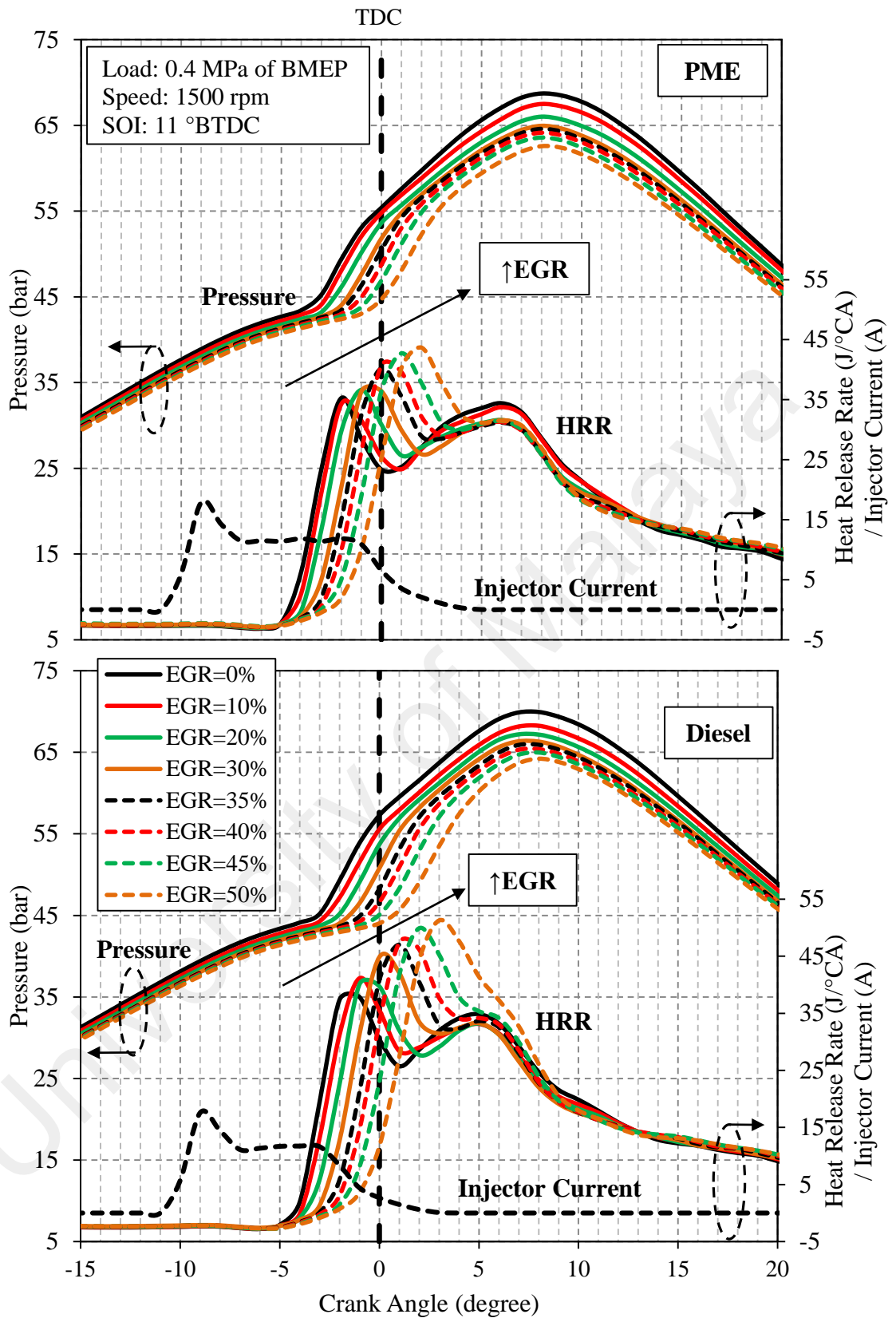


Figure 4.49: In-cylinder pressure, HRR and injector current signal versus crank angle for engine operated with PME (top) and baseline diesel (bottom) at various EGR rates.

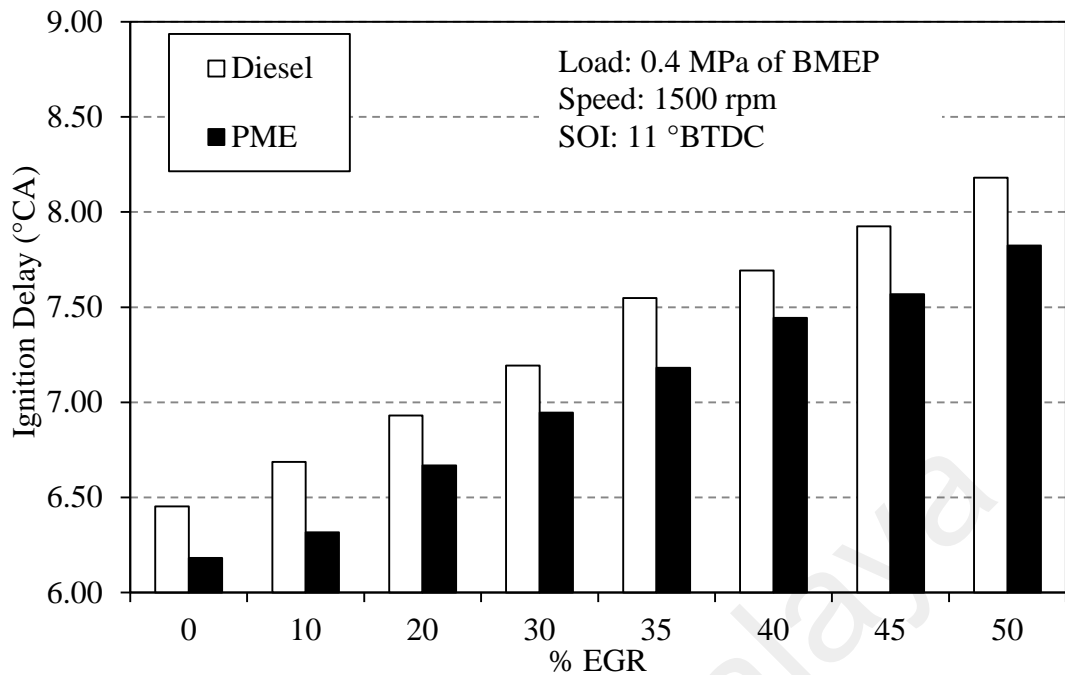


Figure 4.50: Ignition delay at various EGR rates for engine operation with baseline diesel and PME fuels.

Another important aspect is related to in-cylinder combustion pressure traces. A pronounced change in peak combustion pressure is observed with increasing EGR for both fuels. As shown in Figure 4.51, it is observed that, in general, regardless of the EGR setting, the PME fuel exhibited a lower peak pressure than baseline diesel owing to the marginal decrease in the HRR during the premixed combustion phase. On an average, it is found that PME produced 1.2 bar lower maximum combustion pressure compared to baseline diesel across all EGR rates. The results also indicates that a higher EGR rate tends to lower the maximum cylinder pressure during the expansion stroke. This may be due to the combined effect of greater heat capacity, chemical and thermal effects, with the most significant effect being the dilution effect, which extends the ignition delay duration and thus enhances the in-cylinder charge mixing (Ladommatos et al., 2000). Consequently, the premixed phase of combustion would occur late in the expansion stroke, thereby lowering the peak pressure and reducing BSNO_x.

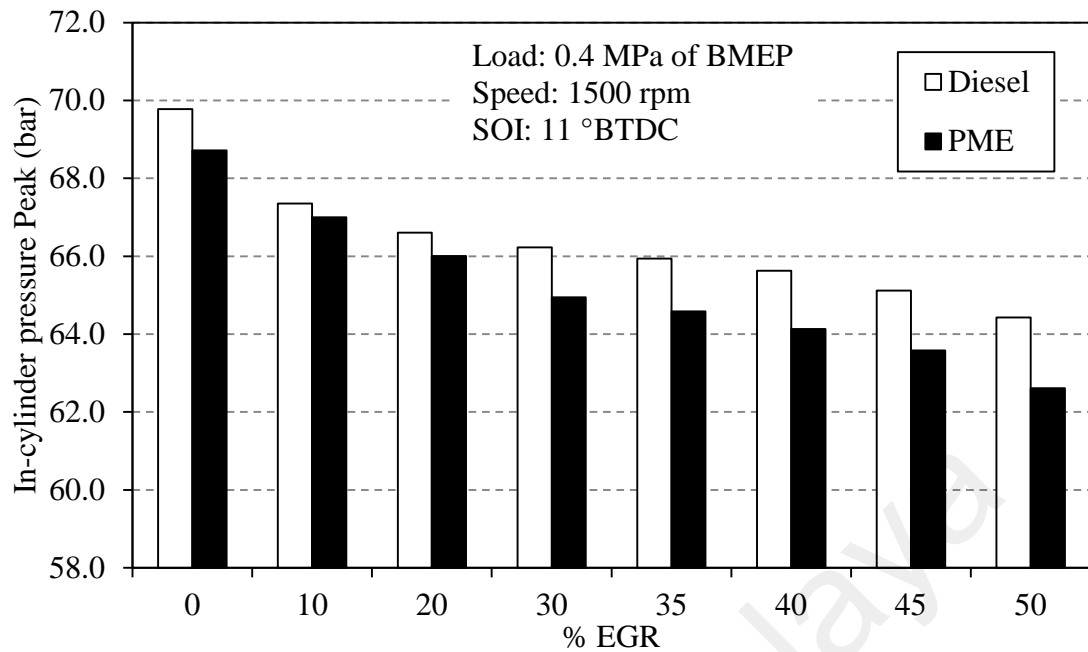


Figure 4.51: Maximum combustion pressure at various EGR rates for engine operation with baseline diesel and PME fuels.

4.5.4 Strategy for simultaneous BSNO_x–smoke reduction

A vast amount of studies have been carried out to reduce the emissions of pollutants from diesel engines and the attempts are still in progress (Agarwal et al., 2006; Bari et al., 2004; Park & Yoon, 2015; Verschaeren et al., 2014). Specifically, the simultaneous reduction of NO_x and smoke is the most challenging aspect in the reduction of diesel engine emissions. Emission controls at the source level are the most effective techniques in reducing the pollutants of a diesel engine since they are economical when compared to the treatment of exhaust gases. Injection timing is a key parameter that directly affects the combustion and exhaust emissions. Using EGR for NO_x reduction is another promising approach in diesel engines, but there could be an increase in smoke emissions. Simultaneous reduction of both emission species from the levels of fossil diesel is possible with the use of biodiesels (Ng et al., 2011). Hence, a comparative analysis of the exhaust BSNO_x and smoke opacity levels between the engine fuelled with neat PME biodiesel and that with fossil diesel is discussed in this section to observe the effect of injection timing and EGR variation on BSNO_x and smoke level.

Figure 4.52 shows the BSNO_x–smoke plot for PME and baseline diesel with various EGR rates and SOI timings. Generally, the overall trend shows that the BSNO_x emissions for both the tested fuels reduces with higher EGR rate and later SOI timing. A substantially lower level of BSNO_x below the EURO V and EURO VI emission standard can be achieved by the late SOI timing of 0° BTDC and over 45% EGR, respectively. The maximum BSNO_x reduction for diesel operation is achieved with the variation of injection timing and with EGR, with a reduction of 72.6% and 97%, respectively. However, both techniques show a penalty on smoke emission as compared to the baseline engine operation without EGR and with SOI of 11° BTDC. With PME fuel operation, it is possible to reduce the smoke emission while maintaining a similar reduction in BSNO_x. The results indicate that about 50% and 46% reduction in smoke emission can be attained with PME biodiesel and adopting the strategies of late SOI timing and a high EGR rate, respectively. Hence, simultaneous BSNO_x and smoke reduction from the levels of fossil diesel is possible with the use of PME biodiesels in parallel with the implementation of late SOI timing or a higher EGR rate in a diesel engine.

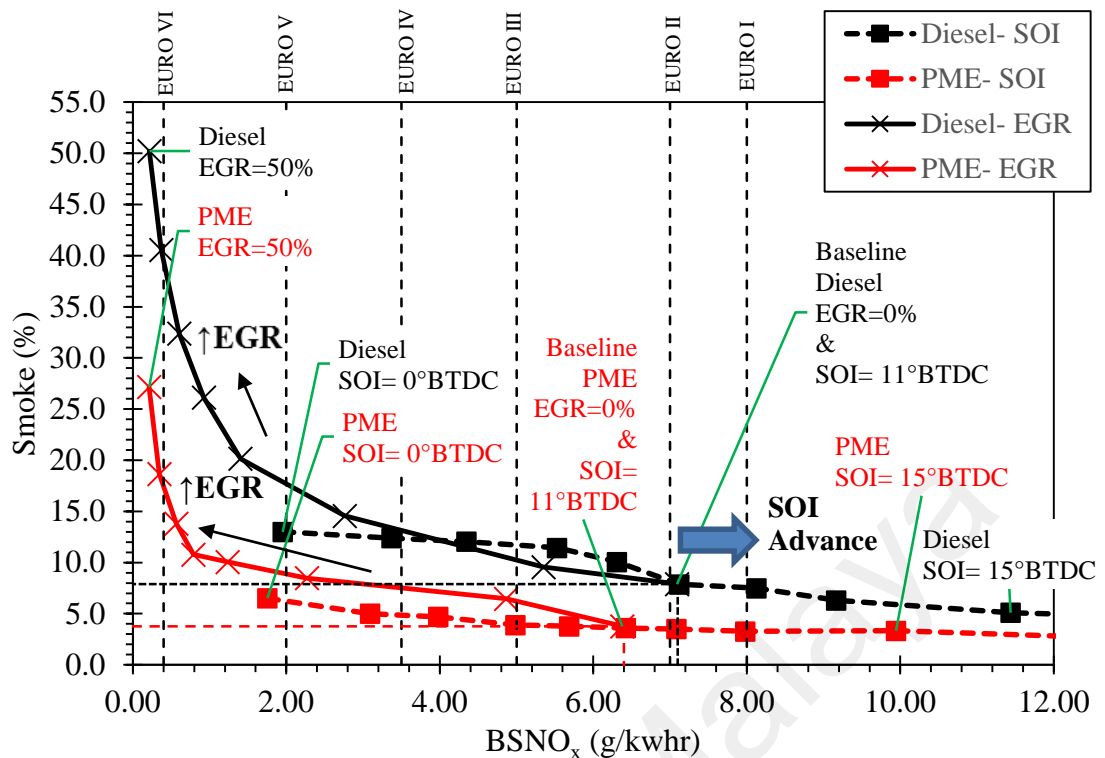


Figure 4.52: BSNO_x–smoke opacity plot for the tested fuels.

4.5.5 Summary

In this test series, the effect of EGR variation on engine performance, emission and combustion characteristics of neat palm biodiesel and diesel fuel have been experimentally investigated in a high-pressure common-rail DI diesel engine. The engine was operated at a constant speed of 1500 rpm and a BMEP of 0.4 MPa. The following main findings can be drawn from this test series.

1. The engine-out-responses with higher EGR (>30%) rates have been investigated in this study using PME biodiesel and compared with baseline diesel. A substantially lower level of BSNO_x, below the EURO VI emission standard, can be achieved with EGR rates of 45% and above.
2. With PME fuel operation, it is possible to reduce the smoke emission while maintaining a similar reduction in BSNO_x. The results indicate that approximately 46% reduction in smoke emission can be attained when the PME biodiesel is operated with high EGR rates.

3. Simultaneous BSNO_x and smoke reduction from the levels of fossil diesel is possible with the use of PME biodiesels in parallel with the implementation of late SOI timing or higher EGR rate in diesel engines.

4.6 Effect of dual-fuel combustion

In this test series, a more comprehensive study which involved operating the engine in dual-fuel combustion mode was conducted. Two kinds of dual-fuel experiments, i.e. the DI diesel with PFI gasoline and the DI PME fuel with PFI gasoline, are compared in terms of performance, emissions and combustion characteristics. Gasoline was port fuel injected onto the opened intake valve at 360° BTDC. Experiments were performed at five EGR rates, 30, 35, 40, 45 and 50%. At each EGR level, SOI timing was varied from 5° BTDC and advanced up to the point at which potential unstable combustion starts to occur.

4.6.1 SOI timing sweep at constant EGR

The engine was operated at an engine speed of 1500 rpm, 30% EGR, and rail pressure of 600 bar. The SOI timing was varied from 5 to 95° BTDC. For each type of DI fuel, the injection quantity was set to 6.5 mg/stroke for baseline diesel fuel and 7.6 mg/stroke for PME fuel. Considering the lower calorific value of PME fuel compared to the baseline diesel, higher injection quantity is necessary to ensure equivalent fuel energy is supplied for every cycle. Due to the introduction of dual fuel, a parameter, R_g , represents the ratio of energy of the premixed gasoline fuel Q_g to the total energy Q_t , which can be obtained from the following equation:

$$R_g = \frac{Q_g}{Q_t} = \frac{m_g h_{ug}}{m_g h_{ug} + m_d h_{ud}} \quad (4.1)$$

where m_g is the mass of the premixed gasoline fuel, m_d is the mass of the directly injected fuel, h_u is the calorific value and subscripts g and d denote premixed and directly injected fuel, respectively. In this study, the gasoline ratio, R_g was maintained at 0.6 for both the direct injected diesel and PME dual-fuel combustion. In addition, the total supplied fuel energy is approximately 760 J/cycle. The operating conditions for this injection strategy is shown in Table 4.3.

Table 4.3: Experimental conditions.

Condition	Diesel/gasoline	PME/gasoline
Engine speed (rpm)	1500	1500
D.I. rail pressure (bar)	600	600
D.I. timing ($^{\circ}$ BTDC)	5 to 95	5 to 95
EGR rate (%)	30	30
D.I. fuel type	Diesel	PME
D.I. fuel quantity (mg/stroke)	6.5	7.6
P.I. fuel type	Gasoline	Gasoline
P.I. fuel quantity (mg/stroke)	10.4	10.4
Gasoline ratio (R_g)	0.6	0.6
Constant total equivalent fuel energy (J) per cycle	760	760

4.6.1.1 Performance analysis

The brake specific fuel consumption (BSFC) as a function of SOI timing for baseline diesel/gasoline and PME/gasoline dual-fuel experiments is shown in Figure 4.53. In general, the results indicated that the BSFC increases with an advance in SOI timing. Furthermore, the BSFC for PME/gasoline operation is constantly greater than that of baseline diesel/gasoline across all SOI timings. The higher BSFC of PME/gasoline corresponds to less efficient operation, thus requiring a greater amount of DI fuel to accomplish the same amount of power. This is due to the lower calorific value of PME compared with diesel, which is about 12% lower than that of baseline diesel fuel. Subsequently, the results also indicate that the BSFC tends to be highly sensitive to variation in SOI timing. For both the dual fuel operations, advancing the SOI timing

resulted in an increase in BSFC initially that reaches the highest value at SOI timing of 55° BTDC and then reduces. With advancing SOI, a large fraction of fuel burns in premixed combustion phase causing earlier occurrence of high peak combustion pressure that potentially resists upward movement of the piston. However, with SOI earlier than 50° BTDC, the fuel air became more homogeneously mixed, and the low equivalence ratio extended the ignition delay of the directly injected fuel and retarded the combustion phasing (Curran et al., 2010). This is the turning point at which BSFC began to drop off with further SOI advancement. However, further SOI advance beyond 95° BTDC caused unstable combustion, and the results are not presented here. With 30% EGR rate, the lowest achievable BSFCs for diesel/gasoline and PME/gasoline operation are found to be 232.9 and 240.6 g/kWhr, respectively, and at an optimum SOI timing of 9° BTDC.

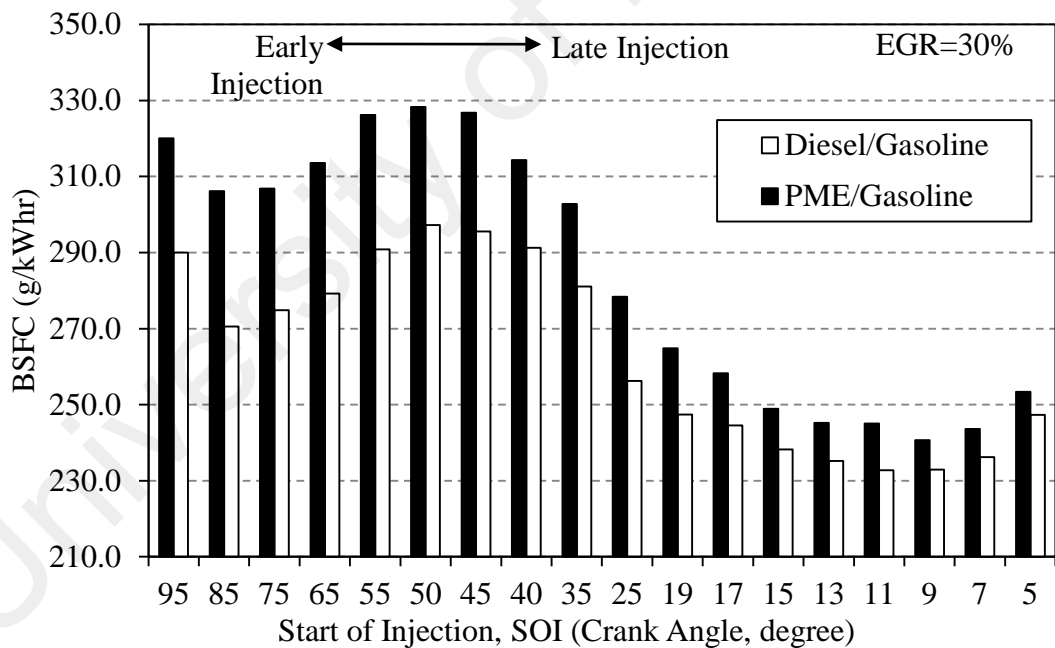


Figure 4.53: BSFC at various SOI timing for dual fuel operation diesel/gasoline and PME/gasoline fuels, with 30%EGR.

Figure 4.54 illustrates the variations in BTE with different SOI timings for engines fuelled with diesel/gasoline and PME/gasoline dual fuel combustion with 30% EGR. The PME/gasoline operation shows slightly higher BTE than diesel/gasoline with SOI between 5 to 15° BTDC, and somewhat lower with further SOI advancement. The highest reported BTE for diesel/gasoline and PME/gasoline is 34.8% and 35.5%, respectively, at SOI timing of 9° BTDC. In both the dual fuel operations, advancing the SOI timing resulted in an increase in BTE initially, reaches the peak value at SOI timing of 9° BTDC, and then reduces. Some improvement in BTE is gained with SOI beyond 50° BTDC. The increment effect is because the combustion phasing retards as SOI advances. This phenomenon also suggests that the extended mixing time of the advanced SOI timings allows the DI fuel to penetrate more thoroughly throughout the combustion chamber. As a result, the local fuel reactivity of the most reactive regions in the combustion chamber is reduced, and the combustion phasing is delayed (Curran et al., 2010). However, shifting the SOI to 95° BTDC caused the BTE to drop off sharply. The excessive advance of SOI timing tends to lean out the direct injected fuel distribution in the cylinder at SOC, which did not permit the combustion progression and caused the engine to begin running rough with intermittent misfiring (Benajes et al., 2015). Thus, further enleanment (i.e., advanced SOI) will only result in worse emissions and performance.

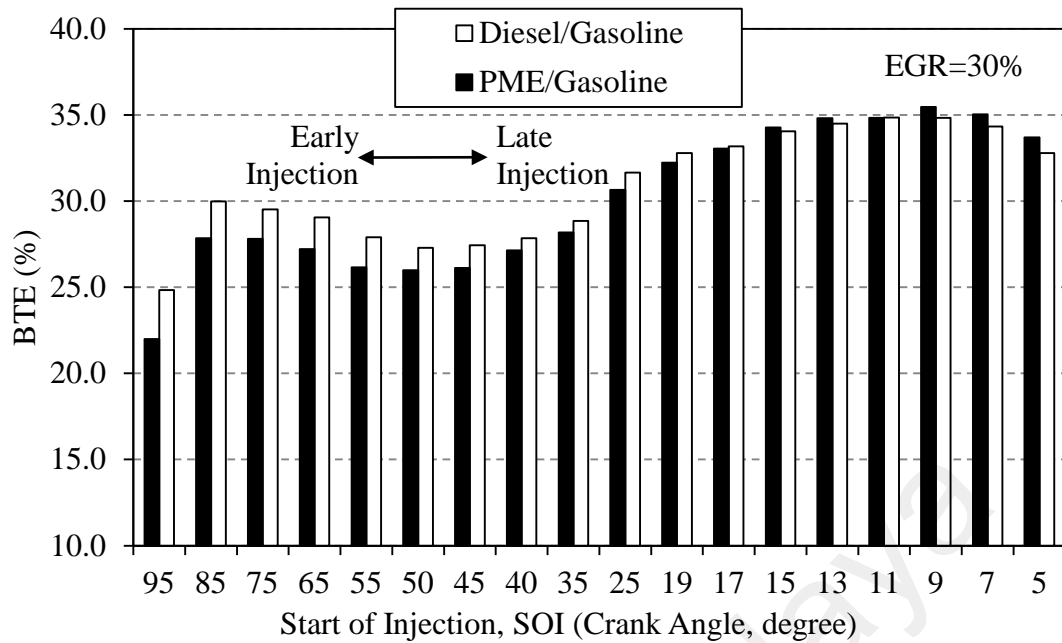


Figure 4.54: BTE at various SOI timing for dual fuel operation of diesel/gasoline and PME/gasoline fuels, with 30% EGR.

4.6.1.2 Emissions analysis

The variation of NO_x emissions for both the dual fuel operations at various SOI timings and with 30% EGR is illustrated in Figure 4.55. Generally, the PME/gasoline operation shows slightly lower NO_x emissions than diesel/gasoline across all SOI timings. In fact, both fuels operation behave the same in terms of NO_x variation as a function of SOI timing. With advancing SOI, NO_x is initially increases and reaches the maximum value of 9.8 and 9.7 for diesel/gasoline and PME/gasoline, respectively, at SOI 35° BTDC, and then is reduces. The results suggest that too advanced or too retarded SOI timing will reduce NO_x . A substantially lower level of NO_x below the EURO VI emission standards can be achieved by early or late SOI timing for both fuel operations. With advanced SOI cases, the early injection tend to lean the local equivalence ratio resulting from extended mixing time. The reduced local equivalence ratios retards the combustion phasing, resulting in lower peak flame temperatures and therefore lower NO_x emissions (Curran et al., 2010). On the other hand, with late injection cases, the combustion phasing is progressively retarded and shifts away from TDC in the expansion stroke. This effect

leads to reduced combustion temperature and lowering NO_x formation via thermal or Zeldovich mechanism. The effect of SOI timing on combustion phasing can be realised from the CA50 plot as shown in Figure 4.56. As can be seen, later or earlier SOI timing will shift the CA50 away from TDC in expansion stroke, which explains the reason for decreased NO_x emissions. A minimum point of CA50 versus SOI timing presents for both cases. This phenomenon has been reported in other investigations of dual fuel combustion in diesel engine (Fang et al., 2014). In addition, it is interesting to note that the same CA50 is possibly obtained by early or late SOI timing. With advanced SOI timing, the leaner local equivalence ratios prolonged the ignition delay and thus caused ignition to occur late. However, when SOI is retarded, ignition delay would become shorter due to the considerably higher cylinder pressure and temperature at that moment, which would result in immediate combustion after DI fuel is injected.

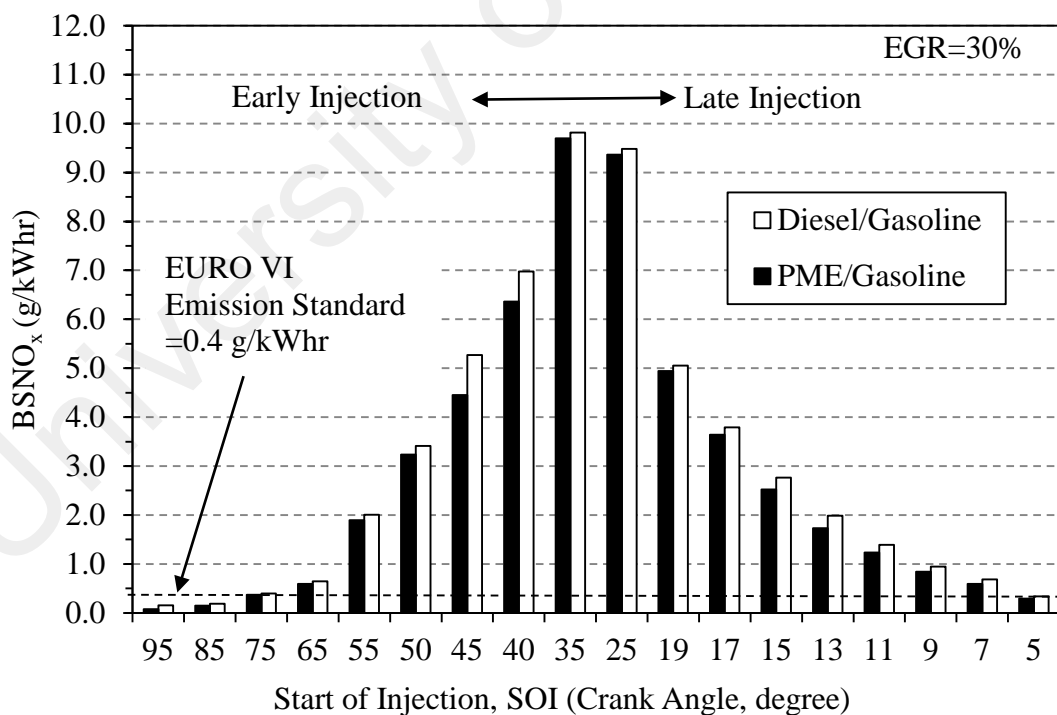


Figure 4.55: BSNO_x emissions at various SOI timing for dual fuel operation of diesel/gasoline and PME/gasoline fuels, with 30% EGR.

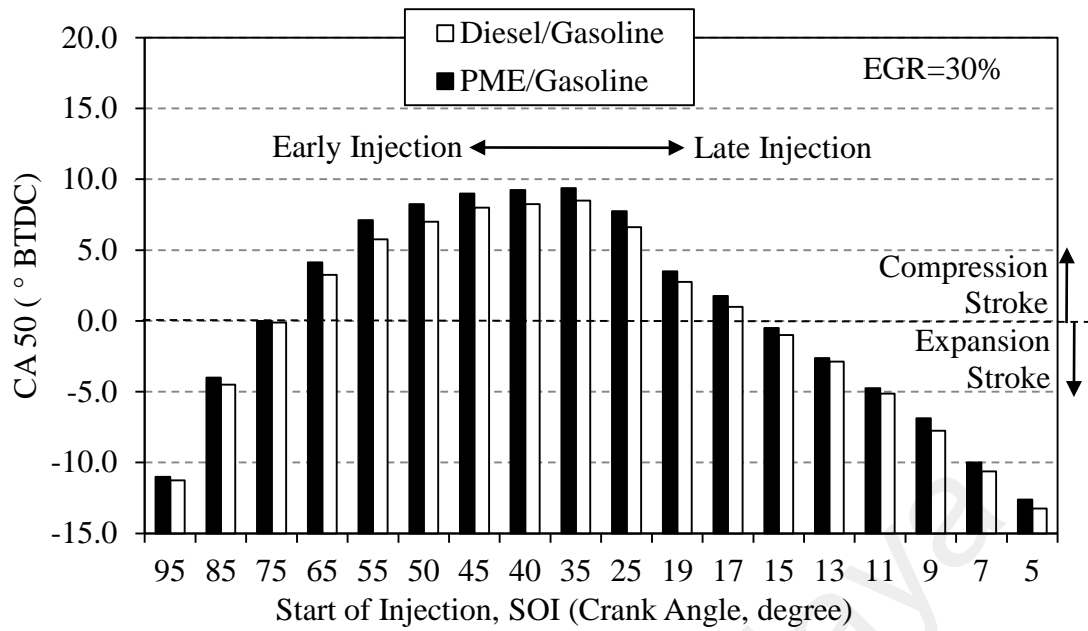


Figure 4.56: CA50 at various SOI timing for dual fuel operation of diesel/gasoline and PME/gasoline fuels, with 30% EGR.

Figure 4.57 shows the variations in HC emissions with different SOI timings for engine fuelled with diesel/gasoline and PME/gasoline dual fuel combustion with 30% EGR. The PME/gasoline operation shows lower HC than diesel/gasoline across all SOI timings. The oxygen content in PME fuel is especially useful in limiting locally fuel rich regions, resulting in improved combustion and thereby reducing HC emissions. Furthermore, it can be seen that the highest HC emissions resulting from diesel/gasoline and PME/gasoline operation are 2.14 and 2.07 g/kWhr, respectively, with earliest SOI timing of 95° BTDC. As previously discussed, the earliest SOI timing tends to lean the overall fuel air mixture and would cause the engine to begin running rough with intermittent misfiring, thereby resulting in higher HC emissions. Some HC increments are observed with SOI advancement between 5° to 17° BTDC. However, a reducing trend in HC emissions is observed with further SOI advancement from 19° to 55° BTDC. The effects of HC reduction with advanced SOI timing have suggests that there is a continuous improvement in DI fuel distribution that permits the premixed gasoline in the squish area to burn more completely, thereby decreasing HC emissions. Figure 4.58 shows the effect of SOI timing on CO emissions for engine fuelled with diesel/gasoline and PME/gasoline

dual fuel combustion with 30% EGR. Similar to HC variation trend, it can be seen that CO emissions first decrease with advancing SOI timing, reaching a maximum at an SOI of 17° BTDC, and then showing a gradual decrease. However, with considerably advanced SOI timing of beyond 65° BTDC, a steep increase in CO emissions is observed. In fact, it can be seen that CO emissions are lower for PME/gasoline than diesel/gasoline across all SOI timings. The use of oxygenated fuel of PME biodiesel would be expected to enhance the combustion efficiency, thereby reducing CO emissions.

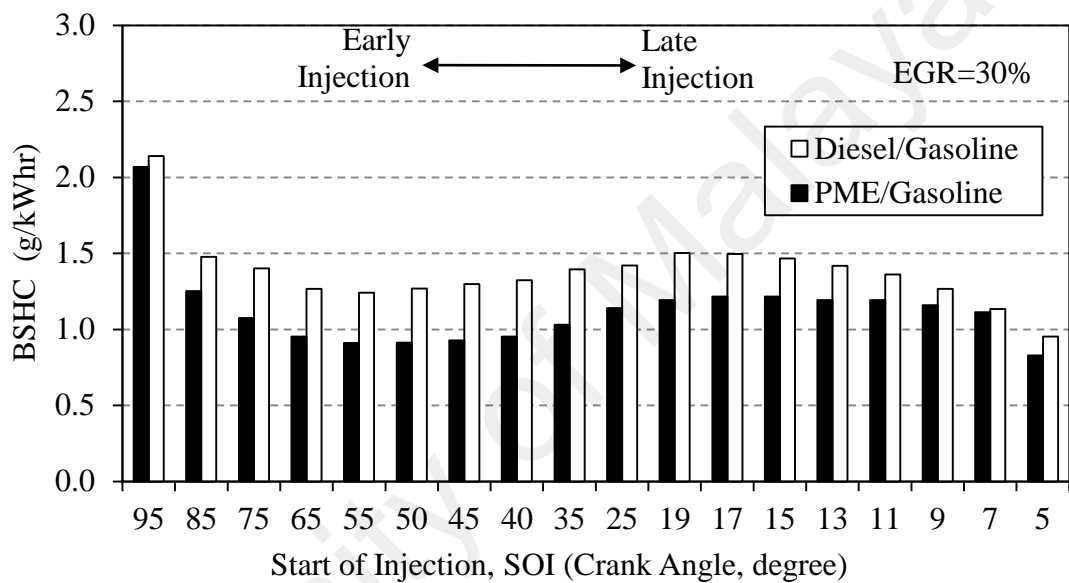


Figure 4.57: BSHC emissions versus SOI timing sweeps with 30% EGR for dual fuel operation of diesel/gasoline and PME/gasoline fuels.

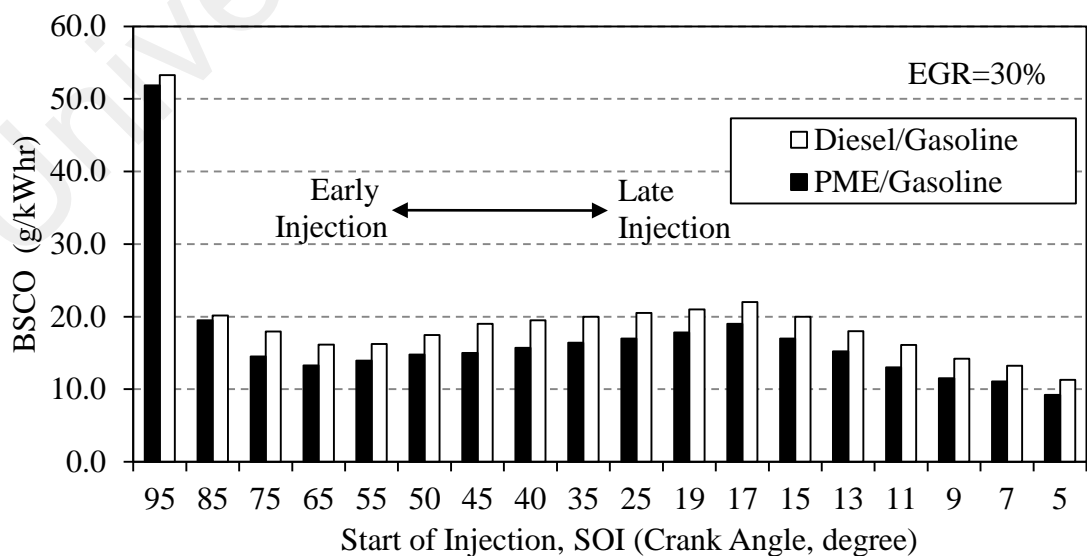


Figure 4.58: BSCO emissions versus SOI timing sweeps with 30% EGR for dual fuel operation of diesel/gasoline and PME/gasoline fuels.

4.6.1.3 Combustion analysis

A more comprehensive study of combustion characteristics resulting from SOI timing variation for both the dual fuel operation with 30% EGR is shown in Figure 4.59. With advanced SOI timing, the peak cylinder pressure is initially increases and reaches the maximum at SOI timing of 35° BTDC, and then reduces. This indicates that too early or too late SOI timing will reduce the peak cylinder pressure and cause delay in combustion phasing. It can be seen that at different SOI timings, the peak cylinder pressure and peak HRR of the PME/gasoline are marginally higher than those of diesel/gasoline cases except for the considerably advanced SOI timing past 35° BTDC. Compared to the case of SOI of 35° BTDC, both late and early SOI timings will reduce the peak cylinder pressure and retard the corresponding crank angle toward the expansion stroke. This interesting effect can be explained because as the SOI is advanced, the in-cylinder mixture would become more homogenous, and the low equivalence ratio would extend the ignition delay of DI fuel, thereby delaying the combustion phasing. For retarded SOI cases, on the other hand, the combustion process becomes more coupled with the variation in SOI timing. From the HRR profile, which is calculated from in-cylinder pressure, it can be observed clearly that a remarkable two-stage HTHR occurred for late SOI timing of 7° to 15° BTDC. In contrast, for advanced SOI timing cases, the combustion process is characterized by single-stage LTHR followed by single-stage HTHR. The first stage is called cool flame reaction, and it proceeds at temperatures below the auto-ignition temperature of the fuel, as explained by Pekalski et al. (Pekalski et al., 2002). In this investigation, this reaction appears consistently as a small peak of HRR at approximately 17° BTDC. This peak reflects low temperature reactions (LTR), and the corresponding crank angle is nearly at the same position of crank angle regardless of the SOI timing. In the LTR stage, part of the premixture of gasoline and injected DI fuel is consumed through an initial breakdown of fuel molecules, leading to the formation of free radicals,

aldehydes and hydrogen peroxide. Because of the heat released in the LTR stage, the mixture temperature rises and causes the remainder mixture to combust, leading to another stage of HTHR combustion. Meanwhile, it can be seen that the peak and the timing of this second stage HTHR are influenced by varying the SOI timing. As the SOI is advanced from 35 to 55° BTDC, the peak of second stage HTHR increases and becomes narrower. However, further advancing the SOI past 55° BTDC reduces this peak. With SOI advancement, more time is being provided for the DI fuel to mix with the premixture of gasoline and air, thus, the mixture becomes more uniform, and the local equivalence ratio decreases. The leaner local equivalence ratio prolonged the ignition delay and retarded combustion events toward TDC in the compression stroke, thus increasing the peak of second stage HTHR. Because the combustion proceeded without flame propagation, resulting in lower local combustion temperature, thereby can be used to explain the reduction in NO_x emissions. Further advancing the SOI past 55° BTDC increased the time for the preparation of a better homogenous mixture and kept reducing the local equivalence ratio, thus further extending the ignition delay and retarding combustion phasing towards the expansion stroke. The extended ignition delay retards combustion phasing, leading to a larger fraction of heat being released near TDC in the expansion stroke and causing a decrease in in-cylinder combustion temperature. Consequently, the NO_x emissions tend to be further reduced. In addition, in general, at most of the SOI timing conditions except for SOI of 75° BTDC, all PME/gasoline operations exhibited advanced SOC timing than the diesel/gasoline operation owing to their relatively higher cetane number. An additional result on the COV (coefficient of variance) of IMEP (indicated mean effective pressure) as shown in Figure 4.60 is often used to indicate combustion stability. In general, better combustion stability corresponds to a lower COV value. The results indicate that advancing the SOI timing past 25° BTDC increases the cyclic variations almost linearly, and they continue to increase rapidly with

the earliest SOI. Cyclic variation in in-cylinder combustion pressure over 100 consecutive cycles for both of diesel/gasoline and PME/gasoline dual fuel operations at four selected SOI timings is shown in Figure 4.61 and Figure 4.62, respectively. Practically speaking, cyclic variation is undesirable because it worsens overall engine efficiency, performance and emissions. From the results, the cause of cyclic variation (COV_{imep}) with the shift in SOI timing can be clearly observed. When SOI is advanced beyond 35° BTDC, an inverse correlation between combustion phasing and SOI timing is noticed from the previously presented HRR results. That is the point at which the cylinder mixture equivalence ratio begins to dominate the combustion stability. In both the dual fuel operations, advancing the SOI timing results in a decrease in COV_{imep} initially, and it reaches the lowest value at SOI timing of 15° BTDC and increases. With the considerably advanced SOI of 85° BTDC, the largest portion of the mixture is at the lowest equivalence ratio, and the extended ignition delay retarded the combustion phasing. The late combustion burned under considerably low temperature and caused incomplete combustion, therefore leading to higher cycle-to-cycle variation. Further advancing SOI timing to 95° BTDC worsened the combustion stability and increased the probability of misfiring. Compared to diesel/gasoline operation, the PME/gasoline operation exhibits higher COV of IMEP with SOI past 25° BTDC. The oxygen content in the PME fuel produced more mixture with much leaner equivalence ratio, thus causing an increase in cyclic variation.

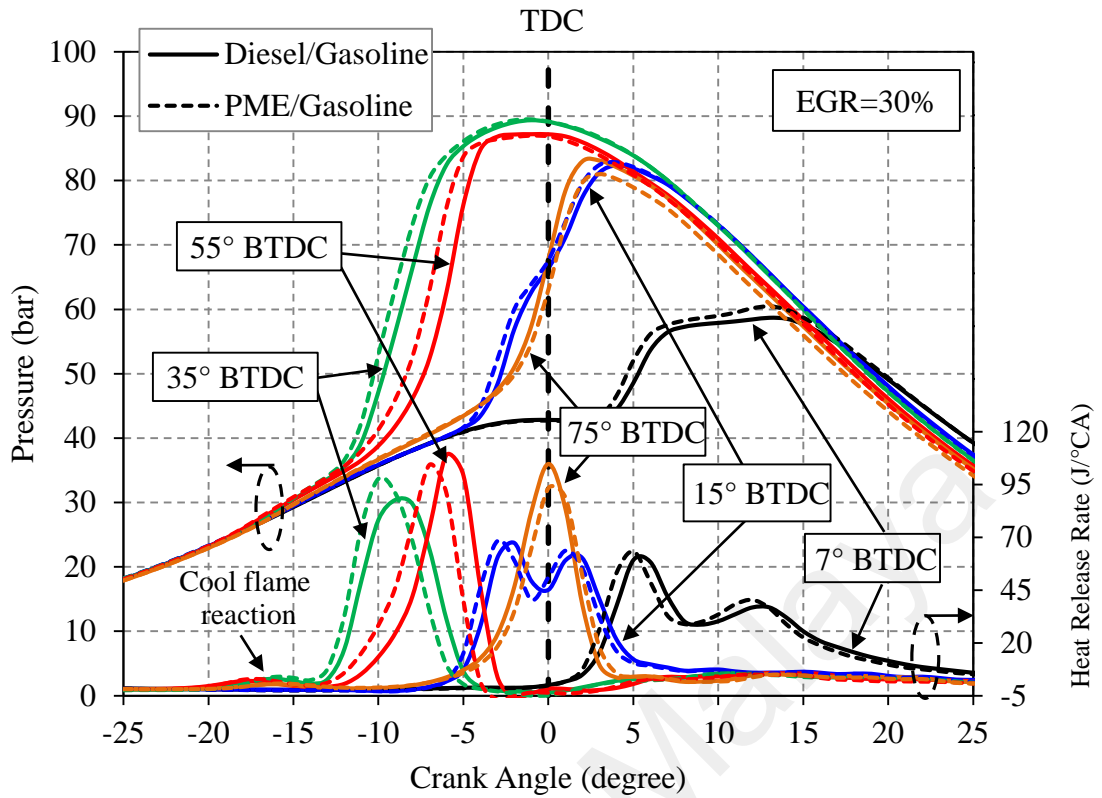


Figure 4.59: Effect of SOI timing on combustion pressure and heat release rate for dual fuel operation of diesel/gasoline and PME/gasoline with 30% EGR.

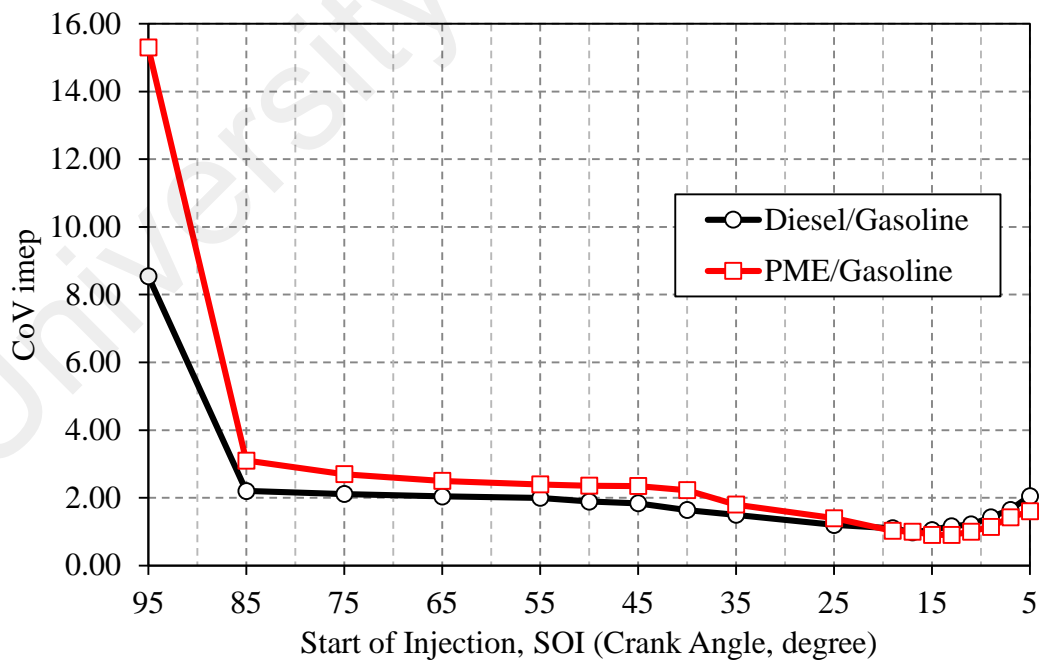


Figure 4.60: Effect of SOI timing variation on the coefficient of variation of indicated mean effective pressure for dual fuel operation of diesel/gasoline and PME/gasoline with 30% EGR.

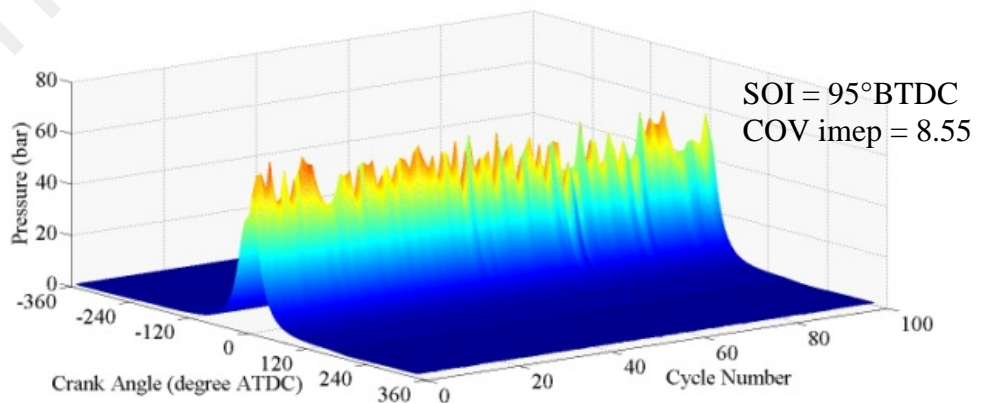
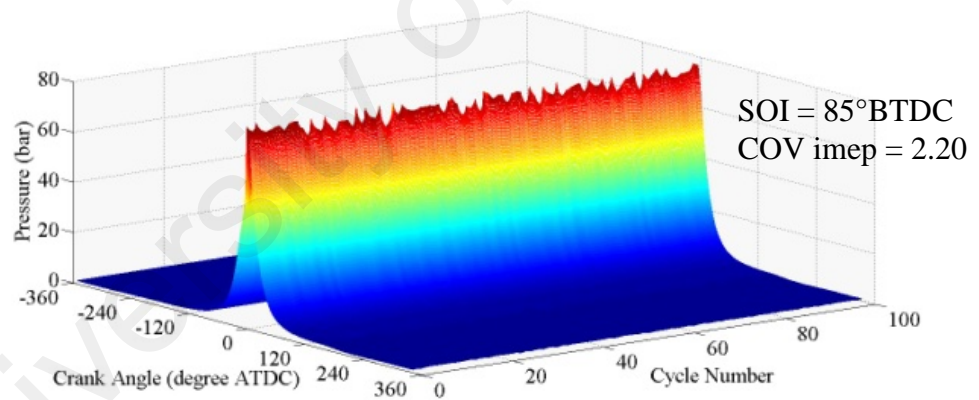
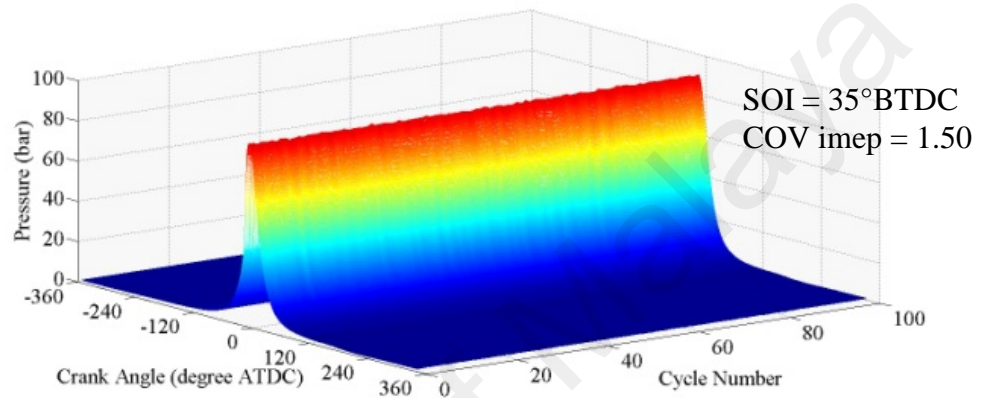
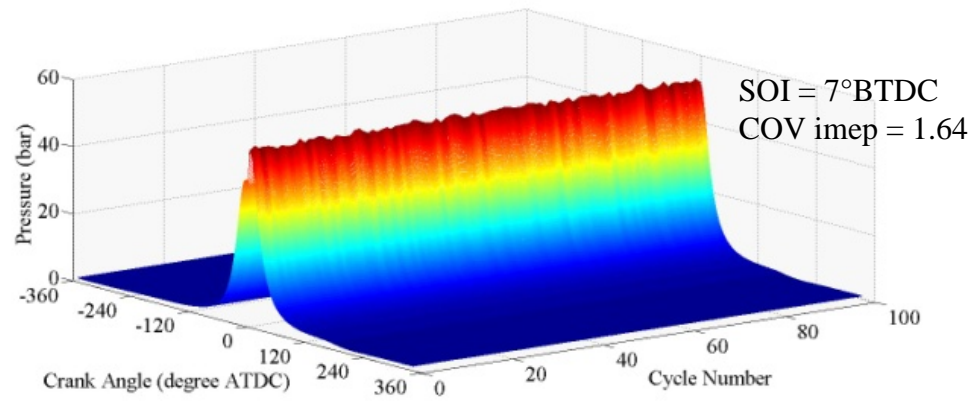


Figure 4.61: Comparison of 100 cycles of cylinder pressure under various SOI timings for diesel/gasoline dual fuel operation with 30% EGR.

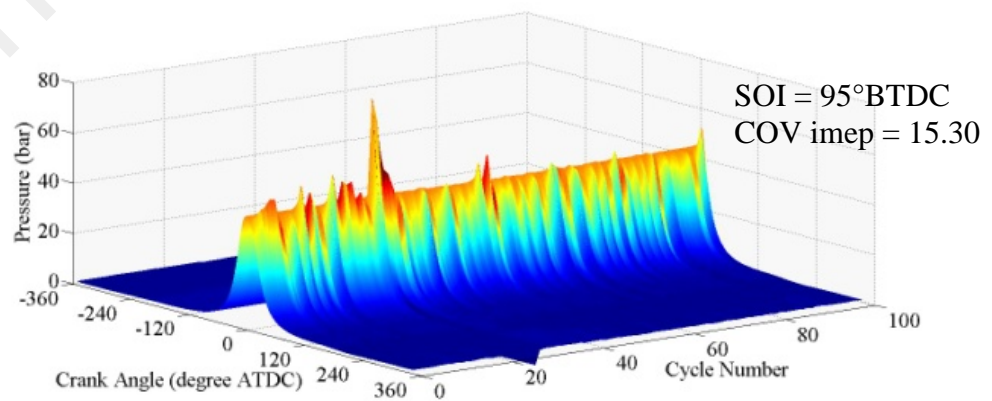
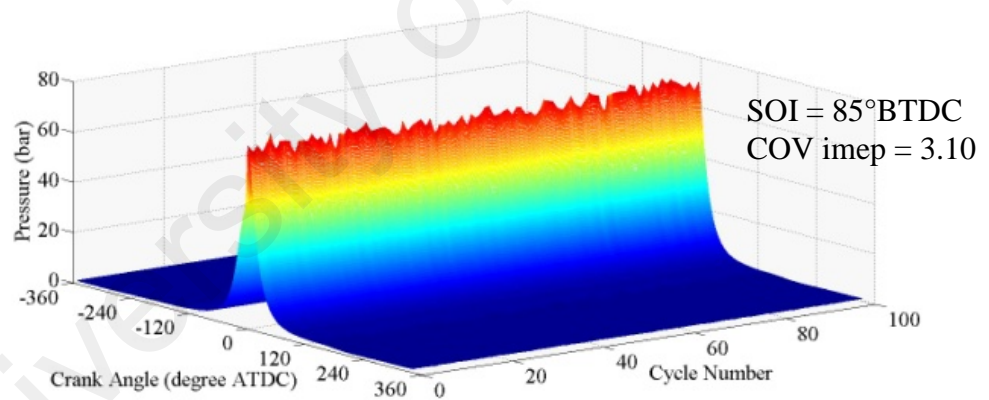
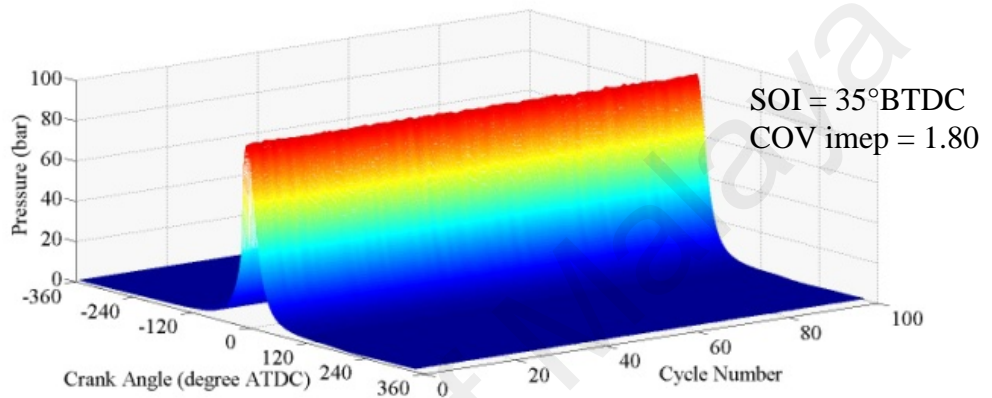
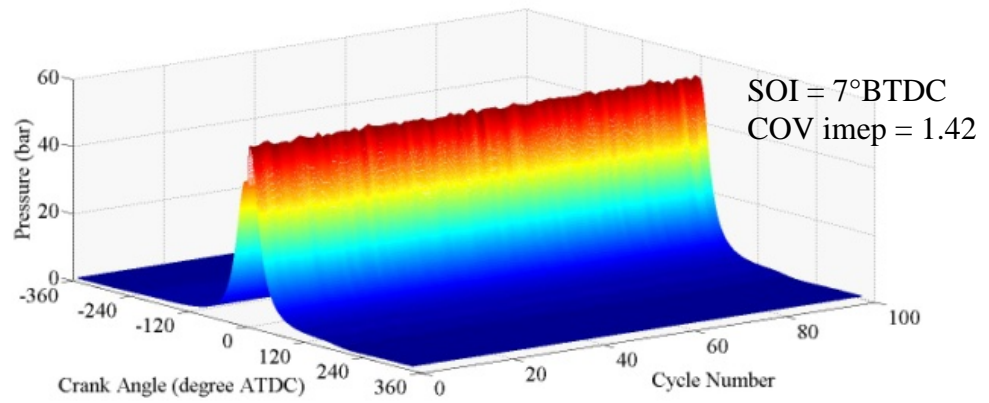


Figure 4.62: Comparison of 100 cycles of cylinder pressure under various SOI timings for PME/gasoline dual fuel operation with 30% EGR.

4.6.2 Dual-fuel with EGR sweep

The previous section (Section 4.5.1) revealed how combustion processes proceeded differently as the SOI timing was changed under a constant EGR rate. In-cylinder charge reactivity and distribution can also be affected by EGR variation. To investigate the dilution effect of EGR on engine performance, emissions, and combustion characteristics for diesel/gasoline and PME/gasoline dual-fuel operation, five EGR levels of 30%, 35%, 40%, 45% and 50% are examined. Figure 4.63 shows the results. With increasing EGR rate, it is feasible to maintain ISFC at the minimum possible magnitude by advancing SOI timing for diesel/gasoline and PME/gasoline operation. This is due to the effect of combustion phasing retardation as EGR increases; thus, the cooperative control of SOI timing adjustment can be used to compensate the drop in combustion efficiency. At a higher EGR rate, the SOI timing for the diesel/gasoline operation is earlier than for the PME/gasoline operation, suggesting that higher cetane number and shorter ignition delay of the directly injected PME fuel improve the combustion of the fuel air mixture. Furthermore, it can be seen that the maximum pressure rise rate (MPRR) decreases with increasing EGR rate for both the cases. This indicates the advantage of EGR in controlling and regulating the HRR, thus lowering the MPRR. In terms of emissions characteristics, HC and CO increase with increasing EGR rate due to the reduced in-cylinder gas temperature with dilution and increased incomplete combustion. Conversely, smoke and NO_x decrease with the increasing dilution effect of EGR. With higher EGR, the prolonged ignition delay has resulted in the formation of more uniform mixtures that burn at substantially lower temperatures, which leads to considerably lower NO_x emissions (below the EURO VI limit of 0.4 g /kWhr).

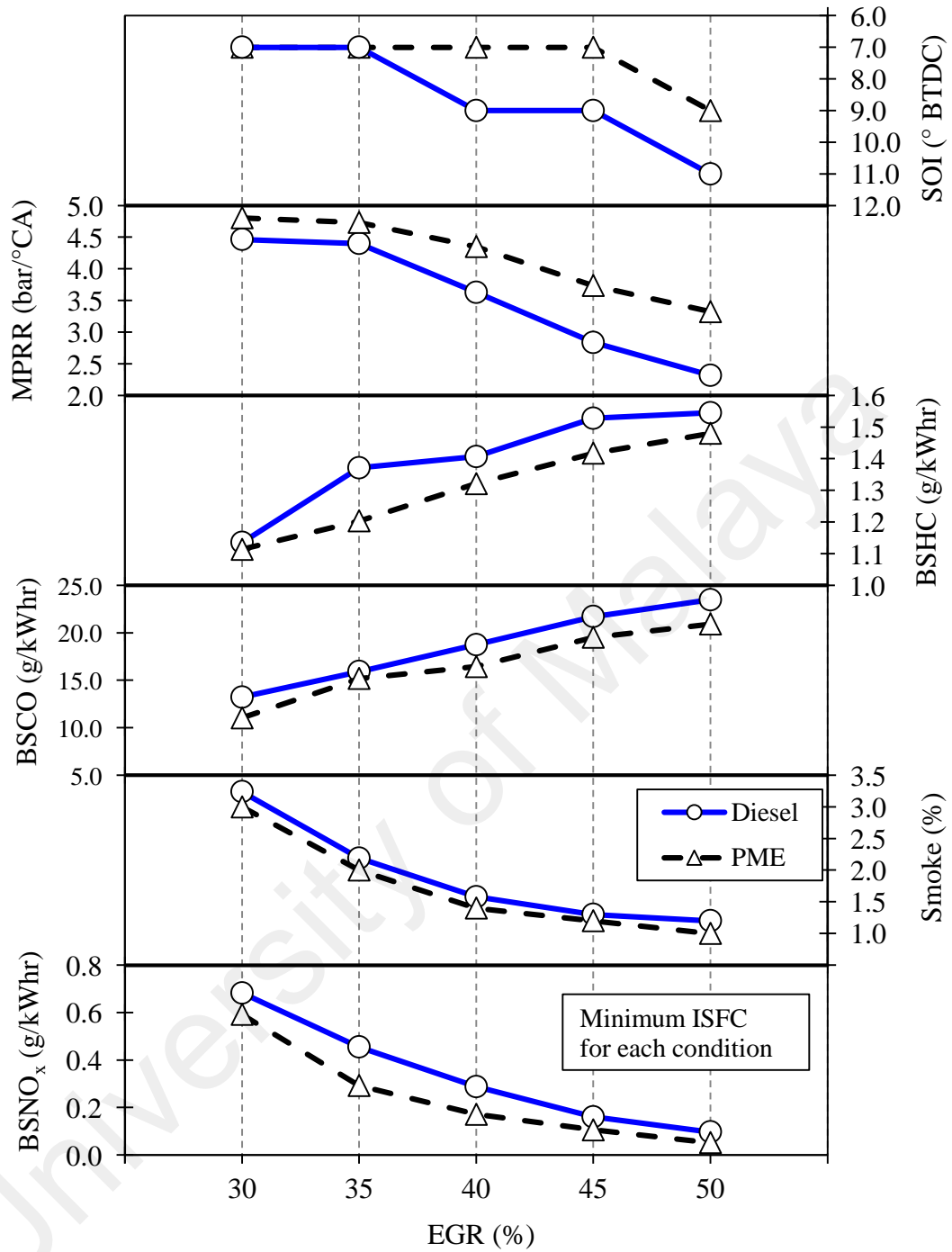


Figure 4.63: Influence of EGR variation on performance, emissions and combustion characteristics for engine operation with dual fuel combustion of diesel/gasoline and PME/gasoline.

4.6.3 Summary

The main objective of this test series is to use biodiesel as an alternative energy source for engines operating in RCCI dual-fuel combustion mode. A series of orderly experiments was conducted to evaluate the use of biodiesel fuels in internal combustion engines operating with dual-fuel combustion strategies. The assessment of engine operation under RCCI dual-fuel combustion mode was carried out using diesel or biodiesel as direct injected fuel and gasoline as port injected fuel. Based on the experimental results, the following main findings can be drawn from this test series.

1. With 30% EGR rate, the lowest achievable BSFCs for diesel/gasoline and PME/gasoline operation are found to be 232.9 and 240.6 g/kWhr, respectively, at an optimum SOI timing of 9° BTDC.
2. The PME/gasoline operation shows slightly higher BTE than diesel/gasoline with SOI between 5 to 15° BTDC, and somewhat lower with further SOI advancement. The highest BTE for diesel/gasoline and PME/gasoline is 34.8% and 35.5%, respectively, at SOI timing of 9° BTDC.
3. A substantially lower level of NO_x below the EURO VI emission standards can be achieved by early or late SOI timing for both fuel operations. Besides, the same CA50 is possibly obtained by early or late SOI timing.
4. The PME/gasoline operation showed lower HC and CO than diesel/gasoline across all SOI timings. The oxygen content in PME fuel is especially useful in limiting locally fuel rich regions, resulting in improved combustion and thereby reducing HC and CO emissions.
5. Compared to diesel/gasoline operation, the PME/gasoline operation exhibited higher COV of IMEP with SOI past 25° BTDC. The oxygen content in the PME fuel produced more mixture with much leaner equivalence ratio, thus causing an increase in cyclic variation.

6. With increasing EGR rate, it is feasible to maintain ISFC at the minimum possible magnitude by advancing SOI timing for diesel/gasoline and PME/gasoline operation. In addition, the prolonged ignition delay with higher EGR level has resulted in the formation of more uniform mixtures that burn at substantially lower temperatures, which leads to considerably lower NO_x emissions (below the EURO VI limit of 0.4 g/kWhr).

Lastly, the results from this test series suggest that alternative fuels from bio resources have high potential as substitutes for petroleum-based fuels for engines operating with low temperature combustion strategies. In addition, the engine operating in RCCI dual-fuel combustion mode is capable of achieving high efficiency with near zero NO_x and smoke emissions.

CHAPTER 5: CONCLUSIONS AND RECOMMENDATION

5.1 Conclusions

A series of experiment were conducted in this research in order to evaluate the use of biodiesel fuels in internal combustion engines for engines operating with current and future combustion strategies. During this investigation, a dedicated experimental system was designed and built. With this system, a variety of injection and combustion strategies under different loads, biodiesel types and blending ratios, injection timings, and EGR were tested and characterized in order to achieve the research objectives. The custom-built common-rail injection system is capable to provide a higher degree of flexibility in varying the injection parameters for achieving optimal performance and reduced engine-out emissions.

In the case of the study of biodiesel blends on common-rail diesel engine, all biodiesel fuels showed a prominent increase in BSFC at all load conditions. Additionally, JB30 and PB10 blends showed a marginal improvement of 3.4% and 1.7%, respectively, in BTE at an engine load of 0.1 MPa. The BSCO emissions showed a decrease with increasing biodiesel blend ratio and engine load. Additionally, the BSNO_x emissions decreased with increase in engine load and biodiesel blending ratio. Besides, both the JME and PME blended fuels showed lower smoke emissions than baseline diesel across all the engine loading conditions. In terms of the combustion aspects, it was found that, the JME and PME biodiesel blended fuels showed a slightly shorter ID and shorter combustion duration in comparison with baseline diesel across the engine load operations. For vibration analysis, the JME and PME biodiesel blended fuels showed direct correlation with RMS of acceleration. JB100 and PB100 showed the largest reduction of 19% in the RMS of acceleration in comparison with the baseline diesel at engine load of 0.6 MPa.

In the study of the effect of injection timing on a common-rail diesel engine, the optimum injection timing of 11° BTDC have translated to the highest BTE and reasonable NO_x level for both the baseline diesel and PME operations. In terms of exhaust emissions, both the tested fuels of diesel and PME showed increased BSNO_x emissions with advancement in SOI timing. The PME fuel showed lower BSNO_x emissions compared to baseline diesel across all the SOI timings. Besides, the PME fuel showed lower smoke emissions compared to diesel fuel across all SOI timings and it showed a reducing trend with advanced SOI timings. In terms of combustion characteristics, the PME biodiesel fuel showed little effect on combustion variation and the pattern is comparable with the baseline diesel at optimum SOI timing of 11° BTDC. In the case of the investigation of EGR variation on a common-rail diesel engine, the engine-out-responses with high EGR ($>30\%$) rates have been investigated in this study using PME biodiesel and compared with baseline diesel. A substantially lower level of BSNO_x , below the EURO VI emission standard, can be achieved with EGR rates above 45%. In terms of exhaust emissions, PME fuel operation showed a reduction in smoke emissions while still maintaining a similar reduction in BSNO_x as compared to the baseline diesel. The operation of PME biodiesel with high EGR rates showed a reduction of about 46% of smoke emissions compared to the baseline diesel. Besides, a simultaneous BSNO_x and smoke reduction from the levels of fossil diesel is possible with the use of PME biodiesels in parallel with the implementation of late SOI timing or higher EGR rate in diesel engines.

In the investigation of dual-fuel combustion strategies, the lowest achievable BSFCs for diesel/gasoline and PME/gasoline operation are found to be 232.9 and 240.6 g/kWhr, respectively, at an optimum SOI timing of 9° BTDC and with 30% EGR. The PME/gasoline operation showed slightly higher BTE than diesel/gasoline with SOI between 5 to 15° BTDC, and somewhat lower with further SOI advancement. The highest achievable BTE for diesel/gasoline and PME/gasoline is found to be 34.8% and 35.5%,

respectively, at SOI timing of 9° BTDC. In terms of exhaust emissions, a substantially lower level of NO_x below the EURO VI emission standards was achieved by early or late SOI timing for both the PME and diesel fuel operations. Besides, the same CA50 is obtained by early or late SOI timing. The PME/gasoline operation showed lower HC and CO than diesel/gasoline across all SOI timings. The oxygen content in PME fuel is especially useful in limiting locally fuel rich regions, resulting in improved combustion and thereby reducing HC and CO emissions. In terms of combustion analysis, the PME/gasoline operation exhibited higher COV of IMEP with SOI past 25° BTDC compared to diesel/gasoline operation. The oxygen content in the PME fuel produced more mixture with much leaner equivalence ratio, thus causing an increase in cyclic variation.

In the investigation of dual-fuel combustion with EGR sweep, the results indicate that with increasing EGR rate, it is feasible to maintain ISFC at the minimum possible magnitude by advancing SOI timing for diesel/gasoline and PME/gasoline operation. In addition, the prolonged ignition delay with higher EGR level has resulted in the formation of more uniform mixtures that burn at substantially lower temperatures, which leads to considerably lower NO_x emissions (below the EURO VI limit of 0.4 g/kWhr). The results from this test series suggest that alternative fuels from bio resources have high potential as substitutes for petroleum-based fuels for engines operating with low temperature combustion strategies. The engine operating in RCCI dual-fuel combustion mode is capable of achieving high efficiency with near zero NO_x and smoke emissions.

Ultimately, the results from this study suggested that alternative fuels from bio resources has high potential as a substitution to petroleum based fuels for engines operating with current and future combustion strategies.

5.2 Recommendation

While this project presents an initial step in the long-term goal of creating a new efficient power source for transport, more advancements and studies will be required in the future.

In this regard, the following recommendations for the future work are suggested:

1. The effects of fuel injection parameters (injection pressure and multiple injections), intake air boosting, piston bowl geometry, and compression ratio should be studied more deeply and optimized.
2. Due to limited facility available, it is suggested that soot or particulate matter emissions should be studied and compared with standards.
3. More intense engine modeling study using three dimensional Computational Fluid Dynamics (CFD) and chemical kinetic modelling are necessary to predict the in-cylinder fuel-air mixing and to optimize the combustion process of the engine.

REFERENCES

- Ackerman, A. S., Toon, O. B., Stevens, D. E., Heymsfield, A. J., Ramanathan, V., & Welton, E. J. (2000). Reduction of tropical cloudiness by soot. *Science*, 288(5468), 1042-1047.
- Agarwal, A. K. (2007). Biofuels (alcohols and biodiesel) applications as fuels for internal combustion engines. *Progress in Energy and Combustion Science*, 33(3), 233-271.
- Agarwal, A. K. (2011). Experimental investigation on intake air temperature and air-fuel ratio dependence of random and deterministic cyclic variability in a homogeneous charge compression ignition engine. *SAE Paper No. 2011-01-1183*.
- Agarwal, A. K., Gupta, T., & Kothari, A. (2011). Particulate emissions from biodiesel vs diesel fuelled compression ignition engine. *Renewable and Sustainable Energy Reviews*, 15(6), 3278-3300.
- Agarwal, D., Singh, S. K., & Agarwal, A. K. (2011). Effect of Exhaust Gas Recirculation (EGR) on performance, emissions, deposits and durability of a constant speed compression ignition engine. *Applied Energy*, 88(8), 2900-2907.
- Agarwal, D., Sinha, S., & Agarwal, A. K. (2006). Experimental investigation of control of NO_x emissions in biodiesel-fueled compression ignition engine. *Renewable Energy*, 31(14), 2356-2369.
- Ahmad, A. L., Yasin, N. H. M., Derek, C. J. C., & Lim, J. K. (2011). Microalgae as a sustainable energy source for biodiesel production: A review. *Renewable and Sustainable Energy Reviews*, 15(1), 584-593.
- Akagawa, H., Miyamoto, T., Harada, A., Sasaki, S., Shimazaki, N., Hashizume, T., & Tsujimura, K. (1999). Approaches to solve problems of the premixed lean diesel combustion. *SAE Paper No. 1999-01-0183*.
- Al-Dawody, M. F., & Bhatti, S. K. (2013). Optimization strategies to reduce the biodiesel NO_x effect in diesel engine with experimental verification. *Energy Conversion and Management*, 68(0), 96-104.
- Alptekin, E., & Canakci, M. (2009). Characterization of the key fuel properties of methyl ester–diesel fuel blends. *Fuel*, 88(1), 75-80.
- Alriksson, M., & Denbratt, I. (2006). Low temperature combustion in a heavy duty diesel engine using high levels of EGR. *SAE Paper No. 2006-01-0075*.
- An, H., Yang, W. M., Chou, S. K., & Chua, K. J. (2012). Combustion and emissions characteristics of diesel engine fueled by biodiesel at partial load conditions. *Applied Energy*, 99(0), 363-371.

- Anand, K., Sharma, R. P., & Mehta, P. S. (2011). Experimental investigations on combustion, performance and emissions characteristics of neat karanja biodiesel and its methanol blend in a diesel engine. *Biomass and Bioenergy*, 35(1), 533-541.
- Aoyama, T., Hattori, Y., Mizuta, J. i., & Sato, Y. (1996). An experimental study on premixed-charge compression ignition gasoline engine. *SAE Paper No. 960081*.
- Arduino. (2015). Arduino MEGA 2560. Retrieved accessed October 2015 <https://www.arduino.cc/en/Main/ArduinoBoardMega2560>
- Armas, O., Yehliu, K., & Boehman, A. L. (2010). Effect of alternative fuels on exhaust emissions during diesel engine operation with matched combustion phasing. *Fuel*, 89(2), 438-456.
- Aroonsrisopon, T., Foster, D. E., Morikawa, T., & Iida, M. (2002). Comparison of HCCI operating ranges for combinations of intake temperature, engine speed and fuel composition. *SAE Paper No. 2002-01-1924*.
- Asad, U., Kumar, R., Zheng, M., & Tjong, J. (2015). Ethanol-fueled low temperature combustion: A pathway to clean and efficient diesel engine cycles. *Applied Energy*, 157(0), 838-850.
- Atabani, A. E., Silitonga, A. S., Badruddin, I. A., Mahlia, T. M. I., Masjuki, H. H., & Mekhilef, S. (2012). A comprehensive review on biodiesel as an alternative energy resource and its characteristics. *Renewable and Sustainable Energy Reviews*, 16(4), 2070-2093.
- Atabani, A. E., Silitonga, A. S., Ong, H. C., Mahlia, T. M. I., Masjuki, H. H., Badruddin, I. A., & Fayaz, H. (2013). Non-edible vegetable oils: A critical evaluation of oil extraction, fatty acid compositions, biodiesel production, characteristics, engine performance and emissions production. *Renewable and Sustainable Energy Reviews*, 18(0), 211-245.
- Atadashi, I. M., Aroua, M. K., Abdul Aziz, A. R., & Sulaiman, N. M. N. (2012). Production of biodiesel using high free fatty acid feedstocks. *Renewable and Sustainable Energy Reviews*, 16(5), 3275-3285.
- Aydin, H., & İlkılıç, C. (2010). Effect of ethanol blending with biodiesel on engine performance and exhaust emissions in a CI engine. *Applied Thermal Engineering*, 30(10), 1199-1204.
- Babu, A. K., & Devaradjane, G. (2003). Vegetable oils and their derivatives as fuels for CI engines: An overview. *SAE Paper No. 2003-01-0767*.
- Bahri, B., Aziz, A. A., Shahbakhti, M., & Muhamad Said, M. F. (2013). Understanding and detecting misfire in an HCCI engine fuelled with ethanol. *Applied Energy*, 108(0), 24-33.
- Baiju, B., Naik, M. K., & Das, L. M. (2009). A comparative evaluation of compression ignition engine characteristics using methyl and ethyl esters of Karanja oil. *Renewable Energy*, 34(6), 1616-1621.

- Bare, J., Young, D., QAM, S., Hopton, M., & Chief, S. A. B. (2012). Tool for the reduction and assessment of chemical and other environmental impacts (TRACI).
- Bari, S., Yu, C. W., & Lim, T. H. (2004). Effect of fuel injection timing with waste cooking oil as a fuel in a direct injection diesel engine. *Proceedings of the Institution of Mechanical Engineers, Part D: Journal of Automobile Engineering*, 218(1), 93-104.
- Baumgarten, C. (2006). *Mixture formation in internal combustion engines*. New Delhi, India: CBS Publishers.
- Benajes, J., Molina, S., García, A., & Monsalve-Serrano, J. (2015). Effects of direct injection timing and blending ratio on RCCI combustion with different low reactivity fuels. *Energy Conversion and Management*, 99(0), 193-209.
- Bendu, H., & Murugan, S. (2014). Homogeneous charge compression ignition (HCCI) combustion: Mixture preparation and control strategies in diesel engines. *Renewable and Sustainable Energy Reviews*, 38(0), 732-746.
- Bensaid, S., & Russo, N. (2011). Low temperature DPF regeneration by delafossite catalysts. *Catalysis Today*, 176(1), 417-423.
- Bessonette, P. W., Schleyer, C. H., Duffy, K. P., Hardy, W. L., & Liechty, M. P. (2007). Effects of fuel property changes on heavy-duty HCCI combustion. *SAE Paper No. 2007-01-0191*.
- Bhaskar, K., Nagarajan, G., & Sampath, S. (2013). Optimization of FOME (fish oil methyl esters) blend and EGR (exhaust gas recirculation) for simultaneous control of NO_x and particulate matter emissions in diesel engines. *Energy*, 62, 224-234.
- Bhave, A., Kraft, M., Mauss, F., Oakley, A., & Zhao, H. (2005). Evaluating the EGR-AFR operating range of a HCCI engine. *SAE Paper No. 2005-01-0161*.
- Bollen, J., & Brink, C. (2014). Air pollution policy in Europe: Quantifying the interaction with greenhouse gases and climate change policies. *Energy Economics*, 46(0), 202-215.
- British Petroleum (BP). (2010). BP statistical review of World Energy June 2010. Retrieved 14th June, 2015, from <http://www.bp.com/productlanding.do?categoryId=6929&contentId=7044622>
- Bunting, B., Wildman, C., Szybist, J., Lewis, S., & Storey, J. (2007). Fuel chemistry and cetane effects on diesel homogeneous charge compression ignition performance, combustion, and emissions. *International Journal of Engine Research*, 8(1), 15-27.
- Bunting, B. G., Crawford, R. W., Wolf, L. R., & Xu, Y. (2007). The Relationships of Diesel Fuel Properties, Chemistry, and HCCI Engine Performance as Determined by Principal Components Analysis. *SAE Paper No. 2007-01-4059*.

- Bunting, B. G., Eaton, S. J., & Crawford, R. W. (2009). Performance evaluation and optimization of diesel fuel properties and chemistry in an HCCI engine. *SAE Paper No. 2009-01-2645*.
- Buyukkaya, E., Benli, S., Karaaslan, S., & Guru, M. (2013). Effects of trout-oil methyl ester on a diesel engine performance and emission characteristics. *Energy Conversion and Management, 69*, 41-48.
- Canakci, M. (2007). Combustion characteristics of a turbocharged DI compression ignition engine fueled with petroleum diesel fuels and biodiesel. *Bioresource Technology, 98*(6), 1167-1175.
- Canakci, M., Ozsezen, A. N., Arcaklioglu, E., & Erdil, A. (2009). Prediction of performance and exhaust emissions of a diesel engine fueled with biodiesel produced from waste frying palm oil. *Expert systems with Applications, 36*(5), 9268-9280.
- Canakci, M., Ozsezen, A. N., & Turkcan, A. (2009). Combustion analysis of preheated crude sunflower oil in an IDI diesel engine. *Biomass and Bioenergy, 33*(5), 760-767.
- Carraretto, C., Macor, A., Mirandola, A., Stoppato, A., & Tonon, S. (2004). Biodiesel as alternative fuel: Experimental analysis and energetic evaluations. *Energy, 29*(12), 2195-2211.
- Cerit, M., & Soyhan, H. S. (2013). Thermal analysis of a combustion chamber surrounded by deposits in an HCCI engine. *Applied Thermal Engineering, 50*(1), 81-88.
- Chauhan, B. S., Kumar, N., & Cho, H. M. (2012). A study on the performance and emission of a diesel engine fueled with Jatropha biodiesel oil and its blends. *Energy, 37*(1), 616-622.
- Chen, Z., Liu, J., Wu, Z., & Lee, C. (2013). Effects of port fuel injection (PFI) of n-butanol and EGR on combustion and emissions of a direct injection diesel engine. *Energy Conversion and Management, 76*, 725-731.
- Cheng, A., Upatnieks, A., & Mueller, C. (2006). Investigation of the impact of biodiesel fuelling on NOx emissions using an optical direct injection diesel engine. *International Journal of Engine Research, 7*(4), 297-318.
- Cheung, C. S., Zhu, L., & Huang, Z. (2009). Regulated and unregulated emissions from a diesel engine fueled with biodiesel and biodiesel blended with methanol. *Atmospheric Environment, 43*(32), 4865-4872.
- Chong, C. T., Ng, J.-H., Ahmad, S., & Rajoo, S. (2015). Oxygenated palm biodiesel: Ignition, combustion and emissions quantification in a light-duty diesel engine. *Energy Conversion and Management, 101*(0), 317-325.
- Choudhury, S., & Bose, P. (2008). Jatropha derived biodiesel—its suitability as CI engine fuel. *SAE Paper No. 2008-28-0040*.

- Christensen, M., & Johansson, B. (1998). Influence of mixture quality on homogeneous charge compression ignition. *SAE Paper No. 982454*.
- Christensen, M., & Johansson, B. (1999). Homogeneous charge compression ignition with water injection. *SAE Paper No. 1999-01-0182*.
- Clean combustion research centre. (2015). Homogeneous Charge Compression Ignition (HCCI) engines research, technology overview. from <http://ccrc.kaust.edu.sa/Pages/HCCI.aspx>
- Colton, B. (2014). The outlook for energy: A view to 2040. EXXONMOBIL: Web accessed. Retrieved on 1st june 2015. from <http://cdn.exxonmobil.com/~media/global/reports/outlook-for-energy/2015/2015-energy-outlook-presentation.pdf>
- Cook, D. J., Pitsch, H., & Nentwig, G. (2008). Numerical investigation of unburnt hydrocarbon emissions in a homogeneous-charge late-injection diesel-fueled engine. *SAE Paper No. 2008-01-1666*.
- Curran, S., Prikhodko, V., Cho, K., Sluder, C. S., Parks, J., Wagner, R., . . . Reitz, R. D. (2010). In-cylinder fuel blending of gasoline/diesel for improved efficiency and lowest possible emissions on a multi-cylinder light-duty diesel engine. *SAE Paper No. 2010-01-2206*.
- Das, P., Subbarao, P. M. V., & Subrahmanyam, J. P. (2014). Study of combustion behavior and combustion stability of HCCI-DI combustion for a wide operating range using a low cost novel experimental technique. *SAE Paper No. 2014-01-2661*.
- Dec, J. E. (2009). Advanced compression-ignition engines—understanding the in-cylinder processes. *Proceedings of the Combustion Institute*, 32(2), 2727-2742.
- Delphi. (2015). Worldwide emissions standards. Passenger cars and light duty vehicles. Retrieved 21st January, 2016, from <http://delphi.com/docs/default-source/catalogs/delphi-worldwide-emissions-standards-pc-ldv-15-16.pdf?sfvrsn=2>
- Delphi France SAS. (2007). Common rail manual- Principles of operation. *DDGX200(EN)* Retrieved 31st December, 2015, from http://www.decbg.com/img/ddgx200_priciples_of_operation-common_rail_manual.pdf
- Demirbas, A. (2008). Comparison of transesterification methods for production of biodiesel from vegetable oils and fats. *Energy Conversion and Management*, 49(1), 125-130.
- Dempsey, A. B., Walker, N. R., Gingrich, E., & Reitz, R. D. (2013). Comparison of low temperature combustion strategies for advanced compression ignition engines with a focus on controllability. *Combustion Science and Technology*, 186(2), 210-241.

- Denso Corporation. (2007). Service manual common rail system (CRS) operation (Diesel Injection Pump). Retrieved 06th July, 2015, from <http://steldiesel.ru/files/crdensoservismanual.pdf>
- Dhar, A., Kevin, R., & Agarwal, A. K. (2012). Production of biodiesel from high-FFA neem oil and its performance, emission and combustion characterization in a single cylinder DIC engine. *Fuel Processing Technology*, 97(0), 118-129.
- DieselNet. (2012). European Union: emission standards – heavy-duty diesel truck and bus engines. Retrieved July 01 2015 <https://www.dieselnet.com/standards/eu/hd.php>
- Directive 2005/55/EC. (2005). Directive 2005/55/EC of the European Parliament and of the Council of 28 September 2005 on the approximation of the laws of the member states relating to the measures to be taken against the emission of gaseous and particulate pollutants from the compression-ignition engines for use in vehicles, and the emission of gaseous pollutants from positive-ignition engines fuelled with natural gas or liquefied petroleum gas for use in vehicles. Retrieved 20th January, 2016, from <http://eur-lex.europa.eu/legal-content/EN/TXT/?uri=CELEX%3A32005L0055>
- Directive 2009/28/EC. (2009). Directive 2009/28/EC of the European Parliament and of the Council of 23 April 2009 on the promotion of the use of energy from renewable sources and amending and subsequently repealing Directives 2001/77/EC and 2003/30/EC. Retrieved 20th January, 2016, from <http://eur-lex.europa.eu/legal-content/EN/ALL/?uri=CELEX%3A32009L0028>
- Dober, G., Tullis, S., Greeves, G., Milovanovic, N., Hardy, M., & Zuelch, S. (2008). The impact of injection strategies on emissions reduction and power output of future diesel engines. *SAE Paper No. 2008-01-0941*.
- Dorado, M., Ballesteros, E., Arnal, J., Gomez, J., & Lopez, F. (2003). Exhaust emissions from a Diesel engine fueled with transesterified waste olive oil. *Fuel*, 82(11), 1311-1315.
- Ekoto, I. W., Colban, W. F., Miles, P. C., Park, S. W., Foster, D. E., Reitz, R. D., . . . Andersson, Ö. (2009). UHC and CO emissions sources from a light-duty diesel engine undergoing dilution-controlled low-temperature combustion. *SAE Int. J. Engines*, 2(2), 411-430.
- Eldering, A., & Cass, G. R. (1996). Source-oriented model for air pollutant effects on visibility. *Journal of Geophysical Research: Atmospheres*, 101(D14), 19343-19369.
- Enweremadu, C., & Rutto, H. (2010). Combustion, emission and engine performance characteristics of used cooking oil biodiesel—A review. *Renewable and Sustainable Energy Reviews*, 14(9), 2863-2873.
- Epping, K., Aceves, S., Bechtold, R., & Dec, J. E. (2002). The potential of HCCI combustion for high efficiency and low emissions. *SAE Paper No. 2002-01-1923*.

- Ergenç, A. T., & Koca, D. Ö. (2014). PLC controlled single cylinder diesel-LPG engine. *Fuel*, 130, 273-278.
- Fang, T., Coverdill, R. E., Lee, C.-f. F., & White, R. A. (2008). Effects of injection angles on combustion processes using multiple injection strategies in an HSDI diesel engine. *Fuel*, 87(15–16), 3232-3239.
- Fang, W., Huang, B., Kittelson, D. B., & Northrop, W. F. (2014). Dual-fuel diesel engine combustion with hydrogen, gasoline, and ethanol as fumigants: Effect of diesel injection timing. *Journal of Engineering for Gas Turbines and Power*, 136(8), 081502-081502.
- Flowers, D., Aceves, S., Westbrook, C. K., Smith, J. R., & Dibble, R. (2000). Detailed chemical kinetic simulation of natural gas HCCI combustion: Gas composition effects and investigation of control strategies. *Journal of Engineering for Gas Turbines and Power*, 123(2), 433-439.
- Folkson, R. (2014). *Alternative fuels and advanced vehicle technologies for improved environmental performance: Towards zero carbon transportation*. United Kingdom: Woodhead Publishing Limited.
- Gan, S., Ng, H. K., & Pang, K. M. (2011). Homogeneous charge compression ignition (HCCI) combustion: Implementation and effects on pollutants in direct injection diesel engines. *Applied Energy*, 88(3), 559-567.
- Ganapathy, T., Gakkhar, R. P., & Murugesan, K. (2011). Influence of injection timing on performance, combustion and emission characteristics of Jatropha biodiesel engine. *Applied Energy*, 88(12), 4376-4386.
- Ganesan, S., Ganesh, D., & Nagarajan, G. (2012). Performance and emission analysis on mixed-mode homogeneous charge compression ignition (HCCI) combustion of biodiesel fuel with external mixture formation. *SAE Paper No. 2011-01-2450*.
- Ganesh, D., & Nagarajan, G. (2010). Homogeneous charge compression ignition (HCCI) combustion of diesel fuel with external mixture formation. *Energy*, 35(1), 148-157.
- Ganesh, D., Nagarajan, G., & Mohamed Ibrahim, M. (2008). Study of performance, combustion and emission characteristics of diesel homogeneous charge compression ignition (HCCI) combustion with external mixture formation. *Fuel*, 87(17–18), 3497-3503.
- Gatellier, B., Walter, B., & Miche, M. (2001). New diesel combustion process to achieve near zero NO_x and particulates emissions. In Duret, P. (Ed.), *A New Generation of Engine Combustion Processes for the Future?* (pp. 43-52). Ginoux, Paris: Editions Technip.
- Ghojel, J., & Honnery, D. (2005). Heat release model for the combustion of diesel oil emulsions in DI diesel engines. *Applied Thermal Engineering*, 25(14–15), 2072-2085.

- Gilpin, G., Hanssen, O. J., & Czerwinski, J. (2014). Biodiesel's and advanced exhaust aftertreatment's combined effect on global warming and air pollution in EU road-freight transport. *Journal of Cleaner Production*, 78(0), 84-93.
- Glewen, W., Meyer, C., Foster, D. E., Andrie, M., & Krieger, R. (2011). Sources and tradeoffs for transient NO and UHC emissions with low temperature diesel combustion. *SAE Paper No. 2011-01-1356*.
- Goldwine, G. (2008). *The effect of fuel injection profile on diesel engine performance*. PhD Thesis, Ben-Gurion University of the Negev.
- Gomaa, M., Alimin, A., & Kamarudin, K. (2011). The effect of EGR rates on NOx and smoke emissions of an IDI diesel engine fuelled with Jatropha biodiesel blends. *Int J Energy and Enviroment*, 2(3), 477-490.
- Graboski, M. S., & McCormick, R. L. (1998). Combustion of fat and vegetable oil derived fuels in diesel engines. *Progress in Energy and Combustion Science*, 24(2), 125-164.
- Gumus, M. (2010). A comprehensive experimental investigation of combustion and heat release characteristics of a biodiesel (hazelnut kernel oil methyl ester) fueled direct injection compression ignition engine. *Fuel*, 89(10), 2802-2814.
- Gumus, M., Sayin, C., & Canakci, M. (2012). The impact of fuel injection pressure on the exhaust emissions of a direct injection diesel engine fueled with biodiesel-diesel fuel blends. *Fuel*, 95, 486-494.
- Han, X., Wang, M., & Zheng, M. (2015). An enabling study of neat n-butanol HCCI combustion on a high compression-ratio diesel engine. *SAE Paper No. 2015-01-0001*.
- Hardy, W. L., & Reitz, R. D. (2006). A study of the effects of high EGR, high equivalence ratio, and mixing time on emissions levels in a heavy-duty diesel engine for PCCI combustion. *SAE Paper No. 2006-01-0026*.
- Hariram, V., & Mohan Kumar, G. (2012). The effect of injection timing on combustion, performance and emission Parameters with AOME blends as a fuel for compression ignition engine. *European Journal of Scientific Research*, 79(4), 653-665.
- Hasegawa, R., & Yanagihara, H. (2003). HCCI combustion in DI diesel engine. *SAE Paper No. 2003-01-0745*.
- Hashizume, T., Miyamoto, T., Hisashi, A., & Tsujimura, K. (1998). Combustion and emission characteristics of multiple stage diesel combustion. *SAE Paper No. 980505*.
- Heywood, J. B. (1988). *Internal combustion engine fundamentals*. New York: Mcgraw-hill.

- Himabindu, M., & Mahalakshmi, N. V. (2007). Experimental studies on dual fuel homogeneous charge diesel combustion engines to improve emission characteristics. *SAE Paper No. 2007-01-4065*.
- Himabindu, M., Sathyanarayanan, G., Thomson, S., & Mahalakshmi, N. V. (2008). Effect of premixed charge of ethanol and exhaust gas recirculation on the performance and emission characteristics in an ethanol-diesel fueled HCDC engine - an experimental investigation. *SAE Paper No. 2008-01-2609*.
- Hosseini, V., Neill, W., Guo, H., Chippior, W., Fairbridge, C., & Mitchell, K. (2011). Effects of different cetane number enhancement strategies on HCCI combustion and emissions. *International Journal of Engine Research*, 12(2), 89-108.
- How, H. G., Masjuki, H. H., Kalam, M. A., & Teoh, Y. H. (2014). An investigation of the engine performance, emissions and combustion characteristics of coconut biodiesel in a high-pressure common-rail diesel engine. *Energy*, 69, 749-759.
- How, H. G., Masjuki, H. H., Kalam, M. A., Teoh, Y. H., & Abdullah, M. A. (2013). Effect of injection timing on performance, emission and combustion characteristics of a common-rail diesel engine fuelled with coconut oil methyl ester. *SAE Paper No. 2013-01-2663*.
- Huang, J., Wang, Y., Qin, J.-b., & Roskilly, A. P. (2010). Comparative study of performance and emissions of a diesel engine using Chinese pistache and jatropha biodiesel. *Fuel Processing Technology*, 91(11), 1761-1767.
- Ibrahim, M. M., & Ramesh, A. (2013). Experimental investigations on a hydrogen diesel homogeneous charge compression ignition engine with exhaust gas recirculation. *International Journal of Hydrogen Energy*, 38(24), 10116-10125.
- Ickes, A., Bohac, S., & Assanis, D. (2009). Effect of fuel cetane number on a premixed diesel combustion mode. *International Journal of Engine Research*, 10(4), 251-263.
- Iida, N. (1997). Alternative fuels and homogeneous charge compression ignition combustion technology. *SAE Paper No. 978449*.
- Inagaki, K., Fuyuto, T., Nishikawa, K., Nakakita, K., & Sakata, I. (2006). Dual-fuel PCI combustion controlled by in-cylinder stratification of ignitability. *SAE Paper No. 2006-01-0028*.
- International Energy Agency (IEA). (2011). Technology roadmaps - biofuels for transport. Retrieved July 01, 2015 www.iea.org/papers/2011/biofuels_roadmap.pdf
- International Energy Agency (IEA). (2012). Tracking clean energy progress. Energy technology perspectives 2012 excerpt as IEA input to the Clean Energy Ministerial. Retrieved July 01, 2015 http://www.iea.org/media/etp/Tracking_Clean_Energy_Progress.pdf

- International Energy Agency (IEA). (2013). World energy outlook special report 2013: Southeast Asia energy outlook. Retrieved 26th January, 2016, from https://www.iea.org/publications/freepublications/publication/SoutheastAsiaEnergyOutlook_WEO2013SpecialReport.pdf
- International Energy Agency (IEA). (2014). World energy outlook 2014 (Executive summary). Retrieved 26th January, 2016, from <http://www.iea.org/textbase/npsum/weo2014sum.pdf>
- Ishibashi, Y., & Asai, M. (1996). Improving the exhaust emissions of two-stroke engines by applying the activated radical combustion. *SAE Paper No. 960742*.
- Ishibashi, Y., & Asai, M. (1998). A low pressure pneumatic direct injection two-stroke engine by activated radical combustion concept. *SAE Paper No. 980757*.
- Ishibashi, Y., & Sakuyama, H. (2004). An application study of the pneumatic direct injection activated radical combustion two-stroke engine to scooter. *SAE Paper No. 2004-01-1870*.
- Iwabuchi, Y., Kawai, K., Shoji, T., & Takeda, Y. (1999). Trial of new concept diesel combustion system - premixed compression-ignited combustion. *SAE Paper No. 1999-01-0185*.
- Jacobs, T. J., Bohac, S. V., Assanis, D. N., & Szymkowitz, P. G. (2005). Lean and rich premixed compression ignition combustion in a light-duty diesel engine. *SAE Paper No. 2005-01-0166*.
- Japan TIOEE. (2013). The institute of energy economics Japan. Retrieved 26th January, 2016, from <https://eneken.ieej.or.jp/en/>
- Jayed, M. H., Masjuki, H. H., Kalam, M. A., Mahlia, T. M. I., Husnawan, M., & Liaquat, A. M. (2011). Prospects of dedicated biodiesel engine vehicles in Malaysia and Indonesia. *Renewable and Sustainable Energy Reviews, 15*(1), 220-235.
- Jia, M., Li, Y., Xie, M., Wang, T., Wang, H., & Reitz, R. D. (2015). The potential of high-load extension by using late intake valve closing for a diesel premixed charge compression ignition (PCCI) engine. *Energy Procedia, 66*(0), 33-36.
- Junjun, Z., Xinqi, Q., Zhen, W., Bin, G., & Zhen, H. (2009). Experimental Investigation of Low-Temperature Combustion (LTC) in an Engine Fueled with Dimethyl Ether (DME). *Energy & Fuels, 23*(1), 170-174.
- Juttu, S., Thipse, S. S., Marathe, N. V., & Gajendra Babu, M. K. (2007). Homogeneous charge compression ignition (HCCI): A new concept for near zero NO_x and particulate matter (PM) from diesel engine combustion. *SAE Paper No. 2007-26-020*.
- Kakaee, A.-H., Rahnama, P., & Paykani, A. (2015). Influence of fuel composition on combustion and emissions characteristics of natural gas/diesel RCCI engine. *Journal of Natural Gas Science and Engineering, 25*(0), 58-65.

- Kalghatgi, G., Risberg, P., & Ångström, H.-E. (2003). A method of defining ignition quality of fuels in HCCI engines. *SAE Paper No. 2003-01-1816*.
- Kalghatgi, G. T. (2005). Auto-ignition quality of practical fuels and implications for fuel requirements of future SI and HCCI engines. *SAE Paper No. 2005-01-0239*.
- Karavalakis, G., Fontaras, G., Bakeas, E., & Stournas, S. (2011). Effect of biodiesel origin on the regulated and PAH emissions from a modern passenger car. *SAE Paper No. 2011-01-0615*.
- Kawamoto, K., Araki, T., Shinzawa, M., Kimura, S., Koide, S., & Shibuya, M. (2004). Combination of combustion concept and fuel property for ultra-clean di diesel. *SAE Paper No. 2004-01-1868*.
- Kawashima, J.-i., Ogawa, H., & Tsuru, Y. (1998). Research on a variable swirl intake port for 4-valve high-speed DI diesel engines. *SAE Paper No. 982680*.
- Keskin, A., Gürü, M., & Altıparmak, D. (2007). Biodiesel production from tall oil with synthesized Mn and Ni based additives: effects of the additives on fuel consumption and emissions. *Fuel*, 86(7), 1139-1143.
- Keskin, A., Gürü, M., & Altıparmak, D. (2008). Influence of tall oil biodiesel with Mg and Mo based fuel additives on diesel engine performance and emission. *Bioresource Technology*, 99(14), 6434-6438.
- Kim, D. S., & Lee, C. S. (2006). Improved emission characteristics of HCCI engine by various premixed fuels and cooled EGR. *Fuel*, 85(5-6), 695-704.
- Kim, H., & Choi, B. (2010). The effect of biodiesel and bioethanol blended diesel fuel on nanoparticles and exhaust emissions from CRDI diesel engine. *Renewable Energy*, 35(1), 157-163.
- Kim, M. Y., & Lee, C. S. (2007). Effect of a narrow fuel spray angle and a dual injection configuration on the improvement of exhaust emissions in a HCCI diesel engine. *Fuel*, 86(17-18), 2871-2880.
- Kim, M. Y., Lee, J. H., & Lee, C. S. (2008). Combustion characteristics and NO_x emissions of a dimethyl-ether-fueled premixed charge compression ignition engine. *Energy & Fuels*, 22(6), 4206-4212.
- Kimura, S., Aoki, O., Kitahara, Y., & Aiyoshizawa, E. (2001). Ultra-clean combustion technology combining a low-temperature and premixed combustion concept for meeting future emission standards. *SAE Paper No. 2001-01-0200*.
- Kimura, S., Aoki, O., Ogawa, H., Muranaka, S., & Enomoto, Y. (1999). New combustion concept for ultra-clean and high-efficiency small DI diesel engines. *SAE Paper No. 1999-01-3681*.
- Kimura, S., Matsui, Y., & Itoh, T. (1992). Effects of combustion chamber insulation on the heat rejection and thermal efficiency of diesel engines. *SAE Paper No. 920543*.

- Kimura, S., Ogawa, H., Matsui, Y., & Enomoto, Y. (2002). An experimental analysis of low-temperature and premixed combustion for simultaneous reduction of NO_x and particulate emissions in direct injection diesel engines. *International Journal of Engine Research*, 3(4), 249-259.
- Kivevele, T. T., Kristóf, L., Bereczky, Á., & Mbarawa, M. M. (2011). Engine performance, exhaust emissions and combustion characteristics of a CI engine fuelled with croton megalocarpus methyl ester with antioxidant. *Fuel*, 90(8), 2782-2789.
- Knight, B. M., Bittle, J. A., & Jacobs, T. J. (2010). *Efficiency considerations of later-phased low temperature diesel combustion*. Paper presented at the ASME 2010 Internal Combustion Engine Division Fall Technical Conference.
- Kokjohn, S. L., Hanson, R. M., Splitter, D. A., & Reitz, R. D. (2009). Experiments and modeling of dual-fuel HCCI and PCCI combustion using in-cylinder fuel blending. *SAE Int. J. Engines*, 2(2), 24-39.
- Körbitz, W. (1999). Biodiesel production in Europe and North America, an encouraging prospect. *Renewable Energy*, 16(1-4), 1078-1083.
- Kwanchareon, P., Luengnaruemitchai, A., & Jai-In, S. (2007). Solubility of a diesel-biodiesel-ethanol blend, its fuel properties, and its emission characteristics from diesel engine. *Fuel*, 86(7), 1053-1061.
- Ladommatos, N., Abdelhalim, S., & Zhao, H. (2000). The effects of exhaust gas recirculation on diesel combustion and emissions. *International Journal of Engine Research*, 1(1), 107-126.
- Lakshmanan, T., & Nagarajan, G. (2011). Experimental investigation of port injection of acetylene in DI diesel engine in dual fuel mode. *Fuel*, 90(8), 2571-2577.
- Lam, M. K., Tan, K. T., Lee, K. T., & Mohamed, A. R. (2009). Malaysian palm oil: Surviving the food versus fuel dispute for a sustainable future. *Renewable and Sustainable Energy Reviews*, 13(6-7), 1456-1464.
- Lapuerta, M., Armas, O., & Rodríguez-Fernández, J. (2008). Effect of biodiesel fuels on diesel engine emissions. *Progress in Energy and Combustion Science*, 34(2), 198-223.
- Lattimore, T., Wang, C., Xu, H., Wyszynski, M. L., & Shuai, S. (2016). Investigation of EGR effect on combustion and PM emissions in a DISI engine. *Applied Energy*, 161, 256-267.
- Leahey, D. M., Jones, B. C., Gilligan, J. W., Brown, L. P., Hamilton, L. J., Gutteridge, C. E., . . . Caton, P. A. (2007). Combustion of Biodiesel- and Ethanol-Diesel Intake Injection Mixtures with. *2007-01-4011*.
- Lechner, G. A., Jacobs, T. J., Chryssakis, C. A., Assanis, D. N., & Siewert, R. M. (2005). Evaluation of a narrow spray cone angle, advanced injection timing strategy to achieve partially premixed spray compression ignition combustion in a diesel engine. *SAE Paper No. 2005-01-0167*.

- Lee, C. S., Park, S. W., & Kwon, S. I. (2005). An experimental study on the atomization and combustion characteristics of biodiesel-blended fuels. *Energy & Fuels*, 19(5), 2201-2208.
- Lemberger, I., & Floweday, G. (2009). 25cc HCCI engine fuelled with DEE. *SAE Int. J. Engines*, 2(1), 1559-1573.
- Li, J., Yang, W. M., An, H., & Zhao, D. (2015). Effects of fuel ratio and injection timing on gasoline/biodiesel fueled RCCI engine: A modeling study. *Applied Energy*, 155(0), 59-67.
- Li, T., Deng, K., Peng, H., & Wu, C. (2013). Effect of partial-heating of the intake port on the mixture preparation and combustion of the first cranking cycle during the cold-start stage of port fuel injection engine. *Experimental Thermal and Fluid Science*, 49(0), 14-21.
- Li, T., Okabe, Y., Izumi, H., Shudo, T., & Ogawa, H. (2006). Dependence of ultra-high EGR low temperature diesel combustion on fuel properties. *SAE Paper No. 2006-01-3387*.
- Liaquat, A. M., Kalam, M. A., Masjuki, H. H., & Jayed, M. H. (2010). Potential emissions reduction in road transport sector using biofuel in developing countries. *Atmospheric Environment*, 44(32), 3869-3877.
- Lilik, G. K., & Boehman, A. L. (2011). Advanced diesel combustion of a high cetane number fuel with low hydrocarbon and carbon monoxide emissions. *Energy & Fuels*, 25(4), 1444-1456.
- Lim, S., & Teong, L. K. (2010). Recent trends, opportunities and challenges of biodiesel in Malaysia: An overview. *Renewable and Sustainable Energy Reviews*, 14(3), 938-954.
- Lin, C.-Y., & Li, R.-J. (2009a). Engine performance and emission characteristics of marine fish-oil biodiesel produced from the discarded parts of marine fish. *Fuel Processing Technology*, 90(7), 883-888.
- Lin, C.-Y., & Li, R.-J. (2009b). Fuel properties of biodiesel produced from the crude fish oil from the soapstock of marine fish. *Fuel Processing Technology*, 90(1), 130-136.
- Liu, H., Zhang, P., Li, Z., Luo, J., Zheng, Z., & Yao, M. (2011). Effects of temperature inhomogeneities on the HCCI combustion in an optical engine. *Applied Thermal Engineering*, 31(14-15), 2549-2555.
- Liu, H., Zheng, Z., Yao, M., Zhang, P., Zheng, Z., He, B., & Qi, Y. (2012). Influence of temperature and mixture stratification on HCCI combustion using chemiluminescence images and CFD analysis. *Applied Thermal Engineering*, 33-34(0), 135-143.

- Mack, J. H., Butt, R. H., Chen, Y., Chen, J.-Y., & Dibble, R. W. (2016). Experimental and numerical investigation of ion signals in boosted HCCI combustion using cesium and potassium acetate additives. *Energy Conversion and Management*, 108, 181-189.
- Mahr, B. (2004). Future and potential of diesel injection systems. In Whitelaw, J. H., Payri, F., Arcoumanis, C. & Desantes, J. M. (Eds.), *Thermo-and Fluid Dynamic Processes in Diesel Engines 2* (pp. 3-17). Berlin, Germany: Springer.
- Masum, B. M., Masjuki, H. H., Kalam, M. A., Rizwanul Fattah, I. M., Palash, S. M., & Abedin, M. J. (2013). Effect of ethanol–gasoline blend on NOx emission in SI engine. *Renewable and Sustainable Energy Reviews*, 24(0), 209-222.
- Maurya, R. K., & Agarwal, A. K. (2014). Experimental investigations of performance, combustion and emission characteristics of ethanol and methanol fueled HCCI engine. *Fuel Processing Technology*, 126(0), 30-48.
- McEwen, M. (2015). ExxonMobil: Fossil fuels will still provide 80 percent of energy by 2040. Retrieved 26th January, 2016, from http://www.mrt.com/business/oil/top_stories/article_44879920-9fa3-11e5-9006-3f8fda67e49f.html
- Mofijur, M., Masjuki, H. H., Kalam, M. A., Ashrafur Rahman, S. M., & Mahmudul, H. M. (2015). Energy scenario and biofuel policies and targets in ASEAN countries. *Renewable and Sustainable Energy Reviews*, 46, 51-61.
- Mofijur, M., Masjuki, H. H., Kalam, M. A., Atabani, A. E., Fattah, I. M. R., & Mobarak, H. M. (2014). Comparative evaluation of performance and emission characteristics of Moringa oleifera and Palm oil based biodiesel in a diesel engine. *Industrial Crops and Products*, 53(0), 78-84.
- Mofijur, M., Masjuki, H. H., Kalam, M. A., Atabani, A. E., Shahabuddin, M., Palash, S. M., & Hazrat, M. A. (2013). Effect of biodiesel from various feedstocks on combustion characteristics, engine durability and materials compatibility: A review. *Renewable and Sustainable Energy Reviews*, 28(0), 441-455.
- Mofijur, M., Masjuki, H. H., Kalam, M. A., Hazrat, M. A., Liaquat, A. M., Shahabuddin, M., & Varman, M. (2012). Prospects of biodiesel from Jatropha in Malaysia. *Renewable and Sustainable Energy Reviews*, 16(7), 5007-5020.
- Mohammadi, P., Nikbakht, A. M., Tabatabaei, M., Farhadi, K., Mohebbi, A., & Khatami far, M. (2012). Experimental investigation of performance and emission characteristics of DI diesel engine fueled with polymer waste dissolved in biodiesel-blended diesel fuel. *Energy*, 46(1), 596-605.
- Monyem, A., & Gerpen, J. H. V. (2001). The effect of biodiesel oxidation on engine performance and emissions. *Biomass and Bioenergy*, 20(4), 317-325.
- Mueller, C. J., Boehman, A. L., & Martin, G. C. (2009). An experimental investigation of the origin of increased NOx emissions when fueling a heavy-duty compression-ignition engine with soy biodiesel. *SAE Int. J. Fuels Lubr*, 2(1), 789-816.

- Murugesan, A., Umarani, C., Subramanian, R., & Nedunchezian, N. (2009). Bio-diesel as an alternative fuel for diesel engines—A review. *Renewable and Sustainable Energy Reviews*, 13(3), 653-662.
- Musculus, M. P. B. (2006). Multiple simultaneous optical diagnostic imaging of early-injection low-temperature combustion in a heavy-duty diesel engine. *SAE Paper No. 2006-01-0079*.
- Musculus, M. P. B., Singh, S., & Reitz, R. D. (2008). Gradient effects on two-color soot optical pyrometry in a heavy-duty DI diesel engine. *Combustion and Flame*, 153(1-2), 216-227.
- Nakano, M., Mandokoro, Y., Kubo, S., & Yamazaki, S. (2000). Effects of exhaust gas recirculation in homogeneous charge compression ignition engines. *International Journal of Engine Research*, 1(3), 269-279.
- Nejat, P., Jomehzadeh, F., Taheri, M. M., Gohari, M., & Abd. Majid, M. Z. (2015). A global review of energy consumption, CO₂ emissions and policy in the residential sector (with an overview of the top ten CO₂ emitting countries). *Renewable and Sustainable Energy Reviews*, 43, 843-862.
- Ng, J.-H., Ng, H. K., & Gan, S. (2011). Engine-out characterisation using speed-load mapping and reduced test cycle for a light-duty diesel engine fuelled with biodiesel blends. *Fuel*, 90(8), 2700-2709.
- Noguchi, M., Tanaka, Y., Tanaka, T., & Takeuchi, Y. (1979). A study on gasoline engine combustion by observation of intermediate reactive products during combustion. *SAE Paper No. 790840*.
- Northrop, W. F., Assanis, D. N., & Bohac, S. (2011). Evaluation of diesel oxidation catalyst conversion of hydrocarbons and particulate matter from premixed low temperature combustion of biodiesel. *SAE Int. J. Engines*, 4(1), 1431-1444.
- NRDC. (2015). From copenhagen accord to climate action: Tracking national commitments to curb global warming. Retrieved 15th June, 2015, from <http://www.nrdc.org/international/copenhagenaccords/>
- O'Connor, J., & Musculus, M. (2014). Effects of exhaust gas recirculation and load on soot in a heavy-duty optical diesel engine with close-coupled post injections for high-efficiency combustion phasing. *International Journal of Engine Research*, 15(4), 421-443.
- Odaka, M., Suzuki, H., Koike, N., & Ishii, H. (1999). Search for optimizing control method of homogeneous charge diesel combustion. *SAE Paper No. 1999-01-0184*.
- Okude, K., Mori, K., Shiino, S., & Moriya, T. (2004). Premixed compression ignition (PCI) combustion for simultaneous reduction of NO_x and soot in diesel engine. *SAE Paper No. 2004-01-1907*.

- Ong, H. C., Mahlia, T. M. I., Masjuki, H. H., & Norhasyima, R. S. (2011). Comparison of palm oil, *Jatropha curcas* and *Calophyllum inophyllum* for biodiesel: A review. *Renewable and Sustainable Energy Reviews*, 15(8), 3501-3515.
- Ong, H. C., Masjuki, H. H., Mahlia, T. M. I., Silitonga, A. S., Chong, W. T., & Leong, K. Y. (2014). Optimization of biodiesel production and engine performance from high free fatty acid *Calophyllum inophyllum* oil in CI diesel engine. *Energy Conversion and Management*, 81, 30-40.
- Onishi, S., Jo, S. H., Shoda, K., Jo, P. D., & Kato, S. (1979). Active thermo-atmosphere combustion (ATAC) - a new combustion process for internal combustion engines. *SAE Paper No. 790501*.
- Ouenou-Gamo, S., Ouladsine, M., & Rachid, A. (1998). Measurement and prediction of diesel engine exhaust emissions. *ISA Transactions*, 37(3), 135-140.
- Owen, N. A., Inderwildi, O. R., & King, D. A. (2010). The status of conventional world oil reserves—Hype or cause for concern? *Energy Policy*, 38(8), 4743-4749.
- Özener, O., Yüksek, L., Ergenç, A. T., & Özkan, M. (2014). Effects of soybean biodiesel on a DI diesel engine performance, emission and combustion characteristics. *Fuel*, 115, 875-883.
- Ozsezen, A. N., & Canakci, M. (2011). Determination of performance and combustion characteristics of a diesel engine fueled with canola and waste palm oil methyl esters. *Energy Conversion and Management*, 52(1), 108-116.
- Ozsezen, A. N., Canakci, M., & Sayin, C. (2008). Effects of biodiesel from used frying palm oil on the performance, injection, and combustion characteristics of an indirect injection diesel engine. *Energy & Fuels*, 22(2), 1297-1305.
- Padala, S., Le, M. K., Kook, S., & Hawkes, E. R. (2013). Imaging diagnostics of ethanol port fuel injection sprays for automobile engine applications. *Applied Thermal Engineering*, 52(1), 24-37.
- Padala, S., Woo, C., Kook, S., & Hawkes, E. R. (2013). Ethanol utilisation in a diesel engine using dual-fuelling technology. *Fuel*, 109(0), 597-607.
- Palash, S. M., Masjuki, H. H., Kalam, M. A., Masum, B. M., Sanjid, A., & Abedin, M. J. (2013). State of the art of NO_x mitigation technologies and their effect on the performance and emission characteristics of biodiesel-fueled Compression Ignition engines. *Energy Conversion and Management*, 76(0), 400-420.
- Park, S. H., & Yoon, S. H. (2015). Injection strategy for simultaneous reduction of NO_x and soot emissions using two-stage injection in DME fueled engine. *Applied Energy*, 143, 262-270.
- Park, S. H., Youn, I. M., & Lee, C. S. (2011). Influence of ethanol blends on the combustion performance and exhaust emission characteristics of a four-cylinder diesel engine at various engine loads and injection timings. *Fuel*, 90(2), 748-755.

- Parks II, J. E., Prikhodko, V., Storey, J. M. E., Barone, T. L., Lewis Sr, S. A., Kass, M. D., & Huff, S. P. (2010). Emissions from premixed charge compression ignition (PCCI) combustion and affect on emission control devices. *Catalysis Today*, 151(3–4), 278-284.
- Pekalski, A. A., Zevenbergen, J. F., Pasman, H. J., Lemkowitz, S. M., Dahoe, A. E., & Scarlett, B. (2002). The relation of cool flames and auto-ignition phenomena to process safety at elevated pressure and temperature. *Journal of Hazardous Materials*, 93(1), 93-105.
- Peterson, C. L., & Reece, D. L. (1996). Emissions testing with blends of esters of rapeseed oil fuel with and without a catalytic converter. *Training*, 2013, 11-04.
- Pradeep, V., & Sharma, R. P. (2007). Use of HOT EGR for NO_x control in a compression ignition engine fuelled with bio-diesel from Jatropha oil. *Renewable Energy*, 32(7), 1136-1154.
- Puhan, S., Saravanan, N., Nagarajan, G., & Vedaraman, N. (2010). Effect of biodiesel unsaturated fatty acid on combustion characteristics of a DI compression ignition engine. *Biomass and Bioenergy*, 34(8), 1079-1088.
- Purushothaman, K., & Nagarajan, G. (2009). Effect of injection pressure on heat release rate and emissions in CI engine using orange skin powder diesel solution. *Energy Conversion and Management*, 50(4), 962-969.
- Qi, D., Leick, M., Liu, Y., & Lee, C.-f. F. (2011). Effect of EGR and injection timing on combustion and emission characteristics of split injection strategy DI-diesel engine fueled with biodiesel. *Fuel*, 90(5), 1884-1891.
- Qi, D. H., Chen, H., Lee, C. F., Geng, L. M., & Bian, Y. Z. (2009). Experimental studies of a naturally aspirated, DI diesel engine fuelled with ethanol– biodiesel– water microemulsions. *Energy & Fuels*, 24(1), 652-663.
- Qi, D. H., Chen, H., Matthews, R. D., & Bian, Y. Z. (2010). Combustion and emission characteristics of ethanol–biodiesel–water micro-emulsions used in a direct injection compression ignition engine. *Fuel*, 89(5), 958-964.
- Qi, D. H., Geng, L. M., Chen, H., Bian, Y. Z., Liu, J., & Ren, X. C. (2009). Combustion and performance evaluation of a diesel engine fueled with biodiesel produced from soybean crude oil. *Renewable Energy*, 34(12), 2706-2713.
- Raheman, H., & Ghadge, S. V. (2007). Performance of compression ignition engine with mahua (*Madhuca indica*) biodiesel. *Fuel*, 86(16), 2568-2573.
- Rahman, S. M. A., Masjuki, H. H., Kalam, M. A., Abedin, M. J., Sanjid, A., & Sajjad, H. (2013). Production of palm and *Calophyllum inophyllum* based biodiesel and investigation of blend performance and exhaust emission in an unmodified diesel engine at high idling conditions. *Energy Conversion and Management*, 76(0), 362-367.

- Rajesh kumar, B., & Saravanan, S. (2015). Effect of exhaust gas recirculation (EGR) on performance and emissions of a constant speed DI diesel engine fueled with pentanol/diesel blends. *Fuel*, 160, 217-226.
- Rakopoulos, C. D., Antonopoulos, K. A., Rakopoulos, D. C., & Giakoumis, E. G. (2006). Study of combustion in a divided chamber turbocharged diesel engine by experimental heat release analysis in its chambers. *Applied Thermal Engineering*, 26(14–15), 1611-1620.
- Reitz, R. D. (2010). High efficiency fuel reactivity controlled compression ignition (RCCI) combustion. *Proceedings of the Directions in Engine-Efficiency and Emissions Research (DEER)*.
- Reitz, R. D., & Duraisamy, G. (2015). Review of high efficiency and clean reactivity controlled compression ignition (RCCI) combustion in internal combustion engines. *Progress in Energy and Combustion Science*, 46(0), 12-71.
- Reveille, B., Kleemann, A., Knop, V., & Habchi, C. (2006). Potential of narrow angle direct injection diesel engines for clean combustion: 3D CFD analysis. *SAE Paper No. 2006-01-1365*.
- Risberg, P., Kalghatgi, G., Ångström, H.-E., & Wåhlin, F. (2005). Auto-ignition quality of diesel-like fuels in HCCI engines. *SAE Paper No. 2005-01-2127*.
- Ryan, T. W., & Matheaus, A. C. (2003). Fuel requirements for HCCI engine operation. *SAE Paper No. 2003-01-1813*.
- Sajjad, H., Masjuki, H. H., Varman, M., Kalam, M. A., Arbab, M. I., Imtenan, S., & Rahman, S. M. A. (2014). Engine combustion, performance and emission characteristics of gas to liquid (GTL) fuels and its blends with diesel and bio-diesel. *Renewable and Sustainable Energy Reviews*, 30(0), 961-986.
- Saravanan, N., & Nagarajan, G. (2010). Performance and emission studies on port injection of hydrogen with varied flow rates with Diesel as an ignition source. *Applied Energy*, 87(7), 2218-2229.
- Saravanan, N., Nagarajan, G., Dhanasekaran, C., & Kalaiselvan, K. M. (2007). Experimental investigation of hydrogen port fuel injection in DI diesel engine. *International Journal of Hydrogen Energy*, 32(16), 4071-4080.
- Saravanan, S. (2015). Effect of EGR at advanced injection timing on combustion characteristics of diesel engine. *Alexandria Engineering Journal*, 54(3), 339-342.
- Saravanan, S., Nagarajan, G., Lakshmi Narayana Rao, G., & Sampath, S. (2010). Combustion characteristics of a stationary diesel engine fuelled with a blend of crude rice bran oil methyl ester and diesel. *Energy*, 35(1), 94-100.
- Saxena, S., Schneider, S., Aceves, S., & Dibble, R. (2012). Wet ethanol in HCCI engines with exhaust heat recovery to improve the energy balance of ethanol fuels. *Applied Energy*, 98(0), 448-457.

- Sayin, C., Ilhan, M., Canakci, M., & Gumus, M. (2009). Effect of injection timing on the exhaust emissions of a diesel engine using diesel–methanol blends. *Renewable Energy*, 34(5), 1261-1269.
- Sayin, C., Uslu, K., & Canakci, M. (2008). Influence of injection timing on the exhaust emissions of a dual-fuel CI engine. *Renewable Energy*, 33(6), 1314-1323.
- Sealand Turbo-Diesel Asia Pte Ltd. (2015). Delphi common rail injectors. Retrieved 25th December, 2015, from <http://www.turbodiesel.com.sg/proddetail.aspx?ID=30&>
- Selim, M. Y. E. (2003). Effect of exhaust gas recirculation on some combustion characteristics of dual fuel engine. *Energy Conversion and Management*, 44(5), 707-721.
- Sellerbeck, P., Nettelbeck, C., Heinrichs, R., & Abels, T. (2007). Improving diesel sound quality on engine level and vehicle level - a holistic approach. *SAE Paper No. 2007-01-2372*.
- Semin, Ismail, A. R., & Bakar, R. A. (2008). Comparative performance of direct injection diesel engines fueled using compressed natural gas and diesel fuel based on GT-POWER simulation. *American Journal of Applied Sciences*, 5(5), 540-547.
- Shahabuddin, M., Kalam, M. A., Masjuki, H. H., Bhuiya, M. M. K., & Mofijur, M. (2012). An experimental investigation into biodiesel stability by means of oxidation and property determination. *Energy*, 44(1), 616-622.
- Shahir, V. K., Jawahar, C. P., & Suresh, P. R. (2015). Comparative study of diesel and biodiesel on CI engine with emphasis to emissions—A review. *Renewable and Sustainable Energy Reviews*, 45, 686-697.
- Sharma, D., Soni, S. L., & Mathur, J. (2009). Emission reduction in a direct injection diesel engine fueled by neem-diesel blend. *Energy Sources, Part A: Recovery, Utilization, and Environmental Effects*, 31(6), 500-508.
- Sharma, Y. C., & Singh, B. (2009). Development of biodiesel: Current scenario. *Renewable and Sustainable Energy Reviews*, 13(6–7), 1646-1651.
- Shibata, G., Oyama, K., Urushihara, T., & Nakano, T. (2004). The effect of fuel properties on low and high temperature heat release and resulting performance of an HCCI engine. *SAE Paper No. 2004-01-0553*.
- Shibata, G., Oyama, K., Urushihara, T., & Nakano, T. (2005). Correlation of low temperature heat release with fuel composition and HCCI engine combustion. *SAE Paper No. 2005-01-0138*.
- Shimazaki, N., Tsurushima, T., & Nishimura, T. (2003). Dual mode combustion concept with premixed diesel combustion by direct injection near top dead center. *SAE Paper No. 2003-01-0742*.

- Shivakumar, Srinivasa Pai, P., & Shrinivasa Rao, B. R. (2011). Artificial Neural Network based prediction of performance and emission characteristics of a variable compression ratio CI engine using WCO as a biodiesel at different injection timings. *Applied Energy*, 88(7), 2344-2354.
- Simescu, S., Fiveland, S. B., & Dodge, L. G. (2003). An experimental investigation of PCCI-DI combustion and emissions in a heavy-duty diesel engine. *SAE Paper No. 2003-01-0345*.
- Singh, A. P., & Agarwal, A. K. (2012). Combustion characteristics of diesel HCCI engine: An experimental investigation using external mixture formation technique. *Applied Energy*, 99(0), 116-125.
- Singh, S., Reitz, R. D., Musculus, M. P. B., & Lachaux, T. (2007). Simultaneous optical diagnostic imaging of low-temperature, double-injection combustion in a heavy-duty di diesel engine. *Combustion Science and Technology*, 179(11), 2381-2414.
- Sjöberg, M., & Dec, J. E. (2007). Comparing late-cycle autoignition stability for single- and two-stage ignition fuels in HCCI engines. *Proceedings of the combustion institute*, 31(2), 2895-2902.
- Soloiu, V., Duggan, M., Harp, S., Vlcek, B., & Williams, D. (2013). PFI (port fuel injection) of n-butanol and direct injection of biodiesel to attain LTC (low-temperature combustion) for low-emissions idling in a compression engine. *Energy*, 52(0), 143-154.
- Song, J.-T., & Zhang, C.-H. (2008). An experimental study on the performance and exhaust emissions of a diesel engine fuelled with soybean oil methyl ester. *Proceedings of the Institution of Mechanical Engineers, Part D: Journal of Automobile Engineering*, 222(12), 2487-2496.
- Srinivasan, K. K., Krishnan, S. R., Qi, Y., Midkiff, K. C., & Yang, H. (2007). Analysis of diesel pilot-ignited natural gas low-temperature combustion with hot exhaust gas recirculation. *Combustion Science and Technology*, 179(9), 1737-1776.
- Stanglmaier, R. H., & Roberts, C. E. (1999). Homogeneous charge compression ignition (HCCI): Benefits, compromises, and future engine applications. *SAE Paper No. 1999-01-3682*.
- Su, W., Lin, T., & Pei, Y. (2003). A compound technology for HCCI combustion in a DI diesel engine based on the Multi-Pulse Injection and the BUMP combustion chamber. *SAE Paper No. 2003-01-0741*.
- Sudheesh, K., & Mallikarjuna, J. M. (2010). Diethyl ether as an ignition improver for biogas homogeneous charge compression ignition (HCCI) operation - An experimental investigation. *Energy*, 35(9), 3614-3622.
- Swami Nathan, S., Mallikarjuna, J. M., & Ramesh, A. (2010a). Effects of charge temperature and exhaust gas re-circulation on combustion and emission characteristics of an acetylene fuelled HCCI engine. *Fuel*, 89(2), 515-521.

- Swami Nathan, S., Mallikarjuna, J. M., & Ramesh, A. (2010b). An experimental study of the biogas–diesel HCCI mode of engine operation. *Energy Conversion and Management*, 51(7), 1347-1353.
- Szybist, J. P., Boehman, A. L., Taylor, J. D., & McCormick, R. L. (2005). Evaluation of formulation strategies to eliminate the biodiesel NOx effect. *Fuel Processing Technology*, 86(10), 1109-1126.
- Szybist, J. P., & Bunting, B. G. (2005). Cetane number and engine speed effects on diesel HCCI performance and emissions. *SAE Paper No. 2005-01-3723*.
- Taghizadeh-Alisaraei, A., Ghobadian, B., Tavakoli-Hashjin, T., & Mohtasebi, S. S. (2012). Vibration analysis of a diesel engine using biodiesel and petrodiesel fuel blends. *Fuel*, 102, 414-422.
- Takeda, Y., Keiichi, N., & Keiichi, N. (1996). Emission characteristics of premixed lean diesel combustion with extremely early staged fuel injection. *SAE Paper No. 961163*.
- Tan, P.-Q., Hu, Z.-Y., Lou, D.-M., & Li, Z.-J. (2012). Exhaust emissions from a light-duty diesel engine with *Jatropha* biodiesel fuel. *Energy*, 39(1), 356-362.
- Tan, Z. (2014). *Air pollution and greenhouse gases: From basic concepts to engineering applications for air emission control*: Springer.
- Tauzia, X., Maiboom, A., Chesse, P., & Thouvenel, N. (2006). A new phenomenological heat release model for thermodynamical simulation of modern turbocharged heavy duty Diesel engines. *Applied Thermal Engineering*, 26(16), 1851-1857.
- Tesfa, B., Mishra, R., Gu, F., & Ball, A. D. (2012). Water injection effects on the performance and emission characteristics of a CI engine operating with biodiesel. *Renewable Energy*, 37(1), 333-344.
- Thring, R. H. (1989). Homogeneous-charge compression-ignition (HCCI) engines. *SAE Paper No. 892068*.
- Tompkins, B., & Jacobs, T. (2012). Low temperature combustion with biodiesel: The role of oxygenation in improving efficiency and emissions. *Spring Technical Meeting of the Central States Section of the Combustion Institute*.
- Torregrosa, A. J., Broatch, A., García, A., & Mónico, L. F. (2013). Sensitivity of combustion noise and NOx and soot emissions to pilot injection in PCCI Diesel engines. *Applied Energy*, 104(0), 149-157.
- TransportPolicy.net. (2014). Global comparison: Heavy-duty emissions. Retrieved 21st January, 2016, from [http://transportpolicy.net/index.php?title=Global Comparison: Heavy-duty Emissions](http://transportpolicy.net/index.php?title=Global_Comparison:_Heavy-duty_Emissions)

- Tsolakis, A., Megaritis, A., Wyszynski, M. L., & Theinnoi, K. (2007). Engine performance and emissions of a diesel engine operating on diesel-RME (rapeseed methyl ester) blends with EGR (exhaust gas recirculation). *Energy*, 32(11), 2072-2080.
- U.S. Energy Information Administration (EIA). (2013). Annual energy outlook 2013 with projections to 2040. Retrieved 26th January, 2016, from [http://www.eia.gov/forecasts/aeo/pdf/0383\(2013\).pdf](http://www.eia.gov/forecasts/aeo/pdf/0383(2013).pdf)
- UNEP. (2013). Status of fuel quality and vehicle emission standards in asia-pacific. Retrieved July 01 2015 http://www.unep.org/transport/pcf/PDF/Maps_Matrices/AP/matrix/AsiaPacific_Fuels_Vehicles_Aug2013.pdf
- Urushihara, T., Hiraya, K., Kakuhou, A., & Itoh, T. (2003). Expansion of HCCI operating region by the combination of direct fuel injection, negative valve overlap and internal fuel reformation. *SAE Paper No. 2003-01-0749*.
- US Energy Information Administration. (2011). International energy outlook 2011.
- USEPA. (2002). Health assessment document for diesel engine exhaust. National center for environmental assessment, office of transportation and air quality.
- Valentino, G., Corcione, F. E., Iannuzzi, S. E., & Serra, S. (2012). Experimental study on performance and emissions of a high speed diesel engine fuelled with n-butanol diesel blends under premixed low temperature combustion. *Fuel*, 92(1), 295-307.
- Vallinayagam, R., Vedharaj, S., Yang, W. M., Saravanan, C. G., Lee, P. S., Chua, K. J. E., & Chou, S. K. (2013). Emission reduction from a diesel engine fueled by pine oil biofuel using SCR and catalytic converter. *Atmospheric Environment*, 80(0), 190-197.
- Vedharaj, S., Vallinayagam, R., Yang, W. M., Chou, S. K., Chua, K. J. E., & Lee, P. S. (2013). Experimental investigation of kapok (*Ceiba pentandra*) oil biodiesel as an alternate fuel for diesel engine. *Energy Conversion and Management*, 75(0), 773-779.
- Veltman, M. K., Karra, P. K., & Kong, S.-C. (2009). Effects of biodiesel blends on emissions in low temperature diesel combustion. *SAE Paper No. 2009-01-0485*.
- Verschaeren, R., Schaepdryver, W., Serruys, T., Bastiaen, M., Vervaeke, L., & Verhelst, S. (2014). Experimental study of NO_x reduction on a medium speed heavy duty diesel engine by the application of EGR (exhaust gas recirculation) and Miller timing. *Energy*, 76, 614-621.
- Walter, B., & Gatellier, B. (2003). Near zero NO_x emissions and high fuel efficiency diesel engine: the NADITM concept using dual mode combustion. *Oil & gas science and technology*, 58(1), 101-114.
- Wang, X., Ge, Y., Yu, L., & Feng, X. (2013). Comparison of combustion characteristics and brake thermal efficiency of a heavy-duty diesel engine fueled with diesel and biodiesel at high altitude. *Fuel*, 107, 852-858.

- Weall, A., & Collings, N. (2007). Highly homogeneous compression ignition in a direct injection diesel engine fuelled with diesel and biodiesel. *SAE Paper No. 2007-01-2020*.
- Wikipedia. (2015). *Common rail*. Retrieved from https://en.wikipedia.org/wiki/Common_rail
- Wu, F., Wang, J., Chen, W., & Shuai, S. (2009). A study on emission performance of a diesel engine fueled with five typical methyl ester biodiesels. *Atmospheric Environment*, *43*(7), 1481-1485.
- Wu, H.-W., Wang, R.-H., Chen, Y.-C., Ou, D.-J., & Chen, T.-Y. (2014). Influence of port-inducted ethanol or gasoline on combustion and emission of a closed cycle diesel engine. *Energy*, *64*, 259-267.
- Wu, H.-W., Wang, R.-H., Ou, D.-J., Chen, Y.-C., & Chen, T.-Y. (2011). Reduction of smoke and nitrogen oxides of a partial HCCI engine using premixed gasoline and ethanol with air. *Applied Energy*, *88*(11), 3882-3890.
- Wu, Y.-Y., Jang, C.-T., & Chen, B.-L. (2010). Combustion characteristics of HCCI in motorcycle engine. *Journal of Engineering for Gas Turbines and Power*, *132*(4), 044501-044504.
- Xue, J., Grift, T. E., & Hansen, A. C. (2011). Effect of biodiesel on engine performances and emissions. *Renewable and Sustainable Energy Reviews*, *15*(2), 1098-1116.
- Yamada, H., Suzaki, K., Sakanashi, H., Choi, N., & Tezaki, A. (2005). Kinetic measurements in homogeneous charge compression of dimethyl ether: role of intermediate formaldehyde controlling chain branching in the low-temperature oxidation mechanism. *Combustion and Flame*, *140*(1-2), 24-33.
- Yokota, H., Kudo, Y., Nakajima, H., Kakegawa, T., & Suzuki, T. (1997). A new concept for low emission diesel combustion. *SAE Paper No. 970891*.
- Zhang, C. H., Pan, J. R., Tong, J. J., & Li, J. (2011). Effects of intake temperature and excessive air coefficient on combustion characteristics and emissions of HCCI combustion. *Procedia Environmental Sciences*, *11*, Part C(0), 1119-1127.
- Zhang, F., Xu, H., Zhang, J., Tian, G., & Kalghatgi, G. (2011). Investigation into light duty dieseline fuelled partially-premixed compression ignition engine. *SAE Int. J. Engines*, *4*(1), 2124-2134.
- Zheng, M., Reader, G. T., & Hawley, J. G. (2004). Diesel engine exhaust gas recirculation—a review on advanced and novel concepts. *Energy Conversion and Management*, *45*(6), 883-900.
- Zhu, R., Miao, H., Wang, X., & Huang, Z. (2013). Effects of fuel constituents and injection timing on combustion and emission characteristics of a compression-ignition engine fueled with diesel-DMM blends. *Proceedings of the Combustion Institute*, *34*(2), 3013-3020.

APPENDIX A

LIST OF PUBLICATIONS

Journal Articles (ISI)

Teoh, Y. H., Masjuki, H. H., Kalam, M. A., & How, H. G. (2015). Comparative assessment of performance, emissions and combustion characteristics of gasoline/diesel and gasoline/biodiesel in a dual-fuel engine. *Rsc Advances*, 5(88), 71608-71619. doi: 10.1039/c5ra14624k [**ISI index; Quartile 1; IF= 3.84**]

Teoh, Y. H., Masjuki, H. H., Noor, I. M., Ali, B. S., Kalam, M. A., & How, H. G. (2015). Effect of injection timing and EGR on engine-out-responses of a common-rail diesel engine fueled with neat biodiesel. *Rsc Advances*, 5(116), 96080–96096. doi: 10.1039/c5ra14831f [**ISI index; Quartile 1; IF= 3.84**]

Teoh, Y. H., Masjuki, H. H., Noor, I. M., Ali, B. S., Kalam, M. A., & How, H. G. (2015). Evaluation of a novel biofuel from unwanted waste and its impact on engine performance, emissions, and combustion characteristics in a diesel engine. *Rsc Advances*, 5(53), 42438-42447. doi: 10.1039/c5ra04294a [**ISI index; Quartile 1; IF= 3.84**]

Teoh, Y. H., Masjuki, H. H., Kalam, M. A., Amalina, M. A., & How, H. G. (2014). Effects of Jatropha biodiesel on the performance, emissions, and combustion of a converted common-rail diesel engine. *Rsc Advances*, 4(92), 50739-50751. doi: 10.1039/c4ra08464k [**ISI index; Quartile 1; IF= 3.84**]

Journal Papers (Non-ISI)

Teoh, Y. H., H. H. Masjuki, M. A. Kalam, M. A. Amalina, and H. G. How. "Impact of premixed kerosene fuel on performance, emission and combustion characteristics in partial HCCI engine." *Energy Procedia* 61 (2014): 1830-1834. [**SCOPUS-Cited Publication**]

Conference Papers

Teoh, Y. H., Masjuki, H. H., Kalam, M. A., & How, H. G. Development of electronically controlled common- rail fuel injection system and its application strategy in single-cylinder diesel engine. 3rd International Conference on Recent Advances in Automotive Engineering & Mobility Research (ReCAR 2015), 1st - 3rd December 2015, Holiday Inn, Melaka, Malaysia.

Teoh, Y. H., Masjuki, H. H., Kalam, M. A., How, H. G., Ashrafur Rahman, S. M., & Ruhul, A. M. Effect of injection timing on gasoline/diesel and gasoline/biodiesel fuelled dual-fuel engine: A comparative study. *Proceedings of the Australian Combustion Symposium (ACS 2015)*, 7th – 9th December 2015, The University of Melbourne

Teoh, Y. H., Masjuki, H. H., Kalam, M. A., Amalina, M. A., & How, H. G. (2014). Impact of premixed kerosene fuel on performance, emission and combustion characteristics in partial HCCI engine. The 6th International Conference on Applied Energy (ICAEE), Taipei, Taiwan, 30th May -2nd Jun 2014.

Teoh, Y. H., Masjuki, H. H., Kalam, M. A., Amalina, M. A., & How, H. G. (2013). Effect of premixed diesel fuel on partial HCCI combustion characteristics. The 2nd International Conference on Recent Advances in Automotive Engineering & Mobility Research (ReCAR 2013), Furama Hotel, Bukit Bintang, Kuala Lumpur, 16th – 18th December 2013.

Teoh, Y. H., Masjuki, H. H., Kalam, M. A., Amalina, M. A., & How, H. G. (2013). Impact of waste cooking oil biodiesel on performance, exhaust emission and combustion characteristics in a light-duty diesel engine. The Proceeding of International Conference on SAE/KSAE 2013 International Powertrains, Fuels & Lubricants Meeting, Seoul, Korea, 21st – 23rd October 2013.

University of Malaysia

APPENDIX B

RESULTS

TABLE B.1: Data for the effect of SOI timing on engine torque under various engine speed and load conditions.

SOI Timing (°BTDC)	Torque (N.m)								
	1000 rpm			1500 rpm			2000 rpm		
	25% load	50% load	75% load	25% load	50% load	75% load	25% load	50% load	75% load
-4	10.0	19.1	-	-	-	-	-	-	-
-2	10.3	19.7	27.9	-	-	-	-	-	-
0	10.6	20.0	28.4	8.9	17.0	25.2	7.2	14.9	22.1
2	10.8	20.1	28.8	9.0	17.2	25.8	7.8	15.7	23.4
4	10.9	20.2	29.0	9.1	17.5	26.2	8.3	16.3	24.3
6	10.9	20.1	29.1	9.2	17.7	26.7	8.7	16.8	25.0
8	10.8	20.0	28.9	9.3	17.8	27.1	8.8	17.3	25.6
10	10.6	19.5	28.5	9.3	18.0	27.2	8.9	17.7	26.4
12	10.3	19.1	28.1	9.2	18.1	27.3	9.0	17.9	27.0
14	9.9	18.8	27.8	9.1	17.8	27.4	9.1	18.0	27.6
16	9.3	18.3	27.3	8.8	17.6	27.3	8.9	18.1	27.9
18	8.7	17.7	26.8	8.5	17.3	27.1	8.6	18.0	28.0
20	8.2	17.0	26.1	8.2	16.9	26.7	8.3	17.9	27.8
22	7.6	16.3	25.3	7.8	16.6	26.5	8.1	17.6	27.7

TABLE B.2: Data for the effect of SOI timing on the first and second HRR peaks and ignition delay.

SOI (°BTDC)	Second HRR Peak (J/°CA)	First HRR Peak (J/°CA)	Ignition Delay (°CA)
0	36.60	52.40	6.32
2	35.44	44.51	6.19
4	35.19	41.67	6.06
6	34.82	40.68	6.06
8	35.03	41.43	6.19
10	34.50	42.02	6.31
12	33.93	44.47	6.56
14	32.70	47.28	6.82
16	30.70	51.96	7.19
18	29.50	58.59	7.69
20	29.30	66.32	8.19
22	28.55	76.56	8.81

TABLE B.3: Data for NO_x and smoke emission with various SOI timing.

SOI Timing (°BTDC)	Smoke (%)	NO _x (ppm)
0	11.8	113
2	10.9	131
4	10.2	163
6	9.1	203
8	8.5	252
10	7.5	324
12	6.7	409
14	5.2	520
16	4.8	646
18	4.5	785
20	4.3	933
22	2.8	1082

TABLE B.4: Data for engine BTE with varying rail pressure and engine speed.

Rail Pressure Set point (bar)	BTE (%)		
	1000 rpm	1500 rpm	2000 rpm
300	27.20	27.07	25.18
400	27.25	27.00	25.16
500	27.27	26.92	25.12
600	27.29	26.95	25.10
700	27.29	26.93	25.08
800	27.29	26.87	25.02
900	27.29	26.84	24.98
1000	27.29	26.81	24.92
1200	27.30	26.66	24.85
1400	27.31	26.54	24.67
1600	27.33	26.45	24.56
1800	27.35	26.17	24.55

TABLE B.5: Data for NO_x emission with varying rail pressure and engine speed.

Rail Pressure Set point (bar)	NO _x (ppm)		
	1000 rpm	1500 rpm	2000 rpm
300	114	149	26
400	173	216	49
500	212	269	65
600	253	335	84
700	291	375	98
800	328	415	113
900	365	452	124
1000	408	514	132
1200	471	571	164
1400	543	650	187
1600	585	721	213
1800	656	791	231

TABLE B.6: Data for smoke emission with varying rail pressure and engine speed.

Rail Pressure Set point (bar)	Smoke (%)		
	1000 rpm	1500 rpm	2000 rpm
300	4.3	6.9	19.8
400	4.0	4.5	10.9
500	4.1	3.9	7.0
600	4.5	3.7	5.6
700	4.5	4.0	5.4
800	3.9	4.2	5.2
900	3.7	4.6	4.4
1000	3.5	4.6	3.0
1200	3.9	4.0	2.7
1400	3.8	4.4	1.8
1600	3.4	4.5	1.7
1800	3.3	4.5	1.6

TABLE B.7: Data for the effect of injection pressure on HRR peak, ignition delay and combustion duration.

Rail Pressure Set point (bar)	1000 rpm			1500 rpm			2000 rpm		
	Premix HRR Peak (J/°CA)	Ignition Delay (°CA)	Combustion Duration (°CA)	Premix HRR Peak (J/°CA)	Ignition Delay (°CA)	Combustion Duration (°CA)	Premix HRR Peak (J/°CA)	Ignition Delay (°CA)	Combustion Duration (°CA)
300	39.93	5.02	18.50	25.38	7.58	24.00	20.01	10.00	34.13
400	48.44	4.77	16.88	31.21	7.20	22.25	24.92	9.51	29.63
500	54.98	4.40	15.88	40.05	6.95	21.75	32.12	9.14	27.75
600	63.72	4.26	15.13	45.95	6.70	20.88	37.92	8.76	27.00
700	73.20	4.15	14.50	50.42	6.45	20.88	42.32	8.41	26.25
800	80.03	3.90	13.88	54.94	6.21	20.75	45.51	8.15	26.00
900	86.60	3.78	13.63	58.64	6.07	20.75	48.37	7.89	26.00
1000	92.44	3.66	13.38	60.82	5.82	20.25	50.92	7.62	25.63
1200	99.87	3.42	13.13	73.26	5.44	20.13	63.94	7.29	24.50
1400	111.68	3.15	13.00	82.35	5.32	19.38	70.91	6.87	24.13
1600	123.55	3.04	12.88	88.92	5.07	19.13	76.67	6.64	24.38
1800	130.46	2.91	12.50	96.41	4.95	18.75	83.29	6.39	24.13

TABLE B.8: Data for the effect of fuel injection strategies on (a) BTE, (b) smoke, (c) NO_x emissions, and (d) pressure rise rate at various fuel injection pressures.

Parameter	Rail Pressure Set point (bar)	BTE (%)		
		Main	Pilot + Main	Pilot + Main + Post
BTE (%)	400	26.6	25.1	27.5
	800	27.3	24.2	26.8
	1200	27.0	22.5	22.5
Smoke (%)	400	4.3	4.0	3.7
	800	4.1	3.7	3.5
	1200	4.9	4.3	2.3
NO _x (ppm)	400	258	327	264
	800	478	627	377
	1200	656	1150	533
Pressure Rise Rate Peak (bar/°CA)	400	3.29	3.11	2.41
	800	5.59	4.50	3.24
	1200	7.77	9.03	8.51

TABLE B.9: Performance and emissions data for the effect of biodiesel blends on common-rail diesel engine.

Fuel Type	BMEP (MPa)	Fuel Flow Rate (L/hr)	Air Mass Flow Rate (kg/hr)	BSFC (g/kWhr)	BTE (%)	Exhaust Gas Temp. (°C)	Smoke (%)	NO _x (ppm)	CO (%)	Relative Air Fuel Ratio (λ)
Diesel	0.1	0.557	40.9	592.7	13.4	200.0	2.0	461	0.047	4.85
	0.2	0.718	40.7	382.2	20.8	242.1	2.6	636	0.041	3.75
	0.3	0.895	40.5	317.9	25.0	287.5	3.8	758	0.037	2.99
	0.4	1.082	40.3	288.1	27.6	334.9	6.2	791	0.034	2.46
	0.5	1.277	40.1	272.1	29.2	382.9	10.3	727	0.037	2.08
	0.6	1.540	40.0	273.1	29.1	439.7	16.5	583	0.033	1.72
PB10	0.1	0.567	40.9	591.5	13.6	200.6	1.8	452	0.041	4.74
	0.2	0.733	40.7	389.9	20.7	243.4	2.1	606	0.035	3.65
	0.3	0.911	40.5	322.4	25.0	286.3	3.5	714	0.034	2.92
	0.4	1.102	40.3	292.5	27.6	334.2	5.9	740	0.035	2.40
	0.5	1.297	40.1	275.3	29.3	382.3	8.8	667	0.034	2.03
	0.6	1.558	40.0	275.3	29.3	435.8	12.2	530	0.030	1.69
PB30	0.1	0.567	40.9	611.4	13.6	199.5	1.7	433	0.034	4.70
	0.2	0.736	40.7	396.4	21.0	243.5	2.0	600	0.034	3.61
	0.3	0.919	40.5	330.9	25.1	288.6	3.0	730	0.028	2.87
	0.4	1.116	40.2	300.8	27.6	333.9	5.5	730	0.025	2.35
	0.5	1.317	40.1	283.9	29.3	381.9	5.9	650	0.028	1.99
	0.6	1.571	40.0	282.6	29.4	431.6	9.9	510	0.031	1.66
PB50	0.1	0.586	40.8	636.0	13.5	201.8	0.8	431	0.016	4.52
	0.2	0.763	40.7	414.5	20.7	244.7	1.3	605	0.011	3.46
	0.3	0.945	40.4	341.9	25.0	287.5	2.6	720	0.009	2.78
	0.4	1.145	40.2	310.8	27.6	334.8	4.1	738	0.009	2.28
	0.5	1.351	40.1	293.1	29.2	382.7	5.3	660	0.011	1.93
	0.6	1.619	40.0	293.1	29.2	432.5	9.6	488	0.017	1.60
PB100	0.1	0.623	40.8	694.0	13.0	199.9	0.2	438	0.015	4.09
	0.2	0.805	40.6	448.7	20.1	242.8	0.6	617	0.008	3.15
	0.3	1.000	40.4	372.1	24.2	285.6	1.6	778	0.007	2.52
	0.4	1.205	40.1	336.2	26.8	334.0	2.8	822	0.006	2.08
	0.5	1.407	40.0	313.5	28.7	379.5	4.8	761	0.008	1.78
	0.6	1.690	39.9	313.7	28.7	433.6	8.6	610	0.012	1.48

TABLE B.9: Performance and emissions data for the effect of biodiesel blends on common-rail diesel engine, continued.

Fuel Type	BMEP (MPa)	Fuel Flow Rate (L/hr)	Air Mass Flow Rate (kg/hr)	BSFC (g/kWhr)	BTE (%)	Exhaust Gas Temp. (°C)	Smoke (%)	NO _x (ppm)	CO (%)	Relative Air Fuel Ratio (λ)
JB10	0.1	0.559	40.8	591.8	13.6	197.5	1.5	464	0.047	4.79
	0.2	0.730	40.6	386.7	20.8	243.2	2.0	640	0.039	3.65
	0.3	0.904	40.4	320.0	25.1	286.0	3.5	750	0.036	2.94
	0.4	1.095	40.2	290.6	27.6	334.3	6.0	790	0.034	2.41
	0.5	1.291	40.0	273.7	29.3	382.0	10.0	720	0.037	2.04
	0.6	1.561	39.9	275.8	29.1	437.6	13.7	580	0.033	1.68
JB30	0.1	0.559	40.7	594.8	13.9	198.5	0.8	453	0.045	4.76
	0.2	0.731	40.6	390.0	21.1	240.6	1.4	633	0.035	3.63
	0.3	0.917	40.4	326.2	25.3	286.8	2.6	740	0.035	2.88
	0.4	1.115	40.2	297.9	27.7	333.3	5.7	780	0.032	2.35
	0.5	1.310	40.0	279.2	29.5	383.2	9.5	740	0.035	1.99
	0.6	1.575	39.8	280.2	29.4	439.4	12.8	600	0.024	1.65
JB50	0.1	0.564	40.7	612.3	13.8	202.4	0.6	460	0.043	4.69
	0.2	0.744	40.6	403.7	20.9	246.6	1.1	640	0.030	3.54
	0.3	0.932	40.3	337.5	25.1	292.1	2.1	783	0.028	2.81
	0.4	1.131	40.1	306.5	27.6	340.2	5.0	821	0.025	2.30
	0.5	1.334	39.9	289.4	29.2	392.2	8.0	742	0.033	1.94
	0.6	1.595	39.8	288.7	29.3	445.3	12.1	595	0.018	1.62
JB100	0.1	0.602	40.7	671.1	13.4	199.0	0.2	488	0.030	4.22
	0.2	0.794	40.4	443.1	20.3	243.9	1.0	699	0.020	3.18
	0.3	0.990	40.3	367.9	24.5	288.4	1.8	873	0.020	2.54
	0.4	1.191	40.0	331.9	27.1	335.6	3.3	932	0.020	2.10
	0.5	1.404	39.8	312.7	28.8	383.0	4.1	877	0.020	1.77
	0.6	1.685	39.7	313.0	28.8	433.9	10.7	714	0.010	1.47

TABLE B.10: Performance and emissions data for the effect of injection timing variation with PME biodiesel and diesel fuel.

SOI (°BTDC)	Fuel Flow Rate (L/hr)		BSFC (g/kWhr)		BTE (%)		NOx (ppm)		BSNOx (g/kWhr)		Exhaust Gas Temp. (°C)		Smoke (%)	
	Diesel	PME	Diesel	PME	Diesel	PME	Diesel	PME	Diesel	PME	Diesel	PME	Diesel	PME
0	1.188	1.359	289.7	343.9	27.6	26.4	103	91	2.0	1.8	372.4	383.4	13.0	6.5
5	1.133	1.297	276.3	327.9	28.9	27.7	178	162	3.4	3.1	349.1	364.1	12.4	5.0
7	1.125	1.278	274.4	323.2	29.2	28.1	230	209	4.3	4.0	342.0	355.7	12.0	4.7
9	1.123	1.268	274.3	320.6	29.2	28.3	293	263	5.5	5.0	336.7	348.8	11.4	3.9
10	1.122	1.262	273.6	319.4	29.2	28.4	334	300	6.3	5.7	335.4	345.7	10.1	3.8
11	1.113	1.252	271.5	316.7	29.5	28.6	377	340	7.1	6.4	332.9	341.7	7.9	3.6
12	1.114	1.256	271.8	317.7	29.4	28.6	431	376	8.1	7.1	331.0	341.4	7.5	3.5
13	1.115	1.267	272.2	320.2	29.4	28.3	486	424	9.2	8.0	330.0	341.5	6.3	3.3
15	1.123	1.275	273.9	322.6	29.2	28.1	607	528	11.4	9.9	331.4	341.6	5.1	3.3
20	1.152	1.302	281.3	329.4	28.4	27.5	976	814	18.3	15.3	335.4	346.0	3.7	2.0
25	1.201	1.369	293.1	346.2	27.3	26.2	1405	1144	26.3	21.5	349.8	362.7	3.0	1.0

TABLE B.11: Data for the total burning angle as a function of SOI timing for diesel and PME fuel.

SOI (° BTDC)	Diesel					PME				
	5% MFB location (°BTDC)	10% MFB location (°BTDC)	50% MFB location (°BTDC)	90% MFB location (°BTDC)	Total Burning Angle (°CA)	5% MFB location (°BTDC)	10% MFB location (°BTDC)	50% MFB location (°BTDC)	90% MFB location (°BTDC)	Total Burning Angle (°CA)
0	-10.125	-11.000	-17.625	-34.250	23.250	-9.500	-10.500	-18.375	-35.250	24.750
5	-3.625	-4.500	-12.250	-26.250	21.750	-3.500	-4.375	-12.750	-27.125	22.750
7	-1.500	-2.375	-10.000	-24.000	21.625	-1.375	-2.250	-10.625	-24.125	21.875
9	0.500	-0.375	-8.000	-22.375	22.000	0.625	-0.250	-8.500	-22.625	22.375
10	1.375	0.500	-7.000	-22.000	22.500	1.625	0.750	-7.500	-21.875	22.625
11	2.375	1.125	-6.125	-21.750	22.875	2.625	1.750	-6.375	-21.250	23.000
12	3.375	2.500	-5.000	-20.750	23.250	3.625	2.750	-5.375	-20.750	23.500
13	4.250	3.500	-4.000	-20.125	23.625	4.500	3.625	-4.500	-20.250	23.875
15	5.875	5.250	-2.125	-19.375	24.625	6.250	5.500	-2.500	-19.750	25.250
20	9.750	9.125	3.000	-17.500	26.625	10.125	9.500	2.375	-17.875	27.375
25	12.875	12.375	8.875	-15.500	27.875	13.375	12.875	7.750	-16.250	29.125

TABLE B.12: Data for the engine performance and exhaust gas emissions for PME compared with diesel fuel at various EGR rates.

%EGR	Fuel Flow Rate (L/hr)		Mass Air Flow Rate (kg/hr)		BSFC (g/kWhr)		BTE (%)		O ₂ (%)	
	Diesel	PME	Diesel	PME	Diesel	PME	Diesel	PME	Diesel	PME
0	1.098	1.241	40.02	39.75	267.8	314.1	29.9	28.9	12.6	12.1
10	1.092	1.234	32.74	32.46	266.3	312.2	30.0	29.1	11.7	11.1
20	1.087	1.223	29.50	29.28	265.3	309.3	30.2	29.3	10.1	9.9
30	1.079	1.212	26.95	26.74	263.4	306.6	30.4	29.6	9.2	8.9
35	1.091	1.204	25.22	25.20	266.1	304.4	30.1	29.8	8.6	8.5
40	1.099	1.211	23.72	23.55	268.1	306.2	29.8	29.6	8.1	8.0
45	1.105	1.215	21.96	21.81	269.3	307.4	29.7	29.5	7.4	7.3
50	1.110	1.218	20.37	20.18	270.7	308.2	29.6	29.4	6.7	6.6

%EGR	NO _x (ppm)		BSNO _x (g/kWhr)		Smoke (%)		Intake Air CO ₂ (%)		Exhaust Gas CO ₂ (%)	
	Diesel	PME	Diesel	PME	Diesel	PME	Diesel	PME	Diesel	PME
0	377	340	7.09	6.38	7.1	3.8	0.04	0.05	6.80	6.88
10	346	316	5.35	4.86	9.6	6.5	0.70	0.72	7.00	7.20
20	198	163	2.76	2.27	14.6	8.5	1.40	1.44	7.00	7.21
30	110	97	1.40	1.23	20.1	10.1	2.31	2.35	7.70	7.82
35	77	66	0.93	0.79	26.1	10.8	2.93	3.03	8.38	8.65
40	53	50	0.60	0.57	32.4	13.8	3.79	3.97	9.48	9.94
45	35	33	0.37	0.35	40.6	18.7	4.67	4.86	10.38	10.81
50	22	22	0.22	0.21	50.2	27.2	5.39	5.57	10.79	11.14

TABLE B.13: Performance, emissions and combustion data for dual-fuel combustion.

Fuel Type	SOI (°BTDC)	Torque (Nm)	IMEP (bar)	Fuel Flow Rate (L/hr)	Mass Air Flow Rate (kg/hr)	BSFC (g/kWhr)	BTE (%)	NO _x (ppm)	CA50 (°BTDC)	HC (ppm)	CO (%)
Diesel/ Gasoline	5	19.87	4.93	0.358	27.28	247.3	32.8	24	-13.250	222	0.130
	7	20.75	5.08	0.357	27.29	236.2	34.3	50	-10.625	276	0.159
	9	20.97	5.04	0.353	27.21	232.9	34.8	70	-7.750	312	0.173
	11	21.02	4.96	0.355	27.19	232.7	34.8	104	-5.125	337	0.197
	13	20.79	4.80	0.354	27.08	235.2	34.5	147	-2.875	348	0.197
	15	20.50	4.64	0.353	27.05	238.2	34.0	202	-1.000	355	0.192
	17	20.04	4.47	0.356	26.99	244.5	33.2	271	1.000	355	0.193
	19	19.78	4.33	0.355	26.95	247.4	32.8	357	2.750	353	0.210
	25	19.09	4.04	0.357	26.99	256.3	31.6	650	6.625	323	0.201
	35	17.30	3.73	0.349	26.80	281.1	28.9	610	8.500	288	0.226
	40	16.67	3.62	0.348	26.74	291.3	27.8	419	8.250	264	0.223
	45	16.39	3.56	0.345	26.67	295.6	27.4	312	8.000	255	0.193
	50	16.24	3.58	0.343	26.67	297.2	27.3	200	7.000	247	0.168
	55	16.57	3.65	0.341	26.70	290.8	27.9	120	5.750	246	0.159
	65	17.23	3.77	0.339	26.79	279.2	29.1	40	3.250	260	0.164
	75	17.52	3.93	0.34	26.90	274.8	29.5	25	-0.125	292	0.185
	85	17.68	4.17	0.335	26.97	270.6	30.0	12	-4.500	309	0.209
95	14.58	3.87	0.328	27.00	290.0	24.8	8	-11.250	367	0.452	

TABLE B.13: Performance, emissions and combustion data for dual-fuel combustion, continued.

Fuel Type	SOI (°BTDC)	Torque (Nm)	IMEP (bar)	Fuel Flow Rate (L/hr)	Mass Air Flow Rate (kg/hr)	BSFC (g/kWhr)	BTE (%)	NO _x (ppm)	CA50 (°BTDC)	HC (ppm)	CO (%)
PME/ Gasoline	5	20.49	4.83	0.396	27.11	253.4	33.7	21	-12.625	200	0.110
	7	21.24	4.95	0.392	26.99	243.6	35.0	45	-10.000	279	0.137
	9	21.48	4.84	0.391	26.87	240.6	35.5	65	-6.875	295	0.136
	11	21.10	4.75	0.395	27.01	245.0	34.8	93	-4.750	300	0.129
	13	21.09	4.60	0.393	26.94	245.2	34.8	131	-2.625	299	0.121
	15	20.70	4.42	0.388	26.88	248.9	34.3	186	-0.500	298	0.120
	17	19.97	4.23	0.39	26.94	258.3	33.0	259	1.750	288	0.122
	19	19.47	4.09	0.389	26.89	264.8	32.2	344	3.500	275	0.141
	25	18.48	3.73	0.387	26.71	278.3	30.7	622	7.750	251	0.136
	35	16.99	3.47	0.387	26.63	302.8	28.2	594	9.375	210	0.133
	40	16.40	3.12	0.389	26.53	314.3	27.1	377	9.250	188	0.153
	45	15.77	2.99	0.389	26.48	326.8	26.1	255	9.000	176	0.141
	50	15.71	3.01	0.389	26.46	328.3	26.0	184	8.250	173	0.138
	55	15.81	3.08	0.389	26.46	326.2	26.2	109	7.125	174	0.131
	65	16.43	3.29	0.39	26.73	313.6	27.2	35	4.125	187	0.129
	75	16.66	3.54	0.384	26.90	306.8	27.8	22	0.000	214	0.143
	85	16.62	3.71	0.38	27.11	306.2	27.9	9	-4.000	247	0.190
	95	10.41	2.08	0.385	27.21	320.0	22.0	3	-11.000	250	0.310

TABLE B.14: Data for the effect of SOI timing variation on the coefficient of variation of indicated mean effective pressure for dual fuel operation of diesel/gasoline and PME/gasoline.

SOI Timing (°BTDC)	CoVimep	
	Diesel/Gasoline	PME/Gasoline
5	2.05	1.60
7	1.64	1.42
9	1.42	1.14
11	1.21	1.00
13	1.16	0.90
15	1.05	0.91
17	0.98	1.00
19	1.10	1.02
25	1.20	1.40
35	1.50	1.80
40	1.64	2.22
45	1.84	2.35
50	1.89	2.36
55	2.00	2.39
65	2.04	2.50
75	2.11	2.70
85	2.20	3.10
95	8.55	15.30

TABLE B.15: Data for the influence of EGR variation on performance, emissions and combustion characteristics for engine operation with dual fuel combustion of diesel/gasoline and PME/gasoline.

%EGR	BSNO _x (g/kWhr)		Smoke (%)		BSCO (g/kWhr)		BSHC (g/kWhr)		MPRR (bar/°CA)		Optimal SOI Timing (°BIDC)	
	Diesel/	PME/	Diesel/	PME/	Diesel/	PME/	Diesel/	PME/	Diesel/	PME/	Diesel/	PME/
	Gasoline	Gasoline	Gasoline	Gasoline	Gasoline	Gasoline	Gasoline	Gasoline	Gasoline	Gasoline	Gasoline	Gasoline
30	0.68	0.59	3.2	3.0	13.2	11.0	1.14	1.11	4.47	4.81	7.00	7.00
35	0.45	0.29	2.2	2.0	15.9	15.2	1.37	1.20	4.40	4.73	7.00	7.00
40	0.29	0.17	1.6	1.4	18.7	16.4	1.41	1.32	3.63	4.35	9.00	7.00
45	0.16	0.11	1.3	1.2	21.7	19.5	1.53	1.42	2.84	3.74	9.00	7.00
50	0.10	0.05	1.2	1.0	23.5	20.9	1.55	1.48	2.32	3.32	11.00	9.00